Investigations on Wood Stability and Related Properties of Radiata Pine

---

A thesis submitted in fulfilment of the
requirement for the Degree
of

Doctor of Philosophy in Chemical Engineering

in the
Department of Chemical and Process Engineering

by Alfred Herritsch

University of Canterbury
October, 2007

Acknowledgements

I would like to thank my supervisor, Associate Professor Shusheng Pang and my associate supervisor, Dr Pat Jordan, for the guidance they have given me during this study.

Many thanks to:

- The Chemical and Process Engineering Department for providing a pleasant working environment;
- Ms Hazel Reeves and Ms June Walter for their support in countless administration matters;
- The departmental workshop for modifying the environment chamber needed in this study. The technical supporting members include: Mr Tony Allen, Mr Trevor Berry, Mr David Brown, Mr Bob Gordon, Mr Peter Jones, Mr Frank Weerts and Mr Glenn Wilson;
- The School of Forestry at University of Canterbury for providing equipment and storage facilities. The technical staff, Mr Lachlan Kirk and Mr Nigel Pink for their support during the sample preparation;
- Selwyn Plantation Board Ltd which generously provided the material for the experimental investigation on moisture diffusion in radiata pine. Particular thanks goes to Mr Les Hurford who cut the trees I had chosen and who also widened my knowledge on New Zealand's forest industry;
- The Wood Quality Initiative Ltd. for the financial support and generous permission for my access to the company data.

Content:

Content: I
List of figures III
List of tables VIII
Abstract XIII
0 Preamble 1
1 Radiata Pine: Review and Analysis of Its Stability Related Properties 3
1.1 Facts and Background of Radiata Pine 4
1.2 Radiata Pine Growth 6
1.3 Wood Structure in General 7
1.3.1 Tracheid structure 8
1.3.2 The microfibril angle 11
1.3.3 Reaction wood (compression wood) 12
1.3.4 Spiral grain 13
1.4 Basic Wood Properties 14
1.4.1 Basic wood density 15
1.4.2 Fibre saturation point 15
1.4.3 Green- and equilibrium-moisture content 16
1.4.4 Shrinkage and swelling 17
1.5 Variation of Wood Properties within an Annual Growth Layer 18
1.5.1 WQI benchmarking study 19
2 Experimental Investigation of Earlywood and Latewood Properties of Radiata Pine 25
2.1 Material and Sample Preparation 25
2.2 Measurements 27
2.2.1 MC and density 27
2.2.2 Shrinkage and EMC 29
2.3 Experimental Results 31
2.3.1 Green MC and wood basic density 31
2.3.2 Properties in desorption 34
2.3.3 Properties in adsorption 48
2.4 Experiment Results for Wood from Juvenile Trees 55
2.5 Discussion of Results 58

2.5.1 Sorption isotherms 58
2.5.2 Fibre saturation point 60
2.5.3 Shrinkage and swelling 62
2.6 Conclusions and Remarks 65
3 Moisture Diffusion in Radiata Pine 67
3.1 Theoretical Background 68
3.1.1 Diffusion coefficient 70
3.1.2 Surface emission coefficient 73
3.2 Experiments 79
3.2.1 Experiment procedure 79
3.2.2 The environment chamber and its performance 81
3.2.3 Experimental results on basic wood properties 84
3.2.4 Inverse determination of the diffusion coefficient 92
3.3 Results and Discussion 97
3.3.1 Diffusion parameters for desorption 99
3.3.2 Diffusion parameters for adsorption 108
3.3.3 Comparison of results with literature data 121
3.3.4 Variation of diffusion parameters with wood types 125
3.3.5 Influence of wood shrinkage and density on the diffusion coefficient 130
3.4 Conclusion and Future Improvement 135
4 Distortion of Radiata Pine Timber 137
4.1 Literature Review 139
4.2 Geometrical Model for Twist in Timber Boards 141
4.2.1 Spiral grain curve 142
4.2.2 Shrinkage of an individual cone layer 144
4.2.3 Geometrical distortion model for twist 147
4.3 Simulation Results and Discussion 151
4.3.1 Segments area distribution 151
4.3.2 Model prediction and comparison 154
4.4 Model Validation with Experimental Data 156
4.5 Discussion and Conclusions 159
5 Conclusions and Applications 163
5.1 Wood Properties Related to Distortion 163
5.2 Model Development and Future Work 167
6 References 171
7 Appendix 181

List of figures

Figure 1-1: Locations and areas (ha) of plantation forests in New Zealand (NZFI, 2006). 5
Figure 1-2: Simplified structure of the cell wall showing orientation of the micro fibril angle in each major wall layers (Dinwoodie, 1975). 9
Figure 1-3: Transverse(x 400) sections early- and latewood from 1-2 and 10-11 ring (Bamber *et al.*, 1983). 10
Figure 1-4: Spiral grain variation within trees (Cown *et al.*, 1991)..... 14
Figure 1-5: Comparison ring width distribution pith to bark (left) and bark to pith (right). 18
Figure 1-6: Ring width distribution from WQI benchmarking study. 20
Figure 1-7: Annual growth rate derived from the distance from the pith and its corresponding ring width. 21
Figure 1-8: Density distribution from WQI benchmarking study. 22
Figure 1-9: Microfibril angle distribution from WQI benchmarking study. 22
Figure 1-10: Modulus of elasticity distribution from WQI benchmarking study. 23
Figure 1-11: Spiral grain distribution from WQI benchmarking study. 24
Figure 1-12: Radii, conical angle and total number of year rings for different heights. 24
Figure 2-1: Appearance and marking of the disc, from which four strips were cut. 26
Figure 2-2: Two strips cut from the disc for preparation of the earlywood and latewood specimens. 27
Figure 2-3: 10 earlywood and latewood specimens were cut out from one strip. 27
Figure 2-4: Longitudinal dial gage mounted on gage plate 30
Figure 2-5: Diameter distribution along the tree height for each of the seven trees. 31
Figure 2-6: Average densities at different heights. 32
Figure 2-7: Radial density distribution at different heights [BH (a), 10 m (b) and 20 m (c)] for early- and late-wood 34
Figure 2-8: RH & temperature progression (EMC cabinet) for the measurements. 35
Figure 2-9: Early (a)- Late-wood (b) EMCs for desorption at different heights. 37
Figure 2-10 (a, b, c): Average EMC and error bars at BH (a), 10m (b) and 20m (c) for early- and late-wood 39
Figure 2-11: Tangential shrinkage at different moisture contents. 40
Figure 2-12: Average oven-dry early- and latewood tangential shrinkage at different heights. 42
Figure 2-13: Average oven-dry early- and latewood longitudinal shrinkage at different heights. 44
Figure 2-14: R^2 values from the fibre saturation point determination. 46

Figure 2-15: Uncertainty of MC and FSP in the linear regression. 46
Figure 2-16: Effect of tree height on the FSP for a low density tree (Tree 12) and a high density tree (Tree 19)..... 47
Figure 2-17: Average FSP for early- and late-wood, at different heights. 48
Figure 2-18: Controlled and actual RH & temperature for the swelling experiment. 49
Figure 2-19: Average EMC for adsorption and comparison with data of Bramhall and Wellwood (Kininmonth and Whitehouse, 1991). 49
Figure 2-20: Earlywood (a) and latewood (b) EMC in adsorption at different heights. 51
Figure 2-21: Average early- and latewood EMC for adsorption and error bars at BH (a), 10 m (b) and 20 m (c). 53
Figure 2-22: Tangential shrinkage of the juvenile tree samples. 57
Figure 2-23: Longitudinal shrinkage of the juvenile tree samples. 57
Figure 2-24: Comparison of tangential dimensional changes of juvenile tree samples between adsorption and desorption. 57
Figure 2-25: Comparison of longitudinal dimensional changes of juvenile tree samples between adsorption and desorption. 57
Figure 2-26: Sorption isotherms for radiata pine at 30°C, including the standard deviations. 59
Figure 2-27: Tangential shrinkage at 12%MC and fibre saturation point at different heights. 61
Figure 2-28: Tangential shrinkage of early- and latewood. 62
Figure 2-29: Longitudinal and Tangential shrinkage at different heights. 63
Figure 2-30: Tangential dimensional changes in desorption and adsorption. 64
Figure 3-1: Siau's Geometrical model for a single cell (Siau, 1984). 71
Figure 3-2: (a) Siau's transverse thermal conductivity model; (b) Analogous electrical circuits. 72
Figure 3-3: Sorption isotherm for radiata pine at 30°C. 76
Figure 3-4: The calculated surface emission coefficient as a function of surface moisture content and wood basic density. 76
Figure 3-5: Surface emission coefficients by Yeo and Siau. 77
Figure 3-6: Comparison of the influence of two applied surface emission coefficient on the drying time of a sample at air velocity of 3.3 m/s. 78
Figure 3-7: Main sample extraction from disc. 80
Figure 3-8: Environment chamber. 82
Figure 3-9: Temperature and relative humidity over time for the performance check of the environment chamber. 83
Figure 3-10: Green moisture content. 85
Figure 3-11: Basic density. 86
Figure 3-12: Equilibrium moisture contents for the 1. Experiment. 87

Figure 3-13: Equilibrium moisture contents for the 2. - 4. Experiment. 88
Figure 3-14: Tangential and radial oven-dry shrinkage. 90
Figure 3-15: Correlation between area shrinkage (oven-dry) and time of flight (TOF) measurements. 92
Figure 3-16: Basic principle and procedures of the inverse algorithm. 94
Figure 3-17: Fitted drying curves with experimental data for one sample in the three diffusion directions. 95
Figure 3-18: Experimental and derived moisture content for desorption, for all samples. 96
Figure 3-19: Experimental and derived moisture content for adsorption, for all samples. 96
Figure 3-20: Desorption D_0 parameter for all experiments. 99
Figure 3-21: Desorption K_0 parameter for all experiments. 100
Figure 3-22: Average diffusion coefficient (thick lines) and values of individual samples (thin lines): (a) longitudinal, (b) tangential, (c) radial. 101
Figure 3-23: Maximum local relative error of all samples for desorption. 102
Figure 3-24: Global relative error of all samples for desorption. 102
Figure 3-25: K_0 versus D_0 in all directions for desorption. 103
Figure 3-26: K_0 versus D_0 in the longitudinal direction for desorption. 103
Figure 3-27: K_0 versus D_0 in the tangential direction for desorption. 104
Figure 3-28: K_0 versus D_0 in the radial direction for desorption. 104
Figure 3-29: Effect of the sample's diffusion dimension on D_0 in longitudinal direction. 105
Figure 3-30: Effect of the sample's diffusion dimension on D_0 in the tangential direction. 105
Figure 3-31: Effect of the sample's diffusion dimension on D_o in the radial direction. 105
Figure 3-32: Average constant diffusion coefficient (D_0) over each tree in the longitudinal direction. 107
Figure 3-33: Average constant (K_0) over each tree in the longitudinal direction. 107
Figure 3-34: Average constant diffusion coefficient (D_0) over each tree in transverse direction. . 107
Figure 3-35: Average constant (K_0) over each tree for desorption in the transverse direction. 108
Figure 3-36: Adsorption constant diffusion coefficient, D_0, for individual samples. 108
Figure 3-37: Adsorption constant, K_0, for individual samples. 109
Figure 3-38: Average diffusion coefficient (thick lines) and values of individual samples (thin lines) for the adsorption process: (a) longitudinal, (b) tangential, (c) radial. 110
Figure 3-39: Maximum local relative error of all samples for adsorption. 111
Figure 3-40: Global relative error of all samples for adsorption. 111
Figure 3-41: K_0 versus D_0 in all directions for adsorption. 112
Figure 3-42: K_0 versus D_0 in the longitudinal direction for adsorption. 112
Figure 3-43: K_0 versus D_0 in the tangential direction for adsorption. 113

Figure 3-44: K_0 versus D_0 in the radial direction for adsorption. 113
Figure 3-45: Effect of the diffusion dimension of the sample on the constant diffusion coefficient in the longitudinal direction for adsorption. 114
Figure 3-46: Effect of the diffusion dimension of the sample on the constant diffusion coefficient in the tangential direction for adsorption. 114
Figure 3-47: Effect of the diffusion dimension of the sample on the constant diffusion coefficient in the radial direction for adsorption. 114
Figure 3-48: Average constant diffusion coefficient, D_0, for each tree in the longitudinal direction for adsorption. 115
Figure 3-49: Average constant, K_0, for each tree in the longitudinal direction for adsorption. 116
Figure 3-50: Average constant diffusion coefficient, D_0, for each tree in the transverse directions for adsorption. 116
Figure 3-51: Average constant, K_0, for each tree in the transverse directions for adsorption. 116
Figure 3-52: Radial distribution of the constant diffusion coefficient, D_0, for desorption in; (a) longitudinal, (b) tangential and (c) radial direction. 117
Figure 3-53: The influence of growth ring and tree height on the constant diffusion coefficient (D_o) and constant (K_o) for desorption 118
Figure 3-54: Radial distribution of constant diffusion coefficient, D_0 for adsorption in; (a) longitudinal, (b) tangential and (c) radial direction. 120
Figure 3-55: Influence of the radial position and tree height on the diffusion parameters for adsorption. 120
Figure 3-56: Basic density influence on surface emission coefficient for desorption (a) and adsorption (b). 121
Figure 3-57: Comparison of the effective diffusion coefficient of radiate pine obtained in this project with the literature data for Scott pine. 124
Figure 3-58: Effective diffusion coefficient for different wood types for desorption. 126
Figure 3-59: Simulated drying behaviour for different wood types, in longitudinal direction. 127
Figure 3-60: Simulated drying behaviour for different wood types, in tangential direction. 127
Figure 3-61: Simulated drying behaviour for different wood types, in radial direction. 128
Figure 3-62: Effective diffusion coefficient for different wood types for adsorption. 129
Figure 3-63: Density influence on longitudinal diffusion for desorption. 132
Figure 3-64: Density influence on longitudinal diffusion for adsorption. 132
Figure 3-65: Density influence on tangential diffusion for desorption. 133
Figure 3-66: Density influence on tangential diffusion for adsorption. 133
Figure 3-67: Density influence on tangential diffusion for desorption. 134
Figure 3-68: Density influence on tangential diffusion for adsorption. 134

Figure 4-1: Cross-sectional- and board distortion of wood (Forest Products Laboratory, 1974)... 137
Figure 4-2: Spiral grain curve. The left diagram represents a tree stem, and the right diagram is the stem seen from the tree top. ... 142
Figure 4-3: Definition of the geometric relationships. ... 143
Figure 4-4: Rolled out cone segment. ... 145
Figure 4-5: Shrinkage in fibre direction. ... 146
Figure 4-6: Combined shrinkage of the rolled out cone segment. ... 147
Figure 4-7: Location of the largest surface area within boards cut from different locations. ... 148
Figure 4-8: Distorted cone segment. ... 148
Figure 4-9: Rotation of the original cross sectional shape ... 149
Figure 4-10: Right hand rule for positive rotation direction around the three principle axes. ... 150
Figure 4-11: Definition of board location in the log cross section. ... 151
Figure 4-12: Segment surface area distribution for a quartersawn board. ... 152
Figure 4-13: Segment surface area distribution for a flatsawn board. ... 152
Figure 4-14: Distribution of the largest segment curve surface area as a function of board location. ... 153
Figure 4-15: Comparison of twist development for quartersawn (a) and flatsawn boards (b), with identical board centre of gravity (100mm), tangential (3%) and longitudinal (0.1%) shrinkage and spiral grain angle (6°). ... 153
Figure 4-16: Predicted twist by the developed model and comparison with results from Stevens and Johnston's model. ... 154
Figure 4-17: Twist variations of flatsawn boards (defined at the mid-length of the board) with different board location angles at the board bottom and top. ... 155
Figure 4-18: Twist variations of quartersawn boards (defined at the board mid-length) with different board location angles at the board bottom and top. ... 155
Figure 4-19: Spiral grain angle distribution of the measured materials. ... 157
Figure 4-20: Shrinkage distribution of the measured materials. ... 157
Figure 4-21: Comparison model results with experimental data for twist. ... 158
Figure 4-22: Spiral grain gradient versus measured twist of the boards. ... 159
Figure 4-23: Experimental results of the board twist as a function of mean radius and board location angle. ... 160
Figure 4-24: Predicted twist of boards as a function of board radius and board location angle. ... 160
Figure 4-25: Distortion of a flatsawn board, predicted by the second approach ... 162
Figure 5-1: Comparison average bow (a), crook (b) and twist (c) per log with the theoretical tangential shrinkage. ... 164
Figure 5-2: Radial distributions of the spiral grain curvatures for different spiral grain angles. ... 168

List of tables

Table 2-1: Moisture content uncertainties arising from the balance used 29
Table 2-2: Average, earlywood and latewood densities for Trees 12, 19, 21 and 23. 33
Table 2-3: EMC values for desorption. 35
Table 2-4: Tangential shrinkage of early- and late-wood for Trees 12, 19, 21 and 23 41
Table 2-5: Comparison of the average longitudinal shrinkage between this study and literature data. 43
Table 2-6: Earlywood and latewood longitudinal shrinkage (LS) for Trees 12, 19, 21 and 23 43
Table 2-7: FSP of early- and late-wood for Trees 12, 19, 21 and 23. 47
Table 2-8: EMC values for adsorption. 50
Table 2-9: Swelling and shrinkage for early- and latewood at 12%MC for Trees 12, 19, 21 and 23. 54
Table 2-10: Longitudinal swelling/shrinkage at 12%MC for early- and latewood for Trees 12, 19, 21 and 23. 54
Table 2-11: Appearance of the juvenile discs. 55
Table 2-12: Comparison desorption EMC juvenile trees with average obtained for seven trees. 56
Table 2-13: Comparison adsorption EMC juvenile trees with average obtained for seven trees. 56
Table 2-14: GAB parameters for radiata pine sorption curves at 30°C and approximately 1 bar. 60
Table 3-1: Basic densities and EMC for the first run of experiment. 88
Table 3-2: Basic densities and EMC for the second run of the experiments. 89
Table 3-3: Basic densities and EMC for the third run of the experiments. 89
Table 3-4: Basic densities and EMC for the fourth run of the experiments. 89
Table 3-5: Summary of the “quality of fit” for the desorption experiment. 95
Table 3-6: Summary of the “quality of fit” for the adsorption experiment. 95
Table 3-7: Average, standard deviation (STD), maxima and minima values of parameters for desorption. 100
Table 3-8: Average, standard deviation (STD), maxima and minima values of parameters for adsorption. 109
Table 3-9: Average, standard deviation (STD), maxima and minima values of parameters for desorption. 122
Table 3-10: Average, standard deviation (STD), maxima and minima values of parameters for adsorption. 122
Table 3-11: Desorption, average constants for different wood types. 125
Table 3-12: Adsorption, average constants for different wood types. 128

Abbreviations

BH	Breast height
CA	Conical angle
CSIRO	Commonwealth Scientific and Industrial Research Organisation
EMC	Equilibrium moisture content
ENSIS	"Joint Forces of CSIRO & SCION"
FSP	Fibre saturation point
GAB	Guggenheim-Anderson-De Boer
ha	hectare
IRL	Industry Research Limited
LS	Longitudinal Shrinkage
MAF	The Ministry of Agriculture and Forestry, N.Z.
MC	Moisture content based on dry matter
MFA	Microfibril angle
MOE	Modulus of elasticity
MOR	Modulus of rupture
NZ	New Zealand
NZFI	New Zealand Forest Industry
RH	Relative humidity
SCION	Trading name of New Zealand Forest Research Institute Limited
SGA	Spiral grain angle
STD	Standard deviation
WQI	Wood Quality Initiative Limited

Nomenclature

a	Ratio of lumen width to cell width [-]
a_w	Water activity [-]
C	Water concentration in wood [kg_{water}/m^3]
C_B	GAB equation parameter
D	Diffusion coefficient [m^2/s]
D_0	Constant diffusion coefficient [m^2/s]
D_{BT}	Transverse diffusion coefficient of the bound water in the cell wall substance
D_{Lumen}	Water vapor diffusion coefficient in the air in the lumens
D_{Wood}	Transverse diffusion coefficient of bound water in wood [m^2/s]
E_b	Activation energy of diffusion [J/mol]

K	GAB equation parameter
L	Length [m]
MC	Moisture content [$kg_{moisture}/kg_{dry\ matter}$]
m	Mass [kg]
R	Gas constant [J/mol K] (8,314 [m^3 Pa/kmol K])
t	Time [s]
T	Temperature [K]
x	Spatial coordinate [m]
X_m	GAB equation parameter
h_{air}	Mass transfer coefficient based on water-vapor concentration in air [m/s]
$D_{H2O,air}$	Diffusion coefficient of water-vapor in air [m^2/s]
Re	Reynolds number [-]
Sc	Schmidt [-]
L_s	Length of the surface along which convection occurs [m]
v	Air velocity [m/s]
μ	Dynamic viscosity [Pa s]
p	Total pressure of air [Pa]
T	Temperature [K]
$C_{,air}$	Concentration in air [kg_{water}/m^3]
h_m	Surface emission coefficient [m/s]
$p_{o,dry}$	Saturated water vapour pressure at dry bulb temperature [Pa]
$p_{o,wet}$	Saturated water vapour pressure at wet bulb temperature [Pa]
$p_{e/s}$	Surface/equilibrium water vapour pressure in air [Pa]
RH_e, RH_s	Relative humidity at equilibrium and at the wood surface [-]
V	Volume [m^3]
D_0	Constant diffusion coefficient [m^2/s]
K_0	Constant
e_1	Local relative error [%]
e_2	Global relative error [%]
CA	Conical angle [radians]
r	Radius of spiral grain curve [m]
ds	Differential cone length [m];
r	Radius of the curve surface at angle φ [m]
SGA	Spiral grain angle [radians]
CA	Conical angle [radians]
dz	Differential height [m]

A	Parameter in spiral grain curve [-]
SH	Shrinkage
l	Length [m]
r	Radius [m]
$dSGA$	Gradient of spiral grain angle [°]

Subscripts

eq	Equilibrium
od	Oven dry
O	Original
e	Equilibrium
s	Surface
Exp	Experimental
$Pred$	Predicted
L	Longitudinal
T	Tangential
R	Radial
V	Volumetric

Greek Letters

ε	Shrinkage/Swelling [-]
ε	Porosity in Chapter 3 [-]
ρ	Density [kg/m^3]
φ	Parameter, for the description of the spiral grain curve, (radians)
ρ_{air}	Density of air [kg/m^3]
ρ_{basic}	Basic density [kg$_{wood}$/m^3]

Abstract

Previous studies on wood instability have identified some wood basic properties which influence the timber distortion and shape changes while the wood is losing or gaining moisture. These properties include wood anisotropic shrinkage, equilibrium moisture content (EMC) in both desorption and adsorption, fibre saturation point (FSP) and water diffusion coefficient.

This study investigated the stability related wood properties and their variations within the stems of the New Zealand grown radiata pine trees. The basic density, EMC and shrinkage for the earlywood and the latewood were also experimentally determined. In taking into account these properties and their variations, an analytical model was developed to simulate the wood distortion.

The equilibrium moisture content was determined at 30°C and humidity range from 27% to 90%. It was found that the EMC difference between the earlywood and the latewood was negligible. The experimental results also show that the EMC decreases from pith towards the bark over the disc cross section and the trend is most obvious at high humidities (70-90%). Along the tree height, the EMC decreases from ground towards the top of the stem.

The tangential shrinkage results were highly variable but, in general, the latewood has higher values than the earlywood. The opposite trend was found for the longitudinal shrinkage, higher values for the earlywood than the latewood. In the tree height direction, the tangential shrinkage was found to decrease with the tree height. This follows the same trend as the microfibril angle which in general also decreases with the tree height. The fibre saturation point (FSP) was determined from the tangential shrinkage values at different equilibrium moisture contents. These were taken as the intersection point of the tangential shrinkage line with the moisture content axis. The experimental results have revealed a trend that the FSP decreases from the pith towards the bark and also decreases with the tree height. Similar behaviour was found for the tangential and longitudinal swelling during the adsorption.

The moisture transport within radiata pine was investigated based on the diffusion theory under transient and isothermal condition of 30°C. The moisture dependant diffusion coefficient was derived from the experimental data using the inverse analysis method. The surface emission coefficient was determined by taking into account the variable surface moisture content, wood density and the ambient conditions. In the experiments, 138 samples in total (46 samples for each

of the longitudinal, tangential and radial directions) were used and their diffusion coefficients were determined for both the adsorption and the desorption with moisture content ranging from 6% to 22%. The derived diffusion coefficients are comparable with the reported data in the literature. Further investigation of the wood type influence on the diffusion coefficient revealed that compression wood has the lowest diffusion coefficients in the three directions (longitudinal, tangential and radial) both in the desorption and in the adsorption. In addition, the moisture content has the least influence on the diffusion coefficient in the compression wood. Investigation on the effects of the wood density has shown that in general, the diffusion coefficient decreases with increasing wood density although the correlations are only significant for the longitudinal direction in desorption.

An analytical model for the simulation of the wood twist was developed which is based on the geometry and geometrical changes of the grains aligning non parallel to the pith. A board consists of numerous such grains which change the length and shape with moisture content change. The model predictions confirm that the grain angle, the tangential and longitudinal shrinkage and the conical angle all affect the development of the board twist. However, the discrepancies between the model prediction and the experimental data are significant, partly due to the experimental uncertainties and partly due to the model errors.

In this study, sound velocity in the longitudinal direction was measured for the test samples used in the shrinkage experiments. The results revealed that the correlations between the sound velocity and the volumetric shrinkage at oven dry are significant. Based on this finding, the relationship between the tangential shrinkage and the radial shrinkage, the tangential shrinkage can be predicted from the sound velocity measurements. As the tangential shrinkage has significant influence on the wood distortion, this method can be used to segregate logs which may be prone to wood distortion.

Preamble

In New Zealand, it is common to dry radiata pine timber in well controlled kilns. During the removal of moisture, timber can alter its shape. The excessive and non-uniform changes of the wood shape result in wood distortion (warp). Distortion of timber is a serious concern for wood quality and can reduce the value of the product. Extensive studies on instability of wood have identified some basic wood properties which influence the wood distortion and shape changes when the wood is losing or gaining moisture. These properties include anisotropic shrinkage (longitudinal and tangential), fibre saturation point and equilibrium moisture content. The abnormal and variations of these properties will generate stresses within timber during drying, which result in distortion or movement in remanufacturing.

The objective of this study was to fill knowledge gaps in regards to earlywood and latewood properties and to investigate the moisture diffusion below fibre saturation point in longitudinal, tangential and radial direction for the desorption and the adsorption. The intention of this thesis was to create a critical view of the property variation within radiata pine. The thesis structure is described as follows:

Chapter 1 introduces wood properties related to wood distortion of radiata pine. Facts and background are discussed and the influence of the climate on the exceptional growth of radiata pine in New Zealand is summarized. The softwood structure, its principal components and variations within the stem are analysed from a literature review and reported data. The basic wood properties, their definitions and importance to the wood distortion are introduced.

Chapter 2 contains the methodology and results of the experiments on the wood properties of earlywood and latewood of radiata pine. The properties investigated in this study are the tangential and longitudinal shrinkage/swelling, fibre saturation point (tangential shrinkage intersection point) and equilibrium moisture contents at 30°C for adsorption and desorption. In the experiments, the radial (along the radius) and longitudinal (along the tree height) distribution of these wood properties were measured and analysed.

Chapter 3 is focused on the moisture transport within radiata pine, based on the diffusion theory (under transient and isothermal condition). The moisture dependant

diffusion coefficient was derived from the diffusion equation by inverse analysis. Theoretical background on the diffusion coefficient is included and the calculation of the surface emission coefficient is introduced. The variation of the water diffusion coefficient with wood type (heartwood, sapwood, compression and opposite wood) and the influences of the wood density on the diffusion coefficient were investigated and the results are included.

Chapter 4 introduces a geometrical twist model. The necessary mathematical algorithm is presented and the model predictions are compared with the twist model of Stevens and Johnston (1962). Additionally, the developed twist model in this work is validated with experimental data.

Chapter 5 includes the general conclusions and recommendations for future work. Furthermore, the possible applications of the results from this thesis are discussed for the identification of logs which are prone to warp.

The aim of the thesis was to critically investigate the property variation within radiata pine trees and to emphasise that exactly these variations have to be considered to prevent the distortion from occurring.

Chapter 1

Radiata Pine: Review and Analysis of Its Stability Related Properties

In New Zealand, it is common to dry radiata pine timber in well controlled kilns. During the removal of moisture, timber can alter its shape. This effect is regarded as distortion or warp. Distortion of timber is a serious concern of wood quality and can reduce the value of the product. Therefore a number of investigations have been conducted to understand and quantify the influences of wood properties on the distortion (Booker, 2005; Ekevad, 2005; Fridley and Tang, 1993; Johansson and Kliger, 2002; Johansson *et al.*, 2001; Kang and Lee, 2002; Kliger *et al.*, 2003; Mishiro and Booker, 1989; Ormarsson *et al.*, 1998, 1999; Ormarsson, Dahlblom *et al.*, 2000; Ormarsson, Petersson *et al.*, 2000; Pang, 2000; Pang and Haslett, 2002; Perstorper *et al.*, 2001; Stanish, 2000; Stevens and Johnston, 1960).

For the above studies, the factors which affect the timber distortion fall into the following three categories:

1. Wood intrinsic properties (Shrinkage, elastic modulus)
2. Log properties (Spiral grain, log diameter and cross sectional shape)
3. Processing effects (Sawing pattern and kiln drying)

Trees consist of a complex biomass structure which enables them to adapt to the surrounding environment. Therefore each individual tree will evolve according to the environment to ensure its survival, and this partly explains the variability in wood properties between trees and within a tree. However, quantitative description of the relationships between growing environment and wood properties are not available in literature. Previous research cited above has tried to derive a common applicable theory to describe the influence of affecting properties on the timber distortion, however, during the investigations, it was realised that the general theory would induce significant errors without knowing the wood properties and their variations. Therefore, this thesis has investigated the factors in the first two categories listed above. This information has further been used to develop an analytical mathematical model to quantify the timber distortion.

1.1 Facts and Background of Radiata Pine

Radiata pine (*Pinus radiata*) was originally named *Pinus insignis* or 'remarkable pine'. It was introduced to the Southern Hemisphere in the 18th century and used initially for amenity and mixed shelter. Indigenous stands of radiata pine are situated on the coast of California, and on two islands west of Baja California. Its natural occurrence reaches from 28°N to 37°N latitudes. Radiata pine was introduced to New Zealand in 1859 (Lavery, 1986), and the typical radiata pine found in New Zealand plantations originated mainly from Aňo Nuevo Point (55 miles south of San Francisco) (Bannister, 1973), which is the northern-most natural population.

Lavery (1990) reported that Australia, Chile and New Zealand share 88% of the world's total plantation of 3.5 million hectares (ha) of radiata pine. The reasons for the extensive planting in these countries can be attributed to its remarkable growth rate, some desirable wood properties and its adaptability to different growing conditions. In New Zealand the economical rotation age of radiata pine is approximately 25 to 30 years.

Recent statistical report (NZFI, 2006) shows that New Zealand plantation forests covered 1.82 million hectares by April 2004 and among the plantations, radiata pine was the dominant species covering 89.2% of the plantation area, followed by Douglas fir with 6.2%. The remaining plantation area was represented by other softwood and hardwood species. The major proportion of the plantation forests (70%) was in the North Island, with the Central North Island as the most favourable place for plantations making up a third of the total area, as shown in Figure 1-1.

Over half of the logs harvested in New Zealand are processed domestically for timber, wood based panels, pulp and paper. It is reported (MAF, 2007) that in 2003 the New Zealand forest industry harvested 21.6 million m^3 of logs and exported the roundwood equivalent of 15.6 million m^3 (including around 7 million m^3 of logs).

The New Zealand wood processing industry processes around 3 million m^3/year of timber for various uses such as building structure and furniture. In the timber processing, wood drying is a key operation which removes the moisture from wood to achieve the required dryness. Wood in its natural occurrence contains variable moisture content, 30-50% in heartwood and 150-200% for sapwood. Most of this water must be removed prior to further processing of the timber such as planing, sanding and varnishing. Additionally, the removal of moisture increases the durability against forest pests, dimensional stability and material stiffness.

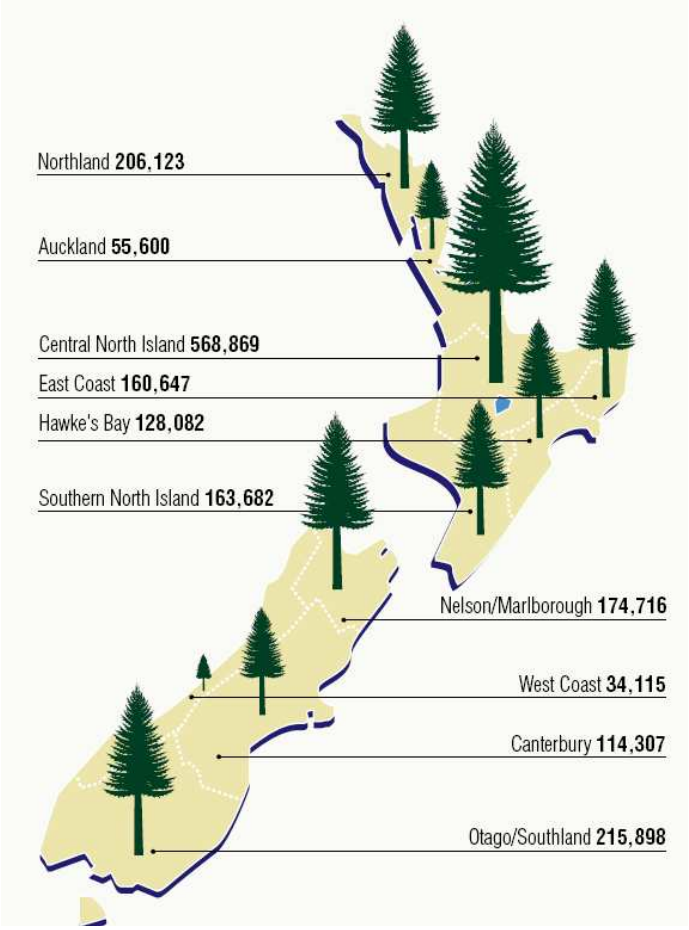

Figure 1-1: Locations and areas (ha) of plantation forests in New Zealand (NZFI, 2006).

1.2 Radiata Pine Growth

The importance of radiata pine as a plantation tree has led to numerous investigations for improving its productivity and wood quality. Rock (1975) studied the exceptional growth of radiata pine in New Zealand, and concluded that the increased productivity was mainly due to its continuous growing ability throughout the year in the prevailing New Zealand climate. The New Zealand climate and its effects on radiata pine growth are summarized below:

1. *Day length:* The geographical location of New Zealand (low latitude) leads to a high number of longer day lengths (up to approximately 16 hours in summer season). Longer day lengths enhance the shoot growth, whereas shorter days cause the trees to stop growing and set dormant buds. This general rule does not apply for radiata pine and allows a continuous yearly growth due to the general mild climate over the winter months.
2. *Climate:* The climate throughout the country is mild, mostly cool temperate to warm temperate, with temperatures rarely falling below 0°C or rising above 30°C in most parts of the county. New Zealand stretches approximately from 47°S to 34°S. The latitudinal position and its geographical features (mountain ranges, plains) cause climate regions varying from continental to subtropical climate. Radiata pine grows most efficiently at day temperatures around 20°C. Higher temperatures lead to lower food production, thus lower growth rates. The prevailing low night time temperatures (around 5°C) are also favourable to the growth. It slows down the metabolism of the tree, and reduces its energy consumption and therefore less energy is wasted during the night time.

The previous mentioned general climate condition explains, to a certain extent, the exceptional growth of radiata pine in New Zealand. Madgwick (1994) investigated in more detail the growth of radiata pine in New Zealand. In his work he pointed out a larger number of aspects affecting the growth including physical conditions (site, soil depth and climate) soil nutrients and biological factors.

In the following section, wood structures and properties of softwood will be discussed. In addition, the microstructure of normal and compression wood will be described. Compression wood differs greatly in its properties from normal wood, and due to its high frequency of occurrence in New Zealand it cannot be neglected. Burdon (1975) examined 12-year-old radiata pine trees growing on four different sites in New Zealand and estimated that 30% to 45% of the stems contained mild to severe compression wood.

Following the discussion of the wood structure, wood basic properties are introduced and their relationship is discussed. In order to understand the impact of moisture content change on the wood distortion, wood-water relations will also be discussed. Due to the variability of the above mentioned properties within a stem their radial and vertical variations are subsequently examined.

1.3 Wood Structure in General

Radiata pine belongs to the specie of conifers which possesses a relative simple anatomy. Around 95% of the wood by volume consists of fibrous elements called tracheids. These cells are aligned axially around the stem axis. Depending on the maturity stage and the formation time, these cells have certain characteristics. The first formed growth layer within the annual growth ring is called earlywood, which is produced in fast growing season of spring and summer. The early wood tracheids have thinner cell walls and lager lumen space than the latewood layer which is formed in slow growing season of autumn and winter. Due to the continuous growth of radiata pine, the transition between the earlywood and the latewood is less apparent compared with other confer species.

When the tree matures the inner zone within the stem is no longer biologically alive and the cells lose moisture. This inner zone is called heartwood. For radiata pine, the heartwood starts to form when the tree reaches the age of 11 to 12 years and increase from pith outward at a rate of 1/3 – 1/2 ring per annum. In the meantime, the outer wood contains living cells which are almost fully filled with water for the transportation of water and storage of nutrients. This part of the wood is called sapwood. Heartwood contains more extractives (resins, tannins, etc.) than the sapwood.

In the following discussion, some terms will be used and it has to be pointed out that the definitions of these terms vary in different sources. In this thesis, the terms and their definitions of Burdon *et al.* (2004) will be accepted and used. In the following, the anatomy of radiata pine is presented with the focus on tracheids and their axial alignment (spiral grain) to the pith. Prior to the spiral grain introduction, the structure of the compression wood is discussed, due to its structural variation from the normal wood tracheids.

1.3.1 Tracheid structure

Longitudinal (Axial) tracheids are the principle cells of conifers, and their length to diameter ratio is around 100. Tracheids contain an open space (lumen) in the middle for water conduction from roots up to the stem. The water transport between cells is established through bordered pits located mainly on the radial cell wall with higher numbers of the pits in the earlywood. For radiata pine, the axial tracheids have average dimensions of 38.35 μm in tangential diameter (range 21.80-56.50 μm), 3.45 μm in wall thickness (range 1.20-6.60 μm) and 2.72 mm in length (range 0.73-4.78 mm) (Kininmonth and Whitehouse, 1991).

Three major chemical components of the wood cells are cellulose, lignin and hemicelluloses. Their concentration varies within the cell wall. Cellulose within the wall occurs as threadlike chains of joined glucoses (microfibrils) which are filled with less regular sugars, which are hemicelluloses. The lignin is a group of more complex and irregular sugars and acts like glue to hold the cells together. More water molecules reside on the hemicellulose sites through hydrogen bonds.

Figure 1-2 shows the simplified tracheid and its cell walls. The layer between cells is called the middle lamella and contains mainly lignin and pectin substances. This is followed by the primary wall which is a thin layer where fibrils are randomly organized. Inside the primary wall is the secondary wall which is subdivided into three layers: S_1, S_2 and S_3, each having a distinct and homogenous microfibril orientation. The secondary wall has the highest concentration of cellulose, but the middle lamella contains the highest concentration of lignin.

In the secondary wall, S_2 has the largest thickness thus the largest volume. Therefore the S_2 layer is believed to have major influence on cell properties which, in turn, affects the wood properties. More accurately, the helical orientation of microfibrils in the S_2 is responsible for the variation of wood properties. The orientation is described by the angle between the longitudinal axis of the tracheid and the microfibril winding around the tracheid, referred as the microfibril angle (MFA). The MFA is an important factor for wood properties and will be discussed in more detail in 1.3.2.

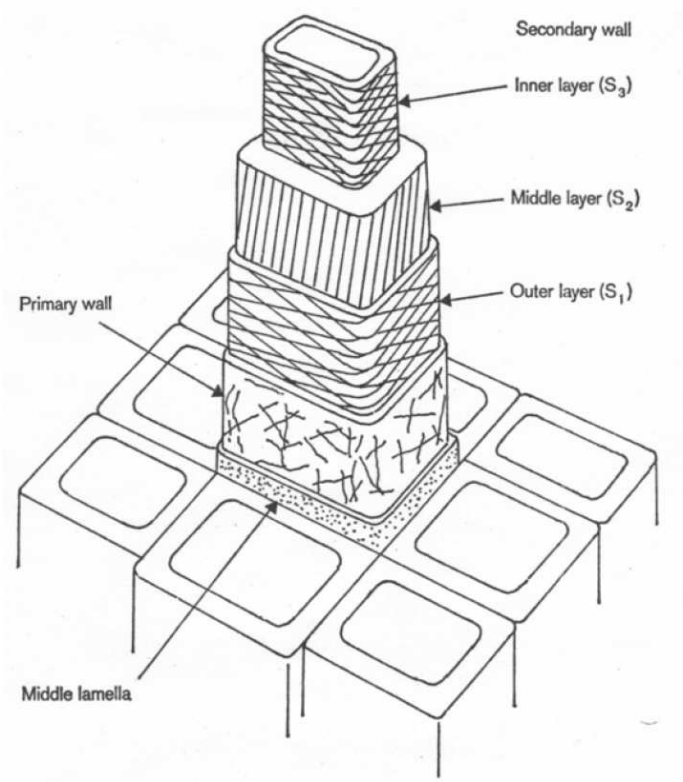

Figure 1-2: Simplified structure of the cell wall showing orientation of the micro fibril angle in each major wall layers (Dinwoodie, 1975).

The Variation of Tracheid Properties within a Stem

There are two anatomical features which differentiate earlywood from latewood, namely the radial diameter and the cell wall thickness of the tracheids. The earlywood cells have a larger diameter and thinner cell wall, and their cell cross section is rectangular. On the other hand, the latewood cells have smaller diameter and thicker cell wall, and their cross section is more towards circular. However, within the first couple of growth rings this feature is not apparently visible, but becomes clearly defined for rings further located from the pith as shown in Figure 1-3. Shepherd (1964) investigated the growth of radiata pine and suggested that diameter of the tracheids is dependant on the sap flow turgor pressure which peaks over the summer period when the earlywood is formed.

Tracheid lengths have been investigated by Sanio (1872). The tracheid length increases with the growth ring from pith and the rate of increase is fairly rapid within the first 15 to 20 rings, and the increase rate slows down in the outer rings (Sanio's law). This pattern has proved to be valid for both softwoods and hardwoods.

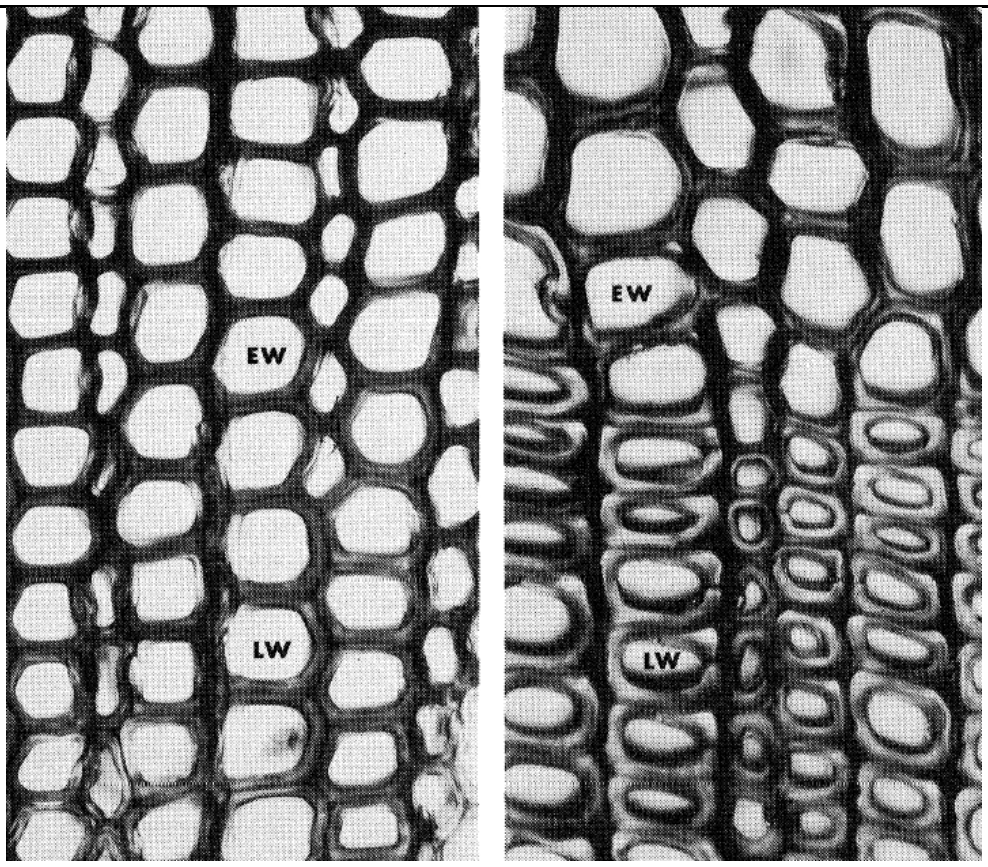

Figure 1-3: Transverse(x 400) sections early- and latewood from 1-2 and 10-11 ring (Bamber *et al.*, 1983).

Earlywood tracheids in conifers are, in general, shorter than the latewood tracheids and inhabit a larger number of bordered pits (Nicholls and Dadswell, 1965). Nicholls and Dadswell (1962) also investigated the tracheid length within a stem for Australian grown radiata pine trees. Investigations on tracheid length for New Zealand grown radiata pine trees have been undertaken by Cown (1975), Cown and McConchie (1983). New Zealand and Australian radiata pines possess the same tracheid pattern and further similar tracheid lengths.

Within a tree, not only do the cell dimensions change, also the chemical composition varies. Uprichard (1971) found that the cellulose content in radiata pine increases from the pith to the 10 to 15 growth rings and outwards from there stays fairly constant. The lignin content is greater for wood closer to the pith than for wood located further away.

It is noticed, that although the cells have variations in dimension and chemical composition, the cell wall density stays remarkably constant around 1500 kg/m^3 for most of the commercial wood species including radiata pine (Stamm, 1964).

1.3.2 The microfibril angle

The homogenous helical winding of micro fibrils in the secondary wall (mainly S_2 layer) is referred as microfibril angle (MFA). A summary of measurement techniques can be found in Barnett and Bonham (2004). The MFA of S_2 layer is widely believed to be one of the key factors influencing stiffness and shrinkage of the cell. Barber and Meylan (1964) introduced a theoretical model explaining the anisotropic shrinkage of wood due the MFA. Harris and Meylan (1965) further investigated the influence of the MFA on longitudinal and tangential shrinkage in radiata pine and found an acceptable agreement between the theoretical model predictions and measured data. The original model was further modified by Pang (2002) to account for the anisotropic shrinkage in tangential and radial direction.

Wood can be treated as a composite structure and therefore the individual fibre properties differ from the continuum properties. This has to be kept in mind when MFA alone is used as predictor of shrinkage as pointed out by Megraw *et al.* (1998). The MFA also varies between the tangential and radial side of the tracheid. Saren (2004) found that the mean MFA for Norway spruce was on average 3.5° higher in radial than in tangential direction in the S_2 wall for the same cell. These findings were consistent with separate studies of Tang (1973), Khalili *et al.* (2001) and Xu *et al.* (2004).

The Variation of MFA within a Stem

Megraw *et al.* (1998) investigated the MFA influence on longitudinal shrinkage (gross sample) in Loblolly pine. They found a wide range of MFA between individual fibres within a sample (20° average range). The highest MFAs were found in the inner rings near the base of the tree with a decreasing trend from pith to bark. Further, the angle also decreases with height within the annual growth ring layer.

Donaldson (1992) investigated the microfibril angle distribution in radiata pine at different heights and ring positions for five trees and found MFAs in a range from 9° to 55°. Donaldson also detected the same pattern of decreasing MFA in radiata pine across the cross section and heights. Furthermore significant variances in the MFA were observed between trees.

This led to further investigation which was focused on the variation in MFA among three genetic groups of radiata pine (Donaldson, 1993). For one genetic group (NZ850-55 progeny) the MFA

decline above breast height could not be found. The strong correlation between tracheid length and MFA was confirmed. This relationship was first mentioned by Preston (1948) and confirmed by Echols (1955).

However, it is noticed that the relationship between tracheid length and MFA is not widely accepted. Preston (1974) pointed out that it is necessary to correct for different girths of the cells and that the relationship is of statistical nature and it is incorrect to say *'any shorter tracheid shows a flatter S_2 helix than any longer tracheid'*.

1.3.3 Reaction wood (compression wood)

The term reaction wood is used to describe wood cut from trees that deviate from the normal growth pattern (vertical stems). Reaction wood in conifers is formed on the lower side of a leaning stem or branch and therefore called compression wood. The compression wood behaves differently to normal wood, and some of its properties are not desirable for structural applications. Therefore for wood processing, the compression wood is classed as defect wood.

Kininmonth and Whitehouse (1991) summarised radiate pine compression wood characteristics as follows:

- More circular tracheids in cross section, so intercellular spaces are formed;
- Typical distinct darker brown of reddish colour from normal wood;
- Less cellulose, and higher contents of lignin and galactan;
- Higher wood density;
- Higher longitudinal shrinkage but less shrinkage in transverse directions;
- Larger MFA in the S_2 layer;
- S_3 layer is absent.

Burdon (1975) examined 12-year-old radiata pine trees growing on four different sites in New Zealand and estimated that 30% to 45% of the stems contained mild to severe compression wood. Due to its frequent occurrence in radiata pine compression wood has significant impacts on distortion of timber because of its abnormal shrinkage properties. More information on the compression wood can be found in Timell (1986), who collected over 8000 references in this field. Compression wood in particular for radiata pine was investigated by Harris (1977).

1.3.4 Spiral grain

Spiral grain refers to the alignment of fibres at an angle to its stem axis. It is believed that the spiral grain has a major influence on the distortional behaviour of the timber. McBride (1967) pointed out that a certain percentage of trees (7% Douglas fir, 2% hemlock) were degraded due to visible spiral grain, resulting in a loss for the timber industry. Kubler (1991) stated that up to 1958 it was suspected that the causes for the spiral grains are wind, rotation of the earth, tree injuries during growth, electric and magnetic fields, leverage of branches, directional aspects, exposure, the sun and even the moon. The origin of the spiral grain is found in the cambium and expanded during the cell divisions (Harris, 1989; Zagorska-Marek and Little, 1986). The three stages of the cell divisions believed to influence the spiral grain are the frequency of pseudo transverse divisions of vertical oriented cambial cells, the intrusive growth and imperfect periclinal divisions. Recently it is also believed that the spiral grain is controlled by genes (Harris, 1989) and affected by environmental factors such as soil conditions (Danborg, 1994b) and wind (Eklund and Sall, 2000; Skatter and Kucera, 1998).

Kubler (1991) emphasised that the spiral grain plays an important role in water supply and uniform distribution of water and food throughout the tree. Leelavanichkul and Cherkaev (2004) looked at the spiral grain from a mechanical perspective and found that excessive grain angles for Ponderosa pine, which possess extra ordinary high spiral grain angles up to 40°, actually reduces the stiffness and further weakens the strength of the tree.

In radiata pine, the spiral grain is inclined to the left of the tree axis as seen from the outside of the tree and is therefore referred to as left-hand spiral grain. Bamber *et al.* (1983) stated that '*there is no evidence to support the contention that trees of the same species grown in the northern and southern hemisphere have spiral grain of opposite sign'*.

The typical radial distribution of spiral grain in radiata pine described by Harris (in Kininmonth and Whitehouse, 1991): Adjacent to the pith, radiata pine tracheids are closely aligned with the stem axis. With increasing distance from the pith, a left handed spiral grain angle is always observed, reaching its maximum value around the second to fifth year ring from the pith, followed by a descending spiral grain angle, which approaches zero or evolves into a right hand spiral grain angle.

Cown *et al.* (1991) investigated the within and between variation of the spiral grain in radiata pine and confirmed the above findings in principle. Their research included fifty 26-year-old trees from Kangaroa Forest (Central North Island, Bay of Plenty Region). The analysis of the height dependency was inconclusive, and also large differences between individual trees were observed. Figure 1-4 shows the measured spiral grain angles (SGAs) in the radial direction and for different heights. Tree number 37 had more uniform SGA with variation of less than 5° over the cross section and between different heights, whereas for Tree 49, large SGAs were observed with steeper gradients in radial direction and significant variation along its height.

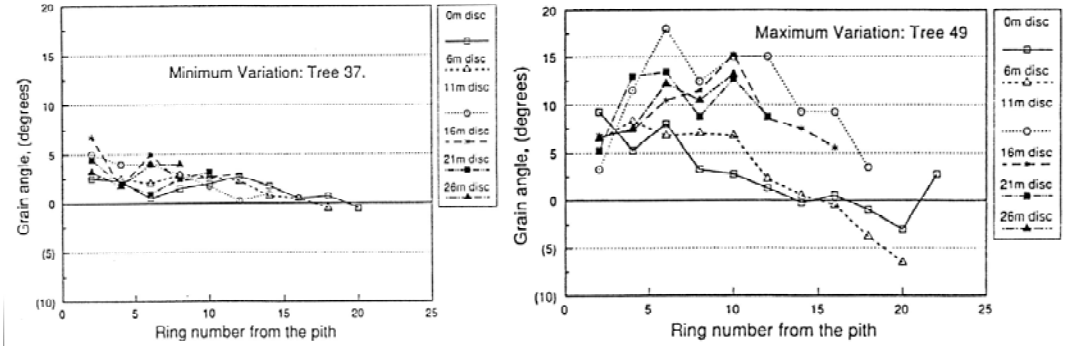

Figure 1-4: Spiral grain variation within trees (Cown *et al.*, 1991).

1.4 Basic Wood Properties

In this section, wood properties that influence the timber distortion are summarised and briefly discussed, and these properties include:

- Basic wood density;
- Fibre saturation point;
- Equilibrium moisture content;
- Shrinkage.

These properties were also part of the investigation with focus on early- and latewood variations within radiata pine (Chapter 2). Therefore in the following only their definitions and their commonly known values are introduced.

In the living tree of radiata pine, heartwood is biologically dead and its moisture content ranges from 30 to 50% in green, whereas the sapwood is active thus the lumens are fully filled with water. The moisture content (MC) is defined as the mass of water in wood divided by the oven dry mass of the wood. The oven dry weight is usually obtained by oven-drying the sample at 102°C to 105°C until no further weight loss is detected.

1.4.1 Basic wood density

Wood density is widely used to classify timber due to its close correlations with strength properties and process abilities (machinability and glueability). The basic density (ρ_{Basic}) is defined as the oven-dry mass (m_{od}) per green volume (V_{green}), as shown in equation 1-1.

$$\rho_{Basic}[\frac{kg}{m^3}] = \frac{m_{od}}{V_{green}} \tag{1-1}$$

For radiata pine, in New Zealand the mean basic density decreases from North to South and also with increasing altitude. Latitude and altitude influence the maritime New Zealand climate. Cown and McConchie (1983) used this relationship to divide the country into three density zones: the high density zone (>475 kg/m^3), the medium density zone (450 – 475 kg/m^3) and the low density zones (<450 kg/m^3).

The wood density also varies significantly within the growth for radiata pine, with the earlywood having much lower density than the latewood. Over the cross section of the log, close to the pith, the earlywood proportion is much higher than the latewood one, thus the average wood density is much lower than for the outer wood where the earlywood proportion is less than the core part of the log. Harris and Cown, in Kininmonth and Whitehouse, (1991), found that the wood adjacent to thepith had a typical density of 320 kg/m^3 and increased to 475 kg/m^3 beyond the 30th growth ring.

1.4.2 Fibre saturation point

The term '*fibre saturation point*' (FSP) was originally applied to wood by Tiemann (1906), cited by Skaar (1988). In Tiemann's studies on the strength properties of wood, he noted that below a certain moisture content, mechanical properties start to increase with decreasing moisture content. Above this point, the mechanical properties seem to be independent of moisture content. Tiemann interpreted this observation as that, at FSP, the cell lumens are free of liquid and the cell wall is fully saturated with bound water. Only the cell wall is responsible for strength properties of wood, thus the loss or gain of bound water affects the mechanical properties of the wood. Liquid stored in the lumens does not affect the mechanical properties, and therefore above FSP no changes are recognisable.

Not only are the mechanical properties affected below the FSP, but also other properties of wood are influenced by the moisture content, such as the shrinkage and the electrical resistance. Skaar (1988) summarised several methods to determine the FSP.

One method, first used by Kelsey (1956), was to determine the FSP from the linear relationship between the transverse shrinkage and moisture content. The derived point is commonly known as the shrinkage intersection point, and can differ from the true FSP. In this study the tangential shrinkage intersection point was determined for earlywood and latewood of radiata pine and is referred as FSP. Harris (1961) measured the shrinkage intersection point for heart and sap wood of radiata pine and found identical values of 30%MC for both types. The fibre saturation point was investigated in this study for radiata pine plantation trees, and the results are included in Chapter 2.

1.4.3 Green- and equilibrium-moisture content

The living tree contains high amounts of moisture, which occurs mainly in three different states, sorbed water in the cell walls (bound water), liquid water in the cell cavities (free water) and water vapour also in the cell cavities. Wood as a natural material has moisture sorption properties, similar to most biologically produced materials.

The water transport within living trees is maintained by the negative pressure resulting from the transpiration of water vapour in the leaves or needles. This theory was initially proposed by Dixon (1914), according to Zimmermann (1983), and known commonly as the 'cohesion theory of sap ascent'.
The moisture content is defined as the percentage of the mass of moisture (m_{wet}) within the sample per moisture free mass (m_{od}) of the sample (Equation 1-2).

$$MC[\%] = \frac{m_{wet} - m_{od}}{m_{od}} \cdot 100 \qquad (1\text{-}2)$$

Green moisture content

The moisture content at the time of felling is referred to as 'Green Moisture Content' and varies considerably amongst trees and also within individual trees. Seasonal variations are also possible (Skaar, 1988). In radiata pine, the moisture content in heart wood is generally lower than for sap wood (Pang and Herritsch, 2005). The green moisture content was also determined in the investigation on moisture diffusion. Highest green moisture contents occurred in trees felled in spring, whereas trees cut in winter showed significant lower green moisture content for heart wood

(below 40%MC). In general, the green moisture content for sap wood was above 100%MC, with highest values around 180%MC.

Equilibrium moisture content

When the tree is felled, the wood is exposed to the atmosphere and loses moisture until it reaches its equilibrium with the ambient atmosphere. This moisture content is referred as the equilibrium moisture content (EMC). The EMC varies between heart and sapwood, cell wall constituents and extractives (Skaar, 1988). It is also dependent on temperature, previous exposure history and mechanical stress.

Several theoretical models exist for the interpretation of moisture sorption of wood, which are based on thermodynamic considerations, either entirely based on theories, of empirical or semi empirical nature. These models have been discussed by several authors (Kininmonth and Whitehouse, 1991; Siau, 1995; Skaar, 1988; Stamm, 1964).

The EMC is of high importance for timber in use, due to its dependency on ambient atmosphere, which can cause shrinkage or swelling of timber structures or flooring. Therefore tradesmen have to apply and follow certain guidelines to account for the wood and ambient atmosphere interaction. For example, timber used for interior design should be processed at the excepted EMC to minimize dimensional changes. Wooden flooring should be laid without constraining it to the under floor and leaving gaps between the wooden floor and side walls to allow unconstrained movement of the wooden flooring.

1.4.4 Shrinkage and swelling

Shrinkage and swelling refers to the dimensional changes below the fibre saturation point. The dimensional changes are traditionally expressed as a percentage of the fully swollen dimension.
Radiata pine has similar shrinkage patterns to most other species. Tangential shrinkage is about twice as great as radial shrinkage and longitudinal shrinkage is a factor of ten smaller than in tangential directions. The same behaviour is found for the uptake of moisture (swelling). Commonly the shrinkage and swelling is given for 12%MC and oven dry.

Cown and McConchie (1980) investigated the shrinkage behaviour of old radiata pine crop at different heights at five or ten year intervals from pith to bark. The shrinkage values followed similar trends as determined in this study for early- and latewood. The general trend for radiata

pine is a decreasing longitudinal shrinkage from pith to bark, but also highly variable. Tangential and radial shrinkage increases from pith to bark. In all directions the values seem to decrease with increasing height, similar to the basic density.

Shrinkage and swelling of early- and latewood for radiata pine plantation trees were investigated in this study, and the results can be found in Chapter 2.

1.5 Variation of Wood Properties within an Annual Growth Layer

The previous sections discussed the basic wood properties and structure in general, and the high variability between trees and within a tree was mentioned. In forest research, it is common practice to illustrate basic wood properties in relation to the year ring from the pith to bark. When investigating the distortion of timber, it is necessary to have knowledge of the annual variation, within the same annual year ring at different heights. By applying the general pith to bark variation, this annual ring height dependency becomes blurred and difficult to extract. Further certain events will vanish when average values are obtained from more than one tree.

Figure 1-5 illustrates these effects. The author has chosen the ring width as an example. The ring width was obtained from the WQI benchmarking study and included ten trees from one stand. The diagram on the left in Figure 1-5 represents the average ring width distribution from the pith to the bark, whereas the right diagram includes the average values calculated from the bark to the pith, also for ten trees. The major differences are annual fluctuations, which are clearly visible even for average values of ten trees. Approximately 17 years before the trees were felled, something caused a significant reduction in the yearly ring width growth rate. Mishiro *et al.* (1986) indicated that the sudden ring width decrease is caused by thinning. This might also be the cause in this study. Further the actual annual growth rate is directly visible in the right diagram of Figure 1-5.

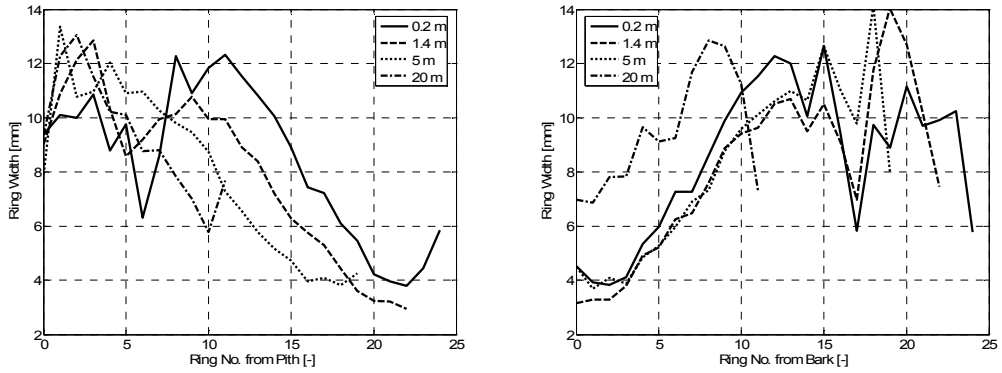

Figure 1-5: Comparison ring width distribution pith to bark (left) and bark to pith (right).

In this section, the results for one stand from the WQI benchmarking study are presented, by applying the numbering system from the bark, and briefly discussed. This study included the continuous measurement of density, microfibril angle and ring width.

Further from the same sample discs as used for the previously mentioned properties, the spiral grain angles have been measured at certain year rings for different tree heights.

1.5.1 WQI benchmarking study

In 2004 the Wood Quality Initiative (WQI) launched a New Zealand wide benchmarking study on radiata pine plantation trees. The intention of this survey was to create a comprehensive database on radiata pine characteristics for seventeen different stands in New Zealand. Approximately ten trees form each stand were recovered. Several wood properties have been measured up the tree.
One objective of this survey was the continuous measurement of the density and microfibril angle from pith to bark for four different heights (0.2 m, 1.4, 5 m and 20 m). These measurements were performed by the Commonwealth Scientific and Industrial Research Organisation (CSIRO, Melbourne). The test is commonly known as SilviScan, which measures density via X-ray densitometry and the microfibril angle is measured by X-ray diffraction. Additionally, the radial and tangential fibre dimensions have been derived by automated image analysis. Further, the modulus of elasticity was derived from the found relationship between density and MFA.
In the following, the SilviScan results for one stand (Golden Downs) are presented. The spiral grain distribution was also measured for the ten trees at 5-ring intervals from the pith at different heights.

The results presented in the following cover:

- Ring width distribution
- Annual growth area
- Density
- Microfibril angle
- Spiral grain angle
- Diameter distribution inside bark
- Conical angle at different heights
- Total number of year rings at different heights

Ring width distribution

Figure 1-6 contains the ring width at 0.2 m, 1.4 m, 5 m and 20 m for ten trees in respect to the ring number from the bark. Furthermore, the average values for the individual ring number from the bark have been derived, and their distribution for different heights is indicated with lines.

Large variations in the individual width are clearly visible with maximum value of approximately 20 mm and minimum value of approximately 1.3 mm. The average ring width values for the heights 0.2 m, 1.4 m and 5 m show similar patterns of a rapid increase in width close to the pith. Then a relatively constant ring width zone is observed from the 20th to 10th ring number from the bark.

This region also includes a sudden decrease of the ring width at ring number 17 from the bark which might have been caused by pruning or weather conditions. From zero to the tenth ring number a uniform decrease is observed for the heights 0.2 m, 1.4 m and 5 m. The ring width at 20 m height decreases at approximately the same rate as for other heights but owning higher individual ring widths within the same growth year. Also the rapid increase of the width form the pith is clearly visible.

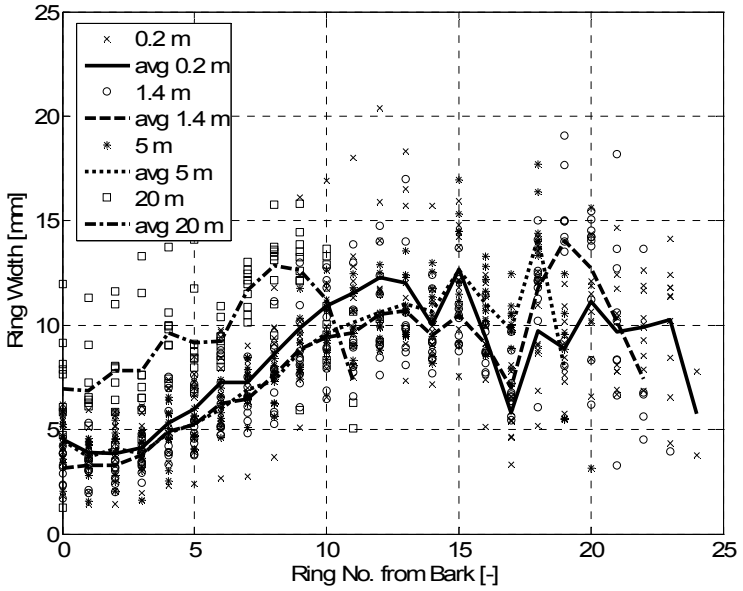

Figure 1-6: Ring width distribution from WQI benchmarking study.

The ring width distribution indicates higher growth rates at higher heights. To validate this fact, the annual growth area is introduced. The annual growth area is calculated from the ring width and the distance from the pith.

Annual growth area

Figure 1-7 contains the calculated annual growth area at 0.2 m, 1.4 m, 5 m and 20 m for ten trees in respect to the ring number from the bark. Furthermore, the average values for the individual ring number from the bark have been derived, and their distribution for different heights is indicated with lines. The area peaks at the tenth ring from the bark, whereas the highest area growth is detected at 0.2 meters and then decreasing with height. At the time of felling the growth rate at all heights approaches similar values (between 4000 and 6000 mm^2). When assuming an average age of 25 years for the trees the beginning of the decline is corresponding to a tree age of 15 years.

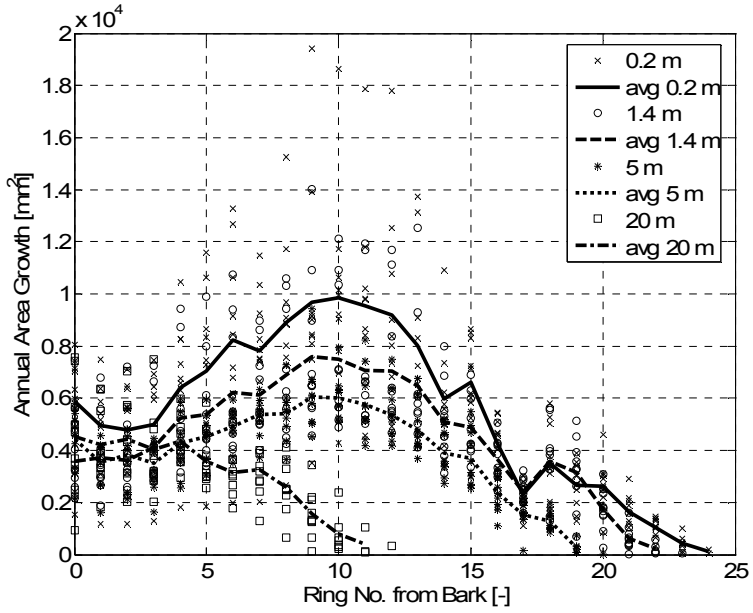

Figure 1-7: Annual growth rate derived from the distance from the pith and its corresponding ring width.

Density

Similar behaviour as for the ring width distribution is observed for the average density (Figure 1-8). The density increases close to the pith followed by a relative long constant density zone (around 475 kg/m^3) between the 20^{th} to 10^{th} ring numbers from the bark, afterwards slowly increasing to the bark. Further a lower density at 20 meters is also clearly visible.

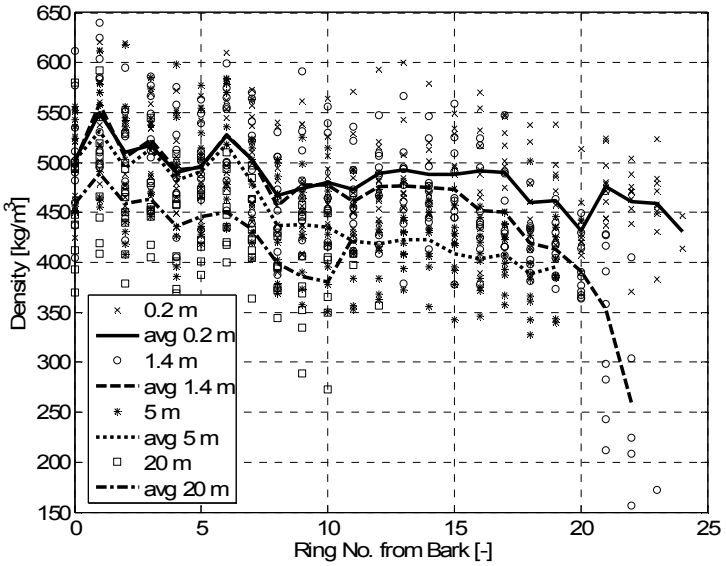

Figure 1-8: Density distribution from WQI benchmarking study.

Micro fibril angle

The average microfibril angles and their individual values are shown in Figure 1-9. As previously mentioned highest MFA, are found close to ground near the pith of a tree. The same behaviour is valid for the average of ten trees. Also clearly visible is the constant value zone between the 17th to 10th ring numbers but with different values at 0.2 m, 1.4 m and 5 m. The measured MFA at 20 m shows a similar decrease, with the same values as at the base of the tree. The lowest values of MFA are found consistently for 1.4 m and 5 m.

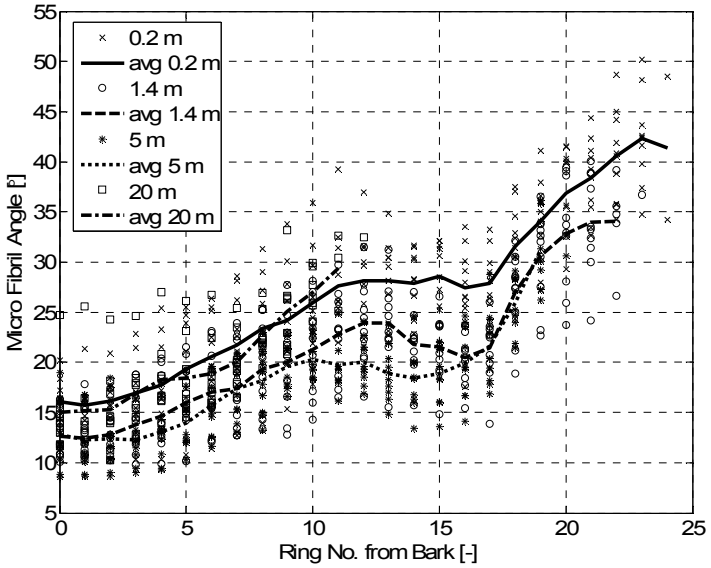

Figure 1-9: Microfibril angle distribution from WQI benchmarking study.

Modulus of elasticity

The MOE (Modulus of elasticity) distribution and their average values for different heights are presented in Figure 1-10. The MOE is derived from the relationship between density and microfibril angle. As for all the other properties measured, the constant value zone is clearly visible. The lowest values of MOE are found closest to the pith. Below the tenth ring number from the bark, all values constantly rise to the bark with the highest values for 1.4 and 5 m and lower values at the base and at 20 m.

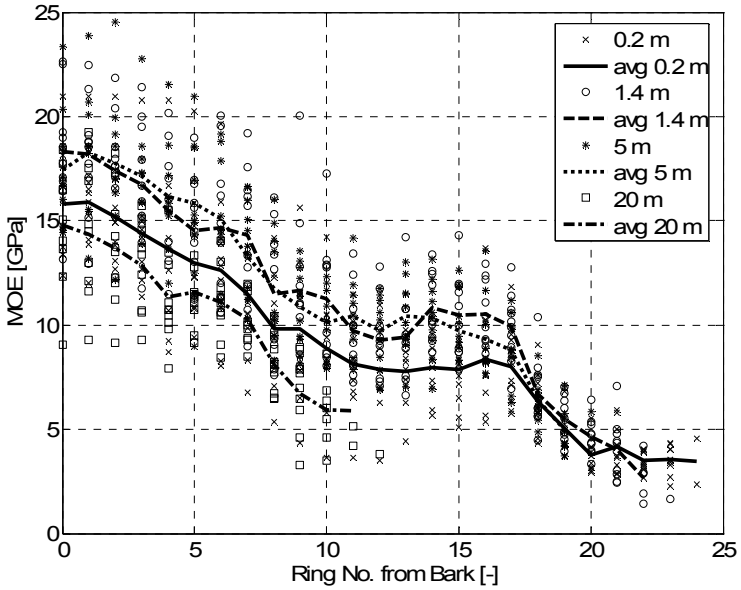

Figure 1-10: Modulus of elasticity distribution from WQI benchmarking study.

Spiral grain and conical angle

The comparison of the average spiral grain angle (SGA) is not as conclusive as for the previously mentioned results due to the localized 5-ring measurement. The spiral grain from each 5th ring was measured twice in one disc. The results, presented in Figure 1-11, are derived from the average of the two measurements and then the numbering system from the bark to the pith was applied. This caused a drift of the data points and therefore the average values at different heights have only been derived when more than two corresponding data points were available. Negative values in Figure 1-11 correspond to a left hand spiral grain which is predominant close to the pith, with the highest values at twenty meters. Up to five meters a similar slope of grain is observed. Where at 0.2 and 1.4 meter the grain angle is changing from a left handed into a right handed one.

Figure 1-12 summarizes the appearance of the individual stems and contains information on the radius distribution at different heights, which were derived from the diameter inside the bark. Further the conical angles (CA) were calculated at different heights and the total number of year rings a disc contained at different heights. Thick lines always correspond to the derived average at certain heights. Clearly visible is the taper curve of the trees. The corresponding conical angles are highest close to the base of the trees and range between 1.1° and 2.3°. Further up the tree values consistently sit below 1°. The range of total number of year rings is widening with increasing with height.

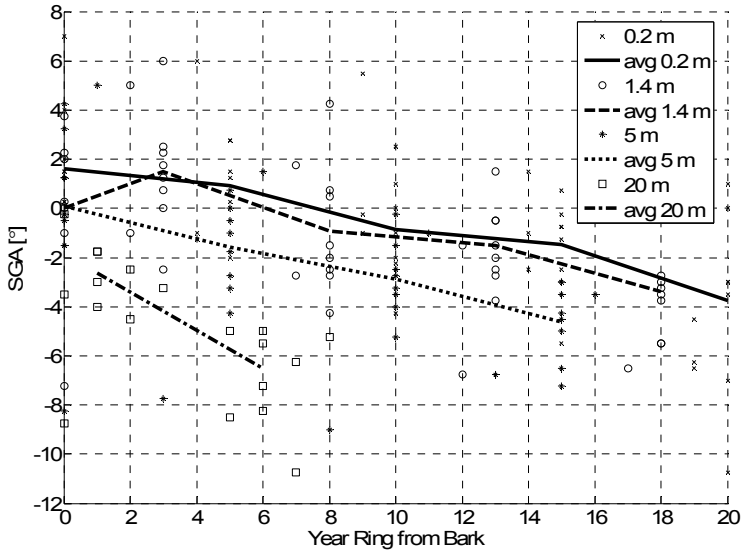

Figure 1-11: Spiral grain distribution from WQI benchmarking study.

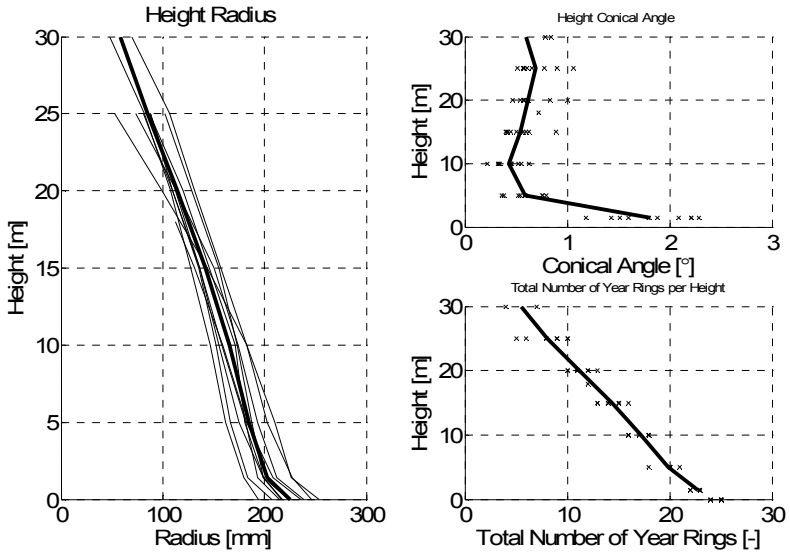

Figure 1-12: Radii, conical angle and total number of year rings for different heights.

Chapter 2

Experimental Investigation of Earlywood and Latewood Properties of Radiata Pine

Extensive studies on instability of wood have identified some wood basic properties which influence the wood distortion and shape changes when the wood is losing or gaining moisture. These properties include anisotropic shrinkage (longitudinal and tangential), fibre saturation point and equilibrium moisture content. The abnormal and variations of these properties will generate stresses within timber during drying, which result in distortion or movement in re-manufacturing. For quantifying the stresses and for predicting distortion of thin wood products, the property difference between earlywood and latewood is important. However, limited information is available in literature on such difference and, therefore, the objective of this chapter is to fill this gap.

This chapter includes the measurements of the shrinkage (tangential and longitudinal) and the equilibrium moisture content of the earlywood and the latewood. From the measured data of the tangential shrinkage, the shrinkage intersection point was determined as FSP at which the wood shrinkage starts to occur. In the experiment, the effects of compression, juvenile wood and wood location in a tree (height and radial distance from pith) were investigated.

The first part of this chapter describes the material selection, sample preparation, the determination of the green moisture content and the basic wood properties. Following this, the measurements and results of dimensional change in longitudinal and tangential direction at different levels of equilibrium moisture content are presented, firstly for desorption (loss of moisture) and then for adsorption (gain of moisture). Finally, the obtained results are analysed and discussed.

2.1 Material and Sample Preparation

In this study, 21 discs of 200 – 250 mm thick were received, which were cut from seven trees (22-years of age) of one single site of Kaingaroa 222 in Central North Island, New Zealand. The discs were cut at three different heights from each tree (breast height = 1.4 m, 10 m and 20 m from ground).

On the disc surfaces, the tree number and height were marked with an arrow indicating the north orientation of the tree. Immediately after cutting, the discs were placed in plastic bags but were neither treated for anti-sapstain nor refrigerated. After arriving at the University of Canterbury, the 21 discs were placed in a freezer at the School of Forestry for approximately three weeks until the preparation of the test specimens.

Before it was possible to cut the samples, the discs had to defrost. Therefore, in each time of the sample preparation, three discs were taken out of the freezer a day before the preparation and then were stored above a drain in a room, the temperature of which was approximately 20°C. After the disc was thawed, the sawing directions were marked and the growth rings were counted. The appearance of the disc was recorded, and a picture of the surface was taken as shown in Figure 2-1.

In the sample preparation, four 30mm strips were cut out for each disc through the pith along the directions of North-South and East-West, respectively. After this cutting, the strips were trimmed to 150 mm along the grain. Two of these 150 mm long strips were further cut to obtain 20 specimens of separated earlywood and latewood bands, 10 from each strip. Small specimens of 30 mm long were cut from each of the earlywood and latewood specimens for green moisture content and density measurements, and the remaining 120 mm specimens were used for the shrinkage/equilibrium moisture content measurements (Figures 2-2 and 2-3 Figure 2-2). The two remaining 150 mm long strips were returned to the freezer for further studies, if needed. The prepared earlywood and latewood specimens were then stored in a cool room (4°C) until all the samples were prepared.

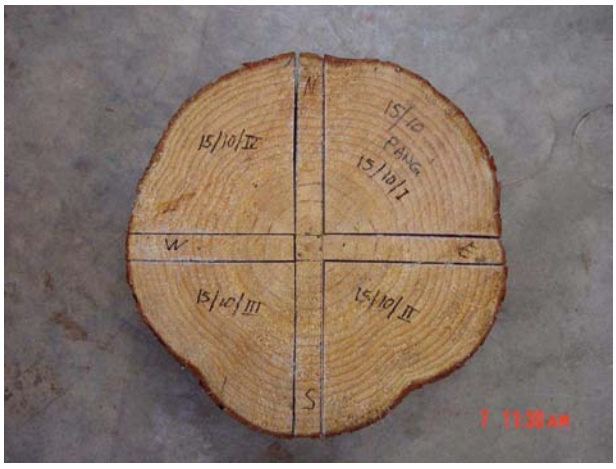

Figure 2-1: Appearance and marking of the disc, from which four strips were cut.

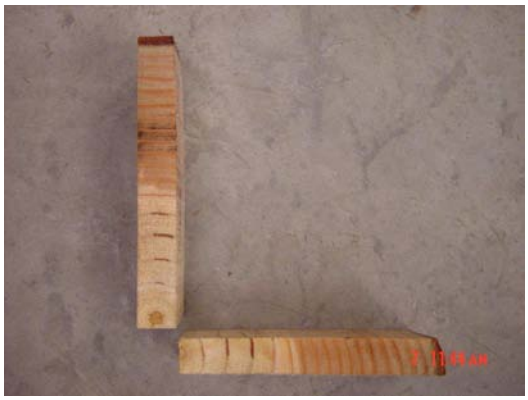

Figure 2-2: Two strips cut from the disc for preparation of the earlywood and latewood specimens.

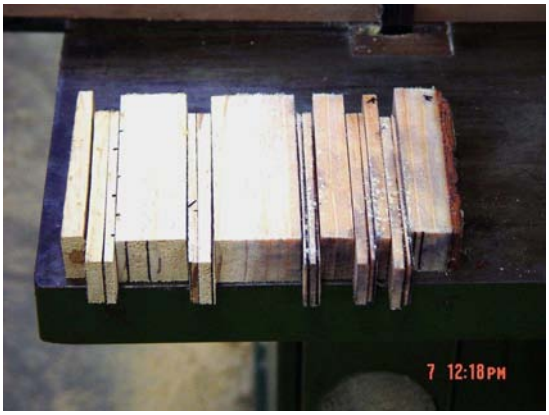

Figure 2-3: 10 earlywood and latewood specimens were cut out from one strip.

In order to compare the effects of tree age on the wood properties, two more discs were cut from two young trees of 10-15 years old which were selected from the Canterbury region. The specimens were prepared in the same manner as described above and were included in the shrinkage and equilibrium moisture content experiment.

2.2 Measurements

2.2.1 MC and density

For the measurement of the green MC and the wood density the following measuring systems were used:

- **Vernier Calliper:** The caliper was used to measure the dimensions of the specimens. The model was a Mitutoyo 500-116 SR-44X2 with a measurement range of 0.01 to 200 mm and accuracy of ±0.02 mm.

- **Balance:** A balance was used for determination of the specimen's weight and the model was a Sartorius BP3100S with a measurement range of 0 to 3100g and an accuracy of ±0.01g.
- **Oven:** An oven was used for obtaining the oven-dry weight of the specimens, which was controlled at 103°C for this experiment.

After all the specimens were prepared, the specimens for determination of green moisture content and wood basic density were taken out of the cool room to measure their weight and dimensions. Longitudinal, tangential and radial dimensions were measured using the vernier calliper to determine the green volume. Immediately after this, the samples were oven dried at 103°C for 48 hours until there was no further loss of weight. Finally, all the samples were re-weighed and their dimensions were re-measured.

MC uncertainties arising from the accuracy of the balance

The accuracy of the balance was ±0.01g, stated by the manufacture. The derived moisture content contained the propagation error arising from its calculation (Equations 2-1 and 2-2). The uncertainty was calculated under the assumption, that the uncertainties of the oven-dry weight and the weight at the EMC were independent and random (Taylor, 1997):

$$\delta MC = MC \cdot \sqrt{\left(\frac{\delta m}{m_{od}}\right)^2 + \left(\frac{\delta m}{m_{eq}}\right)^2} \tag{2-1}$$

In equation 2-1, δm represents the accuracy of the balance, m_{od} the oven-dry mass and m_{eq} the equilibrium mass of the sample. The uncertainty δMC is dependent on the sample's oven-dry mass and on the amount of moisture within the sample.

In this experiment the average oven-dry mass of all samples was found to be 6.4 g with a standard deviation of ±2.3 g. Table 2-1 contains the calculated uncertainties at different MC (5, 10, 15, 20 and 25%MC) for different oven-dry sample weights. For example a sample with an oven-dry weight of 4 grams, at 5 %MC, has an uncertainty of ±0.02%MC, whereas at 25 %MC the uncertainty is ±0.10%MC. The last row in Table 2-1 is only used to illustrate the error propagation for a sample with an oven-dry mass of 0.1 grams. In this experiment the lightest sample was about 2 grams.

Table 2-1: Moisture content uncertainties arising from the balance used

	Uncertainty of MC (δMC)				
m_{OD}	MC range				
[g]	5.00%	10.00%	15.00%	20.00%	25.00%
1	±0.09%	±0.17%	±0.25%	±0.33%	±0.41%
2	±0.04%	±0.08%	±0.12%	±0.16%	±0.20%
3	±0.03%	±0.06%	±0.08%	±0.11%	±0.14%
4	±0.02%	±0.04%	±0.06%	±0.08%	±0.10%
5	±0.02%	±0.03%	±0.05%	±0.07%	±0.08%
6	±0.01%	±0.03%	±0.04%	±0.05%	±0.07%
7	±0.01%	±0.02%	±0.04%	±0.05%	±0.06%
8	±0.01%	±0.02%	±0.03%	±0.04%	±0.05%
9	±0.01%	±0.02%	±0.03%	±0.04%	±0.05%
10	±0.01%	±0.02%	±0.02%	±0.03%	±0.04%
11	±0.01%	±0.02%	±0.02%	±0.03%	±0.04%
12	±0.01%	±0.01%	±0.02%	±0.03%	±0.03%
13	±0.01%	±0.01%	±0.02%	±0.03%	±0.03%
14	±0.01%	±0.01%	±0.02%	±0.02%	±0.03%
0.1	±0.85%	±1.68%	±2.49%	±3.28%	±4.06%

2.2.2 Shrinkage and EMC

For the measurement of the longitudinal shrinkage, a measuring system was designed and manufactured, on which a digital dial gage is mounted (Figure 2-4). The digital dial gage has a Mitutoyo Digimatic Indicator with measurement range of 0.001 to 25.4 mm and accuracy of ±0.003 mm. The vernier calliper was used to measure tangential dimension, and a well-controlled cabinet (Contherm) was used to provide required humidity (20-98%RH) and temperature environment.

The uncertainties in the determination of the tangential and longitudinal shrinkage, arising from the measurement devices, calculated for the tangential shrinkage, for 30 mm in dimension, was ±0.09 %, whereas in the longitudinal direction (120 mm in length), the uncertainty was ±0.004%, and both values were valid for the whole moisture content range.

During the experiment, the temperature and relative humidity inside the environment chamber were measured using a temperature and humidity data logger. The logger model was a HOBO H8 Pro RH/Temp with a measurement range of -30 °C to 50°C for temperature and 0 to 100% for RH. The corresponding accuracies are ± 0.2°C and ±3 %RH.

Figure 2-4: Longitudinal dial gage mounted on gage plate

After all the specimens were prepared, their weights and dimensions were measured. The tangential dimension was measured in two positions as indicated in the specimen of Figure 2-4 by the grey lines. Following this, the longitudinal dimensions were measured. After the measurements, all the specimens were sprayed with an anti-sapstain solution (Oxine Copper, Carbendazim). The treatment was intended to prevent the samples from fungi growing under the initial high humidity condition. Then all of the specimens were placed in the environment chamber where the conditions were initially controlled at 90%RH and 30°C ±0.5°C.

The specimen's weights were checked after 6 days and then every following day, to determine the time for the specimens to reach equilibrium. It was found that two weeks were long enough for the specimens to reach the equilibrium state. Therefore, it was decided to measure the specimens' dimensions after two weeks of equalisation with each new setting of RH, decreasing to 20%RH stepwise.

2.3 Experimental Results

2.3.1 Green MC and wood basic density

Prior to the preparation of the density and shrinkage samples, the diameters of North-South and East-West directions for each disc were measured, and the growth rings were counted. The average year rings were 22, 18 and 12 at breast height, 10 and 20 metres, respectively. Figure 2-5 shows the diameter distribution over the tree heights for each of the seven trees. Tree 12 had the largest diameter and tree 11 had the smallest diameter.

The green moisture content ranged from 30% to 180%. Due to the storing of the samples in the cool room until all samples had been prepared, low values (around 60%MC) were detected for some sapwood samples. It was understandable that the heartwood near the pith had a low green moisture content, but the low values in the sapwood zone were not expected. These deviations could be caused by the storing of the samples in the cool room for approximately two weeks. As the specimens' dimensions are small (2-5mm in thickness), the specimens could lose moisture more easily in handling. However, this moisture loss was unlikely to affect the shrinkage and equilibrium moisture content results, as the fibre saturation point (FSP) of radiata pine lays around 30%MC.

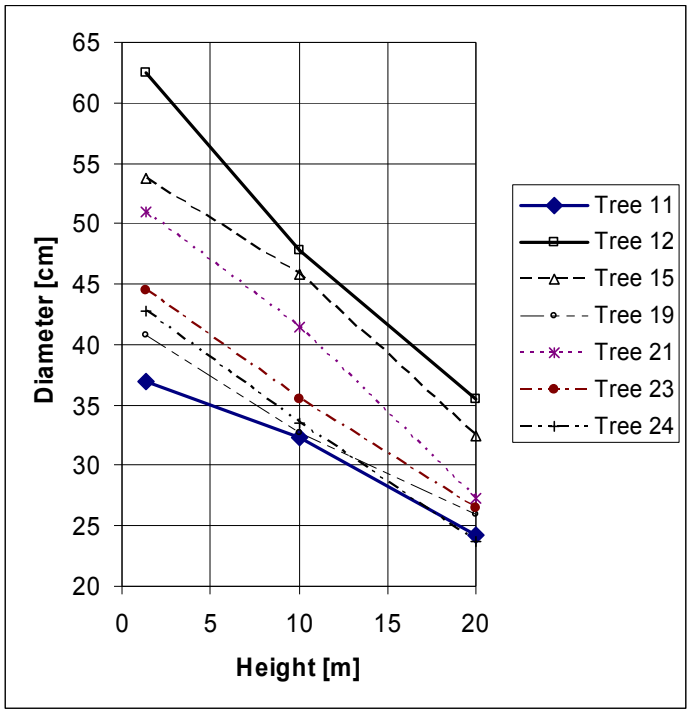

Figure 2-5: Diameter distribution along the tree height for each of the seven trees.

The mean density of our samples (332 kg/m^3) was significantly lower than the mean density reported in literature (Cown and McConchie, 1980, 1983; Kininmonth and Whitehouse, 1991). In this study, the mean density of the earlywood samples was measured to be 294 kg/m^3 and that of the latewood was around 370 kg/m^3. The significant lower latewood density, compared to the available literature data, is partly due to the fact that some latewood samples contained a small proportion of earlywood which decreased the density of the latewood samples. Another reason could be that the selected trees had lower than average density values, which can be confirmed from other studies.

In the experiment, it was not always possible to completely separate the earlywood from the latewood, such as for the small diameter trees (Trees No. 11, 15 and 24), and their deviations from the concentric ring pattern. Therefore these trees are excluded in the discussion of the earlywood and latewood differences. Nevertheless those trees are included in the discussion of the average properties. Figure 2-6 shows the average density for each tree at different heights, and the error bars indicate the maxima and minima measured for the particular trees. The average density does not always follow the same trend, although for most of the trees (4 out of 7) the density decreases with height.

When comparing the diameter with the density, it is found that trees of the same age with a smaller diameter have a higher average density than trees with a larger diameter. In this experiment, Tree 11 and Tree 19 had smaller diameters, whereas the trees 12, 15 and 21 had larger diameters.

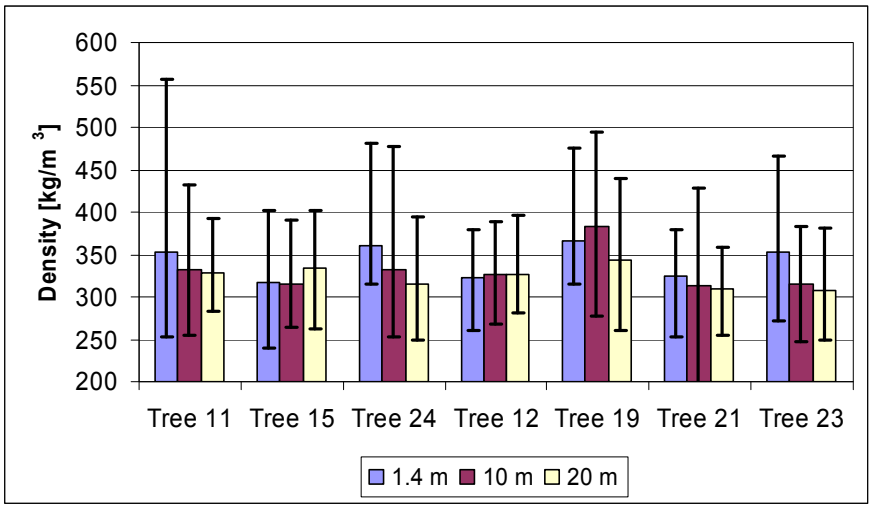

Figure 2-6: Average densities at different heights.

In order to determine the wood density of the earlywood and the latewood, discs from four trees were used, which were No. 12, 19, 21 and 23. The results are given in Table 2-2. Tree 19, with the smallest diameter, had the highest density values for average, earlywood and latewood. The difference in the earlywood density between trees is not as significant as for that of the latewood. The influence of the tree height on the average density and the early/latewood density is not consistent. The average density of the earlywood samples was 287 kg/m^3 and that of the latewood was around 378 kg/m^3. Earlywood and latewood for Trees 11, 15 and 24 were also separated, although the separation was not as complete as for Trees 12, 19, 21 and 23. The earlywood density for trees 11, 15 and 24 was slightly higher, and the latewood was slightly lower, than those of Trees 12, 19, 21, and 23.

Table 2-2: Average, earlywood and latewood densities for Trees 12, 19, 21 and 23.

Tree #	Height [m]	Average [kg/m^3]	E-Wood [kg/m^3]	L-Wood [kg/m^3]
12	1.4	321.7 ±47	279.5 ±21	364.0 ±13
	10	326.3 ±43	290.2 ±23	362.4 ±20
	20	326.9 ±44	289.2 ±14	364.7 ±29
19	1.4	365.7 ±74	305.9 ±34	425.4 ±48
	10	383.3 ±76	325.9 ±51	445.1 ±36
	20	344.2 ±61	291.4 ±28	400.0 ±39
21	1.4	323.9 ±44	286.7 ±22	361.2 ±22
	10	313.3 ±72	259.5 ±53	367.0 ±43
	20	308.5 ±42	280.0 ±29	337.0 ±32
23	1.4	353.8 ±75	302.3 ±42	405.3 ±63
	10	315.1 ±50	280.2 ±28	350.0 ±41
	20	306.7 ±49	262.3 ±13	351.1 ±21

Wood density also varies along the radial position from the pith to bark. The average distribution for the four trees and their maxima and minima are shown in Figure 2-7.

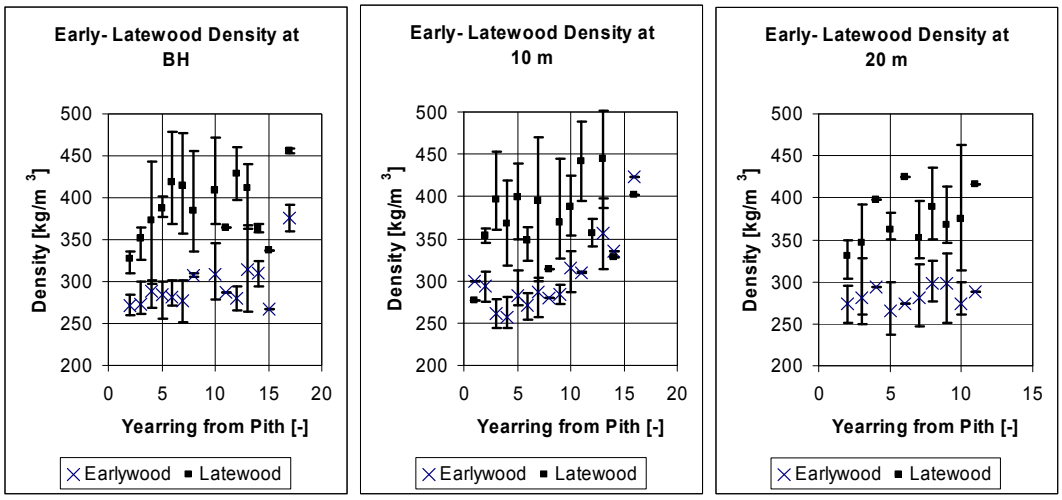

(a) (b) (c)

Figure 2-7: Radial density distribution at different heights [BH (a), 10 m (b) and 20 m (c)] for early- and late-wood.

2.3.2 Properties in desorption

After all the specimens were prepared, and their weights and dimensions measured, the specimens for shrinkage and EMC tests were placed in an environment chamber. The initial set points for relative humidity and temperature were 98%RH and 30°C, respectively. Prior to the experiment the chamber conditions were cross-checked with two identical data loggers and deviation was found between the set humidity and the actual condition within the chamber.

The chamber was not capable of reaching the 98%RH, instead a stable 90%RH was measured with the data loggers (Figure 2-8). The recorded temperature was around 30°C with a maximum deviation of ±0.5°C. Since it was found that two weeks were long enough to reach the equilibrium state, it was decided to measure the specimens' dimensions after 2 weeks of equalisation with each new setting of RH, decreasing from 90% to a setpoint of 30% RH stepwise. However, the final relative humidity was measured as 26%. After reaching the lowest possible RH (30 %) by the EMC cabinet, all the specimens were oven dried for two days at 103 °C.

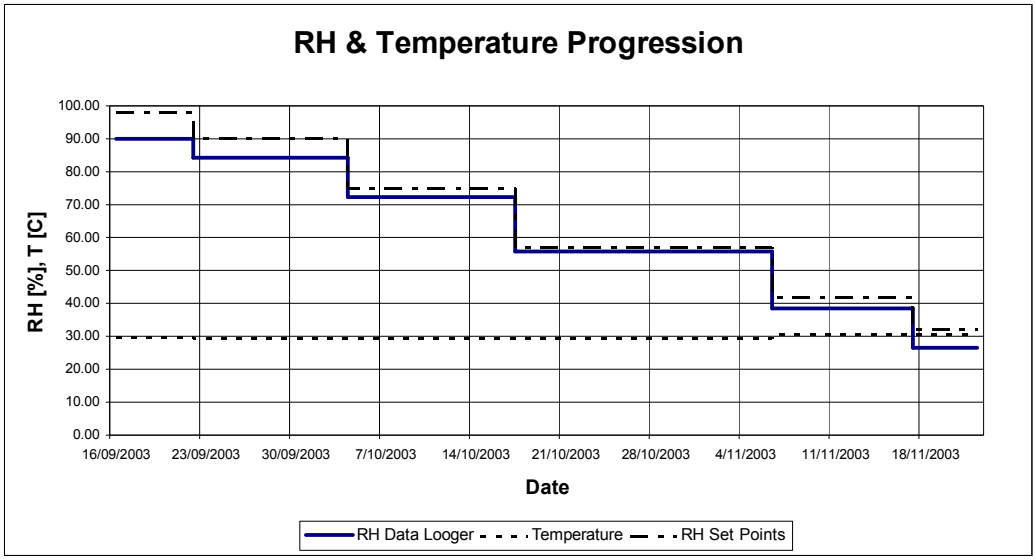

Figure 2-8: RH & temperature progression (EMC cabinet) for the measurements.

Equilibrium moisture content

As described above, once a specimen has reached a stable moisture content at a given relative humidity and temperature for sufficient time, the moisture content is described as the equilibrium moisture content (EMC). After reducing the RH in the environment chamber to approximately 26% RH (setting of 30%RH), the specimens were oven dried and specimens' dimensions and weights were measured. The oven dry weight was used to calculate the moisture content (MC) of the sample by the following equation:

$$MC = \frac{m_{eq} - m_{od}}{m_{od}} \tag{2-2}$$

Where m_{eq} is the weight at equilibrium state, and m_{od} is the oven dry weight of the sample. Table 2-3 contains the average EMC values for all of the samples at different relative humidities. In the table, the standard deviation is also included, and it is shown that, at higher RHs the variation is also higher than for lower RH conditions.

Table 2-3: EMC values for desorption.

RH	EMC
90%	**24.14** ±1.50%
84%	**21.27** ±0.90%
72%	**16.18** ±0.51%
56%	**12.31** ±0.46%
38%	**9.05** ±0.45%
27%	**7.41** ±0.41%

The measured equilibrium moisture contents from this study have been compared with existing data such as those of Bramhall and Wellwood (1976), in Kininmonth and Whitehouse (1991). It is found that the values from the Bramhall and Wellwood table are in close agreement with the average EMC values for adsorption which will be discussed in Section 1.5. However, for desorption, the data produced for North American species are approximately 2.5% to 5%MC lower than measured EMC values in this study.

In the following, the early-late wood equilibrium moisture contents are discussed. The results presented are based on the average values derived for the individual growth ring measured from the bark and are based on the experimental data from the tree 12, 19, 21 and 24. Figure 2-9 illustrates the EMC distribution for both of the earlywood and the latewood at different heights. The data are the average values over samples prepared from the same growth ring and the same tree height. The highest deviations were found at breast height at 90%RH. Not included in this Figure are the maximum and minimum values for the individual rings. At breast height the earlywood EMC (22.5-30%) is more variable than the latewood (22 – 29%EMC) at 90%RH. For the same relative humidity these variations decreased with increasing of the tree height.

It is interesting to note that the EMC of both the earlywood and the latewood tends to decrease towards the bark (sapwood) and this trend is most apparent at high relative humidities (90% – 72%). At the breast height, the growing band was very narrow near the bark thus it was difficult to separate the earlywood and the latewood near the bark. However, at the heights of 10m and 20m from the ground, the growth ring near the bark was sufficiently wide, and thus it was possible to prepare the earlywood and the latewood samples. In general the transition between the different heights is smooth and might suggest that the EMC is independent of height for the individual growth layer.

The decreasing equilibrium moisture content towards the bark was observed for all of the four trees. In order to confirm this trend, the data was rearranged to average the EMC data for each tree height, namely, at the breast height, 10m and 20m from the ground. These averaged values are shown in Figure 2-10 (a) – (c).

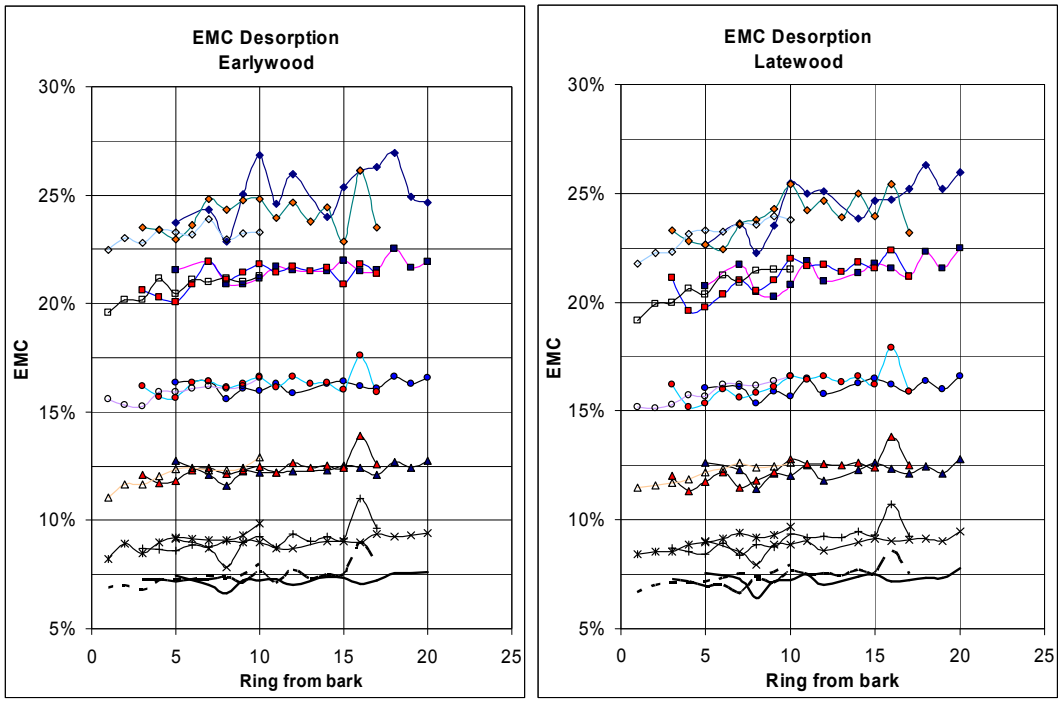

Figure 2-9 (a)	Figure 2-9 (b)

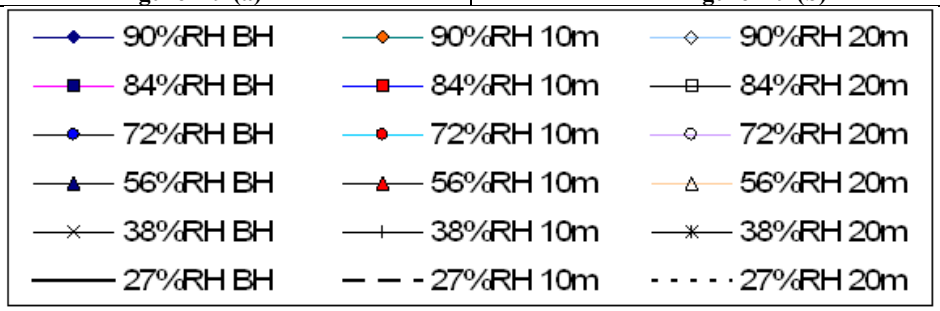

Figure 2-9: Early (a)- Late-wood (b) EMCs for desorption at different heights.

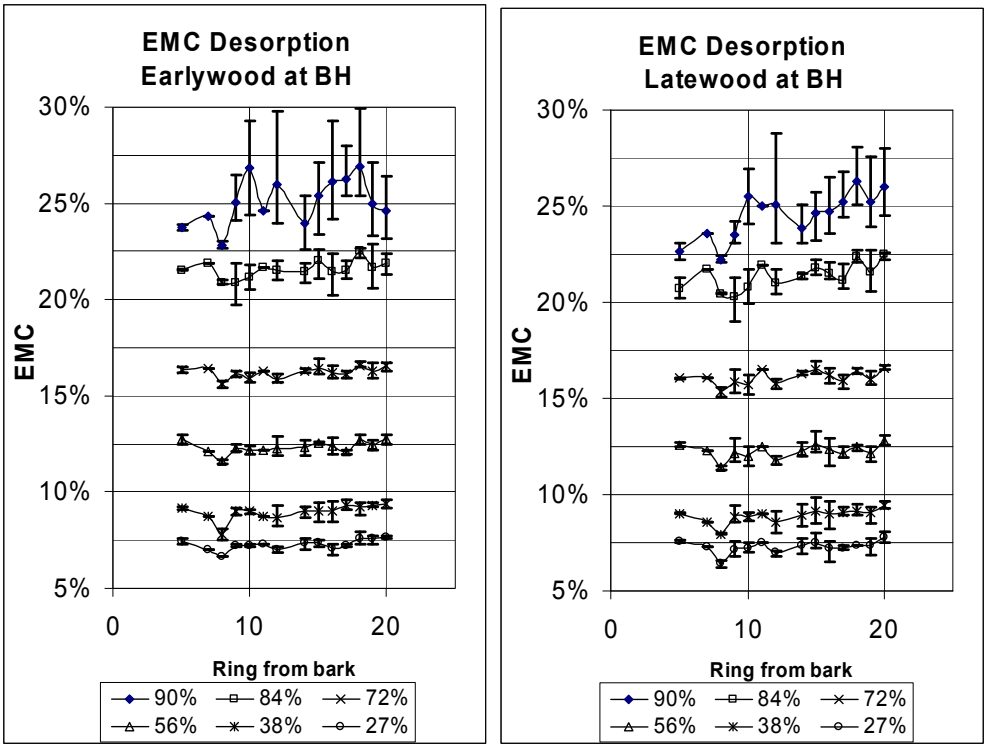

Figure 2-10 (a)

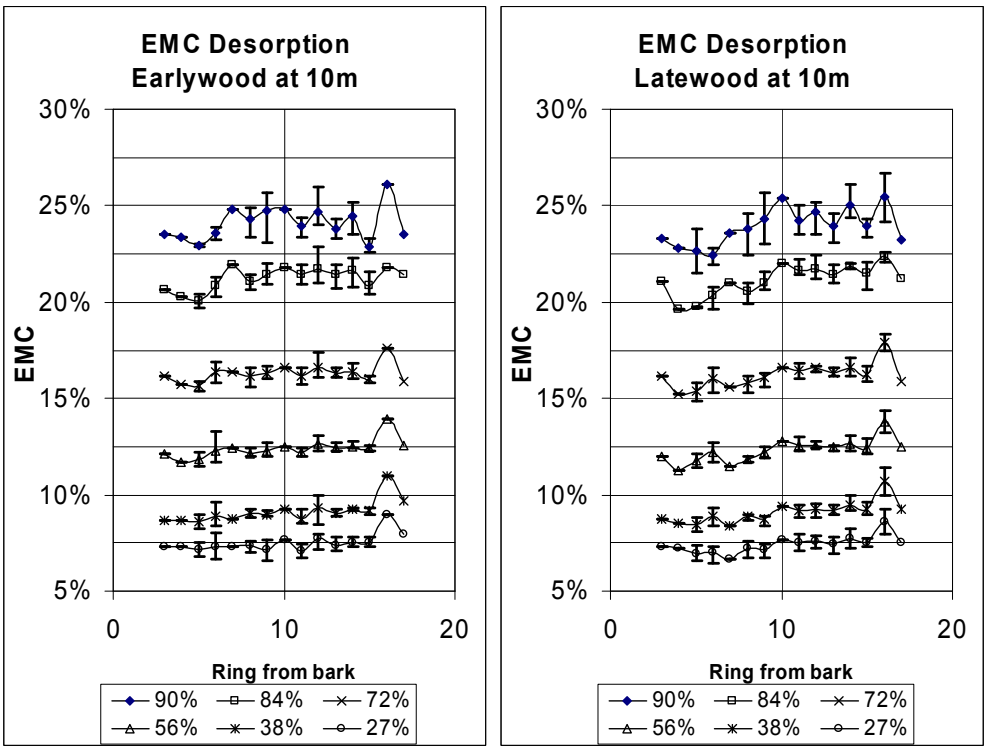

Figure 2-10 (b)

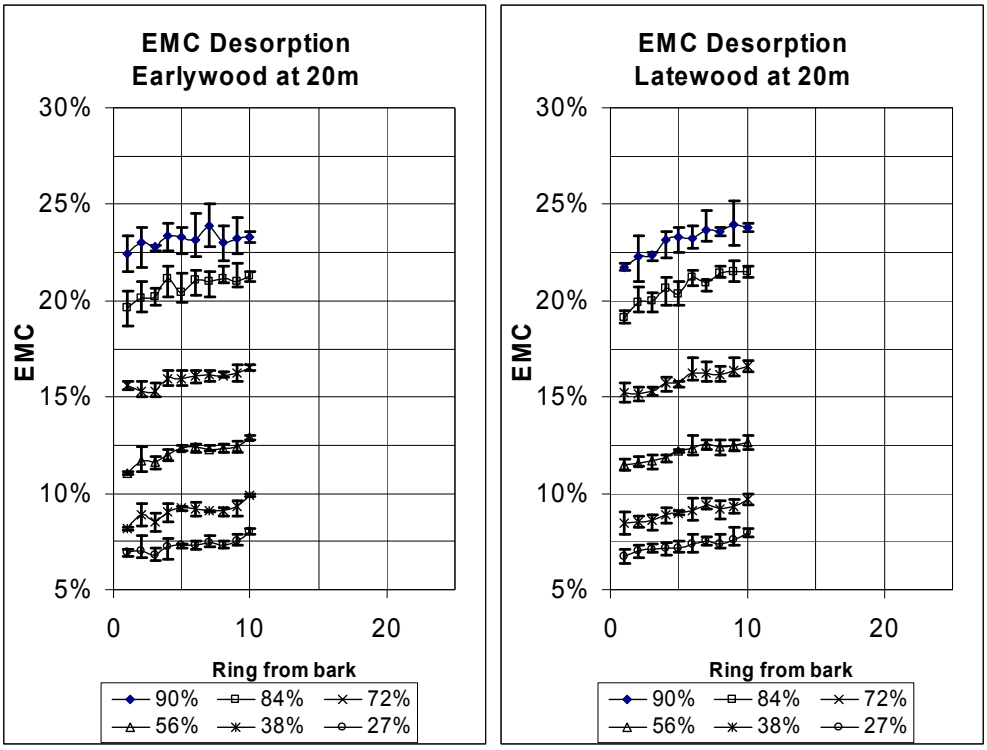

Figure 2-10 (c)

Figure 2-10 (a, b, c): Average EMC and error bars at BH (a), 10m (b) and 20m (c) for early- and late-wood.

Tangential shrinkage

The shrinkage (ε) at given moisture content (MC) below the fibre saturation point (FSP) can be determined from the following equation:

$$\varepsilon = \frac{L_0 - L_{eq}}{L_0} \times 100\% \tag{2-3}$$

Where L_{eq} is the sample dimension at a given MC, and L_0 is the sample dimension in the green state. Equation (2-3) can be applied to both tangential and longitudinal shrinkage measurements. In this section, the average tangential shrinkage results are firstly presented for all seven trees. Afterwards, results are given for the height dependence of the shrinkage. Finally, the radial distribution of the tangential shrinkage and the difference between earlywood and latewood will be presented.

Figure 2-11 shows a typical curve for the tangential shrinkage at different MC. From the figure, it is apparent that a straight line fits the data very closely (details on SH and MC relation accuracies can be found in the results for the fibre saturation point). This allows the tangential shrinkage to be calculated at certain moisture content using the method of least square fitting.

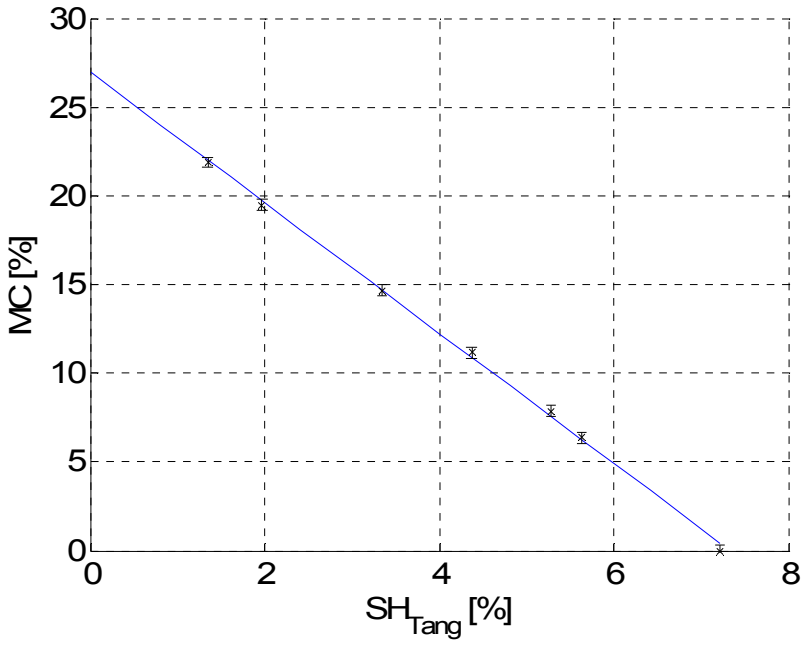

Figure 2-11: Tangential shrinkage at different moisture contents.

The measured values from this project are lower than the published data of Cown and McConchie for older trees (Cown and McConchie, 1980). The overall shrinkage values (seven trees) in tangential directions were 3.28±1.18% and 5.71±1.57% at 12%MC and oven-dry respectively. Cown and McConchie have investigated the shrinkage for 52-year old radiata pine trees and the tangential shrinkage values were 4.2% and 7% at 12%MC and oven-dry conditions respectively. The tangential shrinkage for the older trees is higher than the younger trees, possibly due to increasing tangential shrinkage with distance from the pith.

The average tangential shrinkage values for different heights have shown that the tangential shrinkage decreases with height; the average oven dry tangential shrinkages were 6.21% 5.34% and 4.98% for BH, 10 and 20 metres respectively. When the earlywood was separated from the latewood as for Trees 12, 19, 21 and 23, it was found that the tangential shrinkage is lower for the earlywood bands (3.33±1.49% @12%MC and 5.65±1.68% @OD) than for the latewood bands (3.71 ±0.91% @12%MC and 6.38 ±1.26% @OD).

Following a similar trend to the influence of tree height on the overall average tangential shrinkage, the tangential shrinkage of the earlywood and the latewood also varies with the tree height. For the earlywood, the tangential shrinkage is higher at breast height than at 10 and 20 meters. The same trend also applies to the latewood. Table 2-4 includes the average tangential shrinkage values for the earlywood and the latewood for the four trees. Tree 19 has the highest densities and also has the highest shrinkage values.

Table 2-4: Tangential shrinkage of early- and late-wood for Trees 12, 19, 21 and 23.

Tree	Earlywood			Latewood		
	Density (kg/m^3)	Tangential Shrinkage (12% MC)	Tangential Shrinkage (oven dry)	Density (kg/m^3)	Tangential Shrinkage (12% MC)	Tangential Shrinkage (oven dry)
12	286.3	2.7 ±0.9%	4.9 ±1.3%	363.7	3.4 ±0.8%	5.9 ±1.1%
19	307.7	4.5 ±2.4%	6.8 ±2.3%	423.5	4.3 ±1.2%	7.1 ±1.6%
21	275.4	3.3 ±0.8%	5.7 ±1.2%	355.1	3.8 ±0.6%	6.6 ±1.0%
23	281.6	2.9 ±0.7%	5.3 ±1.1%	368.8	3.4 ±0.7%	6.1 ±1.0%

The tangential shrinkage was highly variable when the average shrinkage values at oven dry for the same growth layer were compared for the three heights as shown in Figure 2-12. In general, the lowest values were found close to the pith at the three heights. The tangential shrinkage also varies within the same growth ring at a given height. Within the same growth ring, the tangential shrinkage decreases with increasing the tree height, especially for the younger annual growth layers. This variation vanishes approximately 5 – 7 years after the initial growth layer formation. This tree height dependent trend is opposite to the trend of microfibril angle which, in general, decreases with the tree height. Higher tangential shrinkage values are expected for smaller MFA (Barber and Meylan, 1964).

The oven-dry tangential shrinkage of the latewood was on average 0.61 % higher than for the earlywood samples, with its corresponding standard deviation of ±0.58%. The high value of the standard deviation underlines the high variability of the tangential shrinkage within the samples.

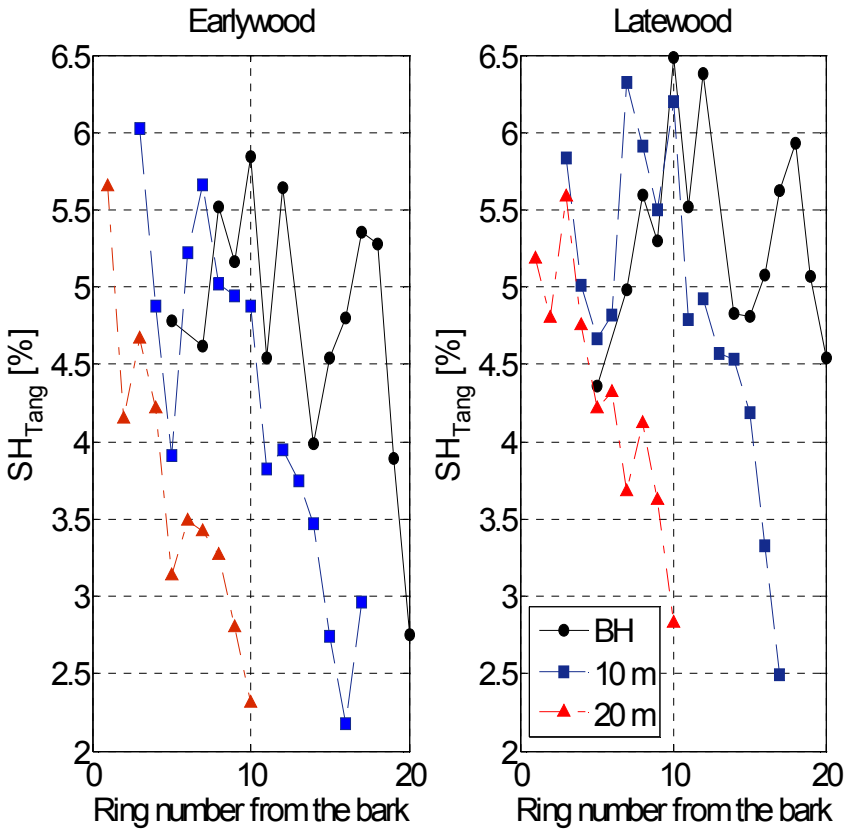

Figure 2-12: Average oven-dry early- and latewood tangential shrinkage at different heights.

Longitudinal shrinkage

In this section the results of the average longitudinal shrinkage for all of the seven trees will be presented first. Then the height dependence of the shrinkage will be discussed. Finally, the longitudinal shrinkage distribution along the radial direction and the influence of the earlywood and the latewood will be presented.

To obtain the longitudinal shrinkage at 12 %MC and oven dry, once again, the least squares method was applied and the results are given in Table 2-5. It has been found that the reported values of Cown and McConchie (1980) are lower than the values from the current experiment, particularly at 12 % moisture content. This can explain the more severe distortion for the new plantation radiata pine, which is normally harvested at 25 – 30 years. However, the experimental values of this study are similar to those of Pang (2001) for trees of a similar age (Table 2-5).

The correlation coefficient (R^2) resulting from the linear least square method was -0.91 with a standard deviation of ±0.12, which shows that the linear behaviour between longitudinal shrinkage

and equilibrium moisture content was not as significant as the found relationship between tangential shrinkage and EMC.

Table 2-5: Comparison of the average longitudinal shrinkage between this study and literature data.

MC Change	Cown and McConchie (1983)	Pang (2001)	This study
Green to 12 %MC	0.02	0.22	0.22 ±0.17
Gren to oven dry	0.25	0.38	0.39 ±0.26

The longitudinal shrinkage dependency on height was investigated, based on the average values of all seven trees. The longitudinal shrinkage tends to increase with height. The relationship between longitudinal and tangential shrinkage will be discussed in Section 2.6. When examining the longitudinal shrinkage of the earlywood and the latewood for trees 12, 19, 21 and 23, it was found that the earlywood had higher longitudinal shrinkage than the latewood. The corresponding shrinkage values for early- and latewood were as follows; 0.25±0.16% @12%MC (0.42±0.22% @OD) and 0.20±0.14% @12%MC (0.34±0.21% @OD).

Table 2-6 contains the average longitudinal shrinkage values for the earlywood and the latewood for the four trees. In the table, wood density is also included for checking the possible correlations between the longitudinal shrinkage and the wood density. It is noticed that Tree 19, with the highest density, has the lowest longitudinal shrinkage with an opposite trend for the tangential shrinkage.

Table 2-6: Earlywood and latewood longitudinal shrinkage (LS) for Trees 12, 19, 21 and 23.

Tree	Earlywood			Latewood		
	Density (kg/m^3)	LS (12% MC)	LS (oven dry)	Density (kg/m^3)	LS (12% MC)	LS (oven dry)
12	286.3	0.42 ±0.15%	0.62 ±0.20%	363.7	0.32 ±0.11%	0.44 ±0.15%
19	307.7	0.14 ±0.12%	0.30 ±0.21%	423.5	0.12 ±0.13%	0.24 ±0.21%
21	275.4	0.26 ±0.08%	0.43 ±0.16%	355.1	0.20 ±0.10%	0.33 ±0.16%
23	281.6	0.17 ±0.09%	0.34 ±0.16%	368.8	0.18 ±0.16%	0.35 ±0.27%

Figure 2-13 shows the radial distribution of the longitudinal shrinkage at oven dry for wood from different heights. It is visible that the shrinkage decreases from pith to bark for the earlywood and the latewood. Over the growth rings near the pith and in ring numbers 8 - 12, the earlywood tends to shrink more than the latewood longitudinally. However, over ring number 12 to bark, the earlywood and the latewood have similar longitudinal shrinkage values.

The oven-dry longitudinal shrinkage of the latewood was on average 0.072% lower than for the earlywood samples, with its corresponding standard deviation of ±0.106%. The even higher value

of the standard deviation in the longitudinal directions also underlines the high variability found in the samples.

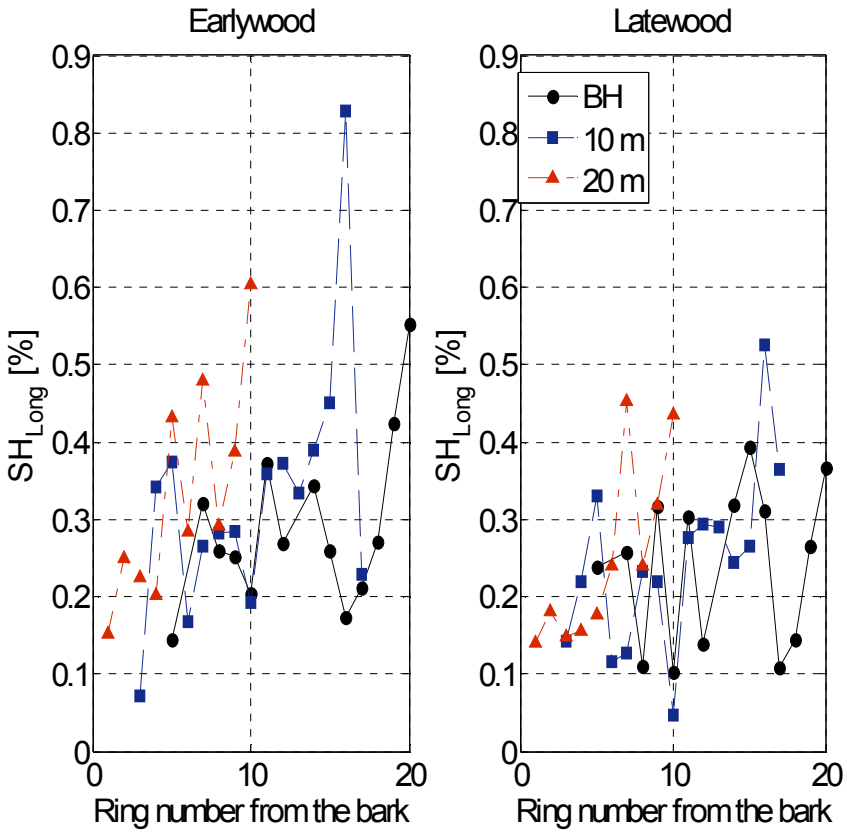

Figure 2-13: Average oven-dry early- and latewood longitudinal shrinkage at different heights.

Fibre saturation point

The fibre saturation point (FSP) is defined as the moisture content at which the cell walls are saturated with bound water, but no free water is present in the lumens. The wood physical and mechanical properties remain unchanged above the FSP but, below the FSP, these properties change with moisture content. FSP is an important parameter both for understanding the drying process and for measuring wood physical and mechanical properties. In wood drying, bound water and free water have different mechanisms for movement. The free water moves mainly by bulk flow while the bound water mainly by diffusion. Most of the wood physical and mechanical properties (such as shrinkage, MOE, MOR, electrical resistance) increase with decreasing moisture content below the FSP.

In this section, the average FSP results for all of the seven trees will firstly be presented. Afterwards the height dependence of the FSP will be discussed. Finally the radial distribution of the FSP and variations between earlywood and latewood will be presented.

In this study, the FSP of each sample was determined from the corresponding plot of the tangential shrinkage against the moisture content. As was mentioned in Section 2.4.2, the relationship between tangential shrinkage and moisture content is linear. Therefore, the fibre saturation point is the moisture content at the intersection of the shrinkage line with the vertical axis. The same procedures have been followed to find the FSP for different type of wood (earlywood and latewood). It was found that the FSP decreases with tree height from 29.95±2.61%MC, 27.45 ±1.91% MC to 26.33 ±2.05% MC, at BH, 10 and 20 meters.

Further analysis was performed to examine the effects of the earlywood and the latewood on the FSP for trees 12, 19, 21 and 23. The results show that the effect of the wood type (early/latewood) is inconsistent (Table 2-7), but when the influence of the wood density was examined, it was observed that the FSP increases with wood density for both the earlywood and the latewood. To further investigate the cross-effect of the density and the tree height, the experimental data were rearranged and two trees selected: one representing a low density tree (# 12) and the other representing a high density tree (#19). The FSP for these two trees as a function of tree height is shown in Figure 2-16.

Uncertainty in the determination of the fibre saturation point

The determination of the fibre saturation point was derived by linear least square regression. For the validation of the FSP results it was necessary to valid the assumption of a linear relationship between the equilibrium moisture contents and the corresponding tangential shrinkage values. The correlation coefficient (R^2) from the regression analysis for all samples is shown in Figure 2-14. The derived average R^2 value for all tested samples was -0.9974 with a standard deviation of ± 0.0064. Therefore it was concluded that the assumption of a linear relation between equilibrium moisture content and the tangential shrinkage is valid.

The uncertainties arising from this assumption (linear relation) were calculated, ignoring the uncertainty of the tangential shrinkage, it was found that the average uncertainty of the moisture content was ±0.58 %MC and the average uncertainty of the fibre saturation point was ±0.47 %MC. Figure 2-15 shows the calculated uncertainties for all samples.

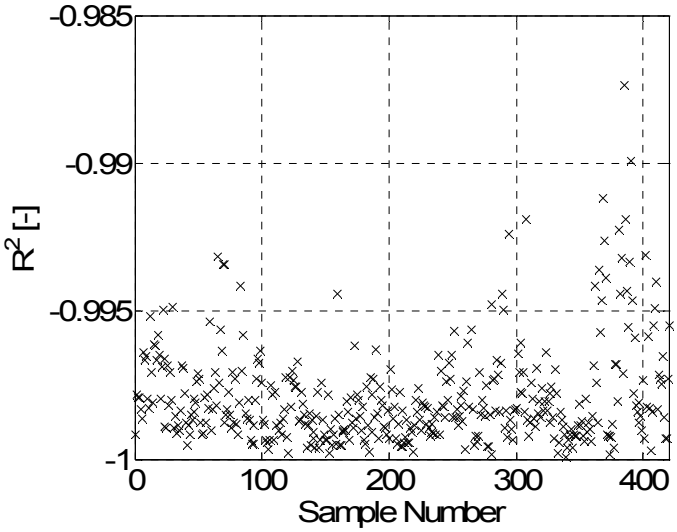

Figure 2-14: R^2 values from the fibre saturation point determination.

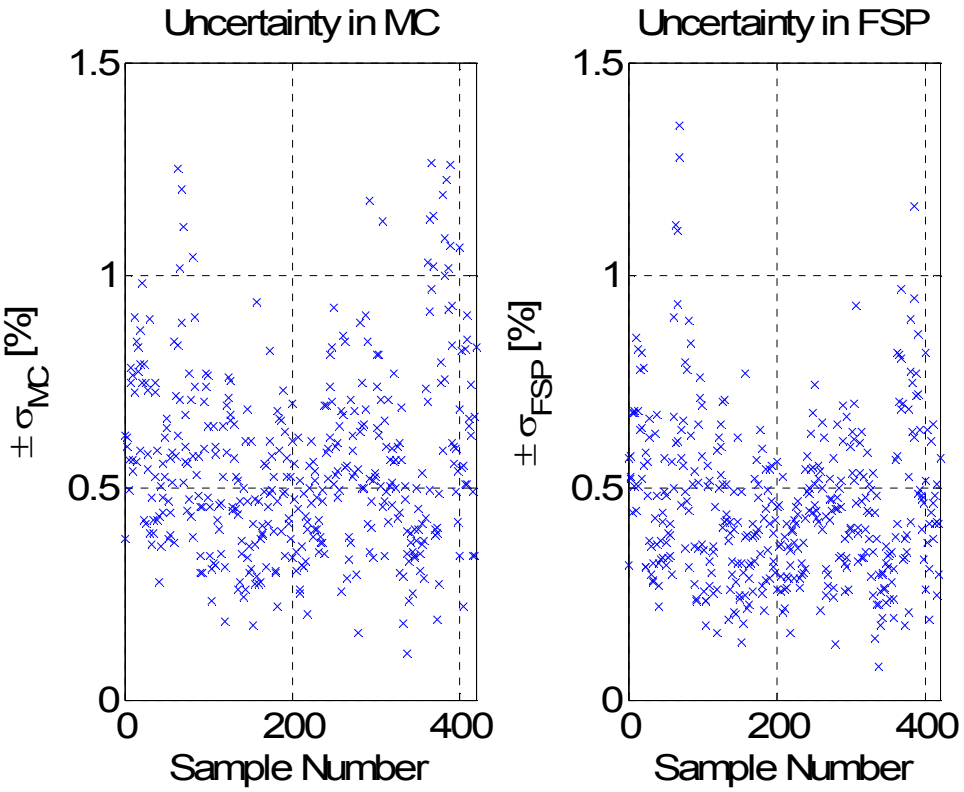

Figure 2-15: Uncertainty of MC and FSP in the linear regression.

Table 2-7: FSP of early- and late-wood for Trees 12, 19, 21 and 23.

Tree	Earlywood		Latewood	
	Density (kg/m^3)	FSP (%MC)	Density (kg/m^3)	FSP (%MC)
12	286.3	27.05 ±2.6	363.7	27.93 ±1.9%
19	307.7	29.95 ±4.3%	423.5	29.49 ±3.1%
21	275.4	27.56 ±2.6%	355.1	28.01 ±1.4%
23	281.6	26.81 ±1.5%	368.8	27.36 ±1.5%

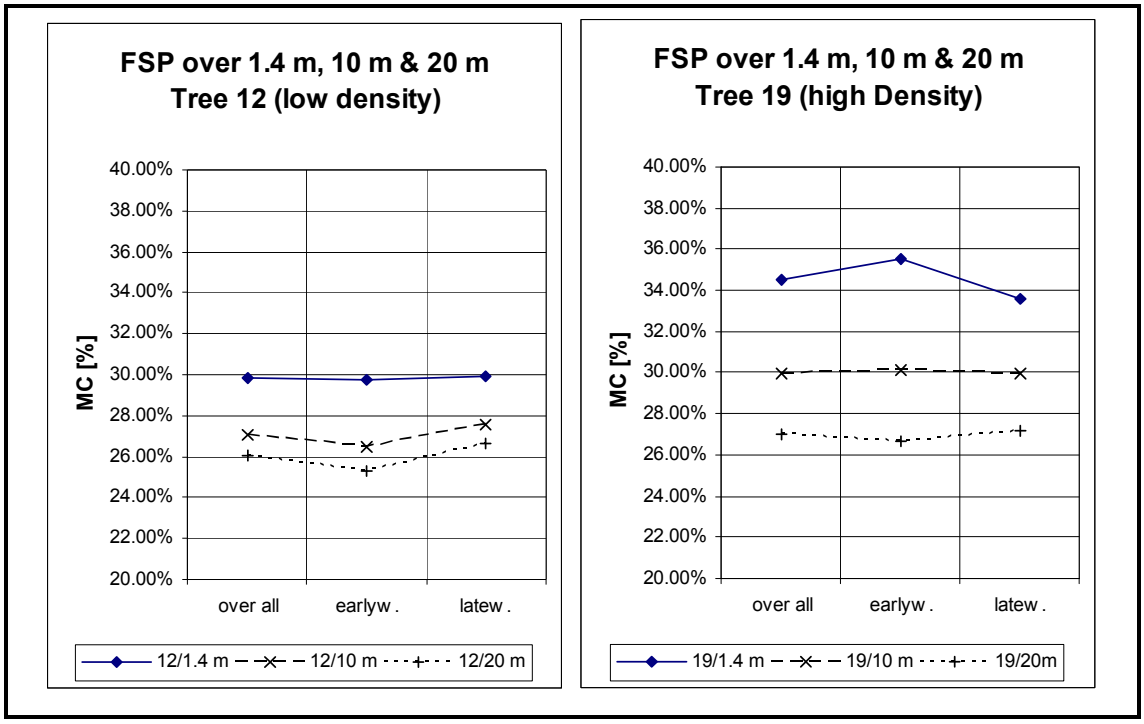

Figure 2-16: Effect of tree height on the FSP for a low density tree (Tree 12) and a high density tree (Tree 19).

As previously mentioned, FSP decreases with height. Figure 2-17 compares the derived FSP of early- and latewood.

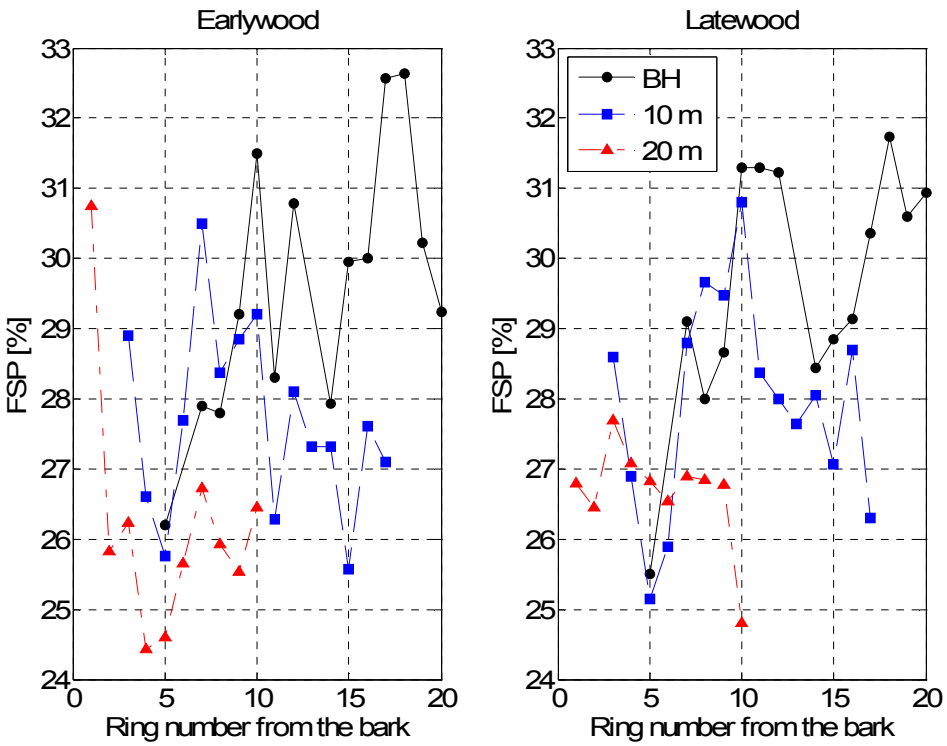

Figure 2-17: Average FSP for early- and late-wood, at different heights.

2.3.3 Properties in adsorption

After finishing the desorption tests, all the oven dried specimens for the shrinkage measurements were put into the EMC cabinet for the adsorption tests, where the relative humidity was increased from 32% to 98% in steps. Similarly to the first part of the desorption experiment, deviations existed between the set humidity and the actual measured humidity inside the cabinet with the data logger, and both of the set and measured relative humidities are shown in Figure 2-18.

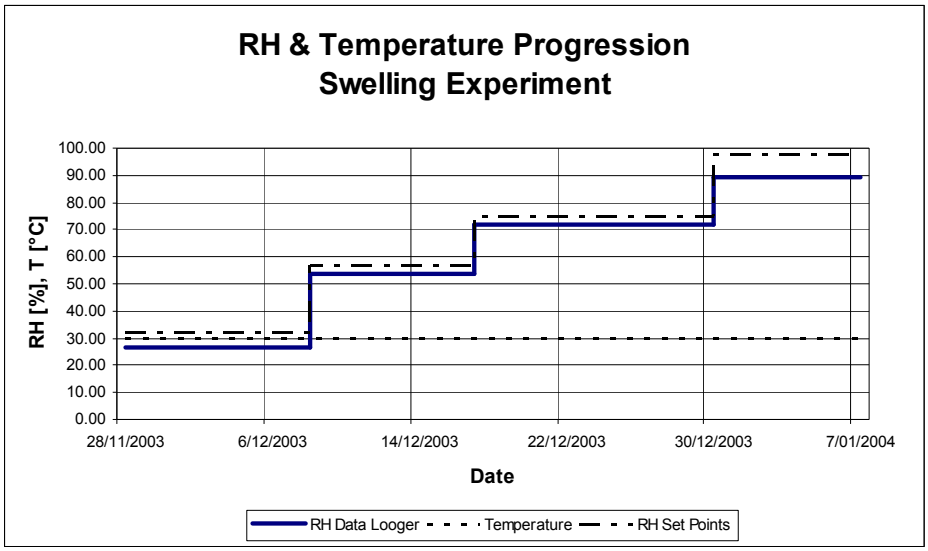

Figure 2-18: Controlled and actual RH & temperature for the swelling experiment.

Adsorption equilibrium moisture content

Figure 2-19 shows the EMC in adsorption for all of the specimens averaged over the earlywood and the latewood. It is very interesting to note that the adsorption values from the current experiment are similar to those of Bramhall and Wellwood (Kininmonth and Whitehouse, 1991). This was not expected because the Bramhall and Wellwood data are the average values for desorption and adsorption. The unusual behaviour of the plotted curve at approximately 12%RH is the result of RH errors in the Bramhall and Wellwood table from Kininmonth and Whitehouse (1991).

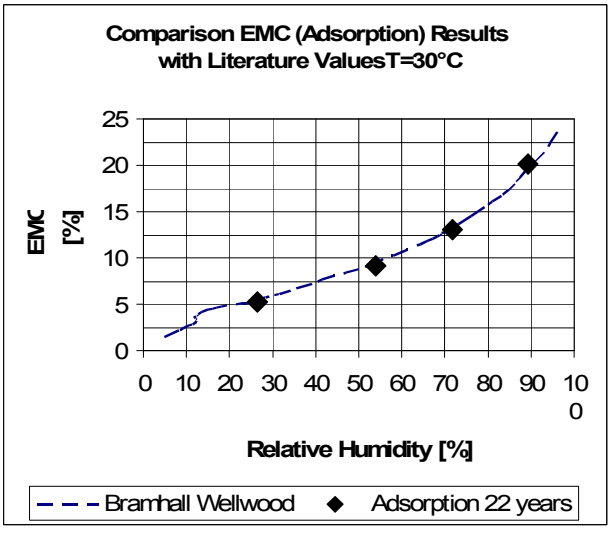

Figure 2-19: Average EMC for adsorption and comparison with data of Bramhall and Wellwood (Kininmonth and Whitehouse, 1991).

Table 2-8 contains the average EMC values with standard deviations for all the samples at different relative humidities. The variations are higher at high relative humidities, as found in the desorption experiment.

Table 2-8: EMC values for adsorption.

RH (%)	EMC (%)
26	**5.28** ±0.35
54	**9.23** ±0.42
72	**13.07** ±0.77
89	**20.29** ±1.19

In the same way as the experimental EMC results have been presented for desorption, the EMC results for adsorption with the earlywood and the latewood are compared for different heights as shown in Figure 2-20 (a) and (b). Figure 2-20 (a) is for the earlywood and Figure 2-20 (b) for the latewood. In the figures, the EMC distribution in the disc radial direction is illustrated which shows the EMC decreasing from pith to bark at high RH (89% and 72%). However, for RH at 54% and 27%, this trend is not apparent. This pattern of the EMC variation in adsorption is consistent with the results in the desorption tests.

In order to further investigate the trend of EMC variations, the EMC data in the same growth ring for each type of wood (earlywood and latewood) were averaged for the three heights and the results are shown in Figure 2-21 (a) to (c). Figure 2-21 (a) is for breast height, Figure 2-21 (b) for the 10m height and Figure 2-21 (c) for the 20m height. From these figures, it is seen that the radial EMC variation trend of decreasing from pith to bark is only noticeable for the 20m heights, whereas at the breast and 10m heights this trend is inconsistent.

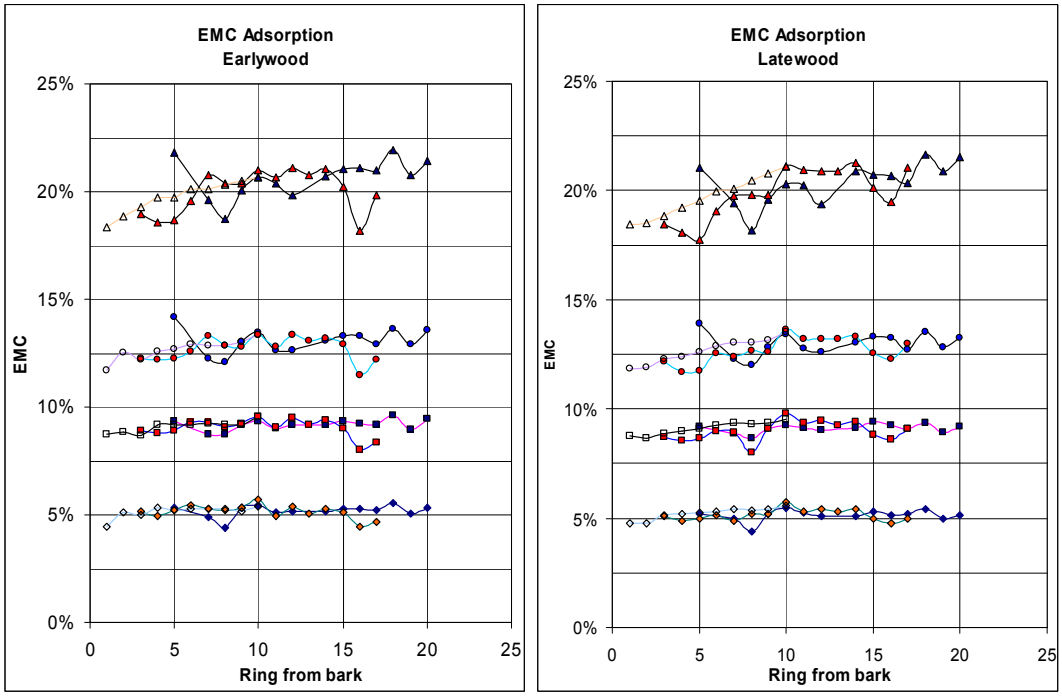

Figure 2-20 (a) **Figure 2-20 (b)**

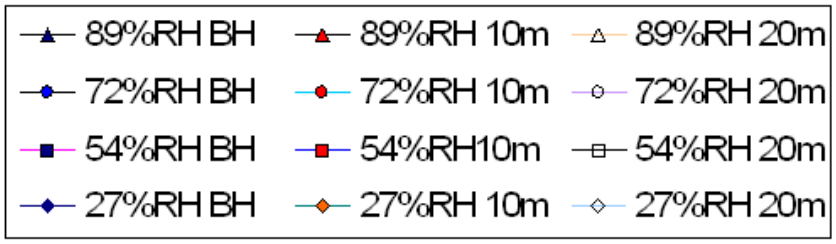

Figure 2-20: Earlywood (a) and latewood (b) EMC in adsorption at different heights.

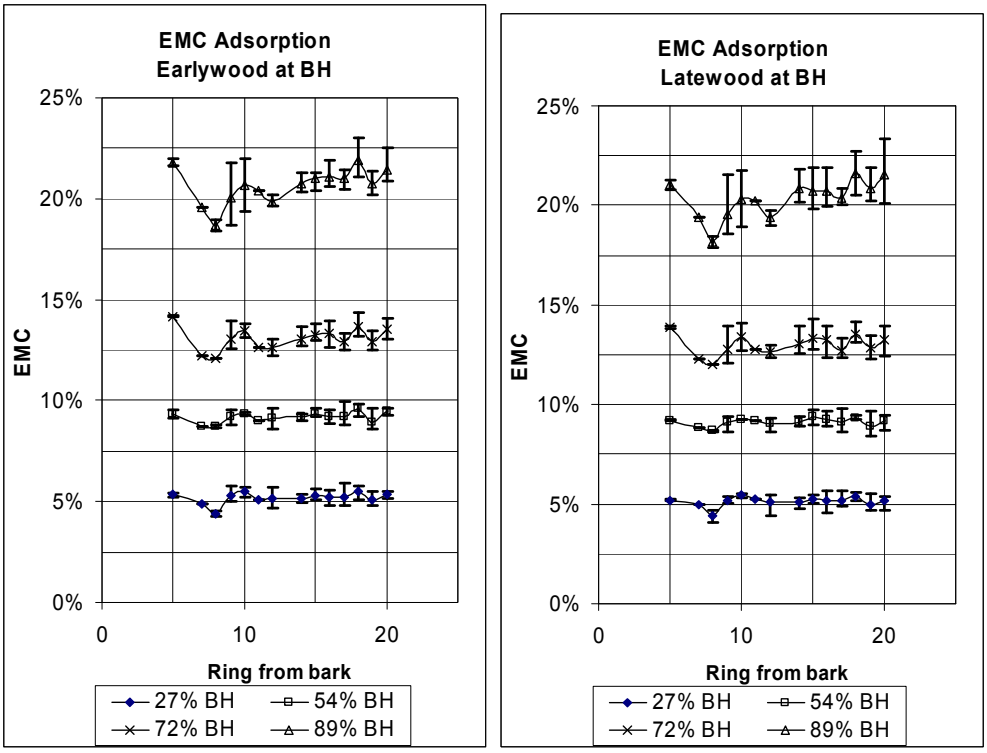

Figure 2-21 (a)

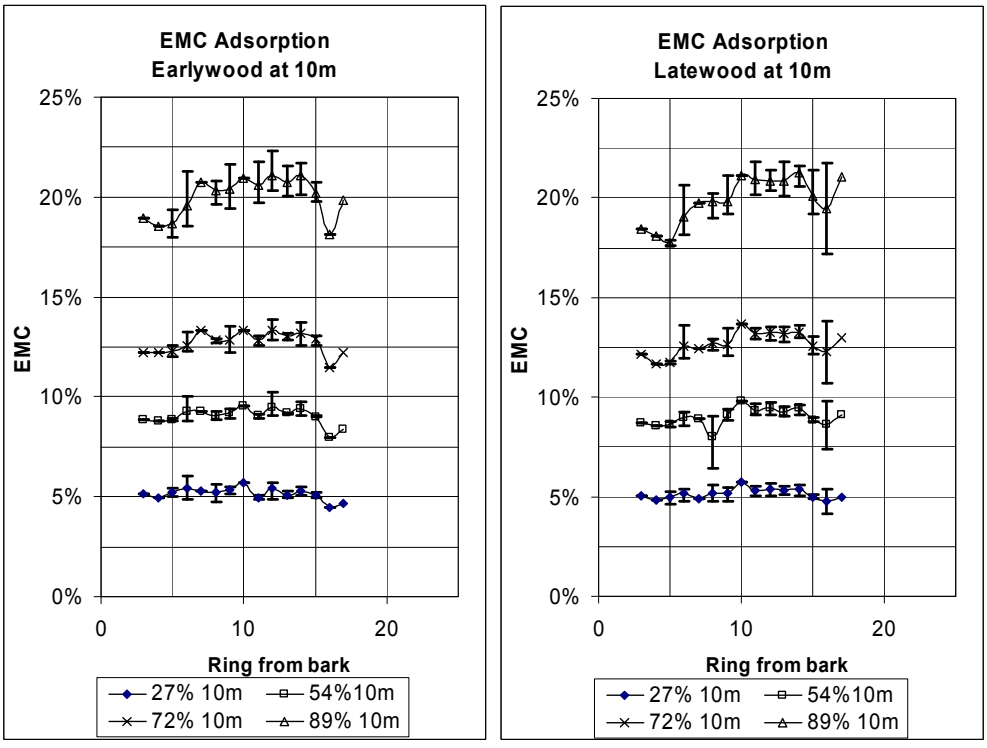

Figure 2-21 (b)

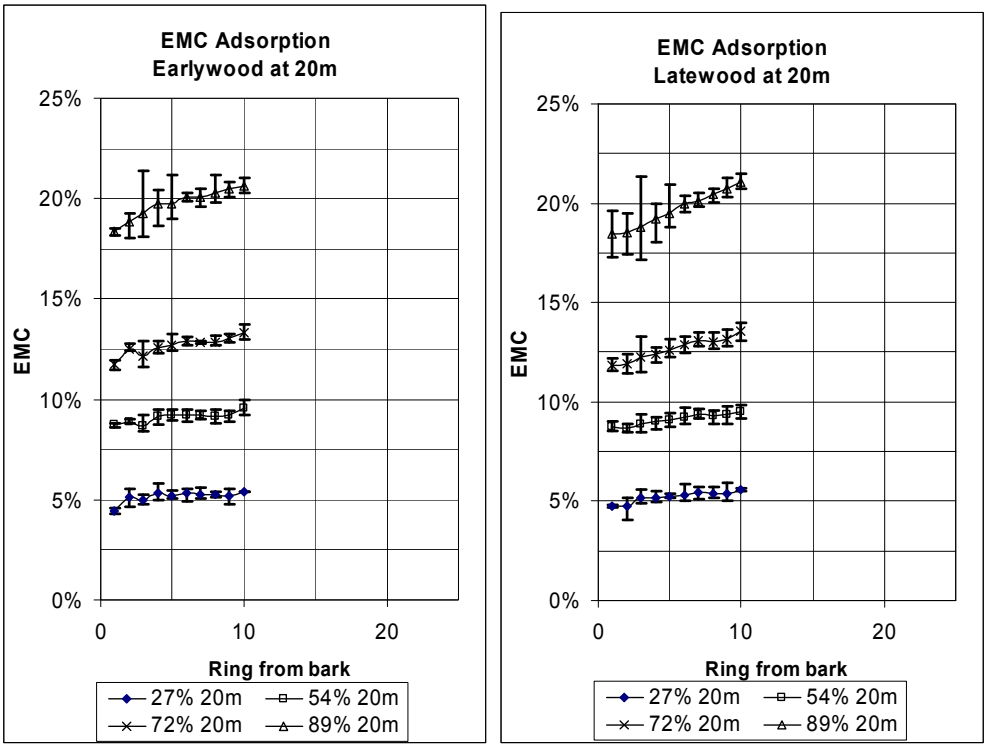

Figure 2-21 (c)

Figure 2-21: Average early- and latewood EMC for adsorption and error bars at BH (a), 10 m (b) and 20 m (c).

Tangential swelling

According to Kininmonth and Whitehouse (1991), swelling is expressed, in the same way as shrinkage, as percentage of the dimensional changes compared with the fully swollen dimension. Therefore equation (2-2) can be used to calculate the swelling. It was found that the relationship between MC and dimensional change was also linear for swelling. Therefore the linear least square fitting method was applied to find the swelling at 12%MC.

The overall average results for tangential swelling were 3.51±1.13% @12%MC. The swelling at the same MC was higher than the tangential shrinkage (3.28±1.18 @12%MC). The difference between adsorption and desorption can be explained by the absence of some bound water connections in the adsorption, which were destroyed during the oven drying. During the adsorption process, these connections could not be re-established, and therefore the swollen dimension in the adsorption is lower than that for desorption at the same MC.

The experimental results have shown that swelling decreases with height, as found for the shrinkage. For direct comparison between the shrinkage and the swelling, the averaged data at 12%MC are given in Table 2-9 together with wood density. It is noticed that Tree 19, with the highest density, has the highest value of tangential swelling, but the correlation for other trees or individual samples is inconsistent.

Table 2-9: Swelling and shrinkage for early- and latewood at 12%MC for Trees 12, 19, 21 and 23.

Tree	Earlywood			Latewood		
	Density (kg/m^3)	**Tangential Swelling (%)**	Tangential Shrinkage (%)	Density (kg/m^3)	**Tangential Swelling (%)**	Tangential Shrinkage (%)
12	286.3	**3.4 ±1.1**	2.7 ±0.9	363.7	**4.1 ±1.0**	3.4 ±0.8
19	307.7	**4.2 ±1.5**	4.5 ±2.4	423.5	**4.5 ±1.2**	4.3 ±1.2
21	275.4	**3.4 ±0.9**	3.3 ±0.8	355.1	**3.9 ±0.6**	3.8 ±0.6
23	281.6	**3.1 ±0.7**	2.9 ±0.7	368.8	**3.7 ±0.7**	3.4 ±0.7

Longitudinal swelling

In this section, the same order of presenting the results as in the previous section is used: Firstly the average longitudinal swelling at 12%MC for all of the seven trees is presented, followed by the results from the earlywood and the latewood for the four trees.

The overall average longitudinal swelling was 0.19±0.17% @12%MC, compared with the longitudinal shrinkage (0.22±0.17% @12%MC). It is observed that the longitudinal swelling in absorption is slightly lower than in the longitudinal shrinkage in desorption. Interestingly, this trend is opposite to that for the tangential swelling, where the swelling is higher than the shrinkage at 12%MC. When comparing the average swelling values for the individual tree as given in Table 2-10, the trend of lower swelling than shrinkage is valid for three trees, but not for tree 12, with no clear reason for this.

Table 2-10: Longitudinal swelling/shrinkage at 12%MC for early- and latewood for Trees 12, 19, 21 and 23.

Tree	Earlywood			Latewood		
	Density (kg/m^3)	**Longitudinal Swelling (%)**	Longitudinal Shrinkage (%)	Density (kg/m^3)	**Longitudinal Swelling (%)**	Longitudinal Shrinkage (%)
12	286.3	**0.45 ±0.17**	0.42 ±0.15	363.7	**0.34 ±0.13**	0.32 ±0.11
19	307.7	**0.12 ±0.11**	0.14 ±0.12	423.5	**0.09 ±0.13**	0.12 ±0.13
21	275.4	**0.23 ±0.07**	0.26 ±0.08	355.1	**0.17 ±0.09**	0.20 ±0.10
23	281.6	**0.14 ±0.08**	0.17 ±0.09	368.8	**0.13 ±0.15**	0.18 ±0.16

2.4 Experiment Results for Wood from Juvenile Trees

In the experiments, two additional discs cut from two juvenile trees were also included. These trees originated from a forest in the Canterbury region. The discs were extracted from a butt log but the exact height location was unknown. The reason for including these two juvenile discs was to find the difference between younger and older trees.

The preparation of the samples followed similar procedures as described in Section 2.2 with the only one exception being that less than 10 samples were cut out from one strip (pith to bark) because of the smaller diameters in the juvenile trees.

The first disc had 7 growth rings and a diameter of 20cm. The second disc had 13 year rings and a diameter of 23.5 cm. Table 2-11 gives more details on the appearance of the discs.

Table 2-11: Appearance of the juvenile discs.

Tree No.	Diameter N–S (cm)	Diameter E–W (cm)	Average diameter (cm)	Growth rings
1	20	19.5	19.75	7
2	23.5	24	23.75	13

As expected, the two juvenile tree discs had a higher green moisture content (120 – 280%) than the mature tree samples, partly due to the juvenility of trees and partly due to the lower loss of water when preparing the samples. The wood density of these two juvenile trees is lower than the older tress, as expected. The disc from Tree 1 had an average density of 299 kg/m^3, with the earlywood density being 258 kg/m^3 and that of latewood being 345 kg/m^3. The corresponding values for the disc cut from Tree 2 were 337, 329 and 359 kg/m^3, respectively.

In the desorption tests, except at 38%RH the average values of the equilibrium moisture content for the juvenile tree samples were higher than those of the mature tree samples as shown in Table 2-12.

Table 2-12: Comparison desorption EMC juvenile trees with average obtained for seven trees.

	EMC in desorption	
RH	**Juvenile tree**	**Mature trees**
90%	26.86±0.95%	24.14±1.50%
84%	22.88±0.36%	21.27±0.90%
72%	16.43±0.38%	16.18±0.51%
56%	12.86±0.30%	12.31±0.46%
38%	8.89±0.28%	9.05±0.45%
27%	7.62±0.33%	7.41±0.41%

Since the tree height for the juvenile tree discs was unknown, comparison of the adsorption EMC between the juvenile tree samples and the mature tree breast height samples was made and the results are given in Table 2-13.

Table 2-13: Comparison adsorption EMC juvenile trees with average obtained for seven trees.

	EMC in Adsorption	
RH	**Juvenile**	**This Study**
26%	5.51±0.32%	5.28±0.35%
54%	10.07±0.49%	9.23±0.42%
72%	15.11±0.53%	13.07±0.77%
89%	23.16±0.48%	20.29±1.19%

Fibre saturation points for juvenile trees are 31.03% for Tree 1 and 34.1% for Tree 2, which are higher than both the mature tree breast height average FSP (29.35%0 and the mature tree overall average value (27.71%). The FSP distribution along the radial direction for the juvenile tree samples follows the same pattern of the mature tree samples as shown in Figure 2-17. It is interesting to note that Tree 2, with the higher FSP has higher tangential shrinkage than Tree 1 as shown in Figure 2-27. However, for the longitudinal shrinkage this trend is reversed. Tree 1 with the lower FSP has a higher longitudinal shrinkage than Tree 2 as shown in Figure 2-28. The tangential shrinkage at 12% MC is 3.17% for Tree 1 and 4.68% for Tree 2. The corresponding values for the oven dry material are 5.22% and 7.27%, respectively. The tangential values for Tree 1 are similar to the mature trees but the values of Tree 2 are much higher than the mature trees. However, the longitudinal shrinkage for Tree 1 (0.51 % at 12 % MC and 0.87 % for oven dry) is much higher than the mature trees. This feature is very important since the longitudinal shrinkage plays an important role in wood instability.

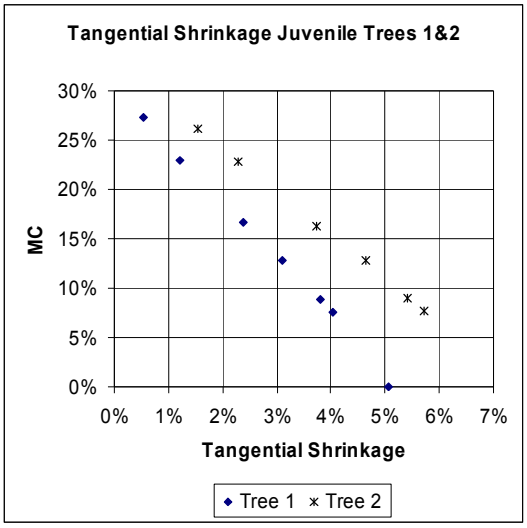

Figure 2-22: Tangential shrinkage of the juvenile tree samples.

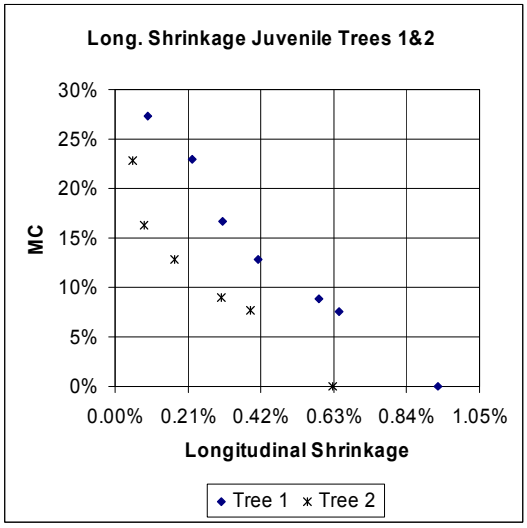

Figure 2-23: Longitudinal shrinkage of the juvenile tree samples.

In order to examine the dimensional change differences between desorption and adsorption for the juvenile tree samples, the experimental results are plotted in Figure 2-24 for the tangential shrinkage and Figure 2-25 for the longitudinal shrinkage. It was found that the juvenile trees follow the same trend as the mature trees. The tangential dimensional change for adsorption is higher than for desorption but the longitudinal dimensional change shows the opposite trend since in the longitudinal direction the wood shrinks more for desorption than for adsorption.

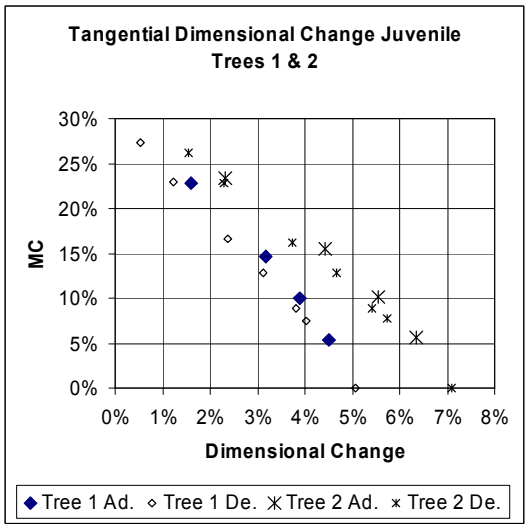

Figure 2-24: Comparison of tangential dimensional changes of juvenile tree samples between adsorption and desorption.

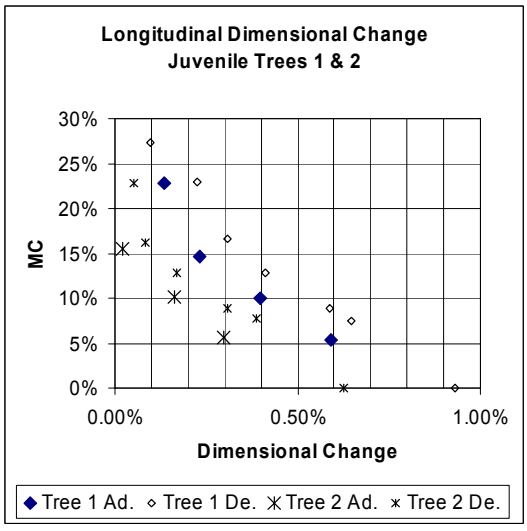

Figure 2-25: Comparison of longitudinal dimensional changes of juvenile tree samples between adsorption and desorption.

2.5 Discussion of Results

2.5.1 Sorption isotherms

When the tree is felled, the wood contains a large amount of water, and this amount of water will eventually be lost either by controlled drying or by natural drying. When the wood is exposed to the atmosphere, it will reach an equilibrium state with the ambient atmosphere with sufficient time, and this moisture content is described as the equilibrium moisture content (EMC). The EMC is strongly dependent on relative humidity (RH) and, to a lesser extent, on the temperature of the surrounding air. At given conditions of RH and the temperature, the wood EMC varies with wood type (heart, sapwood), cell wall constituents and extractives (Skaar, 1988). It is also affected by previous exposure history and mechanical stress. Several theoretical models exist for the interpretation of the moisture sorption of wood, which are based entirely on theories or are of an empirical or a semi empirical nature. These models have been discussed by several authors (Kininmonth and Whitehouse, 1991; Siau, 1995; Skaar, 1988; Stamm, 1964).

The EMC is of high importance for timber in use. Due to its dependency on the conditions of the ambient atmosphere, the wood products can shrink or swell if the wood moisture content is different from the EMC at given conditions. Therefore tradesmen have to apply and follow certain guidelines to account for the wood and ambient atmosphere interaction. For example, timber used for interior design should be dried to a range of expected EMCs to minimize dimensional changes. Wooden flooring should be laid without totally constraining it to the under floor frame to allow an unconstrained movement of the wooden flooring when the moisture content changes.

The sorption isotherms at 30°C using the average values from all samples of radiata pine measured in this study are shown in Figure 2-26. The sorption isotherms follow a typical isotherm ‘S’ shaped curve but are consistently higher than the data in the widely used EMC table, which was obtained from the average values for adsorption and desorption (Bramhall and Wellwood, 1976). Differences have been found between the earlywood and the latewood, but the EMC deviation between the earlywood and the latewood follows no particular trend.

For radiata pine, the EMC varies with growth rings at high relative humidities, decreasing from the pith to the bark. In addition, the EMC variation along tree height is also visible at the high humidities, with the higher values being at the breast height. However, the trends of variation both in the radial direction and along the tree height are inconsistent at low relative humidities.

For a given growth ring along the tree height, the EMC seems not to vary with height. This finding indicates that the EMC may change after the tracheids are formed. Food storage within older tracheids might be causing the later EMC variations.

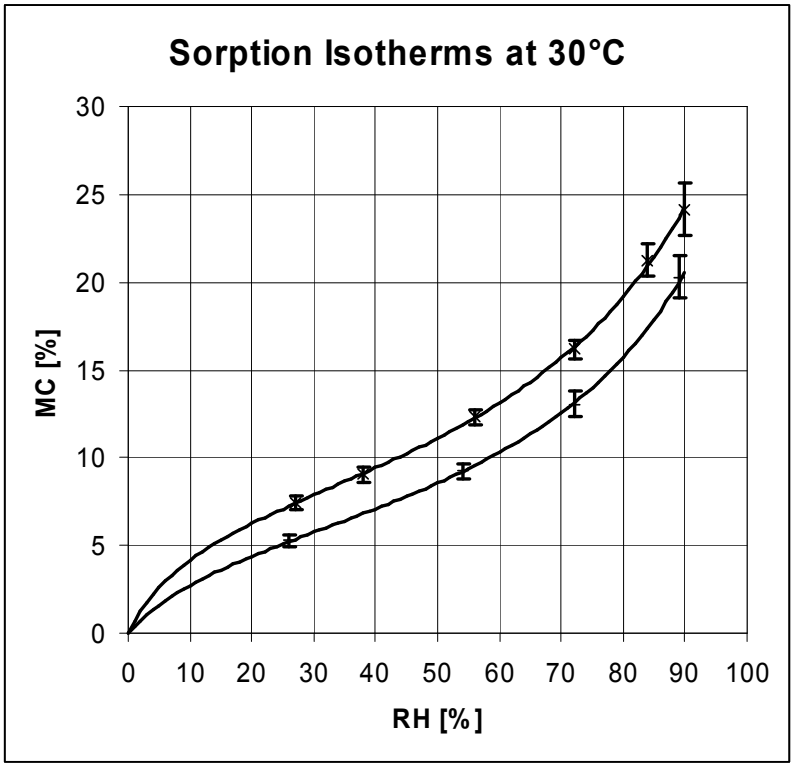

Figure 2-26: Sorption isotherms for radiata pine at 30°C, including the standard deviations.

The typical 'S' curved shape is clearly visible and reflects the manner in which the water is bound to the wood structure. Up to an RH of 30% water is held on its polar sites of relative high energies (monolayer). In the relative humidity region of 30% and 70%RH water is considered to be bound to the first layer by hydrogen bounds (multilayer). Above 70%RH, some of the stored water is described as 'condensed water', and the isotherms reflects solution and capillary effects (Wolf *et al.*, 1972). The lower curve in Figure 2-26 shows the adsorption isotherm obtained when the oven-dried samples were exposed to increasing RH. The difference between the adsorption isotherm and the desorption (upper curve) isotherm at a given RH is described as hysteresis, which reflects the loss of water bounding points. In this study, the hysteresis is significantly formed due to the oven-drying of the samples prior the adsorption. The hysteresis is less significant when wood is not oven-dried, as shown by Orman (1955). The effects of temperature on the sorption isotherms can be found in Skaar (1988). The error-bars in Figure 2-26 represent the derived standard deviations listed in Table 2-3 and 2-8 for all samples.

The fitted curves in Figure 2-26 were obtained by regression analysis of the GAB (Guggenheim-Anderson-De Boer) equation, which is widely accepted model for the sorption isotherms (Ayranci *et al.*, 1990). The GAB equation is defined as follows:

$$EMC = X_m \frac{C_B \cdot K \cdot a_w}{(1 - K \cdot a_w)[1 + (C_B - 1) \cdot K \cdot a_w]} \tag{2-3}$$

The constant a_w represents water activity at ambient conditions which equals the relative vapour pressure (relative humidity). The coefficients, X_m, C_B, and K can be fitted from the experimental data for radiata pine and their values are given in Table 2-14.

Table 2-14: GAB parameters for radiata pine sorption curves at 30°C at approximately 1 bar.

Constants	Desorption	Adsorption
X_m	0.0777	0.0611
C_B	11.7755	8.0012
K	0.7686	0.7966

2.5.2 Fibre saturation point

The term '*fibre saturation point*' (FSP) was originally applied to wood by Tiemann (1906), cited by Skaar (1988). In the studies of Tiemann (1906), he found that below a certain moisture content the mechanical properties of wood start to increase with decreasing moisture content. Above this point the mechanical properties seem to be independent of moisture content. He also found that this critical moisture content, termed as the FSP, corresponds to a state where the cell lumen is free of liquid and the cell wall is fully saturated. Liquid stored in the lumen does not affect mechanical properties, and therefore, above FSP, no changes are recognizable, since only the cell wall is responsible for the strength properties of wood.

In later studies, it was observed that other properties of wood are also influenced by moisture content below the FSP, such as shrinkage and electrical resistance Skaar, (1988). Based on theses observations, Skaar (1988) summarized several methods for fibre saturation point determination. One method, first used by Kelsey (1956), was to determine the fibre saturation point from the linear relationship between the transverse shrinkage and the moisture content.

The derived point is commonly known as the shrinkage intersection point. In this study, the tangential shrinkage intersection point, taken as the FSP, was determined for the earlywood and the latewood of the radiata pine.

Harris (1961) measured the shrinkage intersection point for heart and sap wood of radiata pine and found identical values of 30%MC for both types of the wood. In this study, the variation of the shrinkage intersection point between and within trees was investigated. The overall average FSP (27.7%) measured was slightly lower than the previously reported values of 29 - 30% at room temperature (Pang and Herritsch, 2005). This could be due to the temperature effect, as every 1°C increase in temperature reduces the FSP by 0.1%MC (Bramhall, 1979). In the current study, it is also found the FSP decreases with tree height and increases with wood density as a general trend.

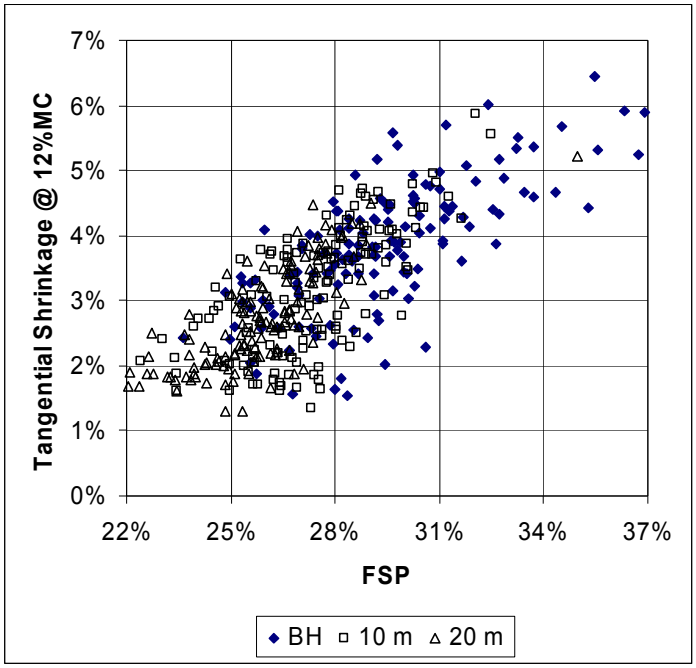

Figure 2-27: Tangential shrinkage at 12%MC and fibre saturation point at different heights.

Since the fibre saturation point was derived from the individual sample's tangential shrinkage in this study, samples with lower tangential shrinkage will generally have lower fibre saturation point values. Figure 2-27 shows the comparison of FSP for samples with different tangential shrinkage at 12% MC. In the figure, the samples collected from different tree heights are also identified to illustrate the trend due to the height effect. The highest tangential shrinkage values are found in breast height samples, which also have the highest FSP. Conversely, the samples cut from 20m tree height show the lowest shrinkage and the lowest FSP.

2.5.3 Shrinkage and swelling

Cown and McConchie (1980) investigated the shrinkage behaviour of a 50 year old radiata pine crop at different heights. The samples used in their study were cut at five or ten year intervals from the pith to the bark. The shrinkage values in their study follow similar trends as determined in this study. The general trend is that, in the radial direction, the longitudinal shrinkage decreases but the tangential and the radial shrinkage increase from the pith to the bark. The shrinkage along all of the three directions (longitudinal, tangential and radial) shows high variability.

Tangential shrinkage

The experimental results show that the younger radiata pine, which has lower basic density, has more variable tangential shrinkage than the mature crops. From this experiment, it was observed that the earlywood tangential shrinkage was lower than the latewood both at 12%MC and at an oven-dry state. Figure 2-28 illustrates the variation of the tangential shrinkage between the earlywood and the latewood at 12%MC.

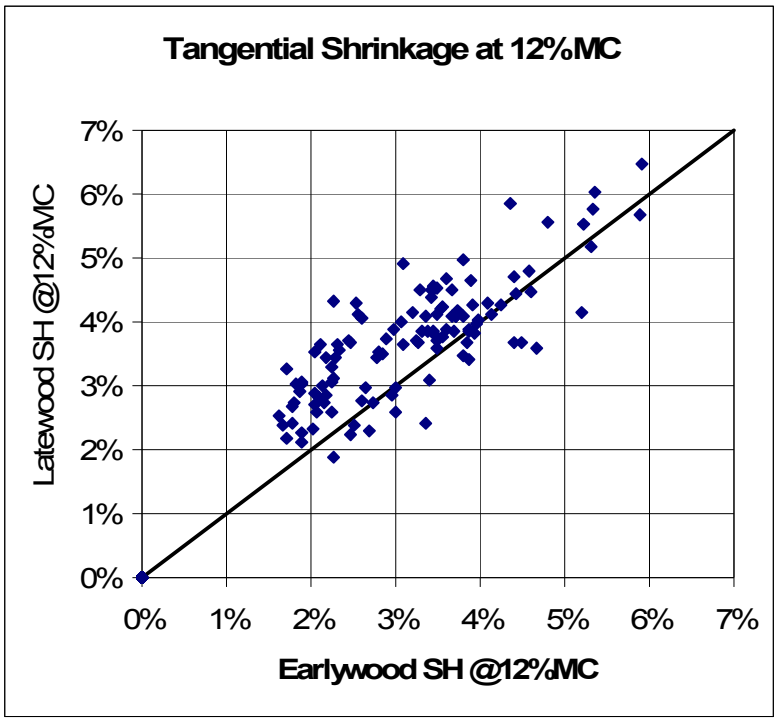

Figure 2-28: Tangential shrinkage of early- and latewood.

The radial distribution of tangential shrinkage from pith to bark follows similar patterns as reported in the literature (Pang and Herritsch, 2005). At 12% MC, the tangential shrinkage of the earlywood increases from a value of 2% near the pith to a value of 4% at around the fifth growth ring.
From this ring outwards to the bark, the tangential shrinkage is relatively constant at 4%. The latewood also has similar pattern to the earlywood, and the lowest value of 4% is found near the pith, while the highest value of 6% is at around the fifth ring.

Longitudinal shrinkage

The most significant feature for the longitudinal shrinkage is that the shrinkage is the highest near the pith and then, from the fifth growth ring, decreases exponentially towards the bark. This pattern is consistent with the earlier reported data (Cown and McConchie, 1983; Pang, 2001). In the longitudinal direction, the earlywood shrinks more than the latewood near the pith. In the middle growth zone in the cross section, the latewood tends to shrink more. The overall longitudinal shrinkage measured in this study is similar to that reported by Pang (2001) but is much higher than the values of Cown and McConchie (1983) who studied older radiata pine crops.

The effect of the tree height was examined in this study, but no consistent trend was found, although the wood at 10m high tends to shrink more longitudinally than the wood at 1.4m and 20m high. Figure 2-29 shows the relationship between the tangential and longitudinal shrinkage of individual samples at 12%MC and in the figure, the tree heights are also identified. There is a general trend that the high tangential shrinkage samples have lower longitudinal shrinkage. This finding is in agreement with model predictions by Barber and Meylan (1964).

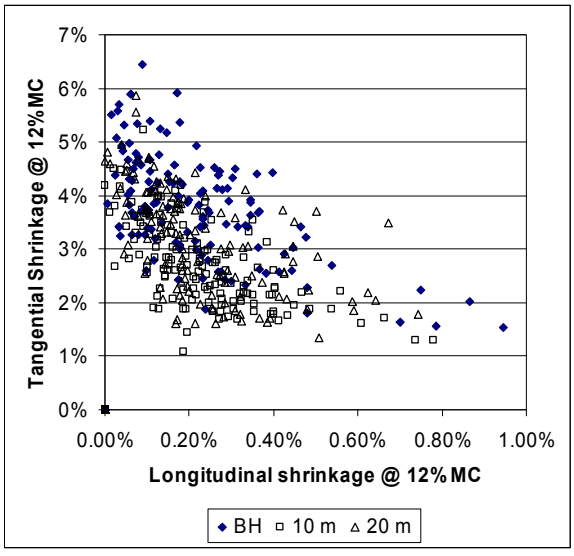

Figure 2-29: Longitudinal and Tangential shrinkage at different heights.

Tangential swelling

The dimensional changes (swelling) in the tangential direction during the adsorption are higher than those in the desorption (shrinkage), as shown in Figure 2-30. This may be caused by absence of bound water connections which were destroyed during the oven drying. During the adsorption process these connections could not be re-established and the shrunken sample could not fully recover its dimensions with the moisture content increasing. Therefore, the swollen length at a given MC is lower in adsorption than in desorption at the same MC. The definitions of the dimensional changes (shrinkage and swelling) are both based on the green dimensions.

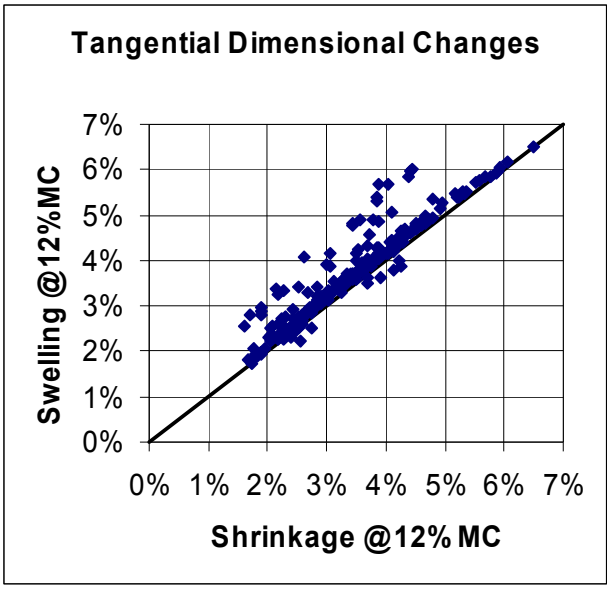

Figure 2-30: Tangential dimensional changes in desorption and adsorption.

Longitudinal swelling

The longitudinal swelling of the earlywood in the adsorption process is similar to the longitudinal shrinkage in the desorption process, whereas the longitudinal swelling of the latewood is slightly lower compared with the shrinkage in the adsorption. The longitudinal swelling, as for the shrinkage, increases with tree height, which is opposite to the trend of the tangential shrinkage. For moisture contents below about 15%, the average longitudinal swelling is lower than the average shrinkage, while for MC above 15% the average longitudinal swelling in the adsorption process is similar to the shrinkage in the desorption process.

2.6 Conclusions and Remarks

The data obtained in this study on equilibrium moisture content (EMC), fibre saturation point (FSP), and shrinkage of earlywood and latewood are very useful in understanding and modelling of wood instability in kiln drying, remanufacturing and in service.

The EMC indicates the moisture content which the wood can eventually retain when it undergoes desorption (drying) or adsorption (wetting) with changes of the ambient humidity and temperature. At given temperature and relative humidity, wood with a higher EMC will lose less moisture in desorption if the wood is originally wet but will gain more moisture in adsorption when the wood is originally dry. On the other hand, wood with lower EMC will lose more moisture in the desorption but gain less moisture in the adsorption. If the range of ambient condition variation is known, the wood should be dried to a target moisture content between the highest and lowest EMCs. One important finding from this study is that radiata pine shows higher EMC than the literature data which has been widely used. Therefore, it is worthwhile to review the recommended target moisture content with kiln drying, particularly for wood from juvenile trees. Further it was found that the EMC at the breast height close to the pith are higher, decreasing towards the bark.

The FSP indicates the maximum moisture content the wood can retain at 100% relative humidity without free water present. The significance of the FSP is that the wood starts to shrink when it is dried from wet. Radiata pine from 25 – 30 year old trees show similar average FSP as most other species (around 30% at room temperature), but FSP variation with tree height (decreasing with height) is significant for radiata pine. For trees with the same age, higher density wood has a higher FSP, but the juvenile trees show higher FSP although having lower densities. Similar to the EMC, the highest FSP values were found for wood close to the pith at the breast height.

Tangential shrinkage and longitudinal shrinkage and their variations are important parameters for wood instability. Qualitatively, with a given spiral grain, the twist increases with increasing the tangential shrinkage but slightly decreases with increasing the longitudinal shrinkage (Stevens and Johnston, 1960). However, the variation of longitudinal shrinkage is the primary cause for crook, bow and residual stresses with kiln drying. The trend that the wood at the breast height has higher tangential shrinkage than the wood at 20 m high may explain the observations that timber cut from the bottom logs tends to have higher twist than timber from second and third logs in the same tree. The spiral grain also plays an important role which needs to be taken into account.

The highly variable longitudinal shrinkage around the pith may be the reason for the higher frequencies of severe bow and crook in the timbers cut from the juvenile zone. The radial distribution of tangential and longitudinal shrinkage data can be used in the modelling of the timber distortion.

The difference in dimensional change between the earlywood and the latewood can be used to predict the distortion and stress development, particularly for thin wood components, which may contain two to three or even less growth rings. The difference is most significant in the tangential direction.

In regards to the historical found correlations between basic density and shrinkage, has to be noted, that for none of the measured properties, within this study, correlations were found between basic densities and other basic wood properties such as tangential-, longitudinal-dimensional changes and fibre saturation points, when analysed for the individual sample.

Chapter 3

Moisture Diffusion in Radiata Pine

Timber distortion can occur when it is dried to below the fibre saturation point. Due to its hygroscopic behaviour, dimensional changes of the wood products will also take place when these products are in use. The objectives of this part of the project were to investigate the wood water diffusion properties of radiata pine and to examine the time for moisture content changes due to adjustment of the ambient conditions (relative humidity changes under constant temperature of 30°C). The properties in the three directions (longitudinal, tangential and radial) were determined from the experiments. The moisture loss or uptake is affected by wood structure and surrounding conditions (temperature, relative humidity and air velocity). This study was focused on the internal moisture diffusion resistance of untreated radiata pine samples for heartwood, sapwood, compression wood and opposite wood with the influence of the tree height also being examined.

In the hygroscopic range, the internal moisture movement is dominated by diffusion and thus can be expressed by the second Fick's law, which states that the transient moisture flux is the product of the moisture concentration gradient and the diffusion coefficient. Research prior to 1970s (Choong, 1963; Choong and Skaar, 1969, 1972; Crank, 1956; Skaar, 1954; Stamm, 1946, 1959) found that the diffusion coefficient for wood is dependent on the moisture content and temperature. Although the water diffusion coefficient is an intrinsic wood property, it cannot be measured directly from an experiment in a way such as to measure density or stiffness. It has to be derived indirectly from observations during the moisture loss or uptake. Depending on the experimental set up, the calculation of the diffusion coefficient varies. In this study the diffusion coefficient was derived from a single drying curve by a non-linear least square fitting method.

In order to solve the Fick's law, the boundary conditions need to be determined and this requires the external moisture mass transfer coefficient or the external resistance. The external resistance was described using the surface emission coefficient as introduced by Yeo *et al.* (2002), which is based on the boundary layer theory (Geankoplis, 2003)

Although the diffusion coefficient is widely used in wood research, very limited information is available on the water diffusion properties for radiata pine. The only information on diffusion coefficients for radiata pine is from two unpublished drying experiments referred to in Kininmonth and Whitehouse (1991). Therefore, this work will fill this knowledge gap by determining the water diffusion properties of the radiata pine.

The material for this study originated from the Canterbury area. Eight trees from different sites close to Christchurch were used to prepare the test samples. In total 138 samples (46 per direction) were used to determine the diffusion coefficients for desorption and adsorption. The samples included heartwood, sapwood, compression wood and opposite wood. One quarter of the total sample pool contained either the compression or the opposite wood.

In this chapter, Section 3.1 provides the theoretical background on the water diffusion in wood and discusses different methods on the determination of the diffusion coefficient. Furthermore the surface emission coefficient used in this study is introduced. Section 3.2 describes the experimental set-up and also includes a summary of the additionally measured basic wood properties. Section 3.3 contains the experimental results and analyses the tree to tree variation and the distribution of the water diffusion properties along the radial direction and the tree height. At last the results are compared with literature data.

3.1 Theoretical Background

Drying of wood is one of the most important operations in wood processing. The drying process and associated development of stresses and deformation have been studied for many years (Martensson and Svensson, 1997a, 1997b; Salin, 1992; Svensson and Martensson, 1999, 2002; Turner and Mujumdar, 1997). A number of models have been developed to predict the water transport. Advanced models considering the more fundamental processes of heat and mass transfer (Pang, 1994; Perre and Turner, 2001a; 2001b; Time, 2002a; 2002b) and are capable of describing the drying behaviour from green to below fibre saturation point. However, there are still gaps in the experimental wood properties to quantify the water transport process.

Even though that diffusion transport in its theoretical definition only occurs below the fibre saturation point where no free water is present, some authors have applied and derived the diffusion coefficient for the whole moisture range above FSP to dry (Cai, 2005; Fakhouri *et al.*, 1993; Hukka, 1999; Yeo *et al.*, 2002).

In general, the models mentioned above do not identify the wood types except for the heartwood and the sapwood (Rosenkilde and Arfvidsson, 1997).

In order to determine the water diffusion coefficient, the experiments can be set up in two ways: (1.) measuring the drying rate curve (moisture loss or gain over time); (2.) measuring the moisture content profile within the sample.

Depending on the surrounding conditions the moisture movement is either steady or unsteady over time. In this work, the diffusion coefficient was derived for unsteady state conditions, which is the most common situation both in wood drying and in wood use for the moisture transport.

In the initial phase of this project, feasible experimental set-ups were investigated with focus on the moisture profile within the sample. An X-ray density measurement device for MDF samples was used to detect the moisture content profile but, unfortunately, the device was not suitable as only one size of sample (50x50x10mm) can be tested. However, several authors have recently determined the coefficient from moisture profiles using the X-ray or nuclear pulsed magnetic resonance techniques (Hartley *et al.*, 1996; Hartley *et al.*, 1994; Rosenkilde and Arfvidsson, 1997; Rosenkilde and Glover, 2002; Sharp *et al.*, 1978). Using this technique certainly increases the accuracy of the derived diffusion coefficient although it is also restricted by the number of samples to be measured. Further work is needed to explore this technique in the future work.

The determination of the moisture profile using the slicing method was dismissed due to the destruction nature and the high variability. Using this method, each sample can only be measured once in each run and thus numerous matched samples are needed if moisture content profiles are developed at different times through the experiment cycle.

In this study the diffusion coefficient was derived from the sample weight loss or gain with elapsed time which makes it possible to determine the diffusion coefficient for a number of samples simultaneously in each run. This technique originated in mid 1950's and was frequently used (Chen *et al.*, 1995; Choong, 1963; Choong and Skaar, 1969, 1972; Comstock, 1963; Crank, 1956) and with the increase of "computer power" further modified for more general boundary conditions.

3.1.1 Diffusion coefficient

Moisture diffusion in a material describes the molecular mass flow caused by a gradient of moisture concentration within the material. Under steady-state conditions, Fick's first law of diffusion can be used to describe the moisture movement. In unsteady-state transport the flux and the gradient will vary in space and with time and this process can be described by Fick's second law. The Fick's second law is derivable from the first law based on the moisture mass balance within an infinitesimal volume:

$$\frac{\partial C}{\partial t} = \frac{\partial}{\partial x}\left(D \frac{\partial C}{\partial x} \right) \tag{3-1}$$

In which,

$\frac{\partial C}{\partial t}$	Rate of moisture movement [kg $_{water}$/m^3 s];
C	Water concentration [kg $_{water}$/m^3];
t	Time [s];
x	Spatial coordinate [m];
D	Diffusion coefficient [m^2/s].

The gradient in the Fick's law is also referred to as moisture transfer driving force and for the convenience for application; gradient of moisture content is commonly used as the driving force for the moisture movement calculation. In other moisture movement models of moisture transport, other driving forces such as vapour partial pressure, chemical potential, water potential, free energy and spreading pressure are also used (Skaar and Babiak, 1982). Although these driving forces can be converted to each other as well as the transfer coefficients, care must be taken when comparing the transfer coefficients with values of the diffusion coefficient due to the different mechanisms for the driving force and the different units used.

The analytical solutions for the unsteady-state diffusion equation are described by Crank (1956). These solutions are based on the following assumptions:

- The diffusion coefficient is constant, independent of moisture concentration;
- The initial temperature and moisture content are uniform through the material;
- The surface moisture content is immediately in equilibrium with the surroundings after contacting; and
- The moisture concentration and moisture transport through the material thickness is symmetrical.

The analytical solutions were firstly used to calculate the constant diffusion coefficient (Skaar, 1954). Stamm (1959) derived the longitudinal bound water diffusion coefficient of the cell-wall substance of Sitka spruce in adsorption. The separation of the internal and external resistance was investigated by Choong *et al* (1969). Several authors then developed models to take into account the influence of moisture content on the diffusion coefficient (Siau, 1984; Skaar, 1988; Stamm, 1946). Stamm (1946) first developed a moisture movement model from the analogy between electrical conduction and mass transfer in wood in which the cell wall structure of wood is regarded as the water transfer resistance. Siau (1984) made a similar but more general approach to account for the wood structure effect and in this work, Siau's model is used to explain the moisture diffusion within wood.

In Siau's model (1984), the analogy between electrical conduction and mass transfer was employed to derive the overall diffusion coefficient of the moisture in the wood. Based on the model, a single cell structure is simplified as shown in Figure 3-1. In the figure, *a* is the ratio of lumen width to cell width which is equal to the square root of the porosity. The porosity can be calculated from the oven-dry density and the wood-cell density:

$$\varepsilon = 1 - \frac{\rho_{oven-dry}}{\rho_{wood-cell}} = a^2 \tag{3-2}$$

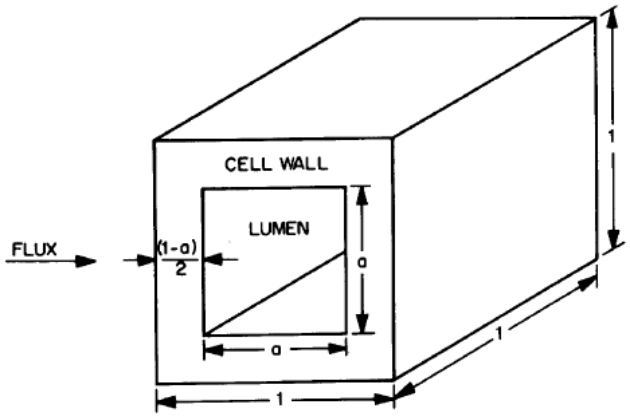

Figure 3-1: Siau's Geometrical model for a single cell (Siau, 1984).

Depending on the moisture transport direction, the water molecules either penetrate or diffuse through the cell wall and lumen, respectively. Figure 3-2 shows this analogy for the moisture transport in transverse direction in which the flux is determined by two resistances (cross wall) in series and a parallel resistance (lumen and side walls).

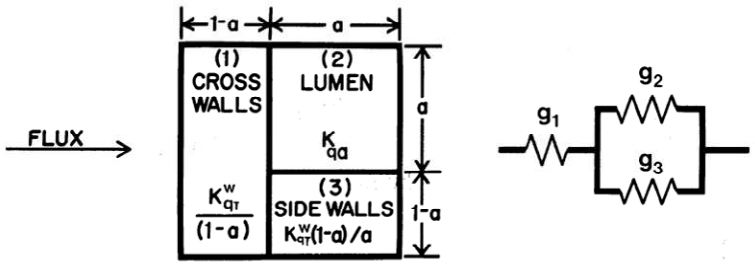

(a) (b)

Figure 3-2: (a) Siau's transverse thermal conductivity model; (b) Analogous electrical circuits.

When neglecting the side walls resistance, the effective diffusion coefficient of wood in the transverse direction is defined as follows:

$$D_T = \frac{1}{(1-a^2)} \cdot \frac{D_{BT} \cdot D_{Lumen}}{D_{BT} + D_{Lumen} \cdot (1-a)} \tag{3-3}$$

In which, D_{BT} is the transverse diffusion coefficient of the bound water in the cell wall substance and D_{Lumen} is the water vapor diffusion coefficient in the air in the lumens. The water vapour diffusion coefficient in the air in the lumens in Equation (3-3) should have the same basis of concentration of bound water in the cell wall (Siau, 1995).

Choong (1963) and Stamm (1964) have found that the diffusion coefficient in the cell wall structure is a function of the constant diffusion coefficient, the activation energy and the temperature expressed by the Arrhenius equation:

$$D_{Wood} = D_0 \cdot e^{-\frac{E_b}{R \cdot T}} \tag{3-4}$$

Where:

D_{Wood}	Transverse diffusion coefficient of bound water in wood [m^2/s]
D_0	Constant diffusion coefficient [m^2/s]
E_b	Activation energy of diffusion [J/mol]
R	Gas constant [J/mol K]
T	Temperature [K]

When analyzing these resistances, the main resistance is considered to be the bound water diffusion through the cell wall. Based on Stamm's data (1959), Siau (1995) derived the activation energy of the bound water diffusion and found that the activation energy decreases with increasing moisture content. Therefore, the diffusion coefficient should increase with increasing the moisture content from Equation (3-4).

This conclusion was confirmed by Hunter (1992), who derived an analytical expression for the activation energy of diffusion as a function of enthalpy and entropy changes associated with the sorption process (Hunter, 1991).

In recent studies (Choong and Skaar, 1969; Liu *et al.*, 2001; Olek *et al.*, 2005; Simpson and Liu, 1991; Yeo *et al.*, 2002), the diffusion coefficient includes both the bound water diffusion and water vapour diffusion which is expressed by an empirical equation as Equation (3-4). Simpson *et al* (1991) proposed that the transverse coefficient increases exponentially with moisture content. Typical values for the diffusion coefficient lie in the range of 10^{-11} to 10^{-7} m^2/s depending on temperature and diffusion direction. The diffusion coefficient in the longitudinal direction is around ten times higher than the diffusion coefficient in the transverse directions.

Different approaches have been used to derive the diffusion coefficients. Choong and Skaar (1969) proposed the unsteady sorption technique to determine the diffusion coefficients. Liu *et al.* (2001) introduced an inverse method based on finite difference method. Yeo *et al.* (2002) developed an technique to measure the diffusion coefficient as a function of average moisture content and wood surface moisture content based on the analytical solution to the diffusion equation. Olek *et al*. (2005) modified the inverse method and applied it to determine the diffusion coefficients. The modified inverse method determines the diffusion coefficient and the surface emission coefficient simultaneously. In this method, the surface emission coefficient is derived from the boundary layer theory and thus only the diffusion coefficient is determined. In this study, the modified inverse approach of Olek *et al.* (2005) is used for the determination of the diffusion coefficient.

3.1.2 Surface emission coefficient

The surface emission coefficient is used to describe the resistance against water vapor movement from the wood surface into the surrounding air. Söderström and Salin (1993) published a review paper on the surface emission coefficient for wood drying and found that the coefficient ranges between 10^{-7} and 10^{-6} m/s.

Rosenkilde and Glover (2002) investigated the surface moisture content of Scots pine using magnetic resonance imaging technique and found that the wood surface dries rapidly in the early phase of drying. Within an hour the surface moisture content drops from 120% to 20%. In drying, it is common to make the assumption that the moisture content is in equilibrium with the surrounding

air immediately after the start of drying, which is valid as the results from Rosenkilde and Glover (2002) have proven.

In this study, the surface moisture content is not assumed to be at equilibrium in the initial start of drying to account for the moisture content change in the early stage of drying. Therefore the surface emission coefficient introduced by Yeo *et al.* (2005) is used to account for the variable surface moisture content. In the following discussion, the surface emission coefficient calculation used in this study is presented. The mass-transfer coefficient (vapour concentration based) calculated by the boundary layer theory for laminar flow is defined as (Geankoplis, 2003):

$$h_{air} = \frac{0.66 \cdot D_{H2O,air} \cdot \mathrm{Re} \cdot Sc}{L_s} \tag{3-5}$$

$$D_{H2O,air} = 2.2 \cdot 10^{-5} \left(\frac{1.013 \cdot 10^5}{p} \right) \left(\frac{T}{273} \right)^{1.75} \tag{3-6}$$

$$\mathrm{Re} = \frac{L_s \cdot v \cdot \rho_{air}}{\mu} \tag{3-7}$$

$$Sc = \frac{\mu}{\rho_{air} \cdot D_{H2O,air}} \tag{3-8}$$

In the above equations,

h_{air}	Mass-transfer coefficient based on water-vapour concentration in air [m/s]
$D_{H2O,air}$	Diffusion coefficient of water-vapour in air [m^2/s] (Dushman's equation cited by Siau,1995)
Re	Reynolds number [-]
Sc	Schmidt [-]
L_s	Length of the surface along which convection occurs [m]
v	Air velocity [m/s]
μ	Dynamic viscosity [Pa s]
p	Total pressure of air [Pa]
T	Temperature [K]
ρ_{air}	Density of air [kg/m^3]

The conversion between the above mass transfer coefficient and surface emission coefficient is based on the analogousness of the flux for the different potentials.

$$h_m \cdot \rho_{basic} \cdot (MC_s - MC_e) = h_{air} \cdot (C_{s,air} - C_{e,air}) \tag{3-9}$$

In which the subscripts e and s stand for equilibrium and surface, respectively. Other variables are defined as:

C_{air}	Concentration in air [kg_{water}/m^3]
h_m	Surface emission coefficient [m/s]
ρ_{basic}	Basic density [kg_{wood}/m^3]

The water-vapor concentration in the air at the surface can be determined by using the following relationship (Yeo *et al.*, 2002):

$$\frac{p_{o,wet} - p_s}{p_{o,wet} - p_e} = \frac{1 - RH_s}{1 - RH_e} \tag{3-10}$$

$$p_s = p_{o,wet} - \left(\frac{p_{o,wet} - p_{o,dry} \cdot RH_s}{1 - RH_e} \right) \cdot (1 - RH_s) \tag{3-11}$$

Where:

$p_{o,wet}$	Saturated water vapour pressure at wet bulb temperature [Pa]
$p_{o,dry}$	Saturated water vapour pressure at dry bulb temperature [Pa]
$p_{e/s}$	Surface/equilibrium water vapour pressure in air [Pa]
RH_e, RH_s	Relative humidity at equilibrium and at the wood surface [-]

From the above relationships, the working formula for the surface emission coefficient can be calculated from the external mass-transfer coefficient and the air conditions:

$$h_m = h_{air} \cdot \frac{\frac{M_{H2O} \cdot p_s}{R \cdot T_s} - \frac{M_{H2O} \cdot p_e}{R \cdot T_{dry}}}{\rho_{basic} \cdot (MC_s - MC_e)} \tag{3-12}$$

In equation 3-12 the outstanding variables M_{H2O} and R represent the molecular weight of water (M_{H2O}= 18 kg/kmol) and the gas constant (R=8,314 m^3 Pa/kmol K) respectively.

Yeo (2002) found that the maximum error when using the dry-bulb temperature (T_e) instead of the wet bulb temperature, at 25%RH, (T_s) is 4.3% at 30°C and therefore the assumption was made that the surface temperature is equal to ambient (equilibrium) temperature. The calculation of the surface emission coefficient requires the knowledge of the sorption behaviour to determine the equilibrium moisture content at give surrounding conditions (MC_e).

The sorption data used in this study originated from the experimental investigation of earlywood and latewood properties of radiata pine (Chapter 2). Figure 3-3 shows the sorption isotherms for radiata pine at 30°C.

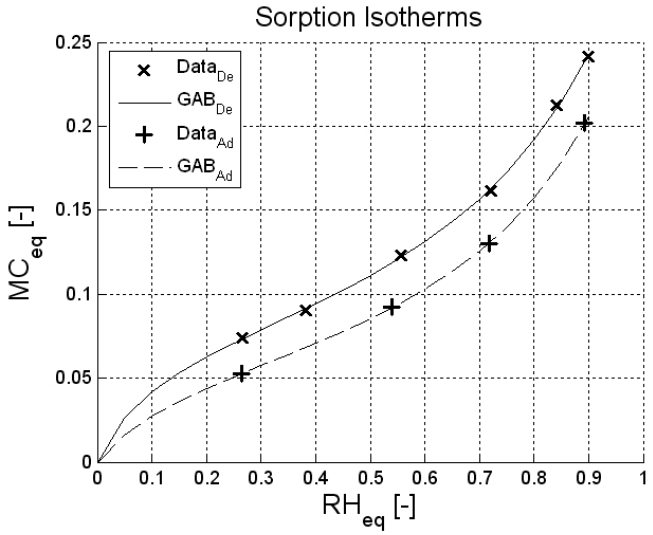

Figure 3-3: Sorption isotherm for radiata pine at 30°C.

Using Equation (3-12), the surface emission coefficient can be calculated at given surface moisture content and density as shown in (Figure 3-4). It should be noted that the surface emission coefficient shown in Figure 3-4 is for desorption. The coefficient for adsorption should use the adsorption isotherm and, therefore, results are slightly different.

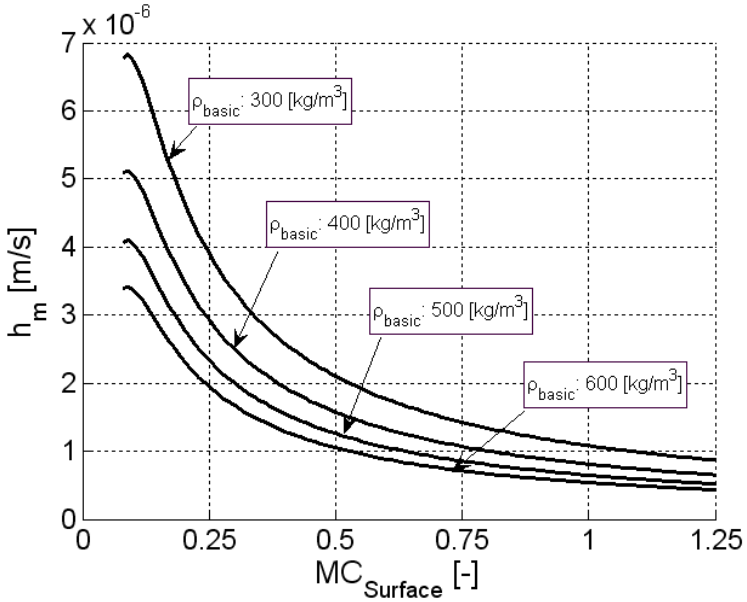

Figure 3-4: The calculated surface emission coefficient as a function of surface moisture content and wood basic density.

Comparison of the surface emission coefficient introduced by Yeo and Siau

To illustrate the difference between the introduced and applied surface emission coefficient and the commonly used mass-transfer coefficient, the wood surface interaction with the surrounding air was further investigated.

In general the assumption is made that at the surface the water vapour pressure is in equilibrium with the surface moisture content. This assumption over-predicts the moisture fluxes at the surface to the surrounding air, as found by Yeo et. al (2002) and Salin (2003). Although their general theories differ both authors found that it is necessary to reduce the surface flux, to be able to obtain a more realistic reflection of the moisture flux from the wood surface to the surrounding air.

Figure 3-5 illustrates the difference between the surface emission coefficient from Siau (1995) and Yeo (2002), and the calculated form equation 3-12. Siau believed that the water vapour pressure on the surface of wood (p_s) is in equilibrium with the wood surface. *This calculation however resulted in large deviations between experimental and theoretical surface emission coefficients (Yeo 2002b).*

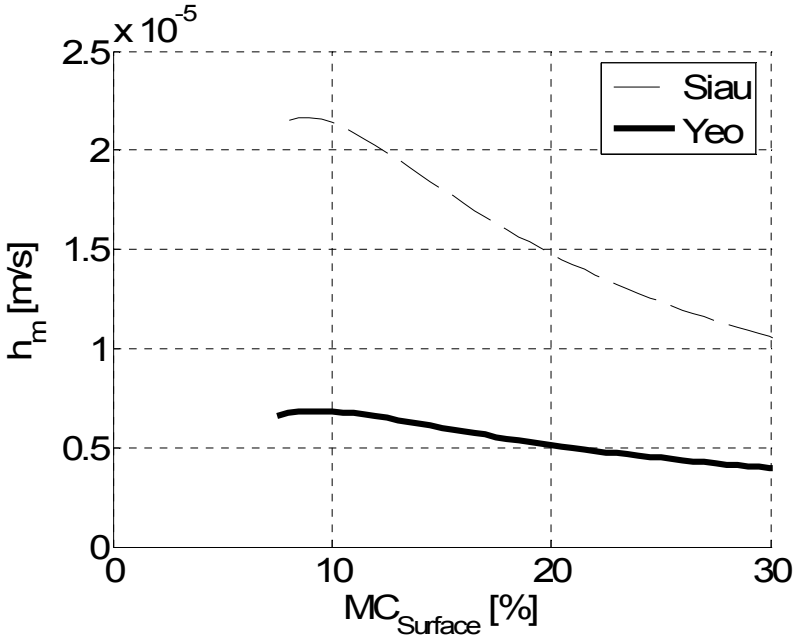

Figure 3-5: Surface emission coefficients by Yeo and Siau.

Due to the high internal moisture movement resistance of the wood, the influence of the two presented surface emission coefficients can be neglected at high air velocities, as used in this experiment and as shown in Figure 3-6. The diffusion coefficient used in this simulation was identical for both simulation (D_0=4.62E-10 m^2/s and K_0=5.95) the air velocity was 3.3 m/s. The emission coefficient introduced by Siau led to a slightly faster drying than the coefficient of Yeo. ΔMC, in Figure 3-6, is the difference between the two drying curves and the highest deviations are found in the first 100 hours of drying, with a maximum value of 0.1%MC within the first 5 hours of drying.

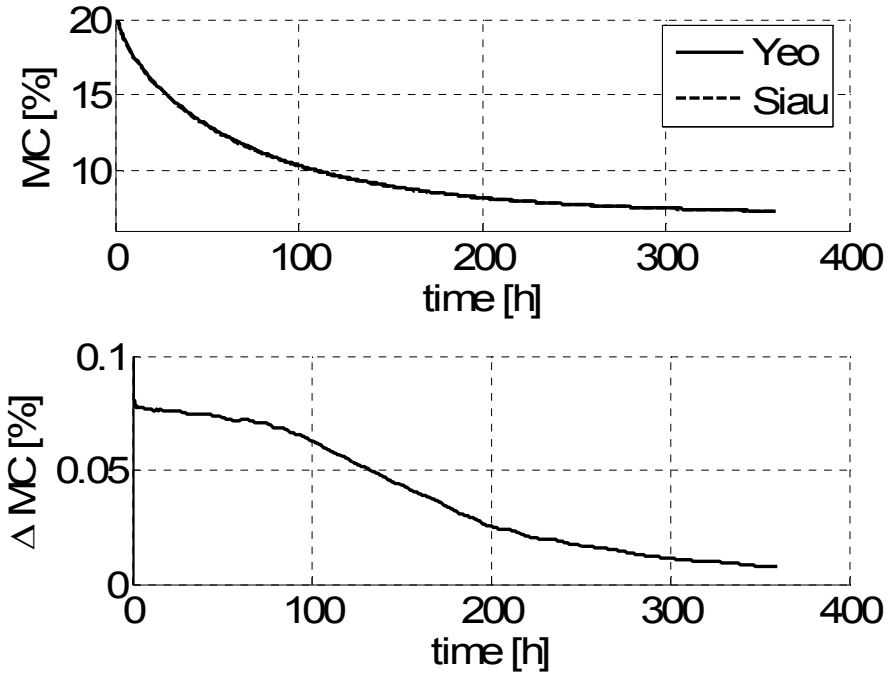

Figure 3-6: Comparison of the influence of two applied surface emission coefficient on the drying time of a sample at air velocity of 3.3 m/s.

The above made comparison clearly show, that at high air velocities the influence of the surface emission coefficient can be neglected. But the author emphasises especially at lower air flow rates, the wood surface interaction with the surrounding air must be considered to achieve a more realistic simulation of the drying behaviour of wood.

3.2 Experiments

This section includes the experimental procedure and the equipment used (environment chamber), followed by the presentation of the basic wood properties summary for the samples tested. These properties include green and equilibrium moisture content, wood basic density, and tangential and radial shrinkage. Finally the procedures for the determination of the diffusion coefficient are presented.

The material in this study originated from the Canterbury area. Two 19 year old radiata pine trees (Tree A1 and Tree A2) were cut down from the University trial stand (Southern Plantation Forest) located near Christchurch for the first run of experiments. Two 20 year old radiata pine trees (Tree 1 and Tree 2) were taken from a forest near Darfield (Canterbury) owned by Selwyn Plantation Board Ltd for the second run of the experiments. This plantation was established in 1986 (20 year old), currently 580 stems/ha with average tree diameter at the breast height being 28 cm and mean stem height 20 m. The stands were pruned twice, 2.6 m pruning in 1995 and production pruning in 1996. In the third run (Tree 3 and Tree 4) and the fourth run (Tree C1 and Tree C2) of the experiments, the material (30 year old radiata pine) originated from the Muirheads plantation forests (Darfield rural area), also owned by Selwyn Plantation Board Ltd.

In the total, four runs of experiments have been carried out with the following objectives:

1. ***Run 1:*** Measure the diffusion coefficient for two butt logs (19 year old) and examine the variations in the diffusion coefficient between heartwood and sapwood;
2. ***Run 2:*** Measure the diffusion coefficient in two 20 year old trees and examine the variations of the diffusion coefficient with the stem height;
3. ***Run 3:*** Measure the coefficient in two 29 year old trees and examine the influence of tree age in comparison with the results of Run 1 and Run 2;
4. ***Run 4:*** Measure the diffusion coefficient for compression and opposite wood for two 29 year old trees.

3.2.1 Experiment procedure

Prior to each experimental run two trees were always selected. After felling of the selected trees, three cross sectional discs were removed at different heights from each tree. On the same day they were transported to the University of Canterbury, where the discs were stored in a cooling room (Forestry School) at 4°C until further use. The thickness of the discs varied from 16 to 20 cm.

Prior the actual sample preparation the actual disc size was reduced for better handling. Afterwards the main sample from a specific location was extracted with a band saw (Figure 3-7). The main samples had a dimension of approximately 4 cm along the tangential and radial directions. The length varied depending on the thickness of original disc from 16 to 20 cm. From this main sample the actual specimens were cut. The longitudinal samples measured approximately 6 cm in length, the radial and tangential samples lengths were approximately 3 cm. In addition to the relevant samples for the diffusion coefficient determination, an additional samples, with an approximate length of 3 cm was prepared from the main sample. This sample was used for cross checking purposes in this experiment and is referred to, in this study, as the reference sample.

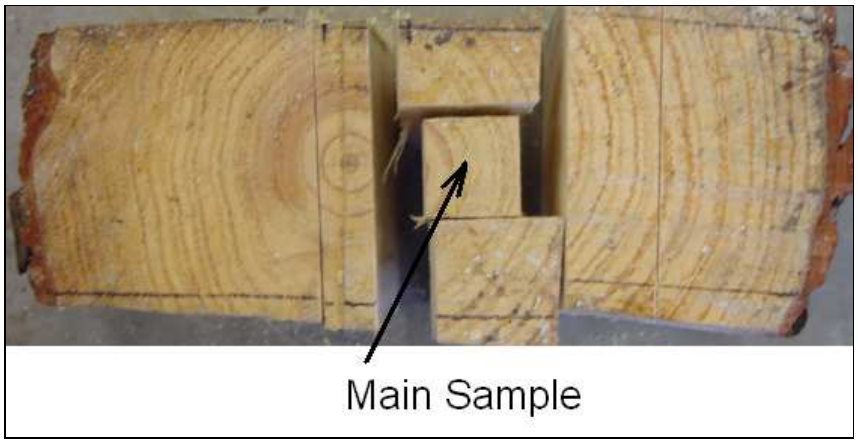

Figure 3-7: Main sample extraction from disc.

Immediately after the samples had been prepared, the weight and the dimensions were measured and then the samples were placed in the sample containers within the environment chamber, this will be discussed in the following section and in Appendix A. The relative humidity in the chamber was maintained as high as possible (over 90%) and the temperature was controlled at 30°C. The air velocity over the samples was adjusted to 3.3 m/s for each sample container. When the samples reached the equilibrium moisture content, the side edges or ends were wrapped with a layer of plastic food wrap (GLAD Wrap) followed by a layer of rubber tape, leaving open the two opposite surfaces of interest which were available for moisture transfer to the surrounding air. For the longitudinal samples, all of the side edges were sealed thus only two ends were exposed to the surrounding air. For the tangential samples, both ends and two side edges parallel to the tangential direction were sealed, thus the moisture moved only along the tangential direction. In a similar way for the radial samples, the two ends and two side edges parallel to the radial direction were sealed allowing the moisture to move in the radial direction.

The first layer prevented the rubber tape from sticking to the sample and also allowed the rubber tape to follow the shrinking material without forming air pockets. Preliminary experiments have shown that this kind of wrapping forms an impermeable coating when all of the four side edges and two ends were sealed. After the samples were sealed the effective length was marked. In this test, the samples were firstly equilibrated at 85% RH and then the samples were fully sealed using then above method. After the sealing, the samples were replaced in the chambers with the RH being decreased from 85% to 25%. The weight of the samples was measured over 9 days and no mass loss was detected over that time period.

In the experiments, both desorption and adsorption tests were performed. In the desorption tests, the sealed samples were placed in the controlled environment chamber in which the relative humidity was reduced to about 25% RH. The weight loss of the samples was recorded at time intervals until all of samples had reached the new equilibrium at the low RH.

In the adsorption tests, the relative humidity was increased to approximately 83%RH, and the weight gain was recorded at time intervals until all of the samples had reached the new equilibrium at the higher RH.

At the start of the desorption or adsorption test the time intervals for the weight measuring were around six hours and extended during the experimental runs up to twenty four hours due to the decreasing moisture loss or gain closer to the equilibrium moisture content.

After the adsorption test the coating of the samples was removed, and all the samples were oven-dried for the determination of the basic wood properties. Due to the high basic wood properties variability found in the samples, the sound of velocity of 38 longitudinal samples was measured and the results confirmed the high variability. The results are discussed in Section 3.2.2.

3.2.2 The environment chamber and its performance

The determination of the diffusion coefficient requires maintaining stable environment conditions over a long period of time. Therefore an existing apparatus and humidification system were modified and an environment chamber designed as shown in Figure 3-8. The volume of the environment chamber is 600 litres. Details on the system modification and the design of the environment chamber can be found in Appendix A. The system is based on one of the simplest and most common method for cooling and/or humidifying a gas stream via a counter current contact

with a liquid in a packed tower. The desired relative humidity is then achieved by heating the saturated gas to the dry bulb temperature. As seen from Figure 3-8, there are two circular windows on the front wall and a rectangular window on the top wall. The front circular windows are for removing the container with the samples in it, thus the environment is interrupted at the minimum when the samples are taken out for measurement. The top window is used for monitoring of the containers, the fans and the samples.

The volumetric flow rate of conditioned air was adjusted to 150 litres per minute. With this air flow rate the volume of air within the chamber (600 L) was replaced every 4 minutes. Controlled trace heating elements were installed on the outside walls of the chamber to maintain constant temperature as required in the chamber. Within the environment chamber, six tube containers are located, each of which is equipped with an adjustable fan for the air velocity. The air velocity was measured with a hot wire anemometer and set to 3.3 m/s. In the experiments performed, each container held 8 samples which were placed on a metal mesh supporter and, in this way, the airflow was always parallel to the exposed surfaces of the samples.

Figure 3-8: Environment chamber.

In the initial preliminary tests of the newly constructed environment chamber, the balance (Sartorius BP 110) was located on the top of the chamber. However, it was found that the balance reading was influenced by the airflow within the chamber and condensation occurred at the bottom of the balance. The condensation was severe at high relative humidity above 80%RH.

Therefore the balance was moved to the table close to the environment chamber during the formal experiments. During the experiments, the 8 samples in one container were removed together from the chamber for the weight measurement.

Time required for measuring all of the samples in the chamber was around 10 minutes. Based on the observation that the moisture movement within the samples was very slow during the experiments and the interruption of the environment in the chamber was minimal, it was assumed that removing the samples from the chamber for the weight measurements had insignificant impacts on the behaviour of drying or wetting of the samples during the experiments.

In order to ensure the conditions in the chamber were stable and the actual conditions to be used in the data analysis, the actual conditions achieved were recorded during the experiments. Figure 3-9 shows the relative temperature and humidity profiles within the chamber in the first run. The results show that, after the initial stabilization period, the temperature can be controlled satisfactorily with fluctuations less than 0.5°C. Similar performance can also be achieved for the RH control, although the initial stage shows slightly higher fluctuations than the two later stages.

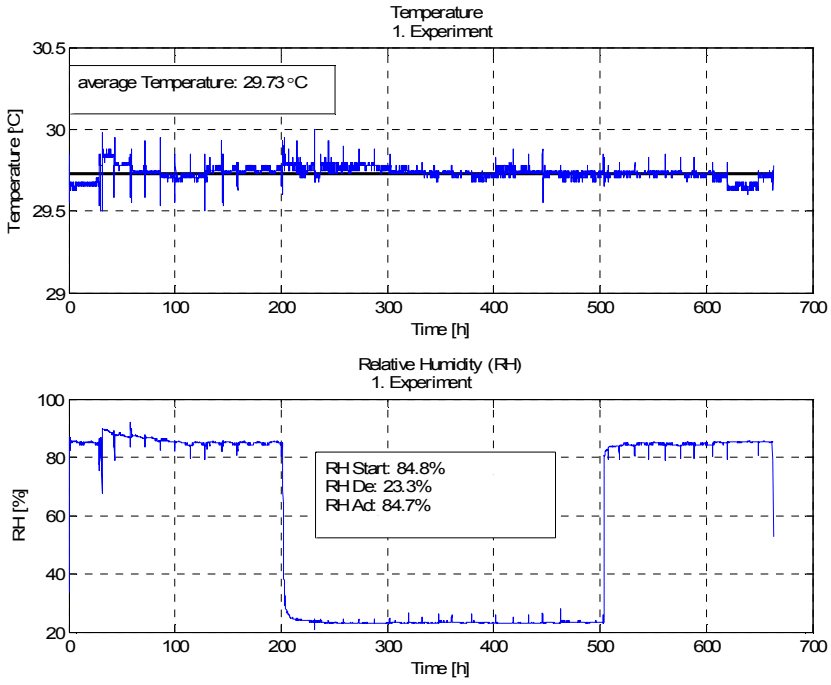

Figure 3-9: Temperature and relative humidity over time for the performance check of the environment chamber.

3.2.3 Experimental results on basic wood properties

The results on basic wood properties presented in this section serve the purpose of providing the reader a general understanding of the material used. A more detailed description of the material and individual samples can be found in Appendix B.

For the first experiment, the samples were identified by a combination of letters. This numbering system was then modified for the following experiments. The samples from the first experiment originated from butt logs of two trees. The first two characters identify the tree (A1, A2), followed by the letter B or T identifying the location within the butt log (bottom of top), and followed by the letter C or O represent the location of the sample (core or outer wood).

For the second and third experiments, the system was changed. In which the first number identifies the tree, followed by the disc location within the stem. The breast height samples, where actual cutting position varied from tree to tree between 1.2 m and 1.6 m, were identified by the combination 1.2m. Samples from higher locations were also identified within the second part with a variation of ±0.3 meters. The radial location followed the disc position where the number one was used to identify core wood sample and the number two for outer wood samples. It has to be mentioned that one disc within the second experiment (2/1.2m) contained compression wood and therefore the same identification system as for the fourth experiment was used.

For the fourth experiment, a similar numbering system was used as introduced for the second and third experiments with only one change. The character C was put in front of the tree number to identify the compression and opposite wood experiment. The last part, which was allocated for the radial location of the samples, was used to differentiate between compression (1) wood and opposite (2) wood.

The above system allowed the identification of the origin, the height and the radial location of the main samples. As mentioned previously, four samples were extracted from this main sample. These samples were used for the actual diffusion experiment and identified with the last characters of the above introduced identification systems of the main sample, where Re, L, T and R represented the reference sample (no coating), longitudinal, tangential and radial sample respectively.

Green moisture content

Green moisture contents were determined for all of the discs in the experiments using Equation 2-1. Due to the different seasons for the felling and different tree ages, the green moisture contents showed high variation between the test discs. As expected, the heartwood samples possessed much lower moisture content than the sapwood samples, but, the heartwood showed higher seasonal variation in the green moisture content. Samples from the third run were prepared over the winter months and the moisture content of heartwood was below 40%, whereas heartwood samples cut in the summer months varied from 80% to 150%MC. Green moisture contents of the sapwood were all above 100% varying from 105% to 190%MC. In general the green moisture content of sapwood had higher fluctuations, and no clear indication of the seasonal influence on the green moisture content could be observed.

Green moisture contents are shown in Figure 3-10 with each bar representing the average value of the four samples (Reference, Longitudinal, Tangential and Radial) from each location within the log.

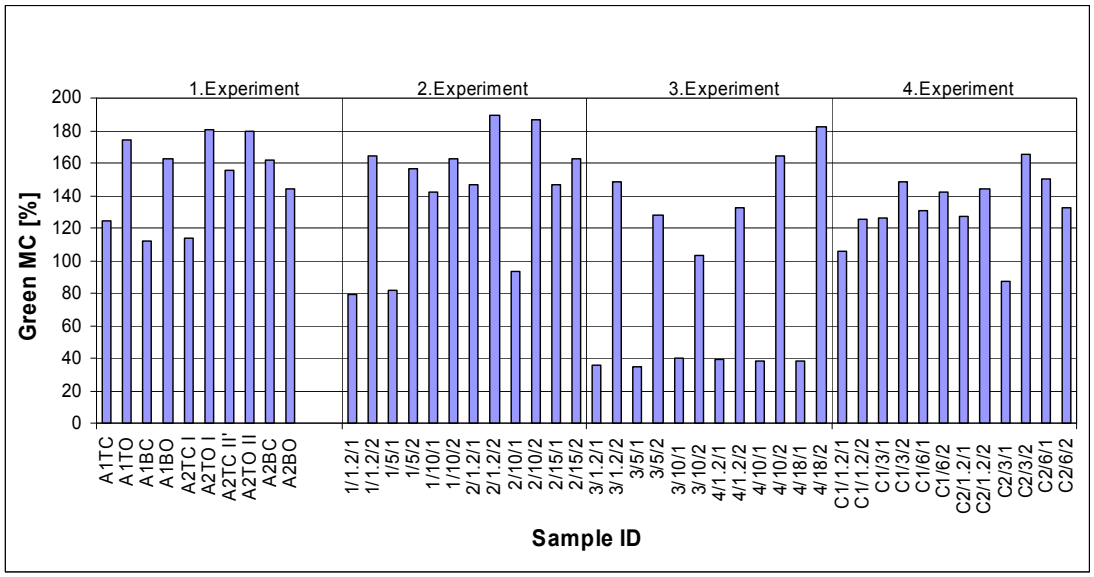

Figure 3-10: Green moisture content.

Wood basic density

Wood basic density was determined from the measured green dimensions and the oven-dry weight of all of the samples. The basic density is defined as follows:

$$\rho_{Basic} = \frac{m_{oven-dry}}{V_{green}} \tag{3-13}$$

The volume (V_{green}) was calculated from the green dimensions, measured with a veneer caliper.
The results of the measured basic density are shown in Figure 3-11, with each bar representing the average value of four samples from one location. The minimum density was 317 kg/m^3 for the sample in the second run. The maximum density was found for the fourth run with the value of 573 kg/m^3. The significant variation for the basic density as shown in Table 3-1 and Figure 3-11 are believed to be caused by the different sample locations within the disc and wood type (heartwood, sapwood, compression wood, opposite wood). The wood samples in the fourth run contained compression wood and opposite wood which were visually identified prior to the experiment. These samples have high density compared with normal wood.

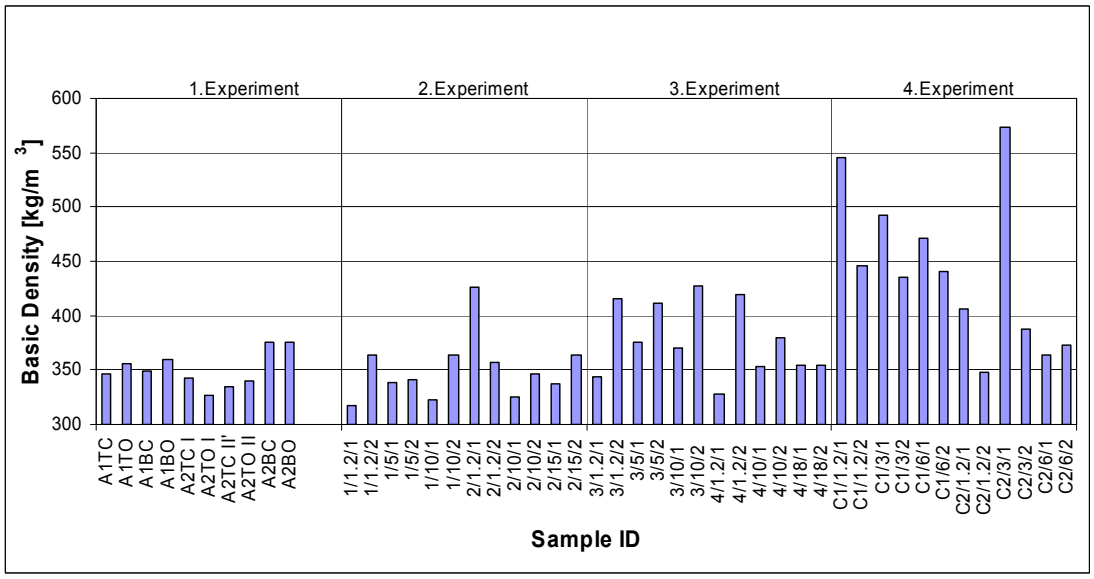

Figure 3-11: Basic density.

Equilibrium moisture content

Equilibrium moisture contents of all of the samples were determined from the measured weights and the oven dry weights of the samples at both high and low relative humidities. The relative humidity set points for the first run differed from the rests runs and, therefore, the equilibrium moisture contents (EMC) for the first run are shown in Figure 3-12 whereas the results from the other runs (run 2-4) are illustrated in Figure 3-13. The values shown in these figures are the equilibrium moisture contents for the reference samples. The reference samples were not sealed in the experiments and, therefore, should have reached equilibrium earlier than other samples.

In Figures 1-9 and 1-10, 'EMC 1' indicates the equilibrium moisture content obtained for the first RH setting (above 80%RH) in the desorption tests; 'EMC 2' represents the equilibrium moisture content obtained for the second RH setting (below 25%RH) in the desorption tests, and 'EMC 3' illustrates the equilibrium moisture content obtained for the third RH setting (above 80%RH) in the adsorption tests.

Average EMC values at 30°C for the first run are found to be around 21.5%MC, 6.2%MC and 18.6%MC for 85%RH, 23.5%RH and 85%RH, respectively. More detailed values for the individual trees and the corresponding standard deviations (STD) can be found in Table 3-1.

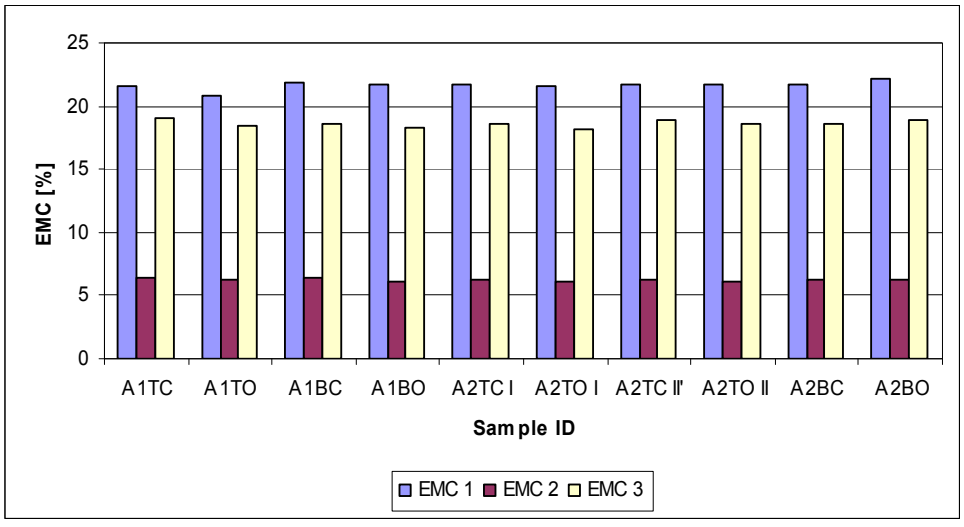

Figure 3-12: Equilibrium moisture contents for the 1. Experiment.

Table 3-1: Basic densities and EMC for the first run of experiment.

1. Experiment @ 30°C						
		Basic Density [kg/m³]	**Green MC [%]**	**EMC 1 85%RH [%]**	**EMC 2 23.5%RH [%]**	**EMC 3 85%RH [%]**
Tree A1	**Mean**	**352.87**	**143.26**	**21.50**	**6.25**	**18.58**
	Minimum	346.64	112.38	20.80	6.11	18.30
	Maximum	359.13	174.04	21.83	6.36	18.97
	STD	5.77	29.63	0.47	0.12	0.29
Tree A2	**Mean**	**348.98**	**155.92**	**21.77**	**6.20**	**18.62**
	Minimum	326.16	113.88	21.55	6.08	18.16
	Maximum	375.69	180.65	22.22	6.30	18.93
	STD	21.19	25.08	0.23	0.09	0.27

The relative humidity set points for the second, the third and the fourth runs of the experiments were identical. In this case, it is possible to directly compare the EMC values between different runs. EMC 1 values in the fourth run are found to be above 20% for all of the samples while the corresponding values (EMC 1) in the second and third runs are all below 20%. The differences in EMC2 and EMC3 between these three runs are not apparent. More detailed values for the individual trees and the corresponding deviations from the mean can be found in Table 3-2, Table 3-3, and Table 3-4 for the second run, the third run and the fourth run, respectively.

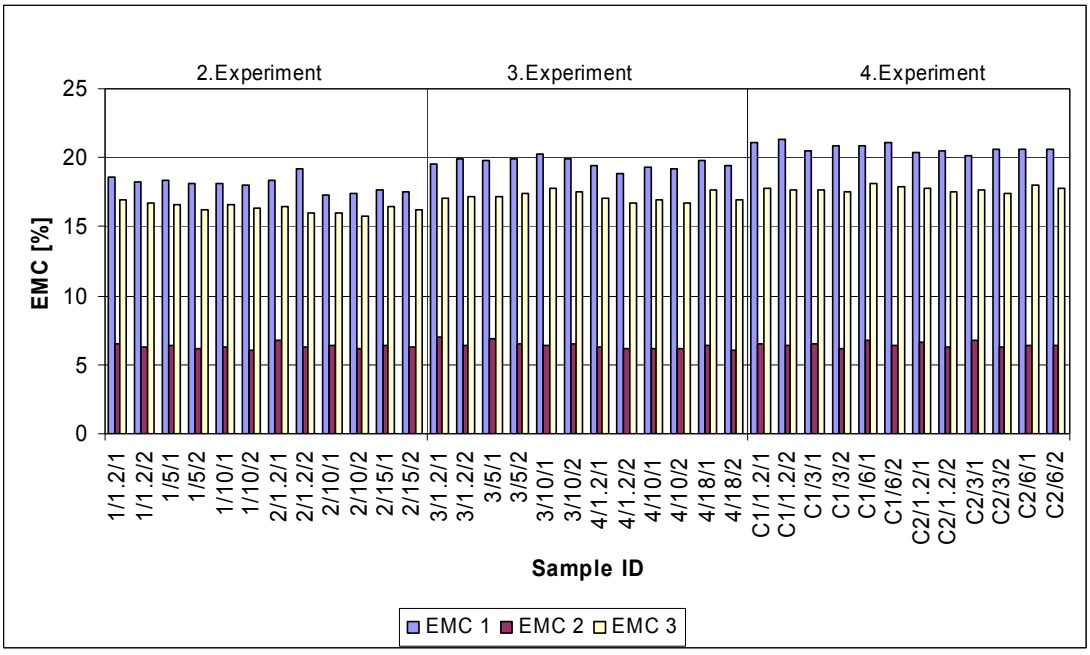

Figure 3-13: Equilibrium moisture contents for the 2. - 4. Experiment.

Table 3-2: Basic densities and EMC for the second run of the experiments.

2. Experiment @ 30°C						
		Basic Density	**Green MC**	**EMC 1 83%RH**	**EMC 2 25.5%RH**	**EMC 3 83%RH**
		[kg/m³]	**[%]**	**[%]**	**[%]**	**[%]**
Tree 1	**Mean**	**341.08**	**131.08**	**18.24**	**6.29**	**16.55**
	Minimum	316.98	79.44	17.97	6.09	16.19
	Maximum	363.67	164.88	18.63	6.48	16.93
	STD	19.64	40.03	0.23	0.14	0.27
Tree 2	**Mean**	**359.23**	**154.36**	**17.91**	**6.40**	**16.13**
	Minimum	322.91	93.75	17.31	6.09	15.74
	Maximum	426.45	189.65	19.23	6.70	16.48
	STD	35.67	35.04	0.74	0.17	0.30

Table 3-3: Basic densities and EMC for the third run of the experiments.

3. Experiment @ 30°C						
		Basic Density	**Green MC**	**EMC 1 83%RH**	**EMC 2 25.5%RH**	**EMC 3 83%RH**
		[kg/m³]	**[%]**	**[%]**	**[%]**	**[%]**
Tree 3	**Mean**	**390.70**	**81.72**	**19.88**	**6.60**	**17.37**
	Minimum	343.93	34.23	19.60	6.39	17.11
	Maximum	426.91	148.62	20.22	6.96	17.73
	STD	32.24	51.46	0.21	0.24	0.24
Tree 4	**Mean**	**364.65**	**99.05**	**19.34**	**6.20**	**17.02**
	Minimum	327.58	37.90	18.82	6.13	16.71
	Maximum	418.95	182.50	19.82	6.38	17.66
	STD	31.18	68.20	0.33	0.13	0.35

Table 3-4: Basic densities and EMC for the fourth run of the experiments.

4. Experiment @ 30°C						
		Basic Density	**Green MC**	**EMC 1 83%RH**	**EMC 2 25.5%RH**	**EMC 3 83%RH**
		[kg/m³]	**[%]**	**[%]**	**[%]**	**[%]**
Tree C1	**Mean**	**472.12**	**129.71**	**20.95**	**6.46**	**17.78**
	Minimum	434.74	105.34	20.48	6.14	17.55
	Maximum	546.07	148.38	21.35	6.72	18.07
	STD	42.33	15.05	0.29	0.20	0.18
Tree C2	**Mean**	**408.53**	**134.39**	**20.47**	**6.45**	**17.70**
	Minimum	348.32	87.22	20.10	6.26	17.41
	Maximum	572.91	165.65	20.63	6.73	18.01
	STD	82.89	26.82	0.20	0.19	0.21

Tangential and radial shrinkage at oven dry

As discussed in section 3.2.1, at the end of the first half adsorption experiment in each run, all of the samples were oven dried and the sample dimensions were measured. This allowed the calculation of the oven-dry shrinkage (SH) in the longitudinal, tangential and radial dimensions. However, the longitudinal shrinkage results are not reliable due to the short length of the samples; therefore the values are not shown here. The results for the tangential and radial shrinkage are shown in Figure 3-14 for the four runs, each bar representing the average values of the four samples from one location. The minimum tangential shrinkage and the minimum radial shrinkage were 3.3 % and 1.5%, respectively, with the corresponding maximum values being 8.1 % and 5%. The results also show that the average radial shrinkage was lower than the corresponding tangential shrinkage, which is consistent with the findings in this work as presented in Chapter 2.

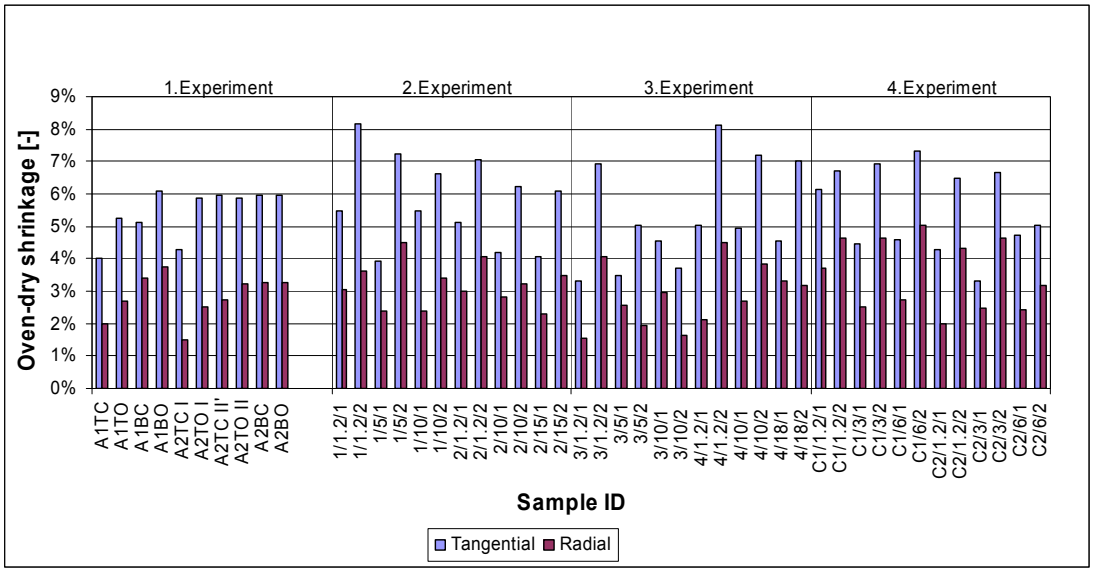

Figure 3-14: Tangential and radial oven-dry shrinkage.

Sound velocity measured using the longitudinal samples

The sound velocity, or the time required for a sonic wave to travel through a certain length of a wood sample referred to as time of flight (TOF), has frequently been used to predict the stiffness property of wood (Bell *et al.*, 1954; Kollmann and Cote, 1968). Cave (1968) investigated the relationship between the microfibril angle and the Young's modulus and found the correlation significant.

In this work, after the completion of the experiments, the TOFs of 38 longitudinal samples were measured in the longitudinal direction by Ensis (Harrington, *personal communication*). Prior to the measurements the samples were stored for approximately a week in an environment chamber to equilibrate all of the samples at the moisture content of around 10%. The TOF measurements were performed for validation purposes to cross check the high variability of the samples. For the TOF measurement a frequency of 500 kHz was used. The measurement device was described as USD-10 by Ensis.

Figure 3-15 shows the correlation between TOF and the oven-dry shrinkage of the samples. Whereas the shrinkage used in this illustration represents the volumetric shrinkage which can be calculated from the tangential and radial shrinkage as the longitudinal shrinkage was negligible in comparison with the tangential and radial shrinkage. The equation for the calculation of the volumetric shrinkage can be found in 3.3.6 (Equation 3-23).

As shown in Figure 3-15 there is a relative strong correlation between the TOF (time of flight) and the oven-dry volumetric shrinkage. Only one sample shows a high variation from the rest of the data, which might have been caused by measurement errors. When ignoring this particular sample, a formula of the second order polynomial can fit to the data closely with the R^2 of 0.71. It is interesting to note the trend that the TOF increases with the volumetric shrinkage of the wood. In Figure 3-15, the samples of compression wood samples are also included as highlighted with the circular marked data points and these samples tend to have lower TOF and lower volumetric shrinkage. The lower TOF (lower stiffness) for the compression wood is expected due to the high microfibril angle with the compression wood. However, the low volumetric shrinkage may can be explained by the high longitudinal shrinkage. Normally wood with high longitudinal shrinkage shows low transverse shrinkage. Due to the low scale of the longitudinal shrinkage compared with the transverse shrinkage, the volumetric shrinkage is lower than the normal wood. Similar behaviour for core wood can be expected.

From Figure 3-15, it is observed that there are a number of wood samples having similar behaviour as the compression wood (low volumetric shrinkage and low TOF). As this was out of the scope of this project no further work was performed to identify these samples.

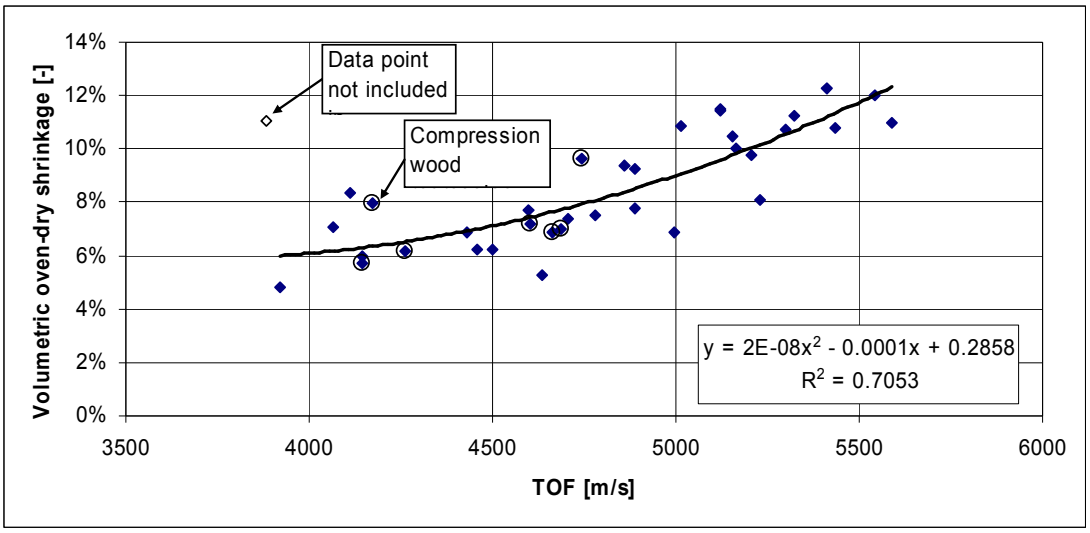

Figure 3-15: Correlation between area shrinkage (oven-dry) and time of flight (TOF) measurements.

3.2.4 Inverse determination of the diffusion coefficient

The mathematical procedure for the determination of the diffusion coefficient is discussed in this section. The mathematical model of the unsteady-state bound water diffusion based on concentration potential is given by the second Fick's law:

$$\frac{\partial C}{\partial t} = \frac{\partial}{\partial x}\left(D \frac{\partial C}{\partial x} \right) \tag{3-1}$$

The water concentration in wood can be determined from the wood basic density (ρ_{basic}) and the moisture content (MC) by the following equation:

$$C = \rho_{Basic} \cdot MC \tag{3-14}$$

From the conclusion of Siau (1995), Hunter (1991; 1992) and Liu (2001), the diffusion coefficient increases with moisture content and thus an empirical model to describe the effect of the moisture content on the diffusion coefficient is proposed as (Droin-Josserand *et al.*, 1989):

$$D = D_0 \cdot e^{K_0 \cdot MC} \tag{3-15}$$

In which,

D_0 Constant diffusion coefficient [m^2/s]

K_0 Constant

In solving the Fick's second law, it is commonly assumed that the initial moisture content distribution within the material is uniform at the beginning of the drying. Assuming the material density is also uniform through the materials, the initial moisture concentration distribution is also uniform:

$$C = C_0 \qquad \text{at } t=0 \tag{3-16}$$

The boundary condition is defined as the moisture flux through the air-wood boundary which can be determined by the surface emission coefficient (h_m) and the concentration difference between the wood surface and the main stream:

$$-D\frac{\partial C}{\partial x} = h_m \cdot (C_s - C_{eq}) = h_m \cdot \rho_{Basic} \cdot (MC_s - MC_{eq}) \tag{3-17}$$

The constant diffusion coefficient (D_o) and the constant (K_o) introduced in Equation (3-15) can be determined by solving the inverse transfer problem. The objective function is defined as the sum of squares of the residuals of the measured and predicted values of the average water concentration at different times through the experiments:

$$F(x) = \sum_{i=1}^{NT}\left[C_{Exp}(t_i) - C_{\Pr ed}(t_i)\right]^2 \tag{3-18}$$

The nonlinear least square problem is solved with the 'Optimization Toolbox' in Matlab 7.0. In doing so, the algorithm is a subspace trust region method and is based on the interior-reflective Newton method described in Coleman *et al.* (1996a; 1996b) and Thomas *et al.* (1994). Each iteration involves the approximate solution of a large linear system using the method of preconditioned conjugate gradients (Matlab Help). The partial differential system at each iteration step is also solved with a pre-defined Matlab function (*pdepe.m*). The ordinary differential equation resulting from discretisation in space are integrated to obtain the solutions at specified times. Detailed description of the algorithm can be found in Shampine *et al.* (1997).

Due to the ill-conditioned nature of the solution matrix and to enable it to determine the moisture dependence on diffusion, the nonlinear least square method constrained the parameter K_0 from 0 to infinity. This assumption was justified with theoretical (Hunter 1992) and experimental studies (Liu 2002, Skaar 1954), which found that the diffusion coefficient increases with increasing moisture content.

Figure 3-16 illustrates the program structure of the inverse method. For a given experiment and sample, the emission coefficient is calculated as described in Section 3.1.2. The concentration is then calculated from the mean basic density and the moisture content at specific times. The nonlinear least square solver minimizes the objective function by varying the constants in Equation

(3-15) until the algorithm terminates based on the preset convergence criteria. At each iteration step the partial differential equation is solved for the new constants and afterwards the average concentration at specific times is calculated from the solution.

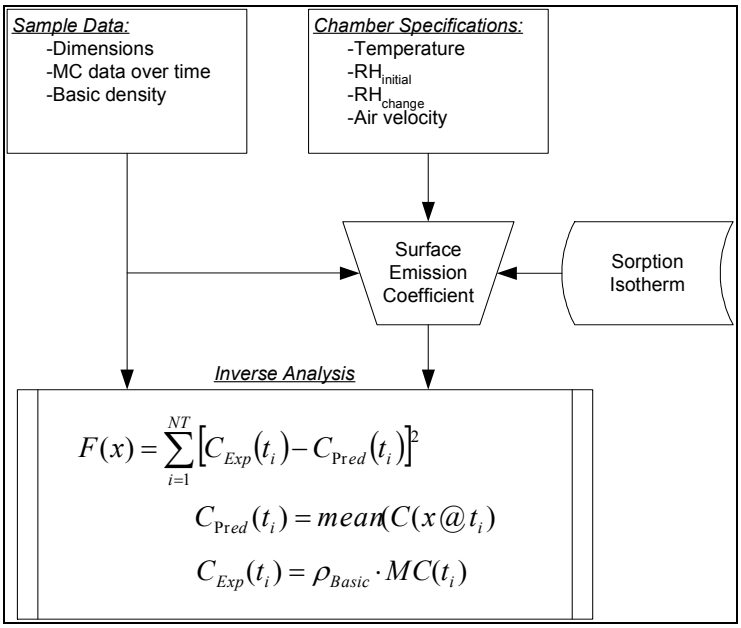

Figure 3-16: Basic principle and procedures of the inverse algorithm.

Discussion of the quality of the fitting parameters

In the following section, the "quality of the fitting" for desorption and adsorption are discussed. Although later in this chapter two different errors are introduced. This section uses commonly used statistical methods to show the accuracy of the applied numerical techniques.

Figure 3-17 shows the obtained fitted drying curves from the inverse method with the experimental results for one sample in the three diffusion directions. Tables 3-5 and 3-6 contain the summary of the analysis of the performed non-linear regression. The average correlation coefficients and standard deviations for all the samples were found to be 99.74% ±0.25% and 99.80% ±0.22% for desorption and adsorption, respectively. The variations of the slopes, between the experimental and the fitted average moisture contents at certain times, were 0.9941 for desorption and 0.9966 for adsorption. Figures 3-18 and 3-19 show the experimental and derived moisture contents for all the experimental data points for desorption and adsorption. Especially for desorption it was found, that at relative high moisture contents the deviations are higher than at lower MCs. Therefore two new errors have been introduced (3.2.1) to allow for a more critical analysis of the derived constants.

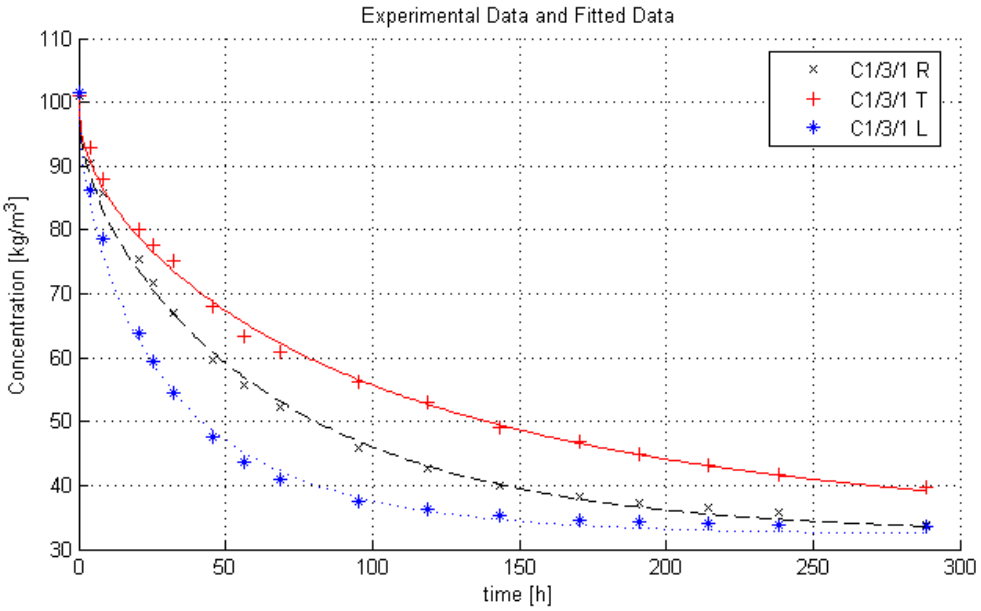

Figure 3-17: Fitted drying curves with experimental data for one sample in the three diffusion directions.

Table 3-5: Summary of the "quality of fit" for the desorption experiment.

Over-All	R^2	Slope	MC uncertaintiy
Desorption	[-]	[-]	[±%MC]
Average	99.74%	0.9941	0.116
Min	98.81%	0.9864	0.009
Max	99.96%	1.0002	0.261
Std	0.25%	0.0033	0.070

Table 3-6: Summary of the "quality of fit" for the adsorption experiment.

Over-All	R^2	Slope	MC uncertaintiy
Adsorption	[-]	[-]	[±%MC]
Average	99.80%	0.9966	0.061
Min	98.70%	0.9813	0.002
Max	99.96%	1.0201	0.210
Std	0.22%	0.0083	0.053

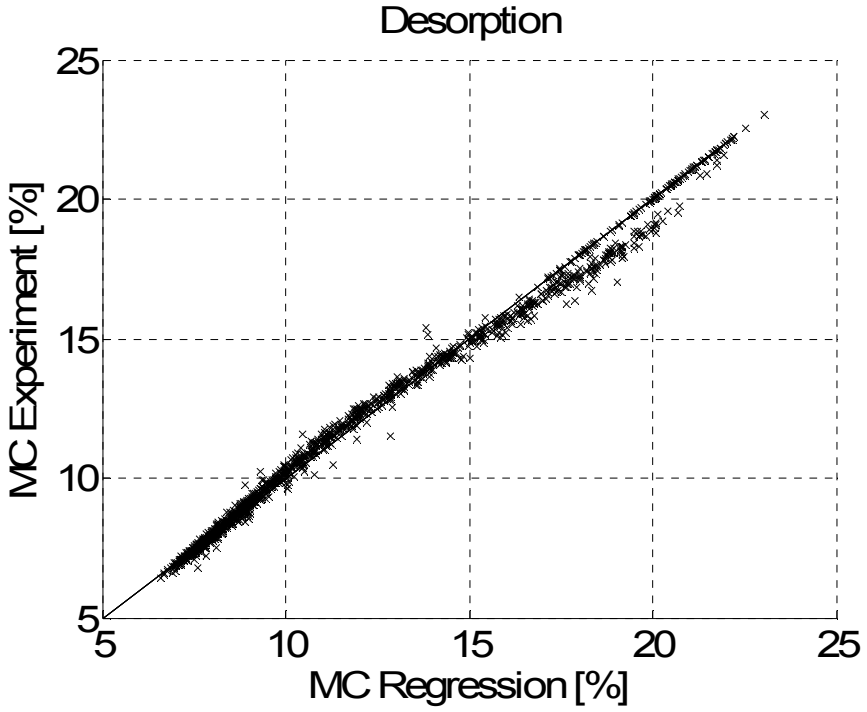

Figure 3-18: Experimental and derived moisture content for desorption, for all samples.

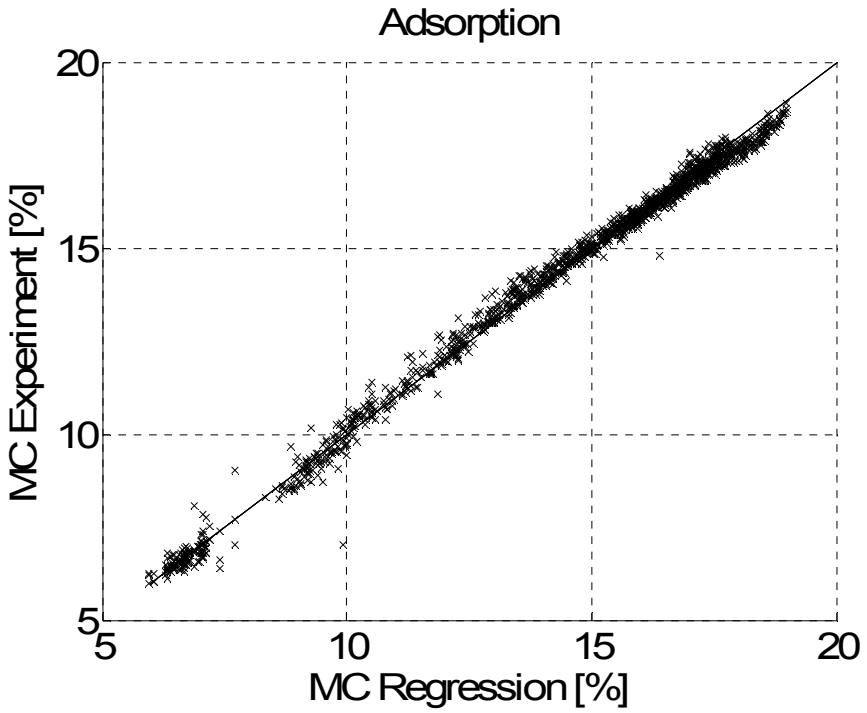

Figure 3-19: Experimental and derived moisture content for adsorption, for all samples.

3.3 Results and Discussion

Prior to the presentation of the results, it is helpful to understand the mechanisms for the water movement in wood during the drying or wetting processes. This can be analysed based on the wood microstructure and wood-water interaction. In this way, we can understand the physical meanings of the water diffusion coefficient and the constants used to determine the diffusion coefficient. From such analysis, the application and limitation of the water diffusion coefficient and the Fick's law can be understood. In the hygroscopic range, water exists in wood as bound water and water vapour with the bound water movement as the dominant phenomenon at low temperature. Water molecules have to cross several barriers on their way through the wood.

Radiata pine is a soft wood species and therefore its cellular structure is relatively simple with most of the wood structures consisting of hollow end-closed cells, which are also called tracheids. For normal radiate pine wood, the tracheids have average dimensions of 38.35 μm in tangential diameter, 3.45 μm in wall thickness and 2.72 mm in length (Kininmonth and Whitehouse, 1991). However, these dimensions vary significantly both between trees and within a single tree. In addition to the tracheid dimension variation, the chemical composition of the tracheid wall also varies, which may affect the water bounding. Between the individual tracheids is the middle lamella which contains a high content of lignin. On the tracheid walls, there are bordered pits which allow for liquid water to flow through the sapwood lumens in a living tree.

However, in the heartwood or during the drying of the sapwood, these pits are aspirated (closed), either completely or partially, which affects the vapour movement when the moisture content is below the fibre saturation point.

The main path obstructions for water movement include the cell wall, the lumen space, the middle lamella, boundaries between the earlywood and the latewood, and boundaries between the heartwood and the sapwood. All of these mentioned obstructions vary significantly within a tree. For example lumen length increases from pith to bark. Latewood content also varies along the radius. In this work, the influence of the above wood structures and chemical components are reflected by the constant diffusion coefficient (D_o) and the constant (K_o) in determination of the effect water diffusion coefficient (D) as described by Equation (3-15).

In general, high values of the diffusion coefficient (D) imply faster movement of moisture. The constant K_0 can be seen as a substitute for the activation energy for the moisture and lower values

can be interpreted as meaning that moisture content has less impact on the water diffusion coefficient.

In the following sections, the diffusion parameters determined from the desorption tests and the variations between trees are analysed, followed by the discussion of the adsorption results. Afterwards the variation of the diffusion parameters in the disc radial direction (growth rings) and with tree height are investigated. Then the derived coefficients are compared with literature data. Finally, the diffusion coefficients for different wood types (heartwood, sapwood, compression wood and opposite wood) are compared.

The sample identification is mentioned in section 3.2.3 and more detailed information on the individual main samples can be found in Appendix B.

3.3.1 Diffusion parameters for desorption

The diffusion parameters were determined by using the inverse method. The input parameters include the sample properties and the surrounding conditions. The sample properties are wood basic density and the effective length through which the moisture diffusion occurred. Prior to the discussion of the results for the individual trees, the solutions for all samples will be presented and possible relationships between the estimated parameters will be examined. Furthermore, two errors will be introduced to quantify the accuracy of the fitted parameters.

Figure 3-20 contains the derived parameter D_0 for the desorption process for all samples in the three directions (longitudinal, tangential and radial). For the results, it can be seen that the constant diffusion coefficient in the longitudinal directions is always higher than in transverse the directions. In addition, for most samples the D_0 constant in the radial is higher than in the tangential direction.

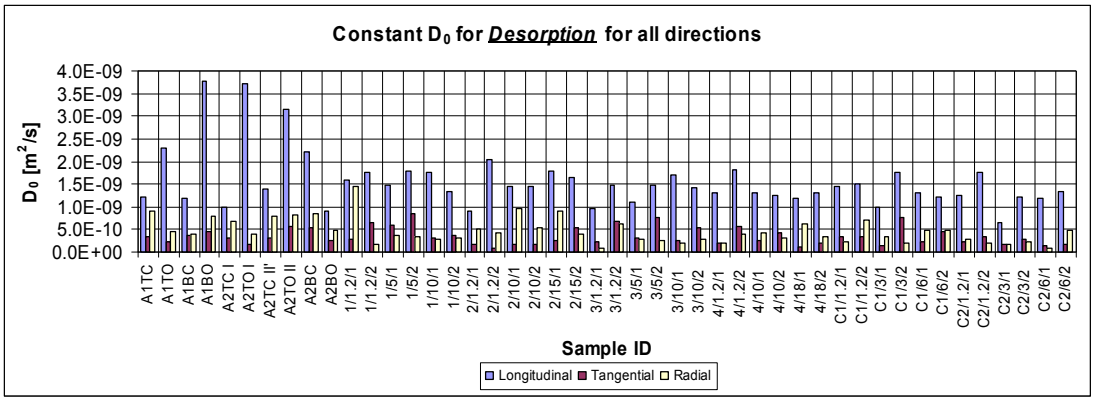

Figure 3-20: Desorption D_0 parameter for all experiments.

The fitted results for the constant K_o are shown in Figure 3-21, from which it is observed that the effect at different directions in the timber is much less but the variation between samples is much higher than those of constant diffusion coefficient D_0. Therefore, no clear distinction between the three diffusion directions can be found for the constant K_o.

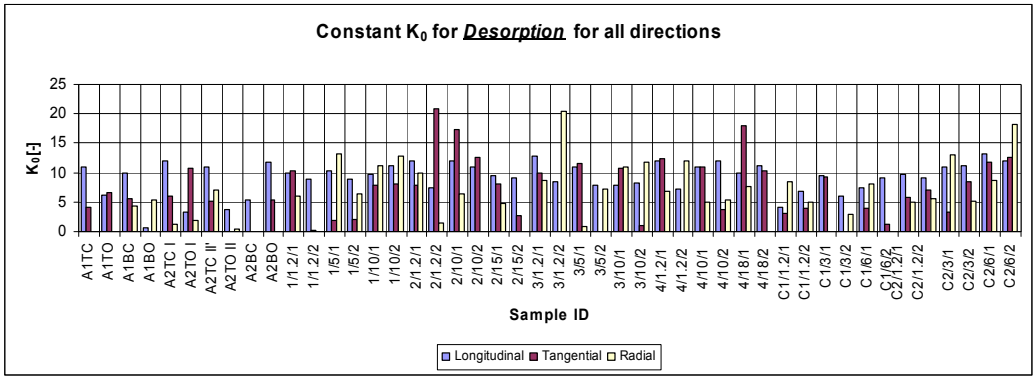

Figure 3-21: Desorption K_0 parameter for all experiments.

Table 3-7 contains the average values of the constant diffusion coefficient D_o and constant K_o for all of the three directions. The average values for D_0 in the longitudinal direction are about 4 times higher than those in the transverse directions, whereas the values for the tangential direction and the radial directions are similar, the difference being within the error range. For the constant K_o, the average values and the range of variations are in the same order for the three directions with average values from 5.95 in the radial direction to 9.2 in the longitudinal direction.

Table 3-7: Average, standard deviation (STD), maxima and minima values of parameters for desorption.

Summary All Samples	Longitudinal		Tangential		Radial	
	D_0	K_0	D_0	K_0	D_0	K_0
	[m^2/s]	[-]	[m^2/s]	[-]	[m^2/s]	[-]
Average	1.56E-09	9.20	3.54E-10	6.58	4.62E-10	5.95
STD	6.25E-10	2.70	1.89E-10	5.19	2.75E-10	4.97
Maximum	3.77E-09	13.15	8.65E-10	20.85	1.46E-09	20.38
Minimum	6.39E-10	0.70	7.60E-11	0.00	7.66E-11	0.00

Once the constant diffusion coefficient (D_o) and the constant (K_o) are known, the effective diffusion coefficient (D) can be calculated at a given average moisture content using Equation (3-15). Figure 3-22 illustrates the calculated results for the three diffusion directions as a function of the average moisture content. In the figure, the subscripts L, T and R in the diffusion coefficient D indicate the longitudinal, tangential and radial directions. The thin lines represent the individual samples and the thick lines show the average values.

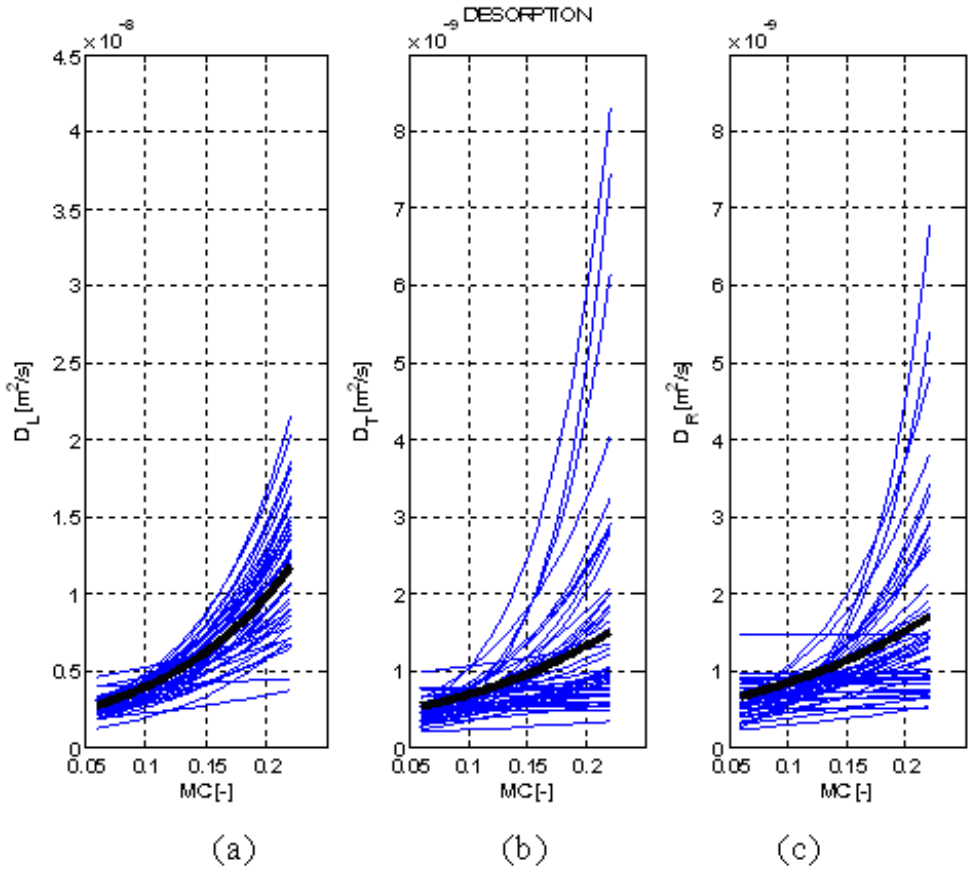

Figure 3-22: Average diffusion coefficient (thick lines) and values of individual samples (thin lines): (a) longitudinal, (b) tangential, (c) radial.

In order to analyse the accuracy in the parameter fitting, Olek *et al.* (2005) introduced a local relative error (e_1) and a global relative error (e_2) in using the inverse method. These errors are defined as follows:

$$e_1 = 100 \cdot \frac{\left| C_{Exp}(t_i) - C_{\Pr ed}(t_i) \right|}{C_{Exp}(t_i)} \tag{3-19}$$

$$e_2 = 100 \cdot \frac{\sqrt{\sum_{i=1}^{NT} \left[C_{Exp}(t_i) - C_{\Pr ed}(t_i) \right]^2}}{\sqrt{\sum_{i=1}^{NT} C_{Exp}(t_i)^2}} \tag{3-20}$$

Figure 3-23 shows the maximum local relative error (e_1) for all samples. The average values are 5.45%, 5.84% and 6.07% for the fitted diffusion parameters in the longitudinal, tangential and radial direction, respectively. In general, all of the samples have local relative errors of less than 10% with only 6 samples exceeding this threshold and only one sample's longitudinal error (2/1.2/2) standing out with a local relative value of 23%.

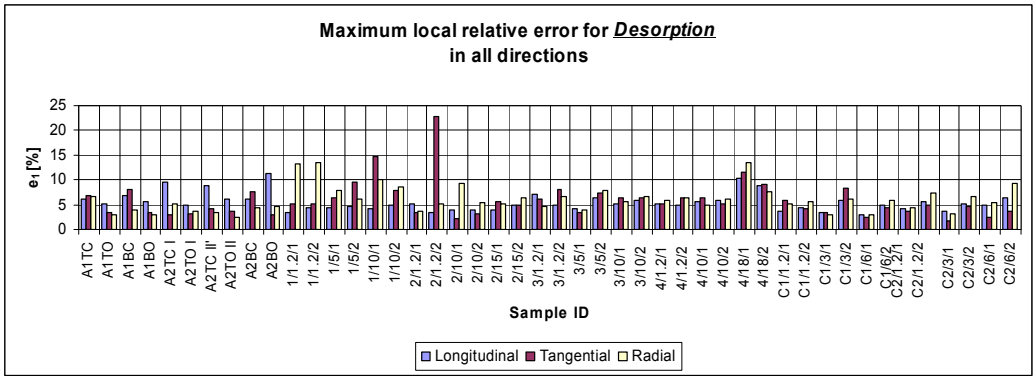

Figure 3-23: Maximum local relative error of all samples for desorption.

Figure 3-24 shows the global relative error (e_2) for all samples. The average error values are 2.95%, 2.9% and 2.75% for the fitted diffusion parameters in longitudinal, tangential and radial directions, respectively. Overall the global relative error was below 6%, with just three samples exceeding this threshold value. Again, the sample 2/1.2/2 shows the highest global relative error of 14.8% in the longitudinal diffusion parameter fitting. Further examination shows that this sample deviated highly from the predicted concentrations especially during the first 100 hours after the start of the desorption experiment, and thus it is believed that there was a fault in the sealing of this sample during the experiment.

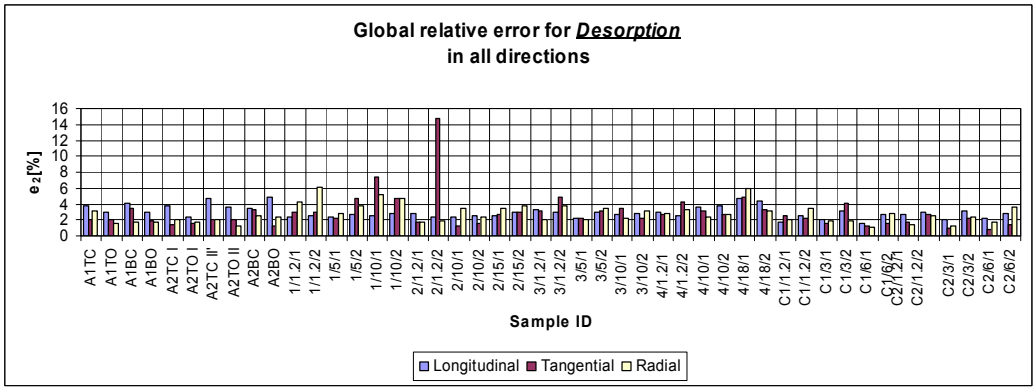

Figure 3-24: Global relative error of all samples for desorption.

Further analysis was performed in this area to examine whether there is any correlation between the constant diffusion coefficient (D_o) and the constant (K_o) both of which are included in Equation (3-15) to determine the effective diffusion coefficient (D). The results are shown in Figure 3-25. As a general trend, the constant, K_o, decreases by increasing the diffusion coefficient, D_0. The correlations for the transverse diffusion are very similar but the longitudinal diffusion shows a much less slope between these two parameters. As already mentioned, the values for D_0 in the longitudinal direction are higher than that in the transverse directions. In addition, most of the values for longitudinal K_0 fall in a range between 4 and 14 which is much narrower than the range of K_o values in the transverse directions (0 to 20).

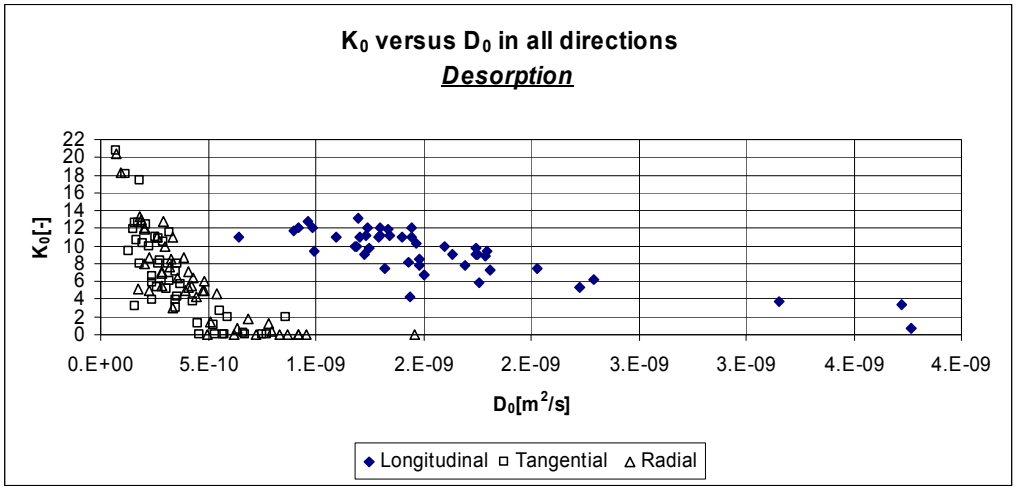

Figure 3-25: K_0 versus D_0 in all directions for desorption.

In Figure 3-25, there seems to be a linear relationship between K_0 and D_0 in the longitudinal direction. Therefore, a linear regression analysis was performed and the results confirm this relationship with reasonable significance (Figure 3-26).

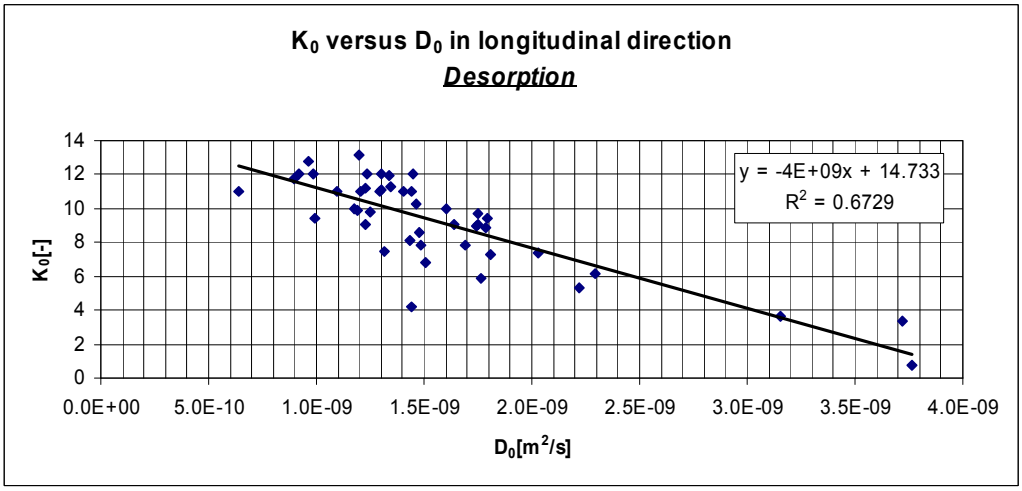

Figure 3-26: K_0 versus D_0 in the longitudinal direction for desorption.

A similar linear regression was also performed for the relationship between K_o and D_o in the transverse directions but the correlation was found not to be significant thus a logarithmic regression analysis was conducted which led to a high R-square value of 0.727 for the tangential direction as shown in Figure 3-27 and 0.788 for the radial direction as shown in Figure 3-28.

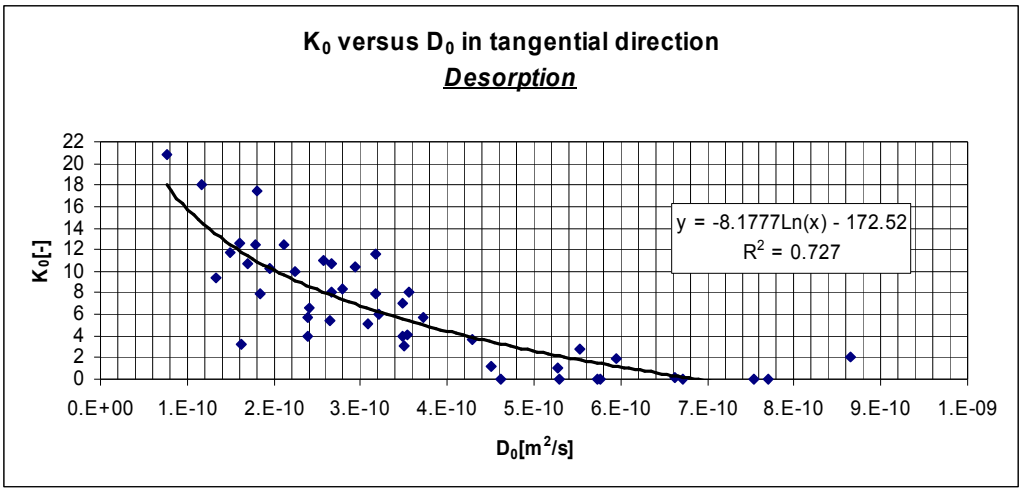

Figure 3-27: K_0 versus D_0 in the tangential direction for desorption.

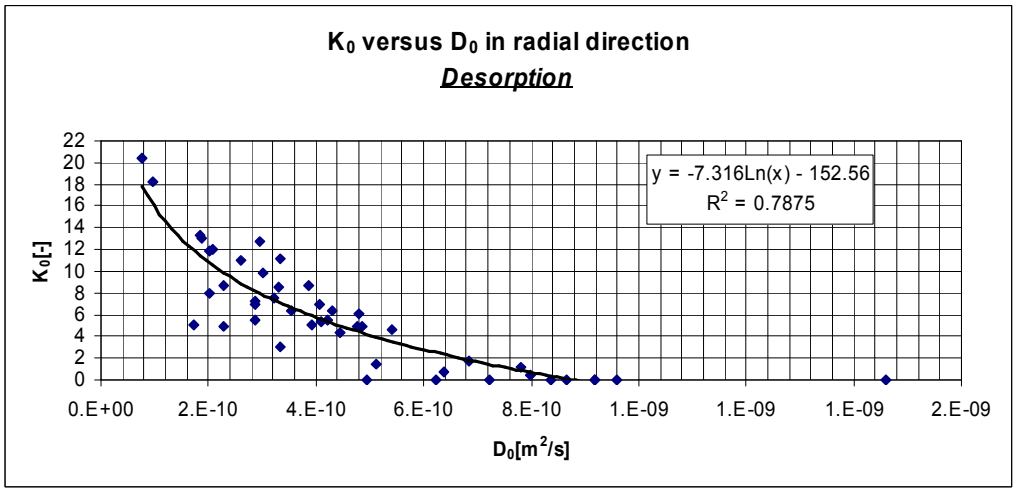

Figure 3-28: K_0 versus D_0 in the radial direction for desorption.

The different correlations between the constant (K_o) and the constant diffusion coefficient (D_o), and, the different correlations between the effective diffusion coefficient (D) and the average moisture content in different directions may be caused by the differences in the resistances for moisture movement.

The parameters may also be influenced by the actual length of the samples where diffusion takes place. Therefore the effect of the diffusion dimension (green) of the samples on the constant diffusion coefficient (D_o) were analysed and the results are shown in Figure 3-29 to Figure 3-31. The diffusion dimension is the sample length for the longitudinal diffusion samples and the width or thickness for the transverse diffusion samples.

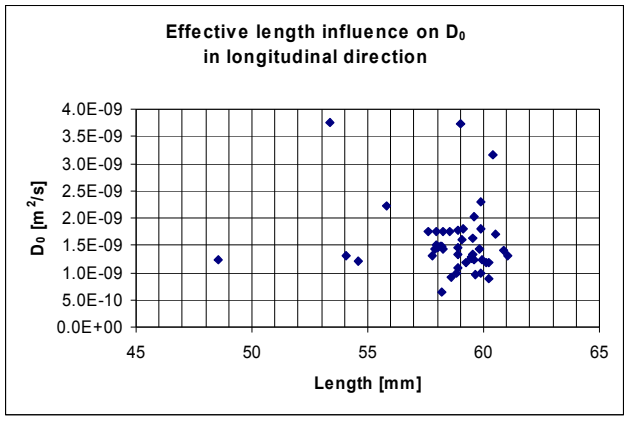

Figure 3-29: Effect of the sample's diffusion dimension on D_0 in longitudinal direction.

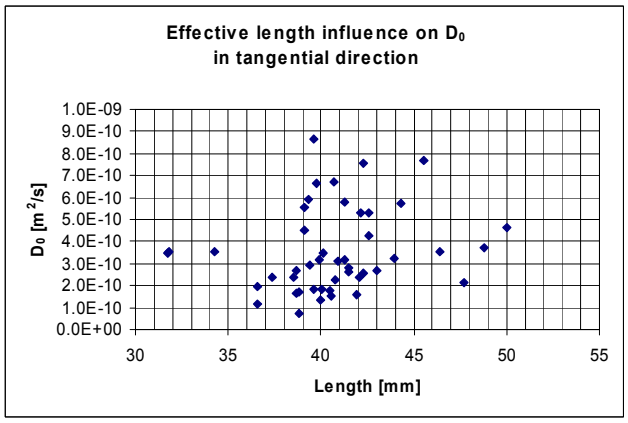

Figure 3-30: Effect of the sample's diffusion dimension on D_0 in the tangential direction.

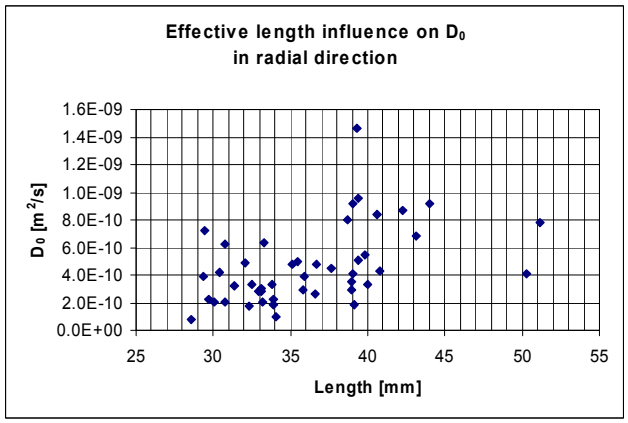

Figure 3-31: Effect of the sample's diffusion dimension on D_o in the radial direction.

From the analysis results in Figure 3-29 to Figure 3-31, there is no evidence to confirm that the diffusion coefficient is influenced by the sample's diffusion dimension in the longitudinal direction. Weak correlation is observed for the tangential and the radial directions, which could be caused by the curvature of the growth rings of the tangential direction and the boundaries between the early and the late wood for the radial direction. The correlation coefficients were 0.02, 0.04 and 0.21 in longitudinal, tangential and radial directions, respectively.

Comparison of diffusion parameters between trees

In this section, the diffusion parameters averaged over individual trees are compared and the results are shown in Figures 3-27 to 3-30. For the longitudinal diffusion, Figures 3-27 and 3-28 show the average constants over each tree and the error bars indicate the maximum and the minimum values within the corresponding tree. Figure 3-34 shows the constant diffusion coefficient (D_o), and Figure 3-35 shows the constant (K_o). in the transverse directions.

For the longitudinal diffusion, Trees A1 and A2 in the first run have the highest constant diffusion coefficient (D_o) and the lowest values for the constant (K_o). For both of these parameters, the Trees A1 and A2 show the highest deviation between samples. These results indicate that the moisture in the younger trees moves faster, and the diffusion coefficient is less dependent on the moisture content, than in the older trees.

However, the trend of the diffusion parameters between trees is not apparent for the transverse moisture diffusion except that the two younger trees (Trees A1 and A2) tend to have higher values for the constant diffusion coefficient (D_O) in the radial direction (Figure 3-34) and lower value for the constant (K_o) in the both of the transverse directions (Figure 3-35). It is interesting to note that the compression wood does not shown apparently abnormal behaviour in terms of the moisture diffusion properties, however, the compression wood tends to have lower values for the constant (K_o) in the transverse directions (Figure 3-35) and the opposite wood tends to have low values for the constant diffusion coefficient (D_o) in the same directions (Figure 3-34).

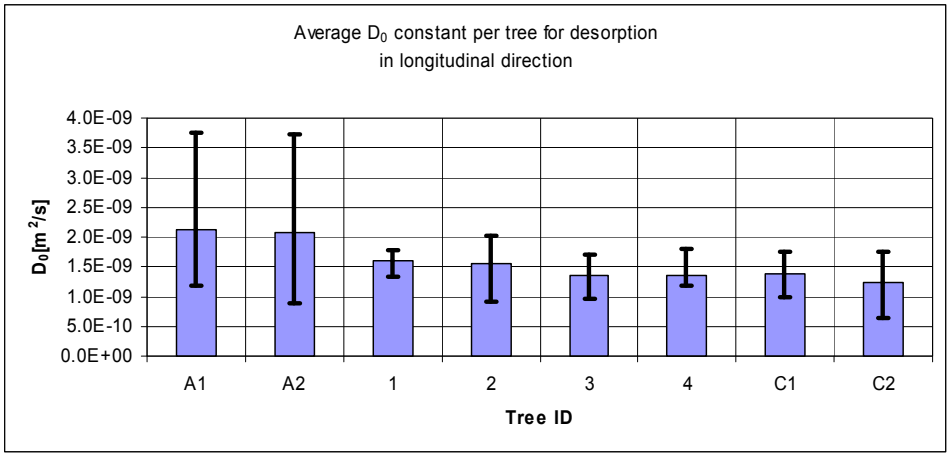

Figure 3-32: Average constant diffusion coefficient (D_0) over each tree in the longitudinal direction.

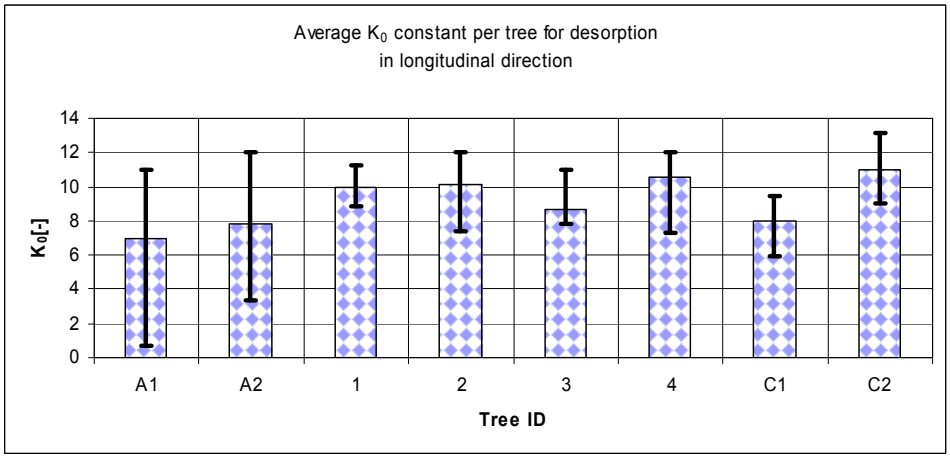

Figure 3-33: Average constant (K_0) over each tree in the longitudinal direction.

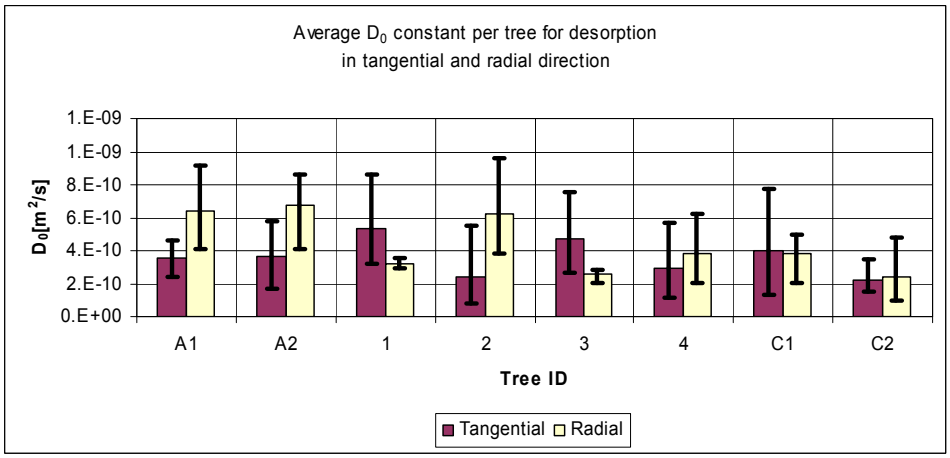

Figure 3-34: Average constant diffusion coefficient (D_0) over each tree in transverse direction.

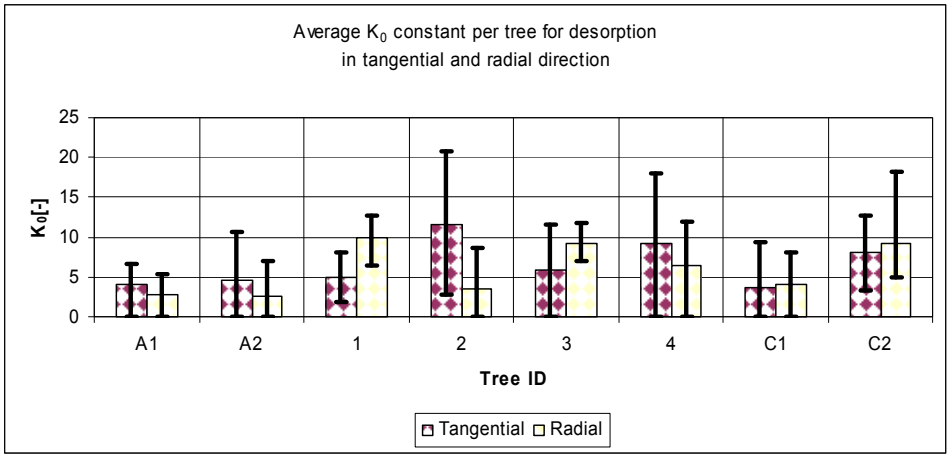

Figure 3-35: Average constant (K_0) over each tree for desorption in the transverse direction.

3.3.2 Diffusion parameters for adsorption

The inverse method has also been applied for all samples with the adsorption tests. The results for the determined values of constant diffusion coefficient, D_0, and constant, K_0, are illustrated in Figures 3-31 and 3-32, respectively.

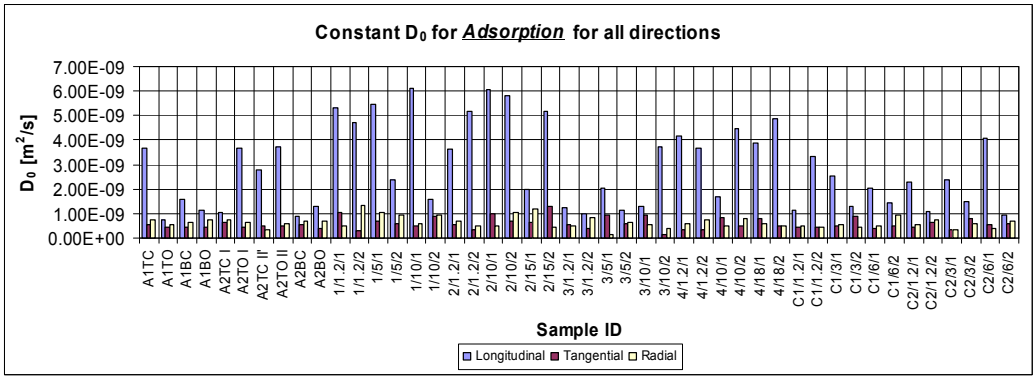

Figure 3-36: Adsorption constant diffusion coefficient, D_0, for individual samples.

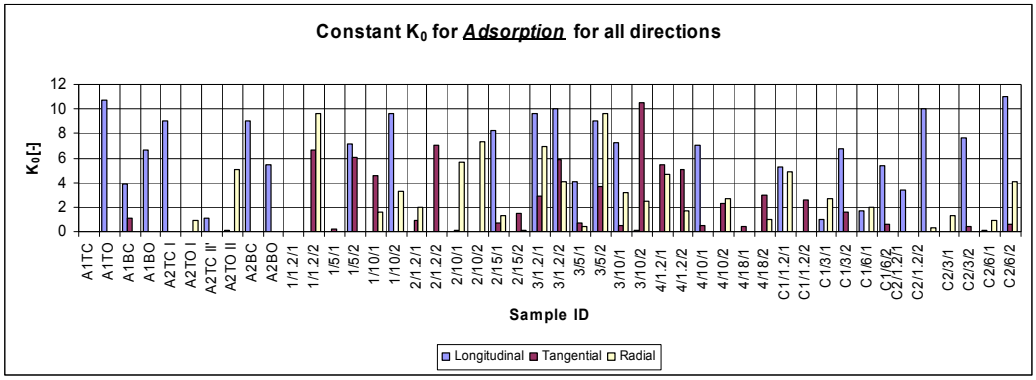

Figure 3-37: Adsorption constant, K_0, for individual samples.

Table 3-8 contains the average values for the diffusion parameters determined for all of the test samples in adsorption. Consistent with the findings in the desorption process, the constant diffusion coefficient, D_0, in the longitudinal direction is approximately five times higher than those in the transverse directions, with the average value for the tangential direction (5.85×10^{-10} m^2/s) being similar to that in the radial direction (6.46×10^{-10} m^2/s). Once again, the values for the constant, K_o, in the three directions are of the same magnitude ranging from 1.64 for the tangential direction to 3.7 for the longitudinal direction. Compared with the results in the desorption process, a clear trend is found that the values of both the constant diffusion coefficient (D_o) and the constant (K_o) in the adsorption are lower than the corresponding values in the desorption process. This trend confirms that the moisture movement in the adsorption is slower than that in the desorption when the wood is dried from green.

Table 3-8: Average, standard deviation (STD), maxima and minima values of parameters for adsorption.

Summary All Samples	Longitudinal		Tangential		Radial	
	D_0	K_0	D_0	K_0	D_0	K_0
	[m^2/s]	[-]	[m^2/s]	[-]	[m^2/s]	[-]
Average	2.85E-09	3.70	5.83E-10	1.64	6.46E-10	1.97
STD	1.64E-09	4.00	2.24E-10	2.47	2.26E-10	2.58
Maximum	6.09E-09	11.01	1.29E-09	10.55	1.33E-09	9.59
Minimum	7.50E-10	0.00	1.57E-10	0.00	1.71E-10	0.00

Using Equation (3-15), the effective diffusion coefficient (D) can be calculated at a given average moisture content. Figure 3-38 illustrates calculated diffusion coefficient as a function of the moisture content, with the thin lines representing the individual samples and the thick lines representing the average values.

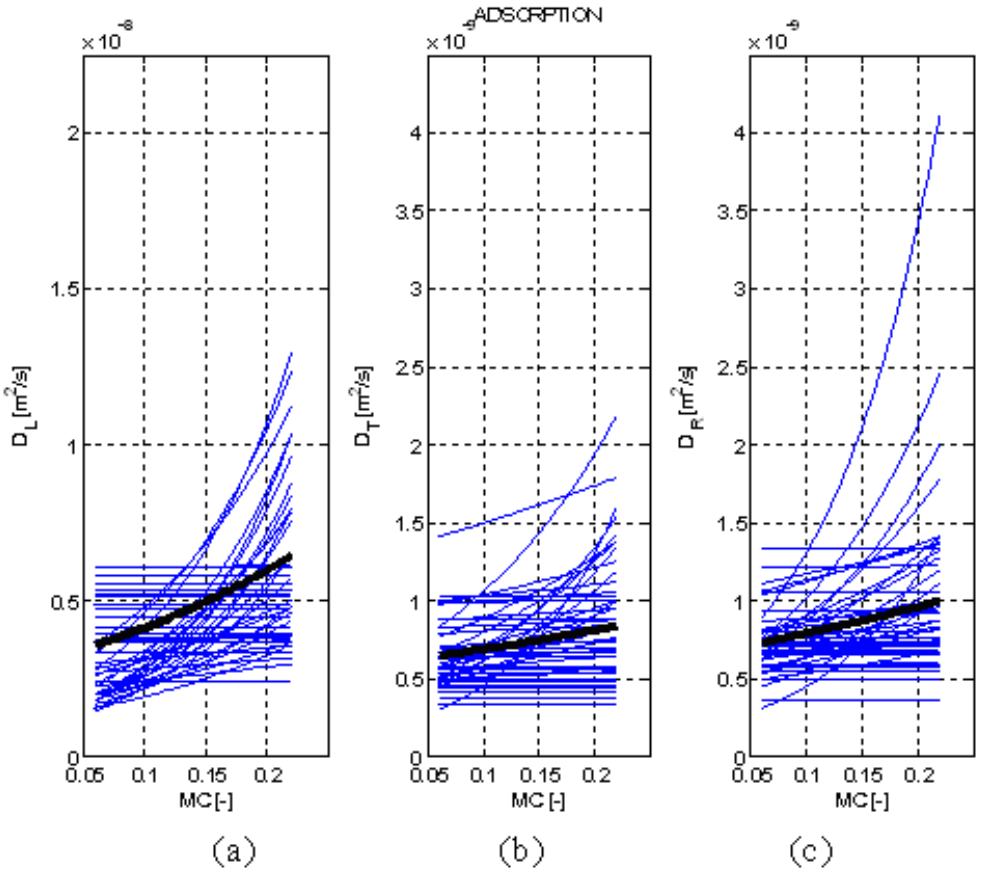

Figure 3-38: Average diffusion coefficient (thick lines) and values of individual samples (thin lines) for the adsorption process: (a) longitudinal, (b) tangential, (c) radial.

As for the desorption experiments, the relative and global relative errors have also been analysed, and the results are presented in Figures 3-34 and 3-35. Figure 3-39 shows the local relative error (e_1) for all samples. The average values are 5.19%, 4.86% and 2.93%, respectively, in the longitudinal, tangential and radial directions. Most of the samples have the local relative errors below 5% and the highest errors were found for the samples 1/1.2/2 and C1/6/1. The sample C1/6/1, in particular, shows an extremely high error of 40% in deriving the longitudinal diffusion parameters.

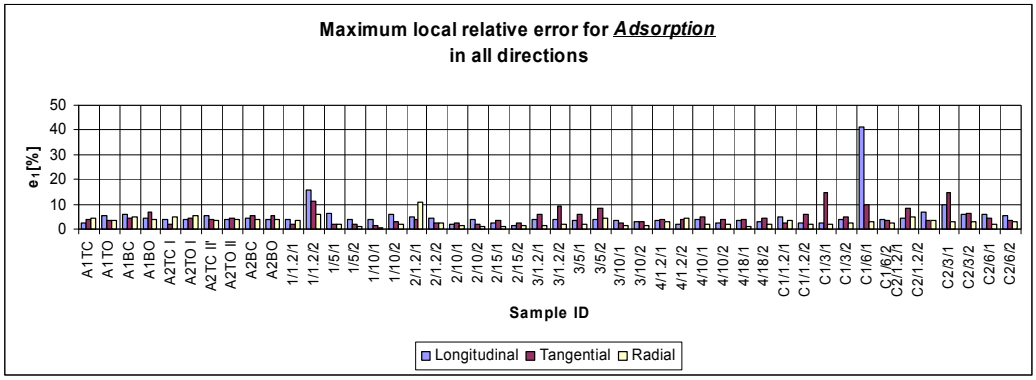

Figure 3-39: Maximum local relative error of all samples for adsorption.

Figure 3-40 shows the global relative error (e_2) for all samples. The average values of the global relative errors are 1.93%, 1.78% and 1.33%, respectively, in the longitudinal, tangential and radial directions. In general, the global relative errors for adsorption are much lower than those for desorption. The maximum global error was found to be less than 6% for all samples, and the majority of the samples have global relative errors lower than 3%.

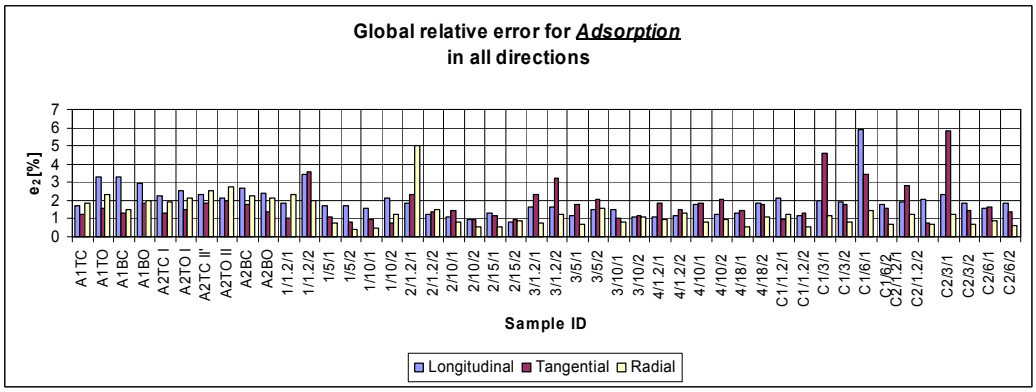

Figure 3-40: Global relative error of all samples for adsorption.

The correlation between the constant diffusion coefficient (D_o) and the constant (K_o) were also investigated for the adsorption process, and the results are shown in Figure 3-41. In adsorption, the values of K_o both in the longitudinal directions and the transverse directions span similar range from zero to 13. The zero value means that the diffusion coefficient is no longer dependent on the moisture content. However, the values of D_o for the transverse directions are lower and fall in a narrower range ($0.2 – 1.2\times10^{-9}$ m^2/s) than those for the longitudinal direction ($0.8 – 6.1\times10^{-9}$ m^2/s).

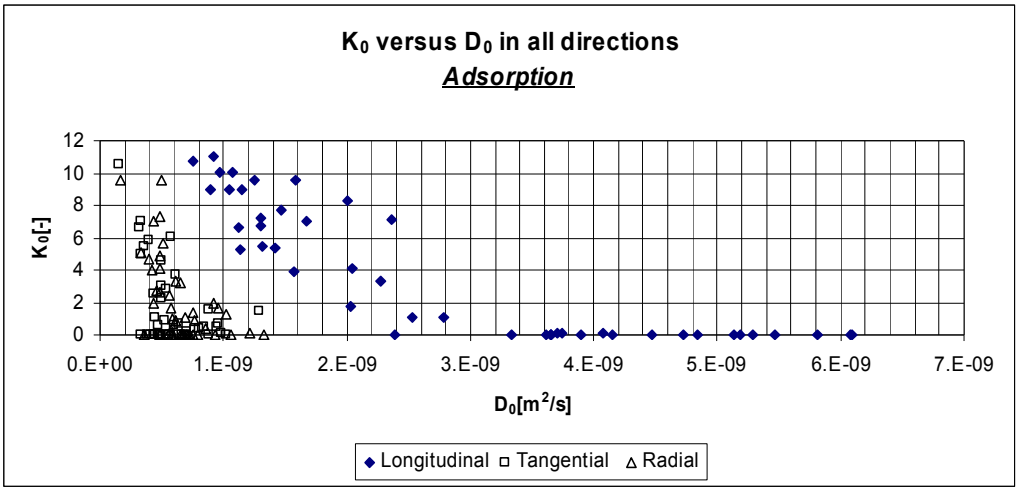

Figure 3-41: K_0 versus D_0 in all directions for adsorption.

More detailed analysis of the correlations are shown in Figure 3-42 for the longitudinal direction, in Figure 3-43 for the tangential direction and in Figure 3-44 for the radial direction. For the longitudinal direction, the constant K_o is linearly related to the constant diffusion coefficient, D_o, for D_o less than 3×10^{-9} m^2/s, above which the values of K_0 approach zero indicating that the diffusion coefficient is independent of the moisture content. However, no such apparent trend is observed for the transverse directions, although the values of K_o tend to be lower for samples with higher D_0 as shown in Figures 3-38 and 3-39.

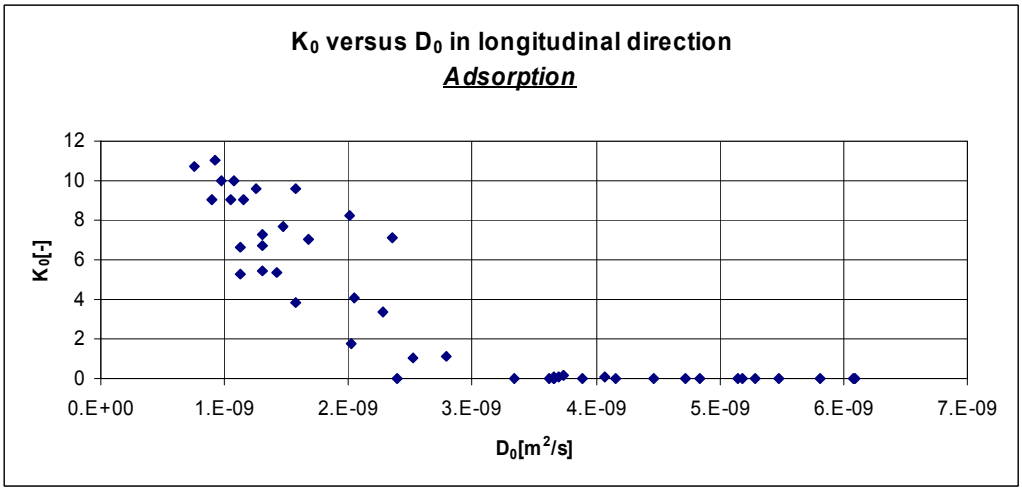

Figure 3-42: K_0 versus D_0 in the longitudinal direction for adsorption.

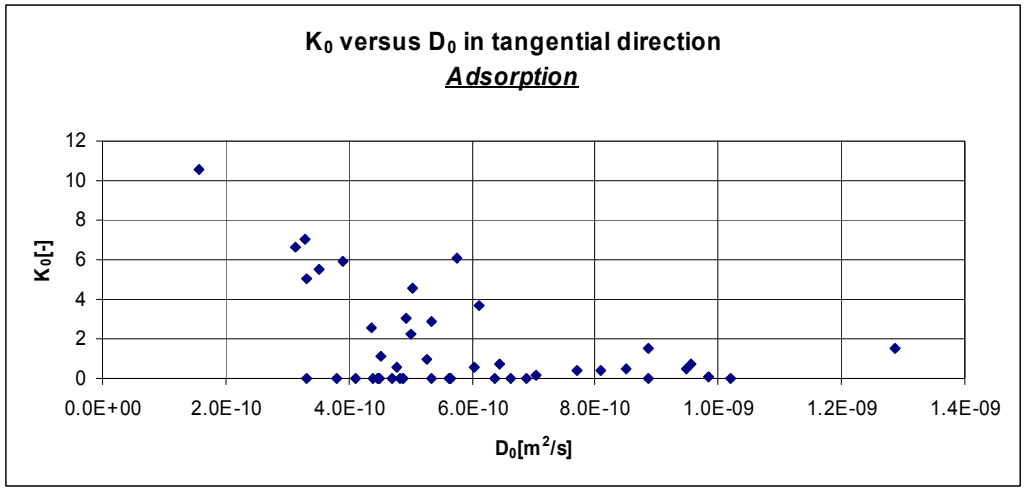

Figure 3-43: K_0 versus D_0 in the tangential direction for adsorption.

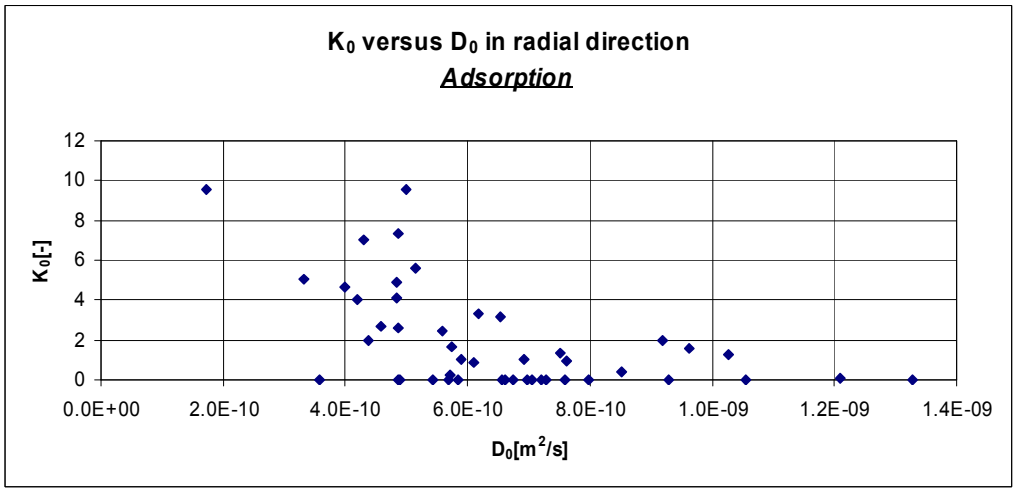

Figure 3-44: K_0 versus D_0 in the radial direction for adsorption.

In the same way as for the desorption, the effect of the diffusion dimension (green) of the samples on the constant diffusion coefficient (D_o) was analysed and the results are shown in Figure 3-45 to Figure 3-47. From the analysed results, no clear trend can be observed for the influence of the diffusion dimension on the constant diffusion coefficient. The correlation coefficients were 0.017, 0.004 and 0.074 in longitudinal, tangential and radial directions respectively.

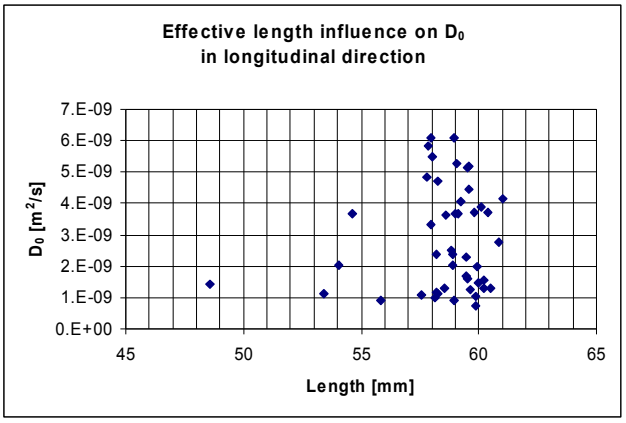

Figure 3-45: Effect of the diffusion dimension of the sample on the constant diffusion coefficient in the longitudinal direction for adsorption.

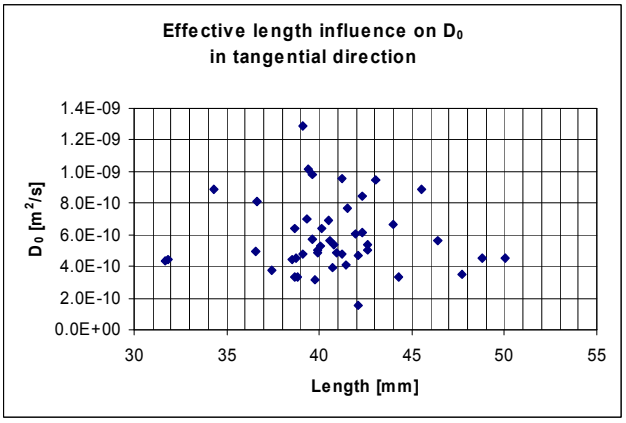

Figure 3-46: Effect of the diffusion dimension of the sample on the constant diffusion coefficient in the tangential direction for adsorption.

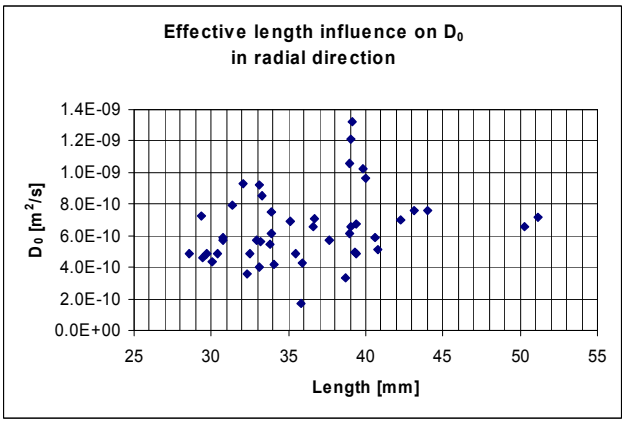

Figure 3-47: Effect of the diffusion dimension of the sample on the constant diffusion coefficient in the radial direction for adsorption.

Comparison of diffusion parameters between trees

In this section, the diffusion parameters averaged over individual trees are compared for the adsorption process and the results are shown in Figure 3-48 to Figure 3-51. For longitudinal diffusion, Figure 3-48 and Figure 3-49 show the average values for the constant diffusion coefficient and the constant in the longitudinal direction for each tree, and the error bars indicate the maximum and the minimum values within the corresponding tree. Figure 3-50 and Figure 3-51 illustrate the corresponding parameters in the transverse directions.

For the longitudinal diffusion (Figure 3-48 and Figure 3-49), Tree 1 and Tree 2 in the second run and Tree 4 in the third run of the experiments have the highest constant diffusion coefficient (D_o) and two of these three trees (Tree 2 and Tree 4) have the lowest values for the constant (K_o). It is interesting to note that the adsorption parameters for these trees are different from those for desorption indicating that the wood in desorption behaves differently. The moisture in the wood of younger trees moves faster longitudinally during drying than the moisture in the wood from older trees but the difference in the wetting behaviour (adsorption) is not apparent. Similar behaviour can be observed for the transverse directions (Figure 3-50 and Figure 3-51), although the moisture diffusion coefficient in the transverse directions in the younger trees and the opposite wood tends to be independent of the moisture content.

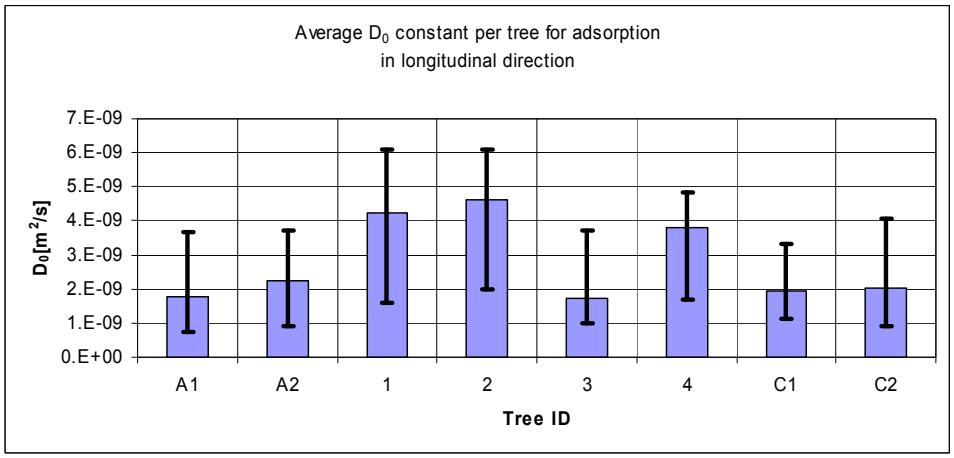

Figure 3-48: Average constant diffusion coefficient, D_0, for each tree in the longitudinal direction for adsorption.

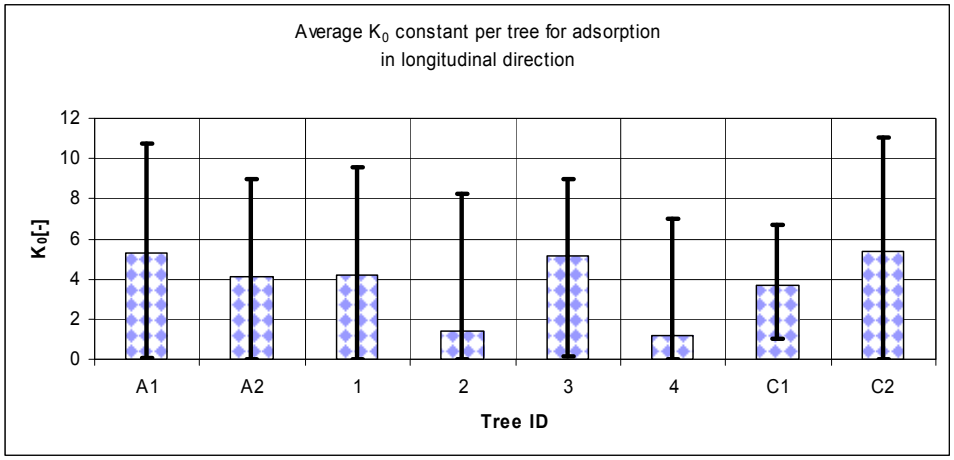

Figure 3-49: Average constant, K_0, for each tree in the longitudinal direction for adsorption.

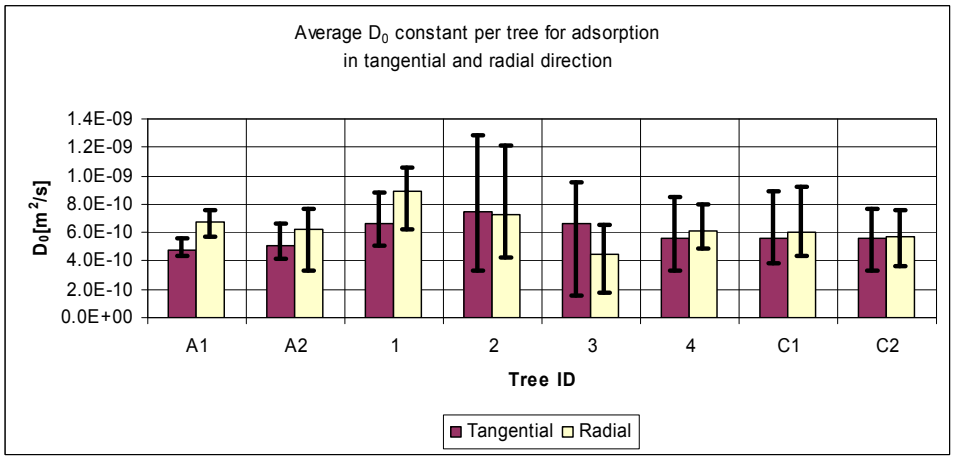

Figure 3-50: Average constant diffusion coefficient, D_0, for each tree in the transverse directions for adsorption.

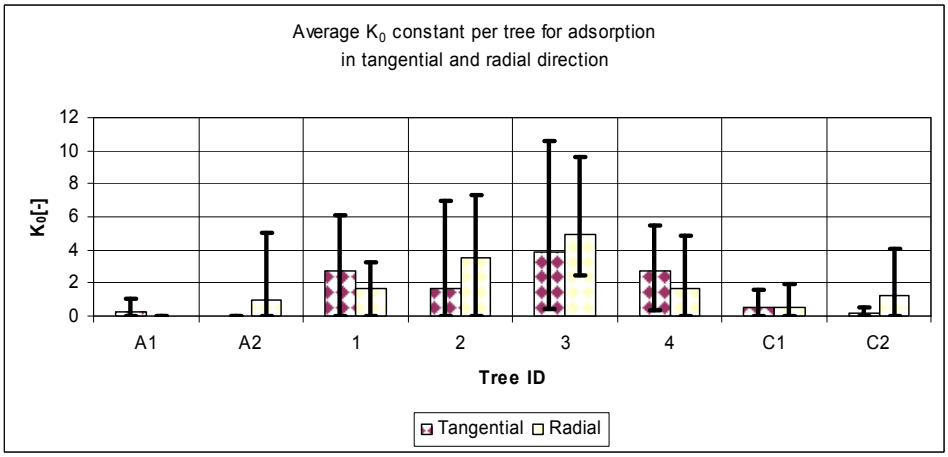

Figure 3-51: Average constant, K_0, for each tree in the transverse directions for adsorption.

Variation of diffusion parameters along the radial direction (growth-ring) and tree height

For the first three runs of the experiments, one sample was always cut from the location close to the pith and one sample close to the bark. The other samples were cut from between the pith and the bark. For the fourth run of the experiments, the disc was used for the preparation of the samples of the compression wood and the opposite wood. In addition, the compression wood samples had the same growth rings as the corresponding opposite wood samples. In all four runs, the discs were cut from each tree at different heights depending on the tree age, but the discs at the breast height (BH) were collected from all of the trees. This kind of sample preparation allows for the comparison of the height versus the radial distribution of the derived constants. The heights which contain the largest number of samples are BH, 5 m and 10 m, with 16, 10 and 8 total number of samples respectively, at each height.

The influence of the radial position (growth rings) over the disc cross section on the derived constant diffusion coefficient values (D_0) for all of the samples for desorption are shown in Figure 3-52. This figure also contains error bars which indicate the growth ring range for the sample concerned. It is noted that the samples cut from near the pith contained less growth rings than the samples cut further away due to the decrease in the growth ring width with the ring number counted from the pith.

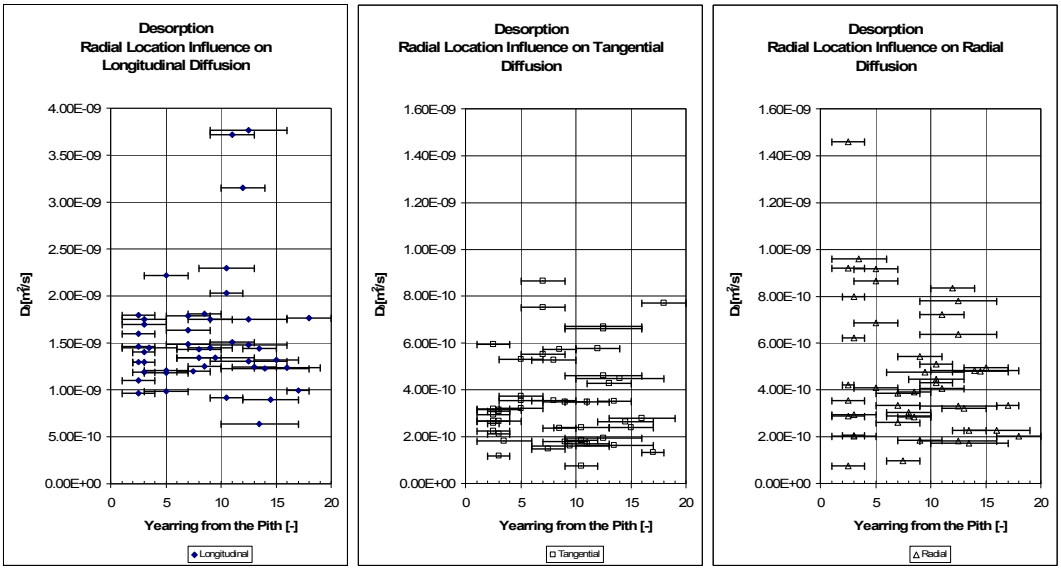

(a) (b) (c)

Figure 3-52: Radial distribution of the constant diffusion coefficient, D_0, for desorption in; (a) longitudinal, (b) tangential and (c) radial direction.

From the results shown in Figure 3-52, no clear trend is found for the distribution of the constant diffusion coefficient (D_o) as a function of the radial location (growth ring). However, some samples cut between 10 and 15 growth rings tend to have higher values for the constant diffusion coefficient, D_0, in the longitudinal direction. For the tangential diffusion direction, values of D_0 are randomly distributed ranging between 1.0×10^{-10} and 9.0×10^{-10} m^2/s. For the radial diffusion direction, the highest values were found for samples close to the pith but, in general, the values are also randomly distributed.

Figure 3-53 contains the derived values of both the constant diffusion coefficient (D_o) and the constant K_o for samples collected from the breast height, 5 m and 10 m high. In this figure the range bars of the growth rings in one sample are not included, with only the average growth ring number being indicated. In addition, the tree heights are also identified in order to show if there is any cross correlation.

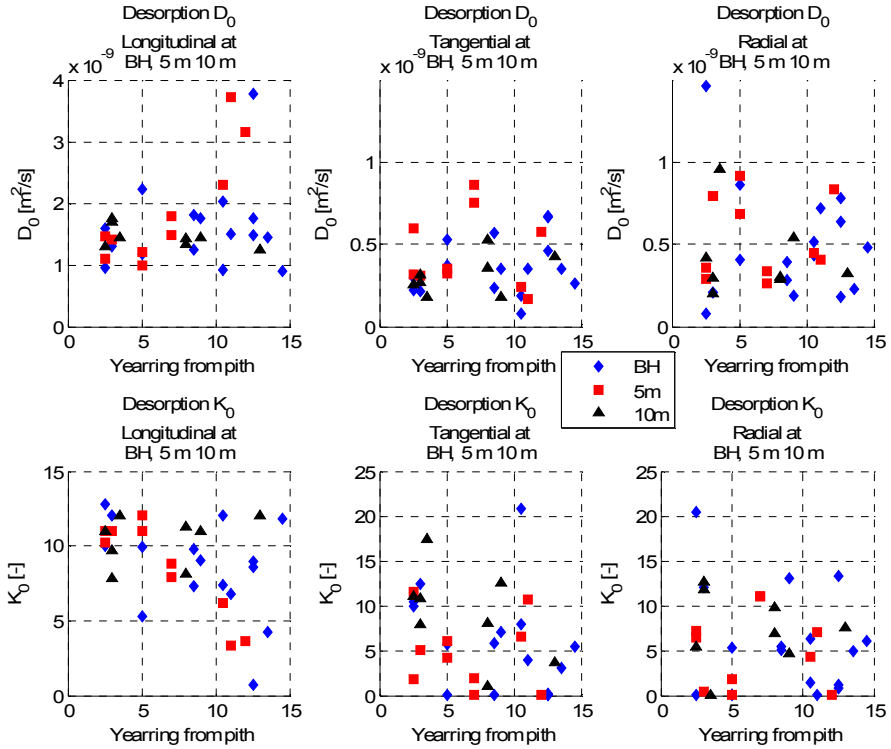

Figure 3-53: The influence of growth ring and tree height on the constant diffusion coefficient (D_o) and constant (K_o) for desorption

In the longitudinal direction, the highest values for the constant diffusion coefficient (D_o) are derived from three samples collected from the first run of the experiments, one from at the breast height of Tree 1 and two from the 5m height of Tree 2. All of these three samples were sapwood.

Despite these exceptional samples, the majority of the samples have a nearly constant diffusion coefficient values (D_0) distributed between 1.0×10^{-9} and 2.5×10^{-9} m^2/s. The corresponding K_0 values are between 0.7 and 14. For some of the breast height samples and 5 m height samples, the K_0 values tend to decrease with increasing growth ring number from the pith. However, the correlation is weak, and no such trend is observed for the 10 m height samples.
In the transverse directions, the values of both D_0 and K_0 are randomly distributed with no apparent trend of variation with the growth ring and the tree height.

For the adsorption experiments, similar analysis to the desorption experiments was performed to examine the influence of the radial location and the tree height on the diffusion parameters. In Figure 3-54 the derived constant diffusion coefficients, D_0, are illustrated for adsorption, including all samples. In general, the derived values in the three directions for adsorption are higher than the corresponding values for desorption. Similar to the desorption, the values for adsorption are also widely spread both across the radial direction and along the tree height.

In the longitudinal direction the bulk data can roughly be divided into three separate regions of values. For the highest value region, it appears that D_0 decreases with distance from the pith. For the middle region there is still a slight relation appearing whereas for the lowest value region no influence of the radial position is visible. The samples that form the highest D_0 value region originated form the Tree 1 (1/1.2/1, 1/1.2/2, 1/5/1, 1/10/1), Tree 2 (2/1.2/2, 2/10/1, 2/10/2, 2/15/2) and Tree 4 (4/10/2, 4/18/2). Nine out of ten samples were identified as normal, while one sample was classified as opposite wood. In the tangential diffusion direction, there seems to be a trend that D_o also decreases with the distance from the pith. However, in radial direction, no trend is observed for the influence of the radial position on the constant diffusion coefficient.

Figure 3-55 contains the derived values of both the constant diffusion coefficient (D_o) and the constant K_o for samples collected from the breast height, 5 m and 10 m high. In this figure, the range bars of the growth rings in one sample are not included, with only the average growth ring number being indicated. In addition, the tree heights are also identified in order to show if there is any cross correlation. From the results, it is found that the values of the constant diffusion coefficient (D_0) are generally higher than those for desorption, but derived K_0 values are, in general, lower than those in desorption, again with a number of data approaching zero.

The mentioned trend in the desorption for K_0 in the tangential direction is also visible for adsorption. However, the three region separation for the longitudinal diffusion seems to disappear in the adsorption when looking at samples at breast height, 5 m and 10 m tree heights.

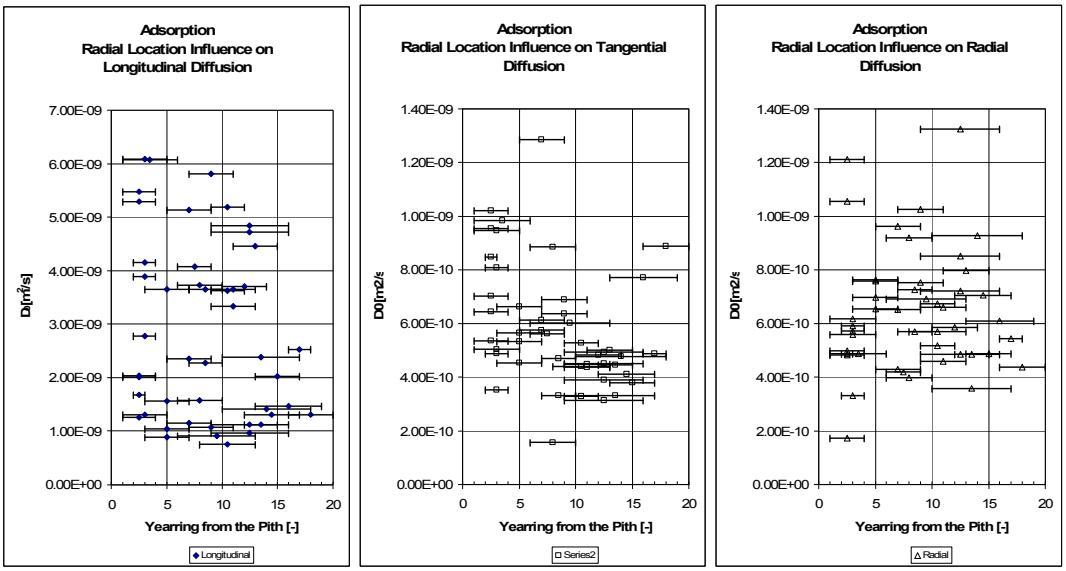

(a) (b) (c)

Figure 3-54: Radial distribution of constant diffusion coefficient, D_0 for adsorption in; (a) longitudinal, (b) tangential and (c) radial direction.

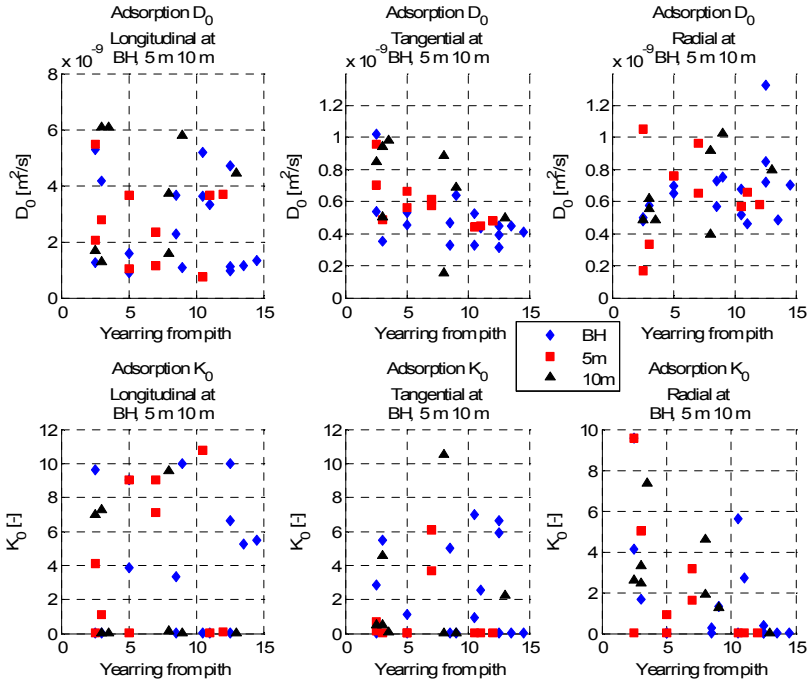

Figure 3-55: Influence of the radial position and tree height on the diffusion parameters for adsorption.

3.3.3 Comparison of results with literature data

The surface emission coefficient calculated in this study ranges from 1.81×10^{-6} to 5.69×10^{-6} m/s. Söderström and Salin (1993) published a comprehensive literature review on the surface emission factors. The review included the values for surface emission coefficient calculated by Liu (1989) with values of the surface coefficient ranging from 1.48×10^{-6} to 1.66×10^{-6} m/s under conditions similar to this work. Liu (1989) derived the coefficient from data published by Choong and Skaar (1969).

In this study, the surface emission coefficient was assumed to be dependent on the surface moisture content (Yeo *et al.* 2002), which influenced the first ten hours after the start of the experiment. We have found that for desorption the surface moisture content reaches faster values close to equilibrium than for adsorption. This is mainly due to the lower surface emission coefficient for adsorption because of the lower sorption isotherm. Figure 3-56 illustrates the basic density influence on the surface emission coefficient (air velocity of 3.3 m/s) for a sample with the length of the surface along on which convection is occurring of 3 cm for the relative humidity range as used in this study. The surface emission coefficient for the individual samples varied due to differences in basic density, the convection length for adsorption and desorption.

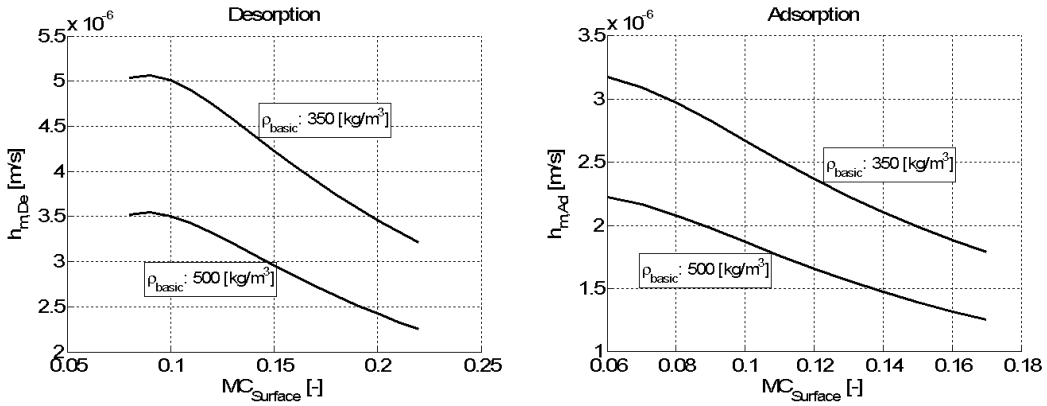

(a) (b)

Figure 3-56: Basic density influence on surface emission coefficient for desorption (a) and adsorption (b).

For comparison of the diffusion parameters of this study with the literature data, the overall average values for the constant diffusion coefficient (D_o) and the constant (K_o) are summarized in Table 3-9 for desorption and Table 3-10 for adsorption.

Table 3-9: Average, standard deviation (STD), maxima and minima values of parameters for desorption.

Summary All Samples	Longitudinal		Tangential		Radial	
	D_0	K_0	D_0	K_0	D_0	K_0
	[m^2/s]	[-]	[m^2/s]	[-]	[m^2/s]	[-]
Average	1.56E-09	9.20	3.54E-10	6.58	4.62E-10	5.95
STD	6.25E-10	2.70	1.89E-10	5.19	2.75E-10	4.97
Maximum	3.77E-09	13.15	8.65E-10	20.85	1.46E-09	20.38
Minimum	6.39E-10	0.70	7.60E-11	0.00	7.66E-11	0.00

Table 3-10: Average, standard deviation (STD), maxima and minima values of parameters for adsorption.

Summary All Samples	Longitudinal		Tangential		Radial	
	D_0	K_0	D_0	K_0	D_0	K_0
	[m^2/s]	[-]	[m^2/s]	[-]	[m^2/s]	[-]
Average	2.85E-09	3.70	5.83E-10	1.64	6.46E-10	1.97
STD	1.64E-09	4.00	2.24E-10	2.47	2.26E-10	2.58
Maximum	6.09E-09	11.01	1.29E-09	10.55	1.33E-09	9.59
Minimum	7.50E-10	0.00	1.57E-10	0.00	1.71E-10	0.00

In previous studies by Yeo *et al.* (2002), Olek *et al.* (2005), Droin-Josserand *et al.* (1989), Cai (2005), Hukka (1999) and Danvind and Ekevad (2006) the effective diffusion coefficients were reported for various wood species.

Yeo *et al.* (2002) used a colorimetric technique to measure the surface emission coefficient and further derived the diffusion coefficient for Maple, Oak and pine at 30°C. Surface emission coefficients for pine were similar to those determined from this study since the same technique was used to determine the surface emission coefficient in both of these studies. In the work of Yeo *et al.* (2002), the diffusion coefficient for the pine wood was found to increase with moisture, content with values ranging from 1.0×10^{-10} to 1.0×10^{-9} m^2/s. In the longitudinal direction, the diffusion coefficient was approximately 10 times higher than that in the transverse directions, whereas the diffusion coefficient in the radial direction was slightly higher than that in the tangential direction.

Olek *et al.* (2005) derived the diffusion coefficient for two European wood species, Scots pine and European beech, for adsorption. In the work of Olek *et al.* (2005), both the diffusion coefficient and the surface emission coefficient were measured. However, the diffusion coefficient was based on the dimensionless bound water content and, therefore the results are not directly comparable with the results of the current study. However, similar determination procedures (inverse method) were used both in the work of Olek *et al.* (2005) and in this project.

Olek *et al.* (2005) also investigated the influence of the moisture content on the diffusion coefficient, but found that the diffusion coefficient decreases with increasing MC, which is contradicts other studies in the literature (Droin-Josserand *et al.*, 1989; Hunter, 1991, 1992; Siau, 1995). Olek *et al.* (2005) found that the diffusion coefficient in the longitudinal direction was approximately 16 times higher than that in the transverse directions, with values in the radial direction being slightly higher than those in the tangential direction for Scots pine.

Droin-Josserand *et al.* (1989) determined the diffusion coefficient in adsorption for Scotts pine. The diffusion coefficient was obtained using the short test technique (Droin *et al.*, 1988; Taverdet and Vergnaud, 1984) under transient isothermal conditions at 30°C. In the work of Droin-Josserand *et al.* (1989), the effective diffusion coefficient was also related to the constant diffusion coefficient, D_o, and the constant, K_o, as in this project. The obtained constant diffusion coefficient, D_0, was reported to be 304×10^{-10}, 1.5×10^{-10} and 1.5×10^{-10} m^2/s, respectively, for the diffusion in the longitudinal, tangential and radial directions. The obtained K_0 values were -0.177, 0.0288 and 0.0228 in the corresponding directions. Droin-Josserand *et al.* (1989) also determined the surface emission coefficient using the method described by Choong and Skaar (1972) and reported a value of 1.0×10^{-6} m/s.

Cai (2005) investigated the diffusion coefficient for sub-alpine fir wood using the method of Siau (1984) and the inverse moisture diffusion algorithm introduced by Liu (2001). The derived diffusion coefficients in transverse directions ranged from 2.7×10^{-11} to 1.1×10^{-10} m^2/s at 20°C. The diffusion coefficient in the longitudinal direction was 7-19 times higher than those in the transverse directions.

Hukka (1999) calculated the effective diffusion coefficient for Nordic softwoods (Scott pine and Norway spruce) at various temperatures in the transverse directions and confirmed the trend that the diffusion coefficient increases with moisture content. The effective diffusion coefficient ranged from 0.2×10^{-10} to 1.9×10^{-9} m^2/s in the temperature range of 20 – 80°C.

Danvind *et al.* (2006) derived the diffusion coefficient for Norway spruce sapwood, using experimental data measured with the non-destructive X-ray computed tomography technique in one and two dimensions. They also found that the diffusion coefficient increases with moisture content, and the values of the diffusion coefficient ranged approximately from 1.2×10^{-9} to 7.5×10^{-9} m^2/s at 50°C.

Figure 3-57 compares the effective diffusion coefficient obtained from the constant diffusion coefficient (D_o) and the constant (K_o) in this study with the literature data for Scott pine (Hukka, 1999; Rosenkilde and Arfvidsson, 1997).

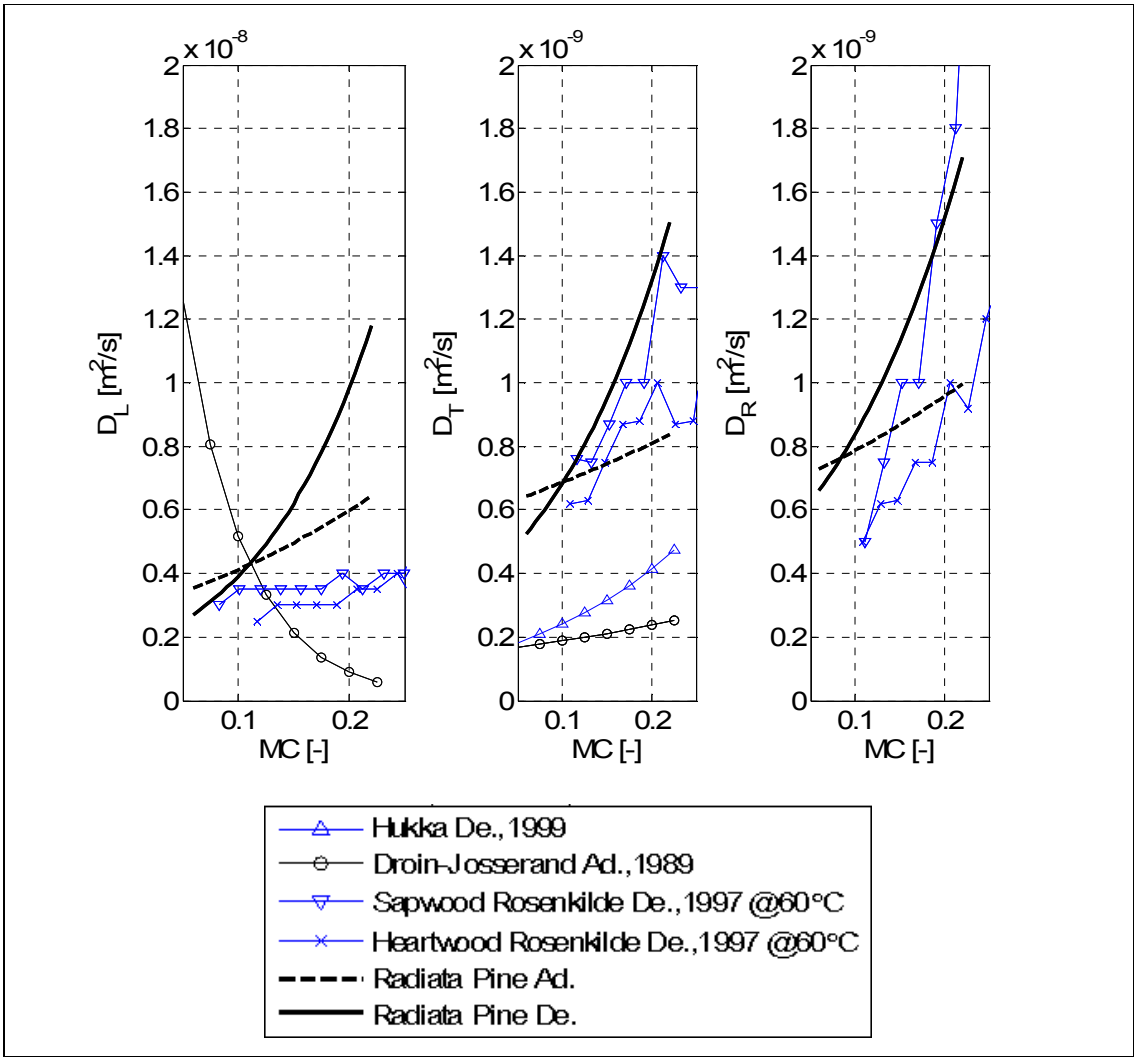

Figure 3-57: Comparison of the effective diffusion coefficient of radiate pine obtained in this project with the literature data for Scott pine.

In this project it was found that the derived values for D_0 for adsorption were higher than those for desorption. However, it was found that the effective diffusion coefficient in adsorption is less dependent on the moisture content than in desorption over the moisture content range of 6% and 25%MC. This is mainly due to the low values of K_0. This behavior was confirmed by previous studies for Scott pine.

In the longitudinal direction, Hukka (1999) found that the diffusion coefficient for Scott pine decreases with moisture content whereas Rosenkilde and Arfvidsson (1997) derived the diffusion coefficient for the same species, which slightly increases with moisture content. The data from Rosenkilde and Arfvidsson (1997) obtained for the transverse directions at 60°C are in close agreement with the results obtained in this project at 30°C.

3.3.4 Variation of diffusion parameters with wood types

The experimental results for the diffusion parameters (D_o, K_o and D) have been analysed based on the wood types, including heartwood, sapwood, compression wood and opposite wood. The numbers of samples for the four types of wood used for this analysis were, respectively, 16, 16, 7 and 7. Table 3-11 contains the average values over these samples in the three diffusion directions for the desorption process.

Table 3-11: Desorption, average constants for different wood types.

Desorption ***Wood Type***	**Average Longitudinal**		**Average Tangential**		**Average Radial**	
	D_0	**K_0**	**D_0**	**K_0**	**D_0**	**K_0**
Summary	**[m^2/s]**	**[-]**	**[m^2/s]**	**[-]**	**[m^2/s]**	**[-]**
Heartwood	1.41E-09	10.33	3.09E-10	8.77	5.92E-10	5.22
Sapwood	1.91E-09	8.11	4.67E-10	3.95	4.33E-10	6.62
Compression wood	1.11E-09	9.58	2.09E-10	6.45	3.03E-10	5.47
Opposite wood	1.55E-09	8.75	3.48E-10	7.74	3.90E-10	6.56

Figure 3-58 illustrates the influence of the moisture content on the effective diffusion coefficient for the desorption process in the three directions (longitudinal, tangential and radial) and for the four types of radiata pine wood. From Figure 3-58, it is observed that the desorption diffusion coefficients in the longitudinal direction for all wood types are approximately four times higher than those in the transverse directions. It is interesting to note that the effective diffusion coefficients of the heartwood and sapwood are similar in the longitudinal and the radial directions, which are higher than the corresponding values for the opposite wood. The compression wood has the lowest value for the diffusion coefficient. In the tangential direction, the sapwood deviated clearly from the heartwood, with the sapwood showing less dependence on the moisture content.

The higher diffusion coefficient for the heartwood indicates that the moisture diffusion in the heartwood is faster than other wood possibly due to the higher porosity of the heartwood and the incomplete aspiration of the bordered pits when the heartwood is formed. On the other hand, the compression wood has higher density and thus lower porosity for the transport of moisture vapour.

The higher diffusion coefficient in the radiata pine heartwood has the opposite trend to the Scott pine as reported by Rosenkilde and Arfvidsson (1997). This difference between the wood types is likely to be caused by the wood species, and further work using larger number of samples will be recommended to validate the results obtained in this project.

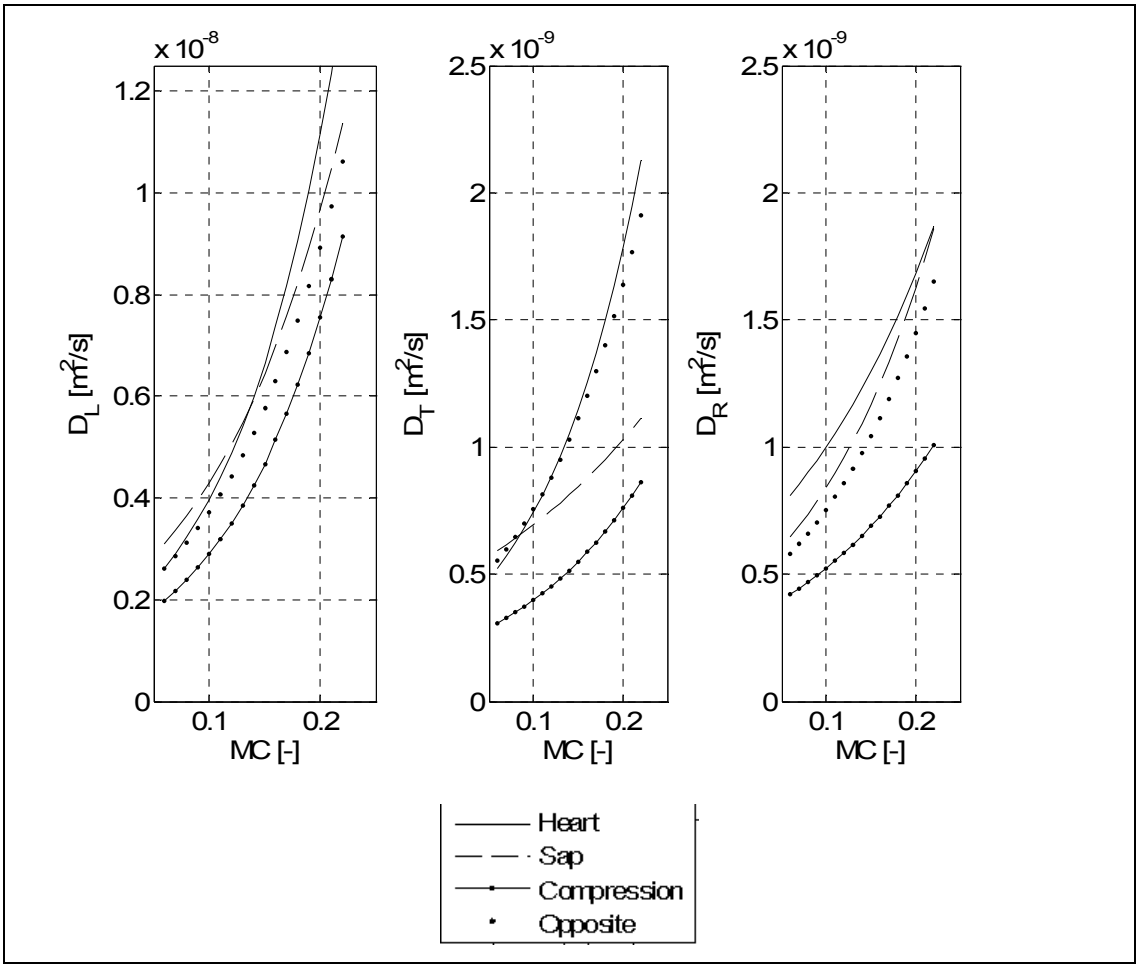

Figure 3-58: Effective diffusion coefficient for different wood types for desorption.

In Figures 3-59 to 3-61, the one-dimensional isothermal (30°C) drying behavior of the different wood types for desorption (Table 3-11), is shown, for an 85 %RH to 25 %RH step. The diffusion directions were assumed to be 5 cm. The air velocity was 3 m/s, with 5 cm as effective convection length. Under these conditions, it was found that all samples, where longitudinal diffusion is occurring, will dry within 40 hours below 10 %MC (Figure 3-59).

It was found that in tangential and radial directions (Figures 3-60 and 3-61) the time to reach the new EMC was about a factor of 10 higher, for samples with the similar diffusion length of 5 cm. In all the simulations the compression wood dried the slowest, whereas the heartwood, sapwood and opposite wood showed similar drying behaviours.

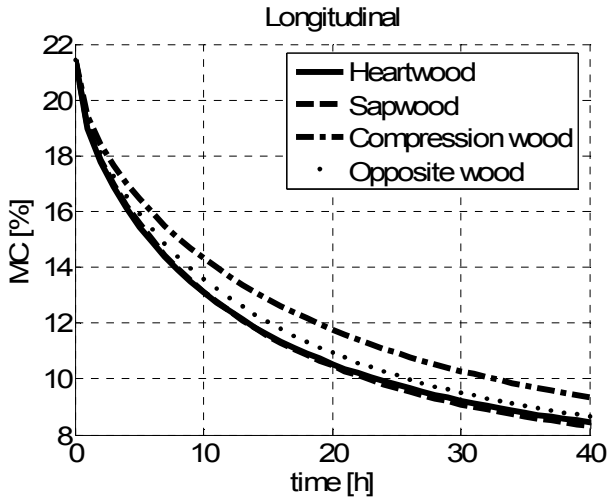

Figure 3-59: Simulated drying behaviour for different wood types, in longitudinal direction.

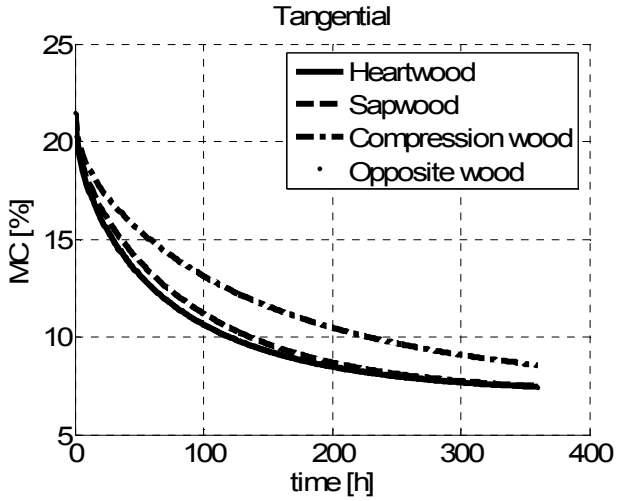

Figure 3-60: Simulated drying behaviour for different wood types, in tangential direction.

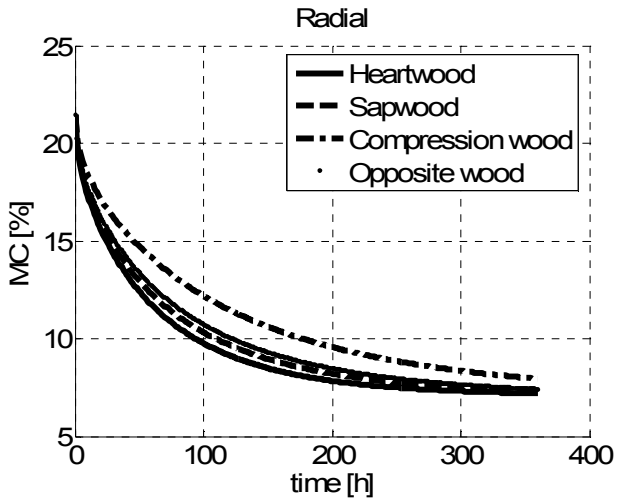

Figure 3-61: Simulated drying behaviour for different wood types, in radial direction.

Table 3-12 contains the average adsorption values for different wood types in the three directions. The adsorption diffusion coefficient in the longitudinal direction for all wood types is 4.6 times higher than that in the transverse direction.

Figure 3-62 illustrates the diffusion coefficient in the adsorption process as a function of moisture content in the longitudinal, tangential and radial directions for the four types of wood of radiata pine (heartwood, sapwood, compression wood and opposite wood). In general, the diffusion coefficient in adsorption is less dependent on the moisture content with lower slopes as compared with the curves presented in Figure 3-58. Compression wood had the lowest diffusion coefficients in all directions. In adsorption, the compression wood again shows the lowest diffusion coefficient, whereas all of the other three types of wood have similar behaviour.

Table 3-12: Adsorption, average constants for different wood types.

Adsorption Wood Type	**Average Longitudinal**		**Average Tangential**		**Average Radial**	
	D_0	**K_0**	**D_0**	**K_0**	**D_0**	**K_0**
Summary	**[m^2/s]**	**[-]**	**[m^2/s]**	**[-]**	**[m^2/s]**	**[-]**
Heartwood	3.08E-09	3.71	6.88E-10	1.07	6.21E-10	2.98
Sapwood	3.06E-09	3.68	5.29E-10	2.79	7.38E-10	1.56
Compression wood	2.58E-09	1.63	4.57E-10	0.13	5.06E-10	0.62
Opposite wood	2.10E-09	5.83	5.92E-10	1.81	6.28E-10	1.94

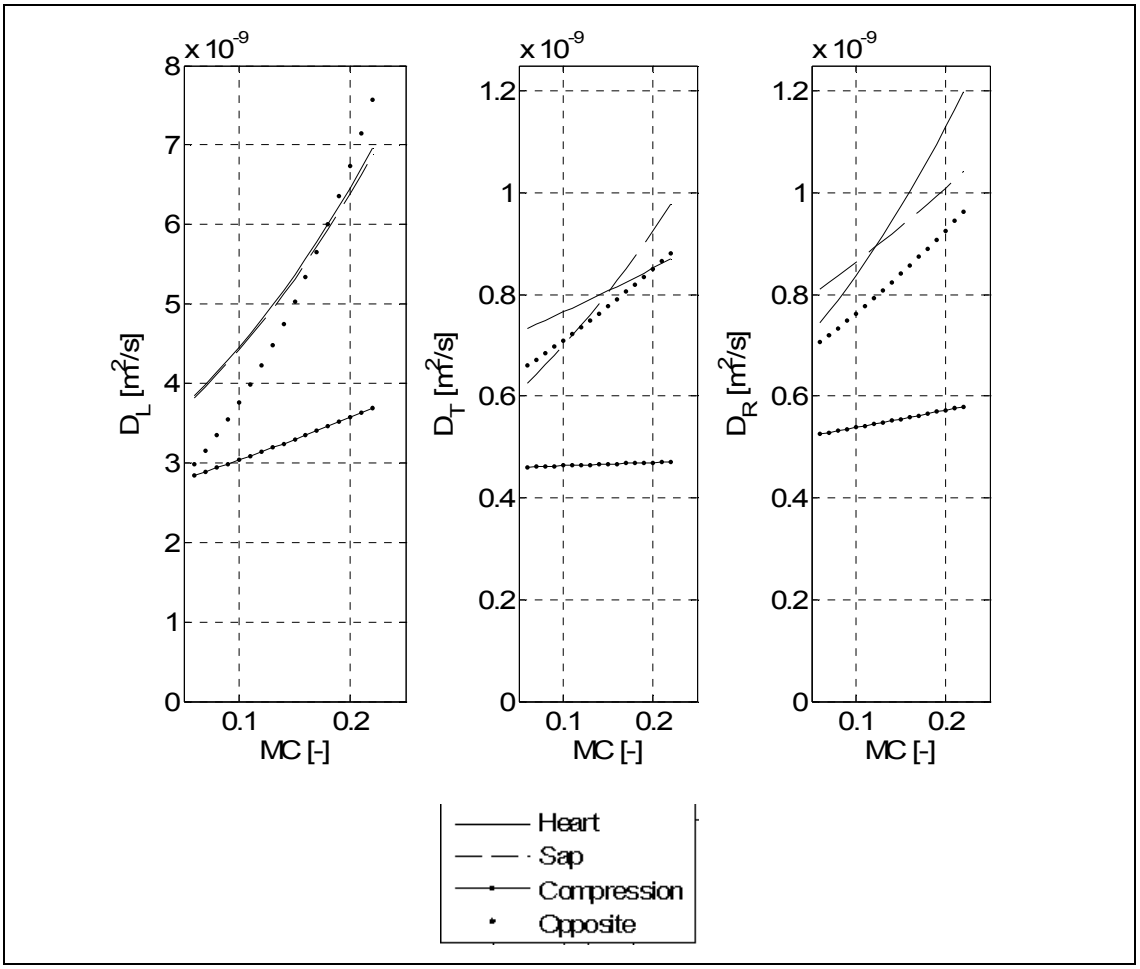

Figure 3-62: Effective diffusion coefficient for different wood types for adsorption.

3.3.5 Influence of wood shrinkage and density on the diffusion coefficient

The derived diffusion parameters have been presented without discussion on the influence of basic wood properties. This section examines the influence of the shrinkage and density on the diffusion coefficient at given moisture contents. The effect of the volumetric shrinkage (ε_V) and the wood basic density (ρ_{Basic}) can be combined and expressed by the actual wood density (ρ) as follows:

$$\rho = \frac{m_{MC}}{V_{MC}} = \frac{m_{od} \cdot (1 + MC)}{V_{green} \cdot (1 - \varepsilon_V)} = \rho_{Basic} \frac{(1 + MC)}{(1 - \varepsilon_V)} \tag{3-21}$$

In the above equation, the actual density is expressed as a function of the basic density, moisture content (MC) and the volumetric shrinkage, which is also dependent on the moisture content. For the calculation of the volumetric shrinkage, the assumption was made that the shrinkage in the each of the three directions (longitudinal, tangential and radial) is linearly related to the moisture content. With this assumption the shrinkage (ε) as a function of moisture content is expressed as:

$$\varepsilon = \varepsilon_{od} \cdot \left(1 - \frac{MC}{FSP}\right) \tag{3-22}$$

The fibre saturation point (FSP), in the following calculations, was assumed to be 29%MC for all samples. The volumetric shrinkage can be related to the three dimensional shrinkages as:

$$\varepsilon_V = \frac{V_{green} - V_{MC}}{V_{green}} = 1 - (1 - \varepsilon_L) \cdot (1 - \varepsilon_T) \cdot (1 - \varepsilon_R) \tag{3-23}$$

Due to then fact that the longitudinal shrinkage is one order lower of magnitude than the transverse shrinkage for normal wood, the longitudinal shrinkage can be neglected without inducing significant errors. With this approach, the volumetric shrinkage is simplified to:

$$\varepsilon_{\overline{V}} = 1 - (1 - \varepsilon_T) \cdot (1 - \varepsilon_R) \tag{3-24}$$

Based on the above discussion, the diffusion coefficients in the three directions for the desorption and adsorption at moisture contents of 10%, 15% and 20% are analysed as a function of wood density. Firstly the relationship in the longitudinal direction is investigated, followed by the the tangential and radial directions.

Influence of wood density on the diffusion coefficient in the longitudinal direction

The density influences on longitudinal diffusion for three moisture contents (10%, 15 and 20%) are illustrated in Figure 3-63 for desorption and Figure 3-64 for adsorption.

For the desorption, an exponential regression analysis was performed, and a significant correlation for the influence of the wood density on the effective diffusion coefficient was revealed with R^2 = 0.67 at 10%MC. With higher moisture contents the correlation becomes less significant with R^2 reducing from 0.63 to 0.43 for 15%MC and 20%MC, respectively. The results indicate that at low level of moisture contents, the water transport can be described by diffusion in the longitudinal direction for the desorption. At higher moisture contents, additional moisture movement mechanisms and resistances might be the causes of the weakening of the correlation.

For adsorption, an exponential regression analysis was also performed, but the correlation becomes weaker than for the desorption. The derived correlation R squares are 0.29, 0.39 and 0.22 for 10%MC, 15%MC and 20%MC, respectively. The weaker correlation might be caused by the performed calculation of the surface emission coefficient used to determine the diffusion constants or that the empirical correlation (Equation 3-15) needs to be modified for the moisture movement during adsorption.

The likely cause for the weakening correlation for the adsorption may lay in the description of the diffusion coefficient as a function of the moisture content (Equation 3-15) or the applied surface emission coefficient for the adsorption process. The surface emission coefficient requires the adsorption isotherm. For the determination of the surface emission coefficient, the adsorption isotherm derived from samples, which were oven-dried prior to the adsorption process, was used (Figure 2-24). For this experiment, the samples would not have developed a significant hysteresis due to the fact that the adsorption experiment started at moisture contents around 6%. The results show that the diffusion coefficient in the adsorption process determined is less dependent on the wood density and the moisture content with the data scattering in a wider range than for desorption.

.

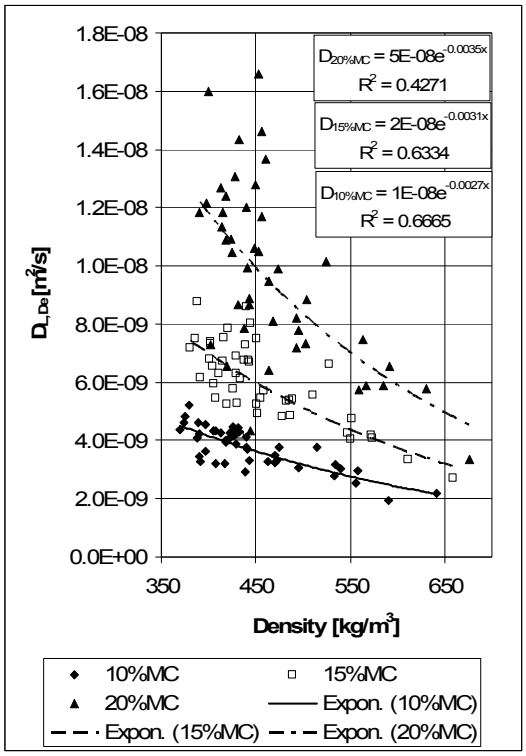

Figure 3-63: Density influence on longitudinal diffusion for desorption.

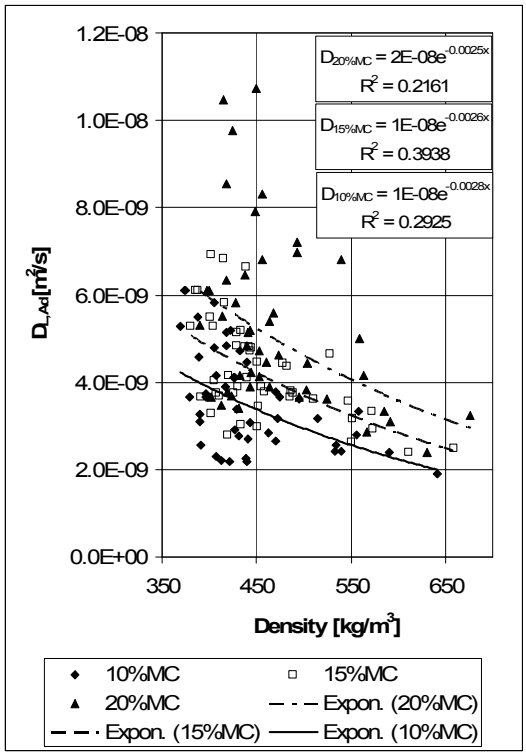

Figure 3-64: Density influence on longitudinal diffusion for adsorption.

Influence of wood density on the diffusion coefficient in the tangential direction

The density effects on the tangential diffusion coefficient for the three moisture contents (10%, 15 and 20%MC) are illustrated in Figure 3-65 for desorption and Figure 3-66 for adsorption. As discussed in the previous section, an exponential regression analysis was also performed for the tangential diffusion for both of the desorption and the adsorption processes.

For the desorption, the correlation factors (R^2) are 0.26, 0.3 and 0.24 at 10%MC, 15%MC and 20%MC, respectively. The corresponding values for the adsorption are 0.12, 0.11 and 0.09. In general, the correlations in the tangential direction are considerablely weaker than in the longitudinal direction. The weaker correlation might be caused by the curvature of the growth rings and the differing wood structure in the tangential direction. On the tangential faces of the tracheids, no bordered pits are located, thus the moisture transfer is through diffusion within the wood cell walls and through the irregular radial rays. In the longitudinal directions, the moisture vapour can move from one tracheid to another through the incomplete bordered pits on the radial cell walls.

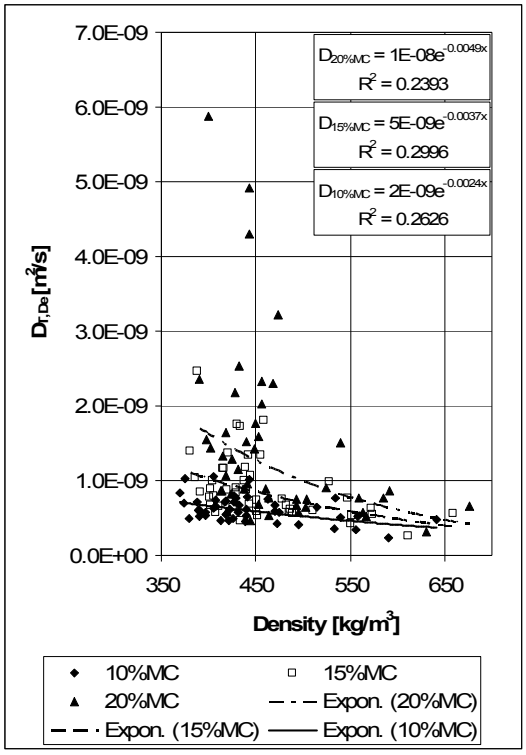

Figure 3-65: Density influence on tangential diffusion for desorption.

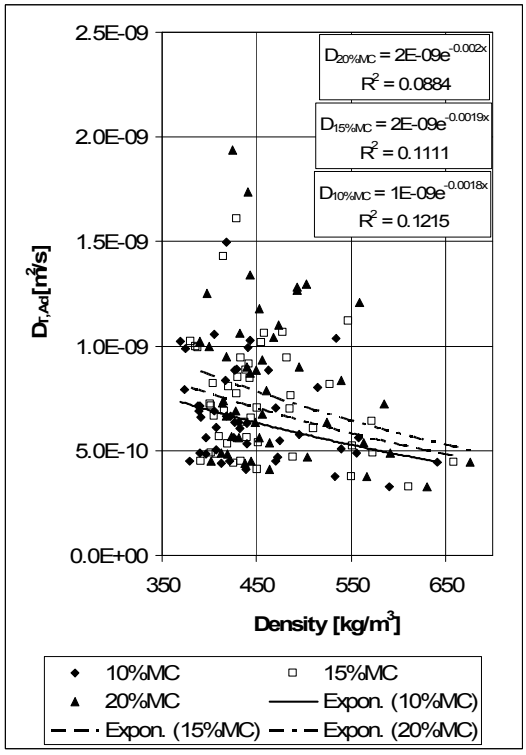

Figure 3-66: Density influence on tangential diffusion for adsorption.

Influence of wood density on the diffusion coefficient in the radial direction

The density effects on radial diffusion for three moisture contents (10%MC, 15%MC and 20%MC) are illustrated in Figure 3-67 for desorption and Figure 3-68 for adsorption. As discussed in previous sections, an exponential regression analysis was performed for the radial diffusion for both the desorption and the adsorption.

For desorption, the correlation factors (R^2) are 0.57, 0.49 and 0.26 at 10%MC, 15%MC and 20%MC, respectively, and the corresponding values for the adsorption are 0.29, 0.36 and 0.34. In general the correlations in the radial direction were weaker than in the longitudinal direction but higher than in the tangential direction. The exact reasons for these differences are not clear but it is believed that the growth ring curvature, the tracheid structure, the ray tissues and the pits have various levels of influence.

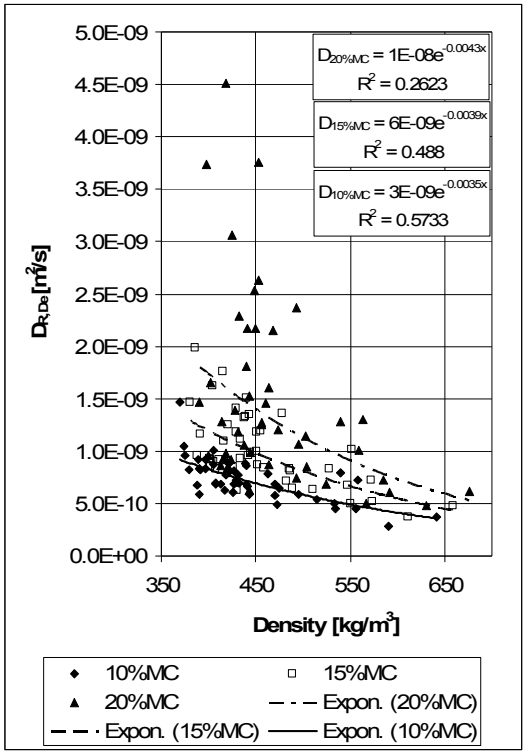

Figure 3-67: Density influence on tangential diffusion for desorption.

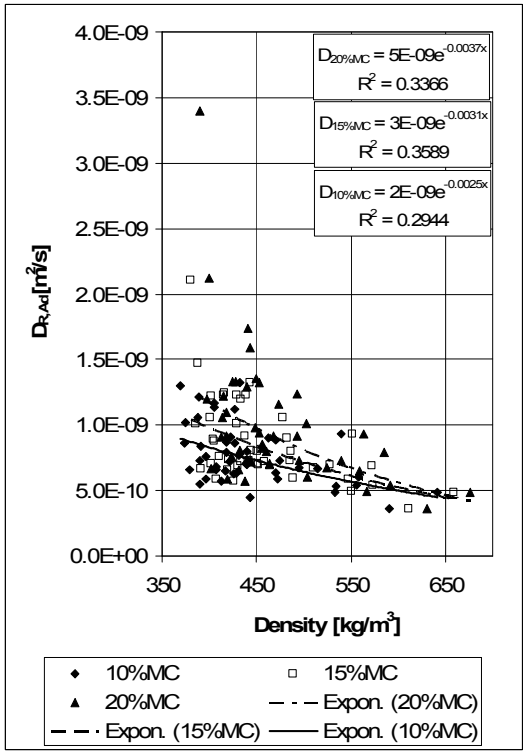

Figure 3-68: Density influence on tangential diffusion for adsorption.

3.4 Conclusion and Future Improvement

The objective of this project was to experimentally determine the intrinsic moisture diffusion coefficient in three directions (tangential, radial and longitudinal) for different moisture contents (6% - 20%MC). This task was solved by applying the inverse method introduced by Olek *et al*. (2005). An empirical exponential equation was used to describe diffusion coefficient dependency on moisture content. For the determination of the constants, due to the ill-conditioned nature of the problem, it was decided to constrain K_0 from zero to infinity, based on theoretical and experimental evidence found in current literature (Hunter, 1992; Liu 2001; Yeo, 2002; Skaar, 1954). The solving of the diffusion equation requires the definition of the boundary condition, which describe the moisture transport from the wood surface into the surrounding air. For the description of the boundary condition, the surface emission coefficient depending on the surface moisture content introduced by Yeo *et al.* (2002) has been implemented into the numerical algorithm.

The algorithm used to determine the constants is not capable of separating the constants to achieve the parameter uniqueness and therefore this study investigated the relationship between the constants. The author strongly recommends that when using the derived constants this “non parameter uniqueness” has to be considered. Further this study introduced the wood surface air interaction, as it was recommended by Olek (2005). The results have clearly shown that the diffusion coefficient is dependent on the moisture content, and also dependent on the wood type. The next step in this study will include the modeling of the cell structure to reduce the number of necessary constants to one and the outcome of the implementation of the wood structure are intended to be published.

Due to the nonexistent information on the parameter relationship describing the moisture dependency on the diffusion coefficient (Equation 3-15), the constants D_0 and K_0 were analysed. Reasonable linear and logarithmic correlations were found for diffusion in desorption, which leads to the conclusion, in combination with the density influence that the diffusion coefficient for high density wood is more influenced by moisture content than for low density wood with radiata pine.

Further it was found that this conclusion is not valid for compression wood, which showed the lowest moisture influence, whereas the opposite wood was highly influenced by the moisture content. For adsorption in general, the diffusion coefficient dependency on moisture content was lower compared with the desorption.

These findings need to be considered for further improvement of the empirical equation (3-15). In this equation the constant K_0 represents the activation energy of diffusion, which Hunter (1992) proposed is derivable from the sorption isotherm. In this study compression wood and opposite wood possessed only slightly higher EMC at high RH and therefore it is questionable if these have a major effect on the activation energy of diffusion. More likely for the high variations of the diffusion coefficient is the actual cell structure and properties of the sample. The influence of the cell structure could be described by Siau's model (1984) and modified for compression wood to take the more circular tracheids in cross section into account. The diffusion equation could further be modified to take the individual shrinkage into account.

The experimental data gathered throughout this experiment can be used to validate newly developed models describing the moisture transport within in radiata pine and also newly developed empirical equations for the diffusion coefficient to be derived.

Due to the high variability of the basic wood properties of the samples, the sound of velocity for longitudinal samples in longitudinal direction was measured. This revealed that some samples of the normal wood (mainly heartwood) behave in a similar manner as compression wood (lower tangential and radial shrinkage, lower modulus of elasticity). This finding should be taken into account for moisture transport experiments in wood, because of its relevance to actual drying applications.

The algorithm used in this study also allows the implementation of the actual moisture content profile within the samples and, in combination with an automation of the weighing process for the individual samples, these improvements of the experimental set-up would lead to higher accuracies of the derived constants.

Chapter 4

Distortion of Radiata Pine Timber

When boards are cut from logs at saw mills, their moisture content can be as high as 150-200% for the radiata pine sapwood. Most of this moisture has to be removed prior to remanufacturing or usage in construction. Radiata pine timber in New Zealand is normally dried in controlled kilns. During the moisture removal, the wood shrinks, and the timber can significantly change its shape, which is usually referred to as distortion or warp. Distortion, or warp, of sawn timber is commonplace in wood, and it is widely accepted that the following factors contribute to its occurrence: moisture content gradients, material inhomogeneity, growth stress, anisotropic shrinkage and spiral grain angle.

The major forms of timber distortion are illustrated in Figure 4-1. In the cross section, depending on the location in the log and shape of the timber the main distortional forms are cup, diamond and oval. Over the entire length of the timber board, the distortion can be categorised as bow, crook and twist.

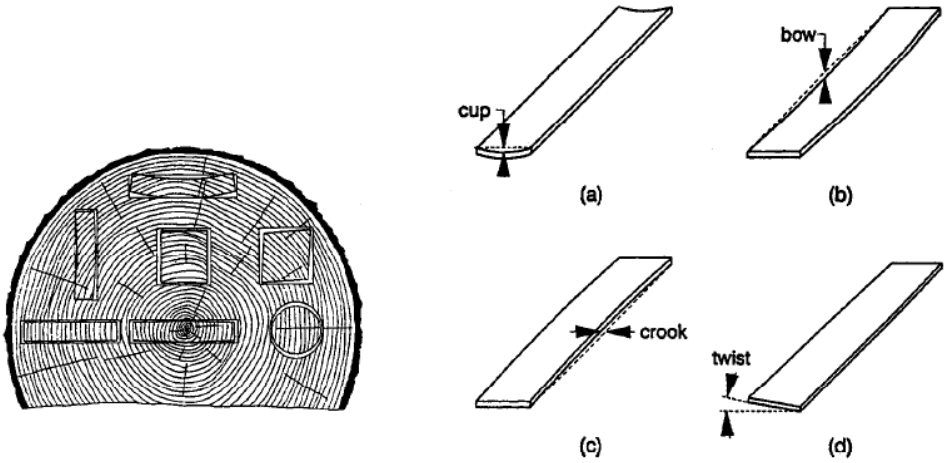

Figure 4-1: Cross-sectional- and board distortion of wood (Forest Products Laboratory, 1974).

In the following, a geometric model will be introduced which originated during the experimental investigation of earlywood and latewood properties of radiata pine (Chapter 2). Due to the small radial and tangential dimensions compared with the longitudinal dimension, the question arose how the individual growth layer within the wooden board contributes to the distortion.

A preliminary literature review revealed several distortion models, which predict the distortion of timber in regards to the location and dimensions of the board within the log, shrinkage variation and spiral grain angle. During the years working in my fathers joinery and the practical saw milling workshops at the Secondary School of Technology for Timber Industry in Kuchl, Austria (Höhere Technische Lehranstalt Kuchl, Holztechnikum), I found that hardly any board was cut perfectly parallel to the pith and further, that different year ring patterns on the bottom and top surface resulted in different distortional shapes after the drying of the board (Figure 4-1). My observation of the non parallel alignment of boards to the pith was confirmed during the validation of the geometrical model with experiment data, where most of the material differed from the parallel alignment to the pith.

During the literature study on distortion it was found that only one model existed which considered the alignment to the pith (Ormarsson, 1999). This model is based on a 3D-finite element formulation and takes into account wood property variations, board dimensions, board location, the convectional drying influence and external loading constraints. Due to the high complexity of this model it is highly valuable for research purposes to analyse certain influence factors in particular, but from a practical point of view it is not well suited for the day to day use by saw milling and drying companies, due to the long numerical solution times and the required resources (high end PC and numerical software package).

The purpose of the model was to create a highly simplified distortion model, which considered the longitudinal shrinkage, tangential shrinkage, spiral grain angle, the 3D board location and the board dimensions as the influencing parameters. The main objective was the effect of the non parallel alignment of boards to the pith. It is important to state that the effect of the actual drying and the resulting moisture gradients and wood property variations are not taken into account. The drying method itself has major influence on distortion; due to the complex inter relations between moisture content, temperature, mechanical behaviour (viscoelastic and mechano-sorptive) and shrinkage of wood.

Distortion of timber has been researched for many decades due to the significant financial losses induced by rejection due to excessive distortion. In general, the research has been focused on the material characteristics responsible for warp and on developing drying methods to prevent the excessive distortion (Arganbright *et al.*, 1978; Simpson and Tschernitz, 1998). The drying methods developed may be able to reduce the degree of distortion but cannot completely eliminate it.

Furthermore, it was observed that certain timber from the same specie can be more prone to deformation than others both in processing (drying) and in use.

For the same materials and the same drying method, the timber distortion increases with decreasing moisture content. Since the timber industry is most interested in twist, bow and crook, the influencing factors on these three distortion forms are discussed in the following section.

4.1 Literature Review

The following literature review on published research is mainly focused on the influences of shrinkage and spiral grain angle on distortion and cannot be seen as complete. Several more investigations have been undertaken in this area and not further discussed in detail due to complexities of the models, which take into account the heat and mass transfer and mechanical phenomena occurring during drying (Pang, 2000; Perre and Passard, 1995).

The literature review was performed in 2003 and extended in 2007 due to additional information made available after the initial review and their relevance in respect to the introduced model (Booker, 2005; Ekevad, 2005).

Most studies have shown that spiral grain angle has significant influence on twist (Balodis, 1972; Danborg, 1994a; Rault and Marsh, 1952). The spiral grain influence on distortion decreases with increasing distance from the pith as shown by Kloot and Page (1959), Mishiro and Booker (1989), Cown *et al.* (1996) and Johansson *et al.* (2001). Other parameters like knots, compression wood, growth ring width and wood density have little influence on twist (Beard *et al.*, 1993; Kliger *et al.*, 1995).

The influence factors responsible for bow and crook are assumed to be the longitudinal shrinkage variations and growth stresses within a log. These stresses can deform a board directly after it was sawn (Archer, 1986; Mishiro and Booker, 1989). The variable longitudinal shrinkage, compression wood and knots influence on bow and crook were investigated in several studies (Gaby, 1972; Shelly *et al.*, 1979; Simpson and Gerhardt, 1984). It was found that these parameters all contribute to the development of the bow and the crook.

Several mathematical approaches exist to predict twist, bow and crook of the timber. These models are either based on statistical correlations or on geometrical analysis. The statistical models (Balodis, 1972; Beard *et al.*, 1993; Cown *et al.*, 1996; Johansson *et al.*, 2001; Kloot and Page,

1959) are correlated from large pools of experimental data with some assumptions to create mathematical formulae. Some of these models can explain up to 65% of the variation of twist.

In general, these models are less accurate for bow and crook, and significant errors are induced if the models are used when the parameters are outside the original experimental conditions.

The first analytical model describing twist in timber was introduced by Stevens and Johnston (1960). The Stevens and Johnston model takes into account the distance of the board from the pith, the tangential shrinkage, the length and the spiral grain angle, and this model was originally used for describing the twist of wooden shells. Balodis (1972) showed that this model is suitable for calculating the twist of boards cut from these shells. Johansson and Kliger (2002) applied the model to Norway spruce studs and found that it explains the twist with reasonable accuracy (R^2=0.73).

Fridley and Tang (1993) introduced a three-dimensional distortion model based on the anisotropic shrinkage. This model takes into account the geometry of the board and location within a log. In this paper, only theoretical predictions were presented as a general indication without any experimental validation of the model's accuracy.

Johansson *et al.* (2001) and Kliger *et al.* (2003) investigated the distortion of Norway spruce timber based on the measurements of 240 studs. They applied the Stevens and Johnston model for the twist prediction and developed a model to simulate bow and crook (spring) as a function of variations of longitudinal shrinkage. From these studies, it was concluded that when the three-dimensional longitudinal shrinkage variation is known, the model can predict the distortion with a discrepancy of 5%.

Booker (2005) published a geometric model to predict twist in unrestrained boards. This model considers the location and dimensions of the board within a log as well as the spiral grain variations within the board. It was found that the spiral grain variation dominates both the twist direction and its magnitude. This is also confirmed by Ekevad (2005) who developed a finite element model for the twist prediction in timber.

Ormarsson *et al.* (1998; 1999; 2000) developed a complicated model which is solved using finite element analysis to describe the deformation process and the stress development during drying. This model predicts the twist development with reasonable accuracy, but underestimates the bow and the crook compared with the experimental data (Johansson and Kliger, 2002).

4.2 Geometrical Model for Twist in Timber Boards

In this section a new geometrical model is developed, based on the observation that the boards are sawn with various cone segments which represent growth rings in the log. Due to the conical nature of the tree stem, these segment areas are not parallel to the board length direction, and the cone segment with the largest area has more influence on board distortion. In the development of the new geometrical model, the mathematical derivations for the spiral grain curve, and the shrinkage of the cone segment is included.
The initial literature review undertaken revealed that none of the geometrical models allowed for boards not parallel aligned to the pith and further the actual conical growth of trees was not taken into account and instead replaced by cylindrical elements.

In the development of the twist model, an expression for a spiral grain curve wound up under a constant spiral grain angle is firstly derived, followed by the derivation of the shrunken cone segment in the longitudinal and the tangential directions in the three-dimensional space. Afterwards the derived geometrical model is applied in actual boards cut from a log. The twist model has been solved analytically in Matlab 7.1. The key feature of the model is that the model is capable of calculating the twist for boards not parallel to the pith. The developed twist model does not include the radial shrinkage, based on the literature review findings that the most important influence factors on twist are the spiral grain angle and tangential and longitudinal shrinkage.

The predicted twist from this model is compared with the predictions from Stevens and Johnston's model, followed by the validation of the model with experimental data provided by Harrington *et al.* (2005). However, the model developed in this work is not designed to predict the twist for boards containing pith, and therefore the results presented do not contain any boards containing the pith.

Boards containing pith are known for their severe distortion, therefore mostly discharged or downgraded pre or post drying due to severe distortion and the poor stiffness quality. Certainly, the model could be modified to give predictions for boards containing the pith, but due to the low quantities of such boards the author did not include this option.

In addition to the validation with the Stevens and Johnston's model, the model behavior is compared with the results from Booker's geometrical model, which has been published after the completion of the model introduced here.

4.2.1 Spiral grain curve

In a tree stem, the grains are aligned at an angle to the stem axis. This angle is called the spiral grain angle. In this model, a single curve will represent the tracheids forming one spiral grain curve. To derive the spiral grain curve, it assumed that each curve contains grains, which have a constant spiral grain angle (SGA) and a constant conical angle (CA).

With the assumption of a constant conical angle (*CA*), the radius of the curve (*r*) will decrease with tree height:

$$r = r_0 - z \cdot \tan(CA) \tag{4-1}$$

Where r_0 represents the radius of the curve (growth ring) at the bottom of the log ($z = 0$). Imagine that a string is wound up at a constant angle (SGA) on a coned curve with a certain conical angle as shown in Figure 4-2; the resulting geometric relationships can be derived as shown in Figure 4-3.

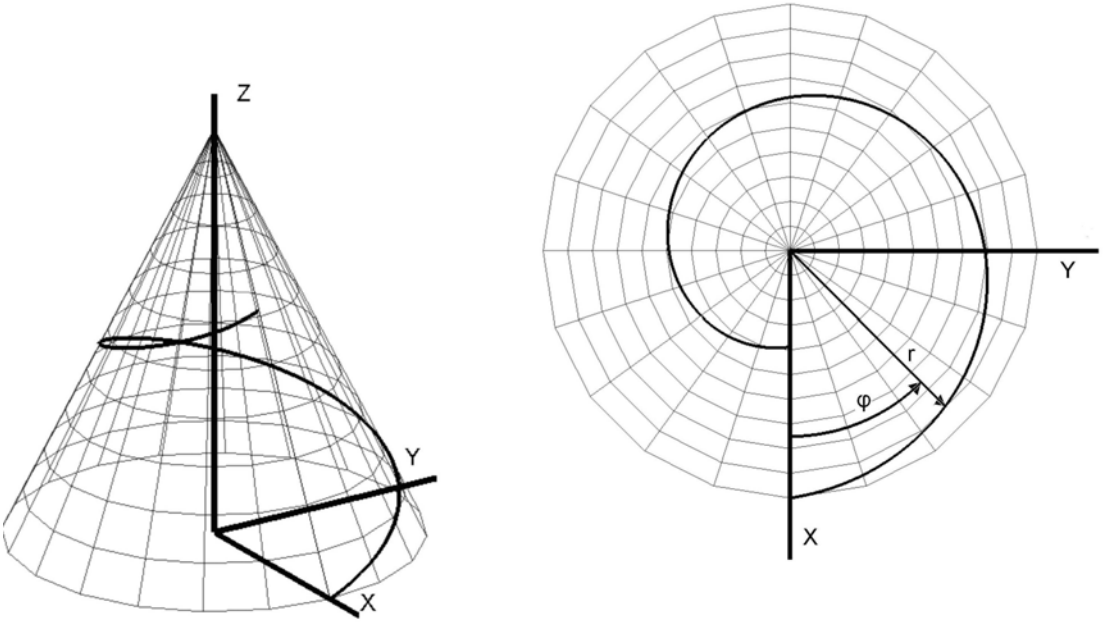

Figure 4-2: Spiral grain curve. The left diagram represents a tree stem, and the right diagram is the stem seen from the tree top.

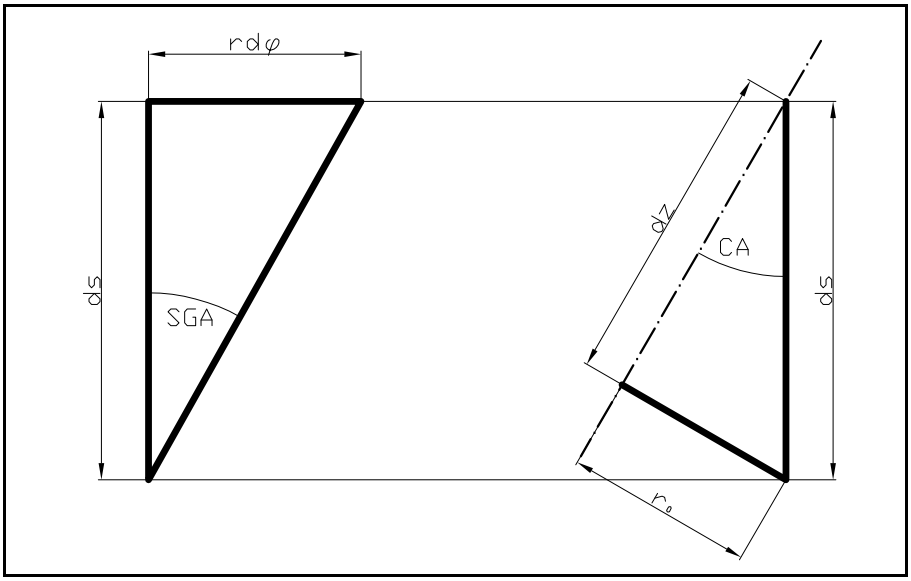

Figure 4-3: Definition of the geometric relationships.

Variables shown in Figure 4-2 and Figure 4-3 are defined as follows:

φ	Parameter, for the description of the spiral grain curve, (radians);
ds	Differential cone length [m];
r	Radius of the curve surface at the angle φ [m];
SGA	Spiral grain angle [radians]
CA	Conical angle [radians];
dz	Differential height [m]

The differential cone length as function of the differential z-coordinate:

$$ds = \frac{dz}{\cos(CA)} \tag{4-2}$$

The spiral grain angle is defined as:

$$\tan(SGA) = \frac{r \cdot d\varphi}{ds} = \frac{\cos(CA) \cdot r \cdot d\varphi}{dz} \tag{4-3}$$

Substituting r from equation 4-1:

$$\frac{\cos(CA)}{\tan(SGA)} \cdot d\varphi = \frac{dz}{r_0 - z \cdot \tan(CA)} \tag{4-4}$$

Integrating Equation (4-4) with the following boundary condition ($z = 0 \rightarrow \varphi = 0$) leads to:

$$z(\varphi) = \frac{r_0}{\tan(CA)} \cdot \left[1 - e^{-A \cdot \varphi}\right] \tag{4-5}$$

Parameter A is the substituted variable:

$$A = \frac{\cos(CA) \cdot \tan(CA)}{\tan(SGA)} = \frac{\sin(CA)}{\tan(SGA)} \tag{4-6}$$

The radius depending on the parameter φ:

$$r(\varphi) = r_0 \cdot e^{-A\varphi} \tag{4-7}$$

Now it is possible to write for the x and y direction:

$$x(\varphi) = r(\varphi) \cdot \cos(\varphi) \tag{4-8}$$

$$y(\varphi) = r(\varphi) \cdot \sin(\varphi) \tag{4-9}$$

Equations (4-5), (4-8) and (4-9) represent the spiral grain curve in parametric form.

4.2.2 Shrinkage of an individual cone layer

Since the cone curve can be expressed by mathematical formulae as discussed in the above section, the shrinkage may be determined once the longitudinal shrinkage and the tangential shrinkage are known. To calculate the shrinkage in the grain direction, it is necessary to know the length of the grain segment. The length of a parameterised curve in space is defined by:

$$ds_{fibre} = \sqrt{\dot{x}^2 + \dot{y}^2 + \dot{z}^2} \cdot d\varphi \tag{4-10}$$

Differentiation of the parameterized curve with respect to parameter φ gives:

$$\dot{x} = \frac{dx}{d\varphi} = r_0 \cdot e^{-A\cdot\varphi} \cdot \left[-A \cdot \cos(\varphi) - \sin(\varphi)\right] \tag{4-11}$$

$$\dot{y} = \frac{dy}{d\varphi} = r_0 \cdot e^{-A\cdot\varphi} \cdot \left[-A \cdot \sin(\varphi) + \cos(\varphi)\right] \tag{4-12}$$

$$\dot{z} = \frac{r_0}{\tan(CA)} \cdot A \cdot e^{-A\cdot\varphi} \tag{4-13}$$

Substituting Equations (4-11), (4-12) and (4-13) into Equation (4-10) and integrating it leads to a relationship for the grain length:

$$s_{fibre} = r_0 \cdot \sqrt{1 + A^2 + \frac{A^2}{\tan^2(CA)}} \cdot \left[e^{-A\cdot\varphi_{start}} - e^{-A\cdot\varphi_{end}}\right] \tag{4-14}$$

In which A is a parameter defined by Equation (4-6), φ_{start} and φ_{end} representing the start and end point of the particular grain in radians. In this case, the starting point of the grain curve $\varphi=0$ sits on the X-axis, due to the definitions of the Equations (4-8) and (4-9).

If it is assumed that, during the changes of the grain curve dimensions, its shape does not change in the grain direction (ε_{fibre}), the resulting new angle can be derived (φ_{end}=constant):

$$s_{fibre} \cdot (1 - \varepsilon_{fibre}) = r_0 \cdot \sqrt{1 + A^2 + \frac{A^2}{\tan^2(CA)}} \cdot \left[e^{-A \cdot \bar{\varphi}_{start}} - e^{-A \cdot \varphi_{end}} \right] \tag{4-15}$$

$$e^{-A \cdot \bar{\varphi}_{start}} = (1 - 0.5 \cdot \varepsilon_{fibre}) \cdot e^{-A \cdot \varphi_{start}} + 0.5 \cdot \varepsilon_{fibre} \cdot e^{-A \cdot \varphi_{end}} \tag{4-16}$$

To better illustrate the shrinkage in directions parallel and normal to the grain direction, the cone segment is rolled out as shown in Figure 4-1 including the grain, whose mid point of the length lies on the Z'-axis. The fibre mid point is defined by the following equation:

$$\varphi_M = -\frac{1}{A} \cdot \ln\left[0.5 \cdot (e^{-A \cdot \varphi_{start}} + e^{-A \cdot \varphi_{end}}) \right] \tag{4-17}$$

For each grain to shrink with the same relationship as the grain mid-length, it is necessary to define the longitudinal shrinkage axis. This particular axis should be normal to each grain. To derive this particular axis, the same procedure was followed as already used for the derivation of the spiral grain curve, just with a new angle which is rotated by 90°.

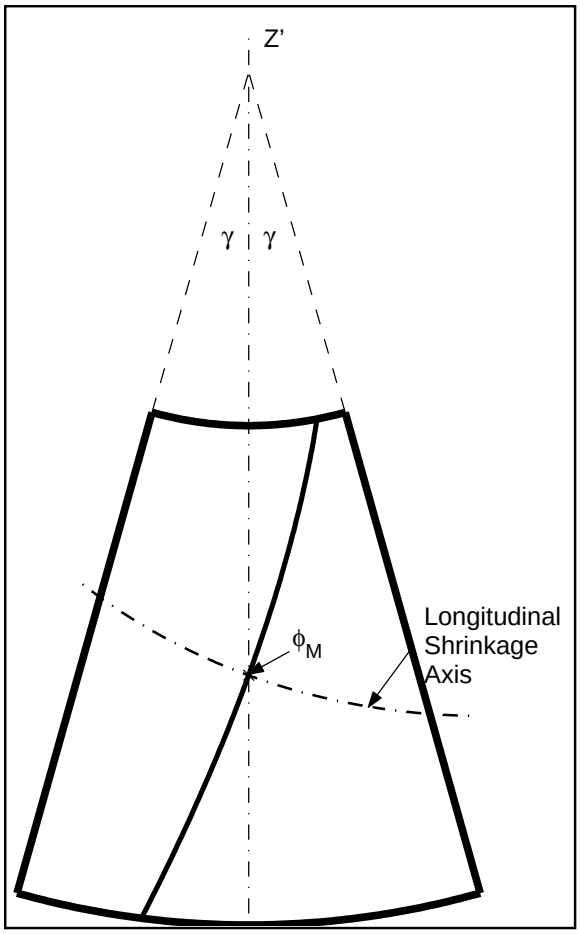

Figure 4-4: Rolled out cone segment.

The resulting curve in parametric form is given by:

$$B = \tan(SGA) \cdot \sin(CA) \tag{4-18}$$

The radius of the curve normal to the grain curve follows:

$$r(\psi) = r_0 \cdot e^{-B\psi} \tag{4-19}$$

The curve normal to the grain curve in parametric form has the form:

$$x(\psi) = r(\psi) \cdot \cos(\psi) \tag{4-20}$$

$$y(\psi) = r(\psi) \cdot \sin(\psi) \tag{4-21}$$

$$z(\psi) = \frac{r_0}{\tan(CA)} \cdot \left[1 - e^{-B \cdot \psi}\right] \tag{4-22}$$

The relationship between φ and ψ can be derived by equating:

$$\begin{aligned} & r(\varphi) = r(\psi) \\ & r_0 \cdot e^{-A \cdot \varphi} = r_0 \cdot e^{-B \cdot \psi} \\ & A \cdot \varphi = B \cdot \psi \rightarrow \frac{\sin(CA)}{\tan(SGA)} \cdot \varphi = \sin(CA) \cdot \tan(SGA) \cdot \psi \\ & \varphi = \psi \cdot \tan^2(SGA) \end{aligned} \tag{4-23}$$

With the above introduced equations it is now possible to calculate the shrinkage of the individual points on the cone segment, when the centre point of the segment is defined. In the following, the centre point of the segment was assumed to be at half of the fibre length and on the symmetry axis (z').

The longitudinal shrinkage, calculated by Equation 4-16, is illustrated on a rolled out cone segment (Figure 4-5).

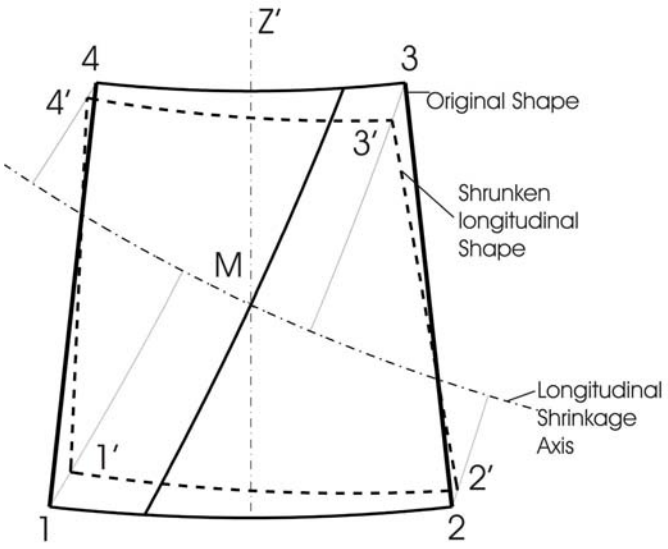

Figure 4-5: Shrinkage in fibre direction.

Equation 4-16 can also be used for the calculation of the shrinkage normal to the fibre by replacing parameter A with parameter B, replacing ε_{fibre} with ε_{normal} and using the correct angles. Figure 4-6 shows the shrinkage in the fibre direction and the shrinkage normal to the fibre.

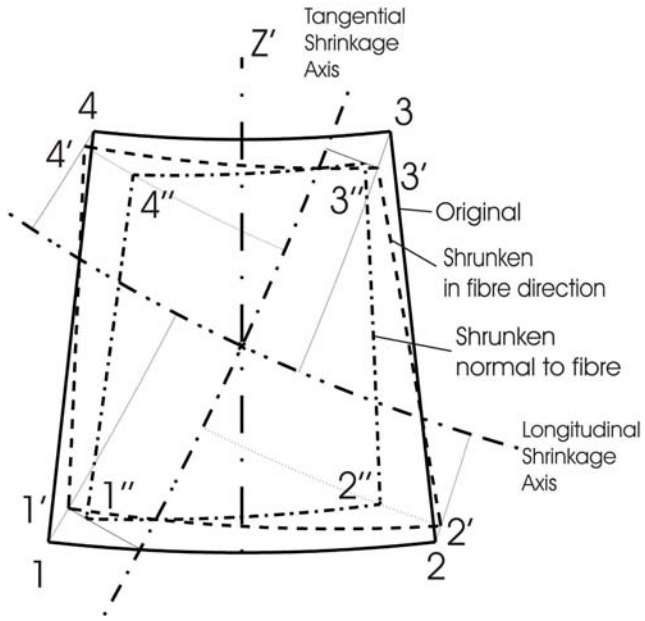

Figure 4-6: Combined shrinkage of the rolled out cone segment.

4.2.3 Geometrical distortion model for twist

After the shrinkage of a cone segment parallel and normal to the grain direction, the board twist can be analysed by considering the cone segment curves. When looking at the distortion of a specific board within a log, the model considers the shrinkage of the cone segment that has the largest surface area, since this surface is dominant in the board twist. Figure 4-7 illustrates the location and shape for boards with dimensions of 2.4 meters long, 50 mm thick and 100 mm wide. Depending on the board location and the position, the largest area segment varies significantly. The largest cone segment area and the area distribution as a function of board location will be discussed in more detail in Section 4.3.

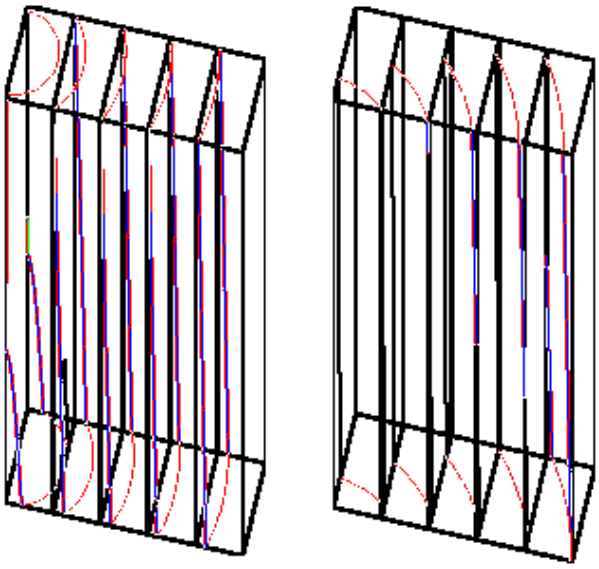

Figure 4-7: Location of the largest surface area within boards cut from different locations.

As an example, the shrinkage of the cone segment within a board with dimensions of 50 mm (thickness) x 100 mm (width) x 100 mm (length) is shown in Figure 4-8. The deformed cone segment's curve surface is illustrated by the black dotted lines. Clearly visible is the twist of the corner points.

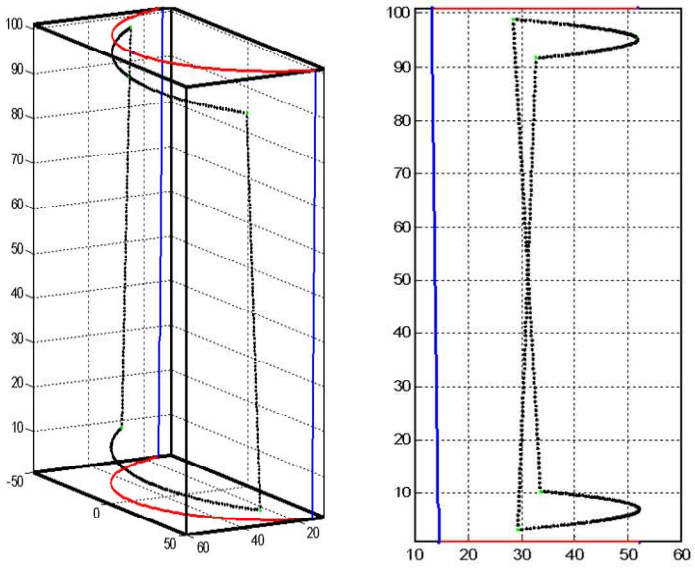

Figure 4-8: Distorted cone segment.

Figure 4-9 illustrates the procedure for the twist calculation. The board twist due to the distortion of the cone segment with the largest area can be calculated by determining the position changes of three points on the cone segment curve. These points are the corner points of the segment and the mid point of the segment at the same height, namely the points P2, P3 and P1, respectively in Figure 4-9. The points P2', P3' and P1' are corresponding positions to the original P2, P3 and P1 with movements in the longitudinal and tangential direction.

With the assumption that the rotation axis is generated with the rotation centres (P1 and P1') and their corresponding centres of gravity (S and S') formed by the two triangles (P1, P2, P3 and P1', P2', P3'), the original cross sectional shape can be rotated onto the shrunk P1' and S' axis. The centre of gravity for the three points in space is defined as:

$$\begin{bmatrix} S_x \\ S_y \\ S_z \end{bmatrix} = \frac{1}{3}\left(\begin{bmatrix} P_{1x} \\ P_{1y} \\ P_{1z} \end{bmatrix} + \begin{bmatrix} P_{2x} \\ P_{2y} \\ P_{2z} \end{bmatrix} + \begin{bmatrix} P_{3x} \\ P_{3y} \\ P_{3z} \end{bmatrix} \right) \tag{4-24}$$

The original shape and the axis created by P1 and S have to be moved firstly by the translation vector. Now the rotation point P1 is located at the origin (0, 0, 0) and the rotation around the X-, Y- and Z-axes onto the new axis P1' and S' can be performed and afterwards moved to P1'.

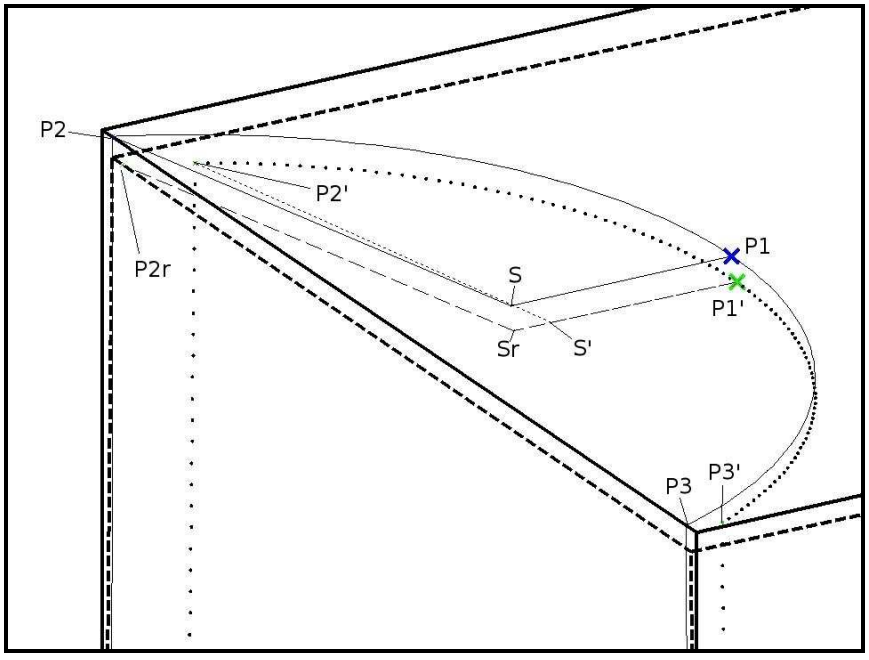

Figure 4-9: Rotation of the original cross sectional shape.

The rotations around the three axes adopting the right hand rule to determine the positive rotation direction was applied, the according axes presentation is shown in Figure 4-10. The corresponding rotation matrices for the three principle directions are given in Equations (4-25) to (4-27).

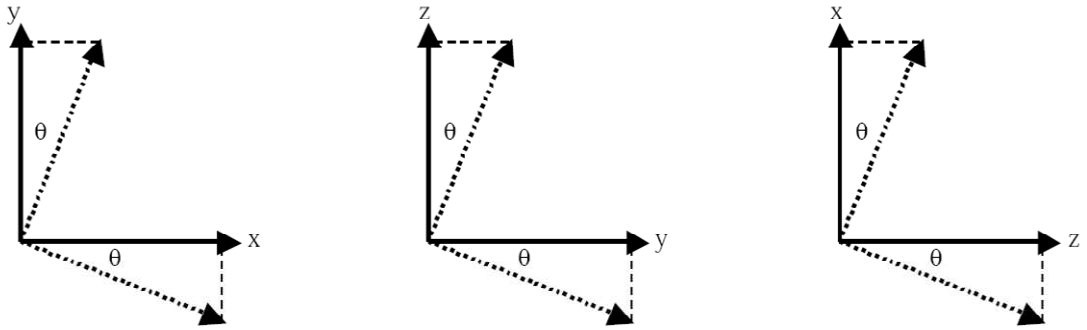

Figure 4-10: Right hand rule for positive rotation direction around the three principle axes.

Z-Axis transformation:

$$\begin{bmatrix} P'_x \\ P'_y \\ P'_z \end{bmatrix} = \begin{bmatrix} \cos\theta & -\sin\theta & 0 \\ \sin\theta & \cos\theta & 0 \\ 0 & 0 & 1 \end{bmatrix} \cdot \begin{bmatrix} P_x \\ P_y \\ P_z \end{bmatrix} \tag{4-25}$$

X-Axis transformation:

$$\begin{bmatrix} P'_x \\ P'_y \\ P'_z \end{bmatrix} = \begin{bmatrix} 1 & 0 & 0 \\ 0 & \cos\theta & -\sin\theta \\ 0 & \sin\theta & \cos\theta \end{bmatrix} \cdot \begin{bmatrix} P_x \\ P_y \\ P_z \end{bmatrix} \tag{4-26}$$

Y-Axis transformation:

$$\begin{bmatrix} P'_x \\ P'_y \\ P'_z \end{bmatrix} = \begin{bmatrix} \cos\theta & 0 & \sin\theta \\ 0 & 1 & 0 \\ -\sin\theta & 0 & \cos\theta \end{bmatrix} \cdot \begin{bmatrix} P_x \\ P_y \\ P_z \end{bmatrix} \tag{4-27}$$

4.3 Simulation Results and Discussion

The geometrical model introduced in Section 4.2 has been solved in Matlab 7.1 and in this section, the simulation results will be presented with comparison to the Stevens and Johnston's model. The board location within the cross section in the log is given by the radius from the origin to the board centroid and the corresponding angle from the X-axis (Figure 4-11). The flatsawn boards are cut when the board centroid is at the vertical axis ($\Theta = \pm 90°$) and quartersawn boards are cut when the board centroid is at the horizontal axis ($\Theta = 0°$ or $270°$).

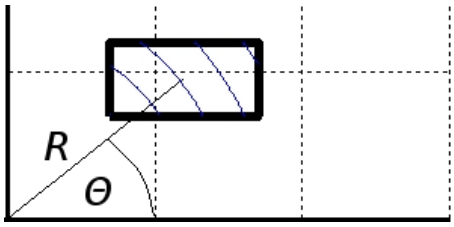

Figure 4-11: Definition of board location in the log cross section.

In the model, the definition of the board location in the 3D-space is achieved by providing the length of the board and the bottom and top cross sectional location. Therefore the model is capable of dealing with boards that are not parallel to the pith.

4.3.1 Segments area distribution

Depending on the length and the location of the board within the log cross section, the segment curved surface with the largest area will vary in size, shape and location within the board. The area distribution for the flatsawn and quartersawn boards can be determined and compared for the board dimensions of 100 mm (width) x 50 mm (thickness) x 2400 mm (length). The distance from the board centroid to the pith was 100 millimetres.

Comparison between the quartersawn with the flatsawn board in Figures 4-12 and 4-13 shows that the segment area is approximately two times greater for the flatsawn board than for the quartersawn board. The quartersawn board contains a higher number of segments of similar areas in the positions from 65 mm to 150 mm from the pith, whereas for the flatsawn board the similar area segments are only found in positions from 95 mm to 125 mm from the pith. The currently developed model only takes into account the maximum area segments, and thus further improvement may be needed to include the area distribution within the board.

Figures 4-12 and 4-13 can also be used to simulate the board twist using the model developed in this work, and the results are compared with the Stevens and Johnston's model. In general, when the Stevens and Johnston's model is applied the radius from the centroid is used to calculate the twist. However, in most cases the developed model in this work calculates the twist from a segment, the radius of which is smaller than the centroid radius (deviation from the fact that the board is not parallel aligned from the pith).

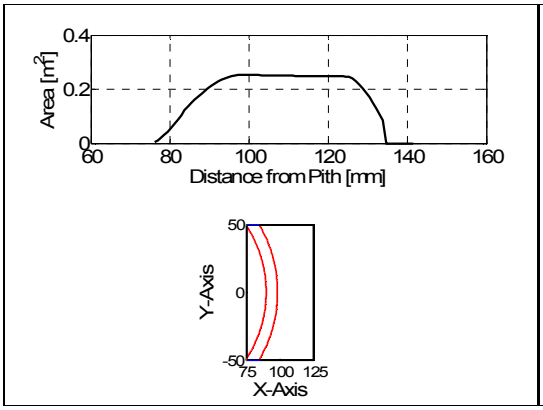

Figure 4-12: Segment surface area distribution for a quartersawn board.

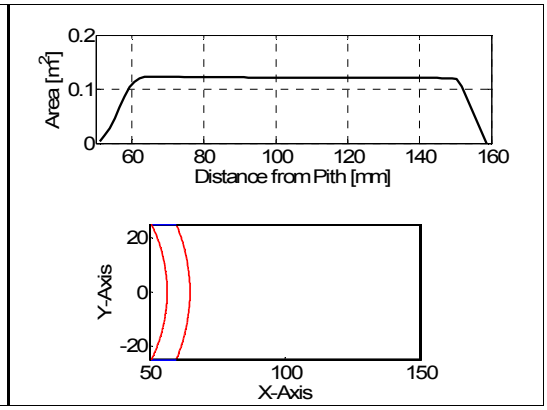

Figure 4-13: Segment surface area distribution for a flatsawn board.

The surface area distribution of the largest segment curve as a function of board location for a board with dimensions 100 mm (width) x 50 mm (thickness) x 2400 mm (length) is shown in Figure 4-14. The minimum radius from the centroid is 60 mm. In general a higher centroid angle starting from 0° (Θ) results in a larger surface area for the maximum segment curve. The peak value for the largest area is found at approximately 65° followed by rapid decreases towards 90°. At the given centroid angle, this maximum surface area decreases, to a lesser extent, with increasing the radius towards the bark, due to the decreased curvature of the surface.

The largest area segment, as well as its location within the board, strongly influences the twist development when the board moisture content is reduced below the fibre saturation point. For the boards with a centre of gravity being outside the twist axis, the boards with lower surface area have more segments outside the rotation layer and, therefore, will result in more severe twist distortion. This characteristic of the geometrical model will further be discussed in the following section (4.3.2), where the simulation results are compared with Stevens and Johnston's model. For completion and to illustrate the statement above, Figure 4-15 contains the simulation results for a quartersawn (100x50x2400mm) and a flatsawn (50x100x2400mm) board with identical board centre of gravity (100mm), tangential (3%) and longitudinal (0.1%) shrinkage and spiral grain angle (6°).

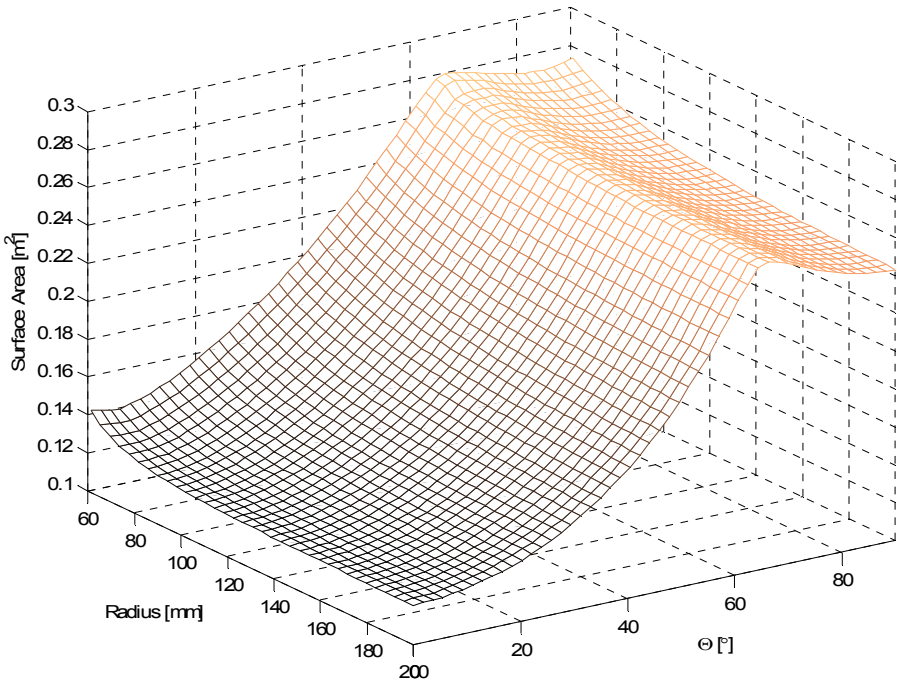

Figure 4-14: Distribution of the largest segment curve surface area as a function of board location.

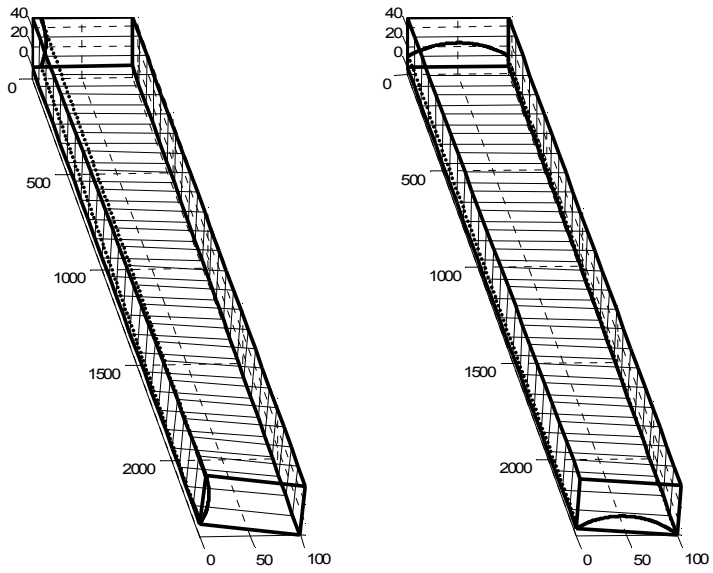

(a) (b)

Figure 4-15: Comparison of twist development for quartersawn (a) and flatsawn boards (b), with identical board centre of gravity (100mm), tangential (3%) and longitudinal (0.1%) shrinkage and spiral grain angle (6°).

4.3.2 Model prediction and comparison

In this section, the developed model is compared with Stevens and Johnston's model, which will be introduced first. Stevens and Johnston's model is based on the twisting of cylindrical shells and the twist can be calculated as follows (1960):

$$\alpha = \frac{l}{r}\frac{2 \cdot SH_T \cdot SGA}{1 + SH_T} \tag{4-28}$$

Where l represents the board length, r is the distance from the pith to the centroid of the board, SGA (in radians) is the spiral grain angle at r and SH_T is the tangential shrinkage of the shell and α represents the twist angle in radians. The above formula assumes that the longitudinal shrinkage is negligible and does not take into account the sawing pattern of the actual board.

For comparison of the two models, it is assumed that the board has a constant and left handed spiral grain angle of 6°, a constant tangential shrinkage of 3%, a constant longitudinal shrinkage of 0.1%, and board dimension of 100 mm (width) x 50 mm (thickness) x 2400 mm (length).

Figure 4-16 shows the predicted twist results for different board locations using the developed model in this work. This figure also includes the twist prediction of the Stevens and Johnston's model. All the predicted twists have the same negative twist angle but their signs have been inverted for better illustration purposes.

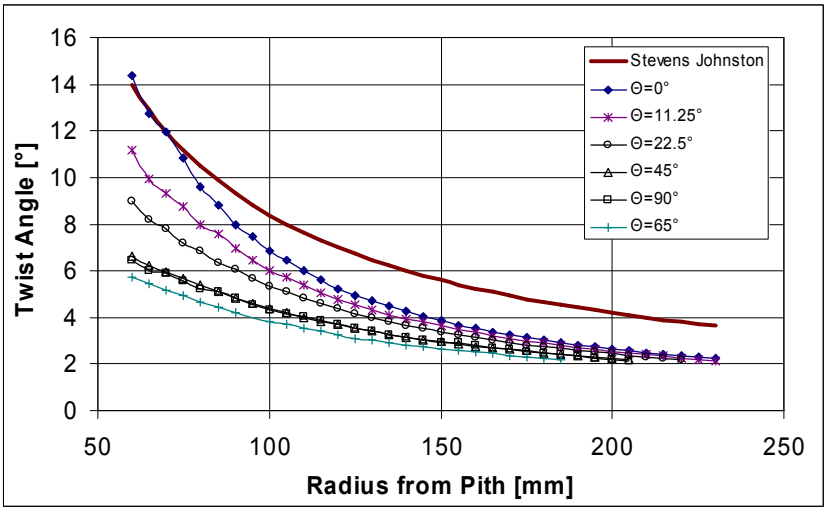

Figure 4-16: Predicted twist by the developed model and comparison with results from Stevens and Johnston's model.

The twist prediction of a +10° and -10° variation of the bottom and top theta angle respectively for flat and quarter sawn boards is shown in Figures 4-17 and 4-18. The board properties are kept constant as used for the comparison of the Stevens and Johnston model. For boards following the spiral grain rotation, the twist is significantly reduced for quarter and flat sawn boards, whereas when boards are aligned against the spiral grain rotation, the twist is slightly increased.

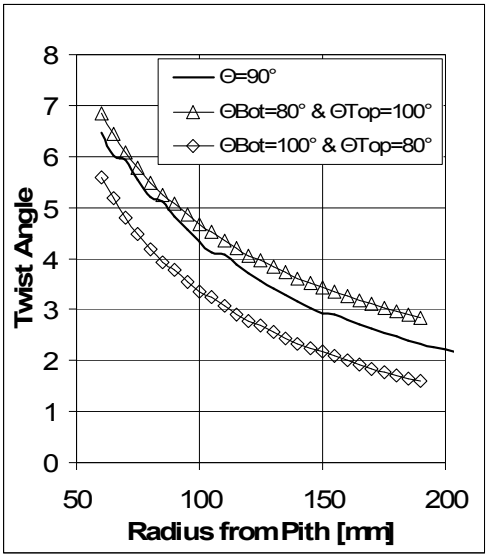

Figure 4-17: Twist variations of flatsawn boards (defined at the mid-length of the board) with different board location angles at the board bottom and top.

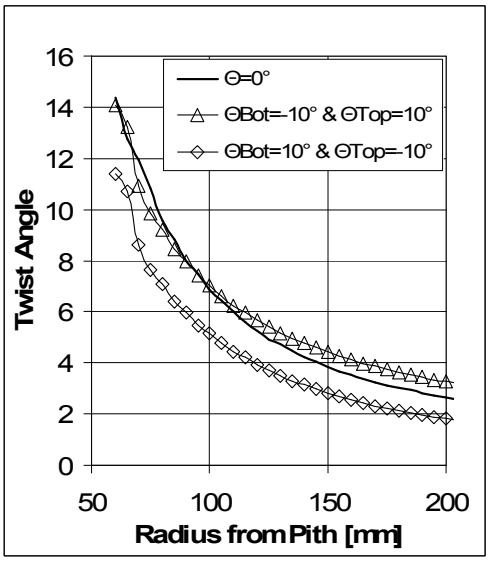

Figure 4-18: Twist variations of quartersawn boards (defined at the board mid-length) with different board location angles at the board bottom and top.

4.4 Model Validation with Experimental Data

The experimental data for the validation of the introduced geometrical model was provided by a group of New Zealand Companies who investigated the potential of existing warp prediction methodologies. Fletcher Challenge Forests Ltd. (now Tenon Ltd.) studied the quality factor; IRL (Industry Research Ltd.) used the Laser Tracheid Imaging technology to predict the board distortion; ENSIS (previously New Zealand Forest Research Institute Ltd.) did the torsional and longitudinal stiffness measurements on green boards and developed correlations of distortion between green boards and dry boards (Harrington *et al.*, 2005).

In the above studies, the materials originated from 20 logs (6 meter long) from the FCF Kawerau Sawmill log yard. Disc samples were removed from each end of the log for wood property measurements from 5-ring groups (density and spiral grain angle). Additional samples were prepared at 29 mm intervals along the diameter from bark to bark for measurements of the shrinkage (longitudinal, tangential and radial) at 12%MC.

The remaining lengths of the logs (after removing the end discs) were sawn to 100 mm (width) x 50 mm (thickness) boards and their positions within the log were recorded. The approximately 5.5 m long boards were cut to 2.4 meter in length and kiln-dried unrestrained in a rack to 10%MC using a 90/65°C schedule. Distortion (twist, bow, crook) was measured both for the green boards and the dry boards.

For the validation of the model with the provided data it was necessary to convert the spiral grain data in the growth ring into the spiral grain angle as a function of distance from the pith. This conversion was based on the derived ring width distribution shown in Chapter 1. This ring width distribution was made dimensionless relative to the log diameter and then this dimensionless growth ring width was multiplied by the actual log diameter in the experiment to obtain the distance of the growth ring from the pith. In general, the spiral grain angle had significant variation between the top and the bottom of the boards and between individual logs. To derive the spiral grain distribution within the boards, a third order polynomial regression was performed for the individual log, represented by solid lines in Figure 4-19.

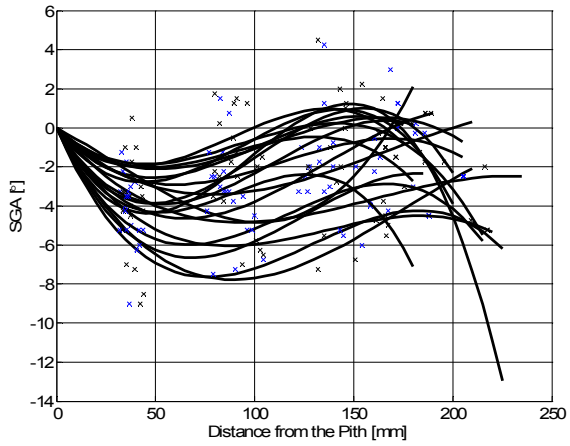

Figure 4-19: Spiral grain angle distribution of the measured materials.

The data for the shrinkage in tangential, radial and longitudinal directions at 12%MC and their corresponding average values (solid lines) for the individual logs are illustrated in Figure 4-20.

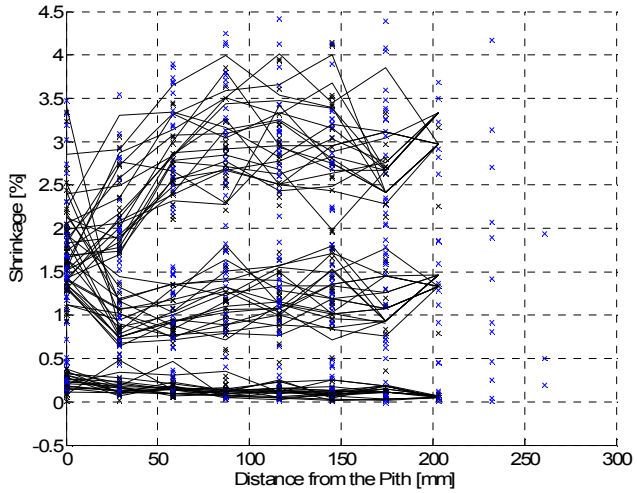

Figure 4-20: Shrinkage distribution of the measured materials.

Using the properties measured from the two end discs and using the corresponding properties for each board, twist for the board is calculated from the developed geometrical model. The results are then compared with the measured results as shown in Figure 4-21. In general, the predicted board twist is lower than the experimental data and the model predictions for the negative twist are rather poor. The lower twist values predicted by the model may be due to the shrinkage values, which were determined at 12%MC, in the model whereas the boards were dried to 10%MC. The poor prediction of negative twist values may be caused by the derived spiral grain distribution.

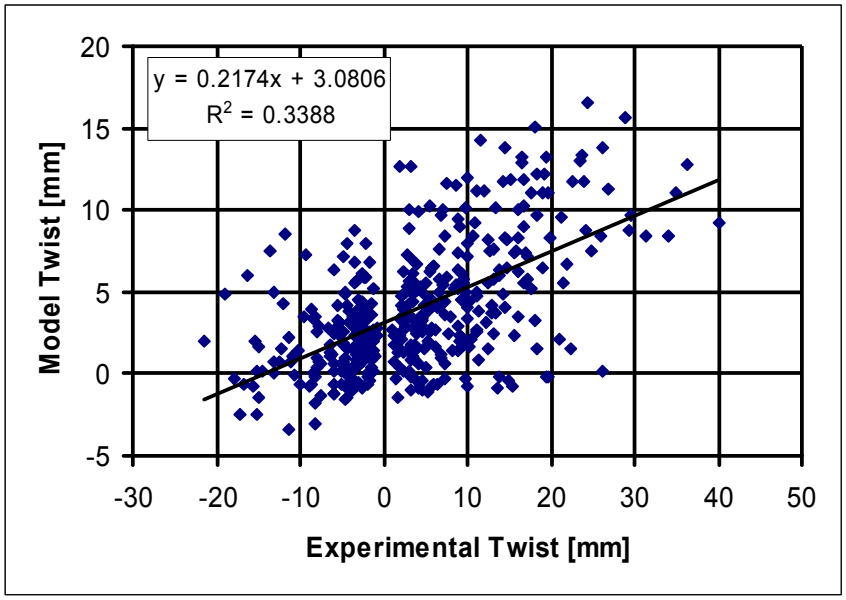

Figure 4-21: Comparison model results with experimental data for twist.

Booker (2005) and Ekevad (2005) stated that the spiral grain angle gradient over the board cross section is the major reason for the large twist of the board. The twist model developed in this work has only taken into account the properties at one position of the board (at the location of the largest cone segment).

If the statement made by Booker (2005) and Ekevad (2005) is correct, then it is necessary to check if the measured spiral grain angles from the two end-discs accurately represent the spiral grain angle gradients of the individual board. In order to investigate the relationships between the spiral grain angle gradient and the board twist, the derived spiral grain curves for the individual tree (Figure 4-19) were used to calculate the spiral grain gradient. In Figure 4-22, the board spiral grain gradient was plotted against the measured twist. No relationship was found between twist and the gradient of spiral grain angle (dSGA), and for this reason the procedure of deriving a continuous spiral grain curve (third order polynomial regression) failed. An improvement of the spiral grain distribution was not possible due to the insufficient amount of spiral grain data in the radial direction.

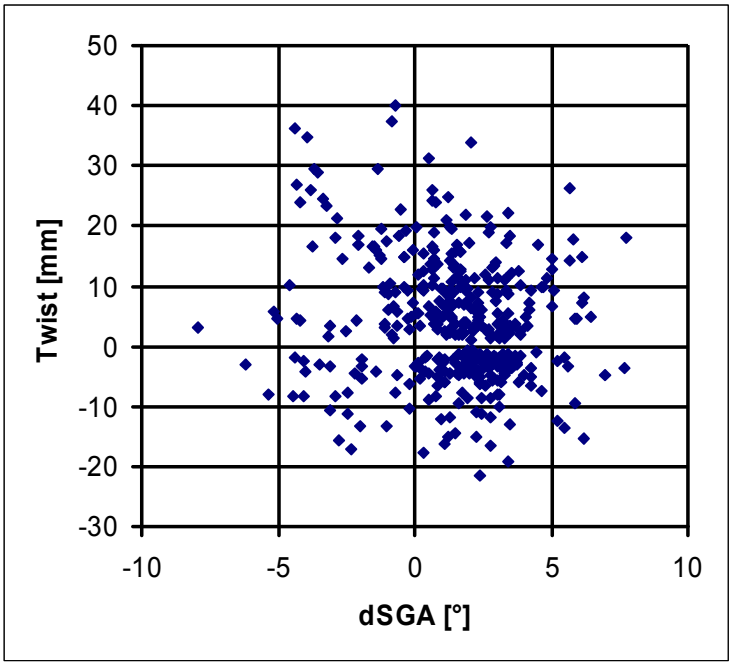

Figure 4-22: Spiral grain gradient versus measured twist of the boards.

4.5 Discussion and Conclusions

In this chapter a simple geometrical model was developed to predict the twist of timber when the boards are dried to below the fibre saturation point. The model is based on the longitudinal and tangential shrinkage of the cone segment which has the largest surface area. The cone angle and the spiral grain angle are also included in the model. The model calculates the twist of individual boards and has shown that the twist is dependant on the board location within a log and its alignment to the pith. The model predicted that the quartersawn boards twist more than the flatsawn boards, which is contradictory to predictions of Ormarsson et al. (2000) and Booker (2005). Figure 4-23 shows the experimental data for the twist (Harrington *et al.*, 2005) depending on the mean radius and mean board location angle (Θ). From the figure, it is found that there is no clear evidence to prove the difference in the board twist between the two sawing patterns. It is believed that these inconclusive results are due to the significant variation in the wood properties within a board.

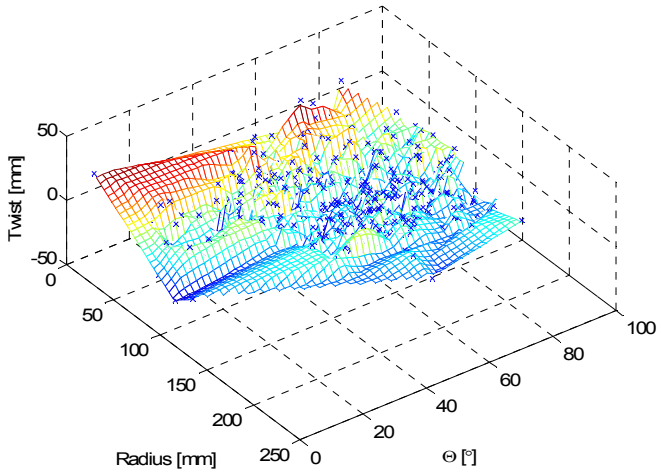

Figure 4-23: Experimental results of the board twist as a function of mean radius and board location angle.

Quantitative comparison between the model predictions and experimentally measured twists as a function of the board radius and the board location angle is extremely difficult, since the influence of other parameters cannot be eliminated. Nevertheless, Figure 4-24 shows the predicted twist development for boards (50 x 100 x 2400 mm) using constant longitudinal and tangential shrinkage (0.1% and 3%, respectively) and constant spiral grain angle (6°). The trend that the higher twist occurs for board with low radius seems consistent between the measured results and the model predictions. Also the low twist can be seen for the board location angles (Θ) between 40 and 60°. However, as mentioned previously, the model predicts higher twist for the quartersawn boards (Θ = 0°) than for the flatsawn boards (Θ = 90°), which is not apparent in the experimental results.

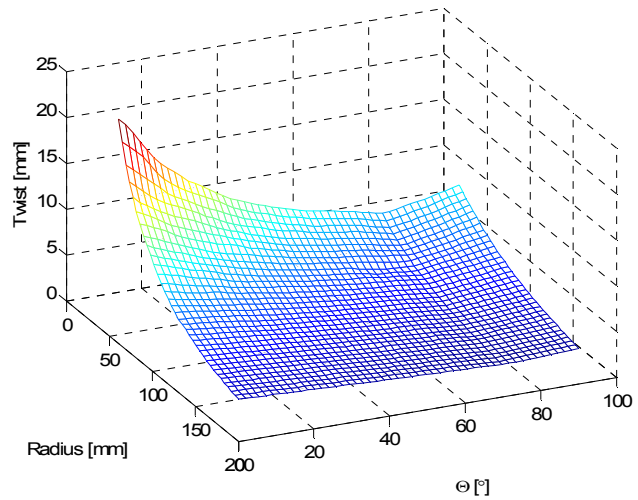

Figure 4-24: Predicted twist of boards as a function of board radius and board location angle.

The accuracy of the developed model is strongly dependent on the accuracy of the input wood properties. The data provided for the spiral grain has shown that the angle is highly variable and the information on continuous distribution of other needed properties from the pith to the bark for radiata pine does not exist in literature. Furthermore the height dependency of the wood properties is not known. Therefore, in order to improve the accuracy of the model prediction, both the wood properties for each independent board and the wood property variation within the log are needed.

Despite the wood properties, the drying method itself has to be mentioned as possible cause for distortion. The lignin and its thermoplastic behavior allow for the reduction of developed stresses induced by moisture concentration differences and the accompanied shrinkage. Klaiber *et al.* (2004) investigated the drying method influence on distortion for Norway spruce and found that air-dried boards show, in general, less twist than kiln-dried boards using a conventional drying schedule at a constant dry-wet bulb temperature of 55°C and a stepwise adaptation of the wet-bulb temperature. For bow and crook, the drying method influence was not observed. In this study, the provided material was kiln dried at higher temperatures (90°C), which might have caused a more severe distortion development.

A remark to the model developed here is that the actual programming effort for establishing the geometrical boundaries is by far more extensive than the actual shrinkage calculations. This point might be one of the reasons for the non-existent studies on the non-parallel alignment to the pith and its influences on distortion.

The model introduced here was the first approach to the development of a geometrical model for distortion. In the second approach the individual cone segment layers were shrunken independently from each other with differing spiral grain angle and shrinkage values. The interesting findings in this approach were that the cross-sectional distortion (cup, diamond) was clearly visible and further the lengthwise distortion (bow, crook) started to develop. The lengthwise distortion due to longitudinal shrinkage variation was concluded by several authors (Johansson *et al.*, 1999; Ormarsson, 1999; Simpson and Gerhardt, 1984) and seemed to be also valid for the second approach. However, the second approach was intended as an intermediate step in the formulation of an analytical distortion model. A preliminary comparison with literature data, the model introduced here and a cross-check with the provided data has shown that the second approach underestimated the three length wise distortion appearances (bow, crook and twist).

In Figure 4-25 the second approach was applied to a flatsawn board and to make the distortion clearly visible higher shrinkage values have been used.

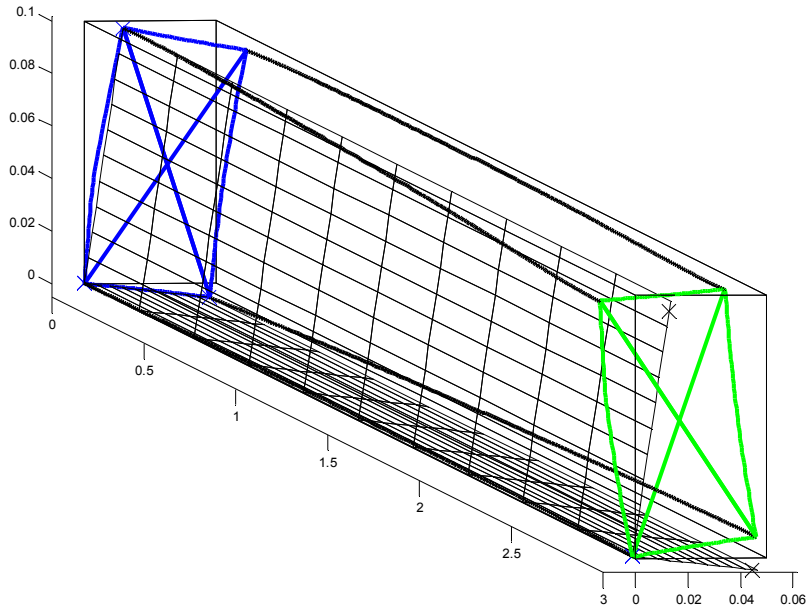

Figure 4-25: Distortion of a flatsawn board, predicted by the second approach

Due to the lower distortion predictions but the in general good agreement with the developing distortion forms, a third approach was initiated. This approach was based on the shrinkage calculations introduced here and to allow for interactions between the individual conical elements stress-strain-shrinkage relationships were included. It has to be noted, that my intention was to derive an analytical solution for the distortion to allow the analysis of the separate influence factors and further a tool which supports timber related industries in their decision making.

During his studies the author was not able to solve and establish all the necessary equations and solving algorithms, due to other commitments in the fulfilment of this thesis.

The author further recommends, based on the model simulations results that due to the low influence of the conical angle on the twist. The conical angle should be disregarded, which would lead to a significant reduction of the mathematical complexity, but not disregarding the actual board location.

A schematic flow-diagram of the twist model algorithm can be found in the appendix.

Chapter 5

Conclusions and Applications

This study has investigated some of the wood properties of radiata pine that are believed to have influence on wood distortion. By considering all of these properties and the grain alignment in a board, an analytical model was developed to simulate the wood distortion with changing moisture content. From the studies undertaken in this work, the following conclusions are drawn, and the potential applications are identified.

5.1 Wood Properties Related to Distortion

In order to better understand the twist of the board and more accurately quantify the influence of the wood properties, it was proposed in this work to experimentally investigate the wood property distribution within cross sections and variations along the tree height as well as the difference between the different wood types (earlywood, latewood, compression wood and opposite wood). These properties include shrinkage, equilibrium moisture content, fibre saturation point and diffusion coefficient. The difference between desorption (drying) and adsorption (wetting) was also examined.

The results of the shrinkage measurements can be further evaluated to find correlations with spiral grain angle and microfibril angle reported in literature. Such correlations can then be used to create statistical or analytical models for the prediction of the wood properties based on the log cross sectional shape.

Tangential Shrinkage influence on the Wood Distortion

Anisotropic shrinkage, particularly tangential and longitudinal shrinkage, is believed to significantly affect the wood distortion. The experimental results show that wood with high tangential shrinkage normally has lower longitudinal shrinkage (Chapter 2). This finding can be explained by the microfibril angle and its influence on the shrinkage. The tangential shrinkage decreases with increasing microfibril angle, whereas the longitudinal shrinkage increases with increasing microfibril angle. From this relationship, the volumetric shrinkage can be determined

once the tangential and radial shrinkage is known and, based on the measured sound velocity in the longitudinal direction, the volumetric shrinkage (ε_V) can be linked to the sound velocity (*TOF*) as discussed in Chapter 4. From the data provided by WQI, an empirical relationship between the sound velocity and volumetric shrinkage was found to be:

$$\varepsilon_V = 1.709 \cdot 10^{-8} \cdot TOF^2 - 1.246 \cdot 10^{-4} \cdot TOF + 0.286 \tag{5-1}$$

The literature review in Chapter 4 revealed that the longitudinal shrinkage is believed to have a major influence on the bow development, whereas the tangential shrinkage influences the twist the most. By considering the interaction between the tangential and the longitudinal shrinkage as discussed in Chapter 2, the influence of the tangential shrinkage on the different distortion forms can be analysed as follows.

The theoretical tangential shrinkage can be derived from the volumetric shrinkage under the assumptions that the longitudinal shrinkage is negligible and that the tangential shrinkage is twice the radial shrinkage:

$$\varepsilon^2_{theo,T} - 1.5 \cdot \varepsilon_{theo,T} + \varepsilon_V = 0 \tag{5-2}$$

The above equation has been solved by ignoring the unrealistic solution of the second order polynomial solution, and the results have been used to correlate the measurements of the board distortion with the tangential shrinkage (WQI data) as shown in Figure 5-1.

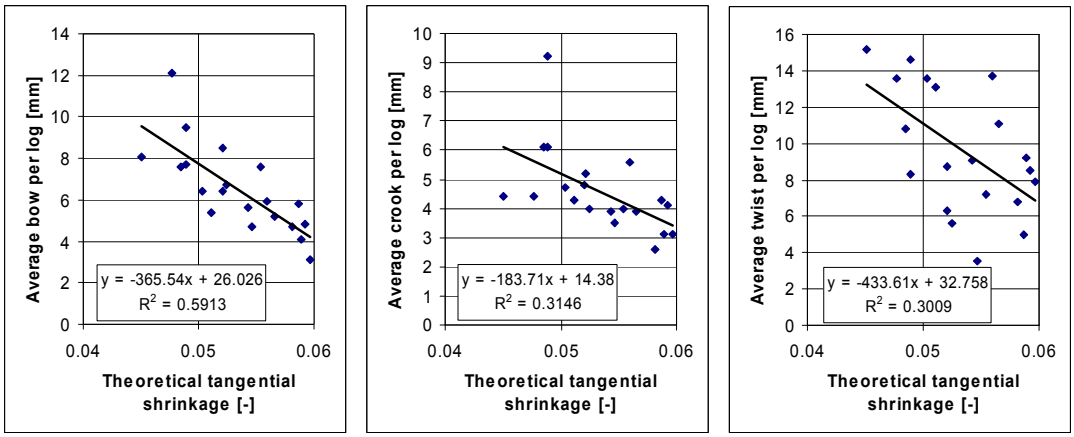

(a) (b) (c)

Figure 5-1: Comparison average bow (a), crook (b) and twist (c) per log with the theoretical tangential shrinkage.

By taking into account the relationship between the volumetric shrinkage and the sound velocity, the above correlations can potentially be used to predicting logs which are prone to distortion. The

prediction for the bow gives reasonable accuracy, but further work is needed to verify the accuracy of the predictions for the twist and the crook. To increase the predictability for the individual boards, the location of the board and the spiral grain angle has to be also taken into account in addition to the tangential shrinkage.

Radiata Pine Growth Characteristics

Chapter 1 included the wood properties variations of ten radiata pine trees based on continuous SilvaScan measurements, provided by WQI (Benchmarking study, 2004). The average ring widths, microfibril angles and densities were derived for different heights (0.2m, 1.4m, 5 and 20m) based on the year ring count from the bark. The radial ring width distributions revealed that, after seven years from the planting of the trees, an event occurred which had significant influence on the steadily improving wood quality (MOE, density and microfibril angle). After the event, which might have been pruning, the density, modulus of elasticity and microfibril angle stayed constant for approximately seven years and after this stagnation period the wood quality started to improve again. While the wood quality was significantly affected by this incident, the actual cambial productivity was only disturbed in the year of the incident. The cambial productivity was analysed by the annual growth rate, which was derived from the yearly growth ring area increase. The tree height influence on the microfibril angle was analysed, and the highest MFAs were found in the core at the base of the tree. The tree height influence on MFA for a growth ring showed that the same growth ring at 0.2 metres and 20 metres possessed similar values, whereas the MFA for the breast height and 5 metres were in general lower than at 0.2 metres and 20 metres. This finding contradicts the generally assumed decreasing microfibril angle with height for the annual growth ring.

The WQI data also included spiral grain increment measurements, which revealed large angle variations and therefore the conclusion was drawn that published literature data on spiral grain has to be critically viewed when these data are intended for further use.

Longitudinal and Tangential Shrinkage Variations in regards to Earlywood and Latewood

In general, the latewood possessed higher tangential shrinkage values than earlywood within the same growth ring whereas the earlywood had higher longitudinal shrinkage values than the latewood. This general linkage was also found for the tangential shrinkage when neglecting the differentiation between the latewood and the earlywood. High tangential shrinkage was always

accompanied by low longitudinal shrinkage values. This finding might reflect the microfibril angle influence on the tangential and longitudinal shrinkage.

The found differences between shrinkage of the earlywood and latewood within one growth ring need to be taken into account when the distortion of thin wood products is investigated. The sudden changes in shrinkage values (tangential and longitudinal) will cause stresses, which will lead to the deformation of thin wood products.

Wood Property Variations in Radial and Tree Height Directions

Wood type (heart- and softwood) seasonal variations of the green moisture content were found during the investigations. In general, heartwood possessed lower green moisture contents, and samples cut during the winter months had moisture contents close to the fibre saturation point, whereas the green moisture contents of sapwood stayed above 100% MC during the winter season. These variations have to be considered during kiln drying. Timber located in the transition zone will have high moisture content gradients, which can lead to the development of stresses when not considered in the drying schedule.

Variations of the equilibrium moisture contents were observed during the experimental investigation. Minor differences between the earlywood and the latewood of the same growth ring were found. The equilibrium moisture content showed the highest variations in the radial direction and the tree height for high relative humidities (70% - 90%RH). Highest EMC values were found for core wood at the base of the tree with a decreasing trend towards the bark and in the tree height direction. For a given growth ring along the tree height, the EMC seems not to vary with height. This finding indicates that the EMC may change after the tracheids are formed. Food storage within older tracheids might be causing the later EMC variations. The sorption isotherms for the adsorption and desorption at 30°C were derived. The typical ‘S’ curves were obtained, but the values are consistently higher than the data in the widely used EMC table (Bramhall and Wellwood, 1976).

The tangential shrinkage distribution within trees was highly variable, but the generally known trend of increasing tangential shrinkage in the radial direction towards the bark could be confirmed. The earlier mentioned linkage between the longitudinal and tangential shrinkage results in the opposite radial behavior of the longitudinal shrinkage, namely highest values close to the pith decreasing towards the bark.

The fibre saturation point was derived from the tangential shrinkage values at certain equilibrium moisture contents and also described as the shrinkage intersection point. It was found that the FSP increases from the pith to the bark and decreases with the tree height. The FSP is highly important during drying, because it indicates the start of wood property changes (stiffness, shrinkage) and therefore the variations found here need to be considered in timber production.

The wood property behaviour in adsorption was also investigated during this study, derived from prior oven-dried samples. This experimental set-up led to higher swelling values than the corresponding shrinkage values at the same moisture content. In the praxis, these differences will usually not be as significant as in this experiment for low temperature drying (below 90°C) but have to be considered for high temperature drying due to the resulting dimensional differences in the conditioning phase of the drying, which can result in the stress development.

Water Diffusion

Chapter 3 investigated the diffusion coefficient for different types of wood. Under the ambient conditions, the wood with high values of the diffusion coefficient picks up or loses moisture faster than wood with lower values of the diffusion coefficient. From the experimental results, it was found that diffusion coefficient of radiata pine is comparable to other species such as Scott pine and Norway spruce, and the trend for the radial distribution over the cross sectional disc and the variation along the tree height is inconsistent. However, it was found that the diffusion coefficient for compression wood was the lowest compared with other wood (normal wood and opposite wood). This indicates that the compression wood will change its moisture content slower than other wood although the compression wood normally shows high tendency to distort.

The highly variable moisture content dependency on the diffusion coefficient for the individual samples and directions led to the conclusion that the wood structure has to be taken into account in future experimental investigations and theoretical models. The current knowledge about the activation energy for diffusion in combination with the wood structure can not explain the high fluctuations in the moisture dependency on the diffusion coefficient and has to be further improved.

5.2 Model Development and Future Work

In Chapter 4, an analytical model for simulation of the wood twist was developed which is based on the geometry and geometrical changes of the grains aligning at different angles to the pith. This model has a unique feature in that it considers the grow ring curves within the board, and the model

includes factors of conical angle and variations of the growth ring curvatures. The model can predict the impacts of the wood properties, including shrinkage, spiral grain angle, density and conical angle.

The spiral grain angle has been found to be the key parameter influencing the twist of the board. The model can predict this influence through the relationship between the spiral grain angle and the curvature of the growth ring, as shown in Figure 5-2. Clearly visible is the change of the apparent radius of the curve, which does not correspond to the cone radius at the certain height. The grains themselves bend over the three dimensional surface. The curvature decreases with the spiral grain angle and the distance from the pith (radius). The highest values of the curvature are found for the segment surfaces close to the pith axis for all the spiral grain angles with a rapid decrease up to 5 cm from the pith. Afterwards the rate of the decrease slows down, approaching a constant value as the bark is approached for a given spiral grain angle.

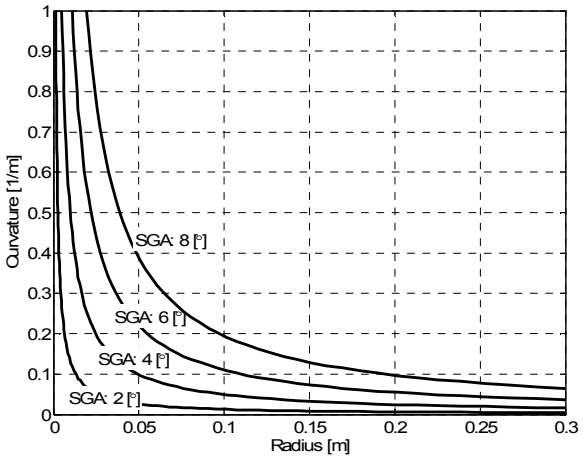

Figure 5-2: Radial distributions of the spiral grain curvatures for different spiral grain angles.

Although the curvature may affect the wood properties, the above calculated curvature cannot be directly applied to wood due to the interaction between fibres. The coarseness of the segment surface may play an important role in the formation of the individual tracheids in respect to their lengths and internal properties. The spiral grain has its origin in the cambial zone, which is also the place where tracheids are formed. The pre-given growth direction might not allow the tracheid to develop straight, and therefore it has to adjust its properties to the given situation.

In the current model, the largest growth ring segment area is assumed to be the dominant one for the board distortion, and the property variation along the board length is not included. Therefore, the model needs to be further improved by including these factors and by considering the moisture distribution, which will lead to the application of the finite element method. In regards to moisture

content distribution within the board, the water diffusion coefficient measured in this work needs to be included to predict the water movement when the wood is dried, or the dried wood is placed in given ambient conditions (temperature, relative humidity and air flow).

From the current study, it is concluded that in order to achieve accurate predictions of the wood distortion, it is important for the models to include the variations of the wood properties within the board, since this study has shown that there are significant variations within a tree (along the radial direction over the cross sectional disc and along the tree height) for most of the wood properties.

Furthermore, wood property variations between trees also need to be included since trees at different locations differ even at the same forest site. Trees near the site edges or on higher terrain may contain higher proportions of compression wood, which is formed for tree survival and growth.

References

Archer, R. R. (1986). *Growth stresses and strains in trees*. Berlin ; New York: Springer-Verlag.

Arganbright, D. G., Venturino, J. A., andGorvad, M. (1978). Warp reduction in young-growth ponderosa pine studs dried by different methods with top-load restraint. *Forest-Products-Journal, 28*(8), 47-52.

Ayranci, E., Ayranci, G., andDogantan, Z. (1990). Moisture Sorption Isotherms of Dried Apricot, Fig and Raisin at 20-Degree-C and 36-Degree-C. *Journal of Food Science, 55*(6), 1591-&.

Balodis, V. (1972). Influence of grain angle on twist in seasoned boards. *Wood-Science, 5*(1), 44-50.

Bamber, R. K., Burley, J., andCommonwealth Agricultural Bureaux. (1983). *The wood properties of Radiata Pine*. Slough: Commonwealth Agricultural Bureaux.

Bannister, M. H. (1973). The origins of radiata pine in cultivation. *What's New in Forest Research, No. 2*.

Barber, N. F., andMeylan, B. A. (1964). The anisotropic shrinkage of wood. A theoretical model. *Holzforschung,-Berlin, 18*(5), 146-156.

Barnett, J. R., andBonham, V. A. (2004). Cellulose microfibril angle in the cell wall of wood fibres. *Biological Reviews, 79*(2), 461-472.

Beard, J. S., Wagner, F. G., Taylor, F. W., andSeale, R. D. (1993). The influence of growth characteristics on warp in two structural grades of southern pine lumber. *Forest-Products-Journal, 43*(6), 51-56.

Bell, E. R., Peck, E. C., andKrueger, N. T. (1954). Modulus of elasticity of wood determined by dynamic methods. *Rep-US-For-Prod-Lab,-Madison*(1977), 10.

Booker, R. E. (2005). Geometric model to predict twist in unrestrained boards. *Wood-Science-and-Technology, 39*(4), 269-289.

Bramhall, G. (1979). Mathematical-Model for Lumber Drying .1. Principles Involved. *Wood Science, 12*(1), 14-21.

Bramhall, G., andWellwood, R. W. (1976). Kiln drying of western Canadian lumber. *Information-Report,-Western-Forest-Products-Laboratory,-Canada*(VP-X-159), ii.

Burdon, R. D. (1975). Compression wood in Pinus radiata clones on four different sites. *New-Zealand-Journal-of-Forestry-Science, 5*(2), 152-164.

Burdon, R. D., Kibblewhite, R. P., Walker, J. C. F., Megraw, R. A., Evans, R., andCown, D. J. (2004). Juvenile versus mature wood: a new concept, orthogonal to corewood versus outerwood, with special reference to Pinus radiata and P. taeda. *Forest-Science, 50*(4), 399-415.

Cai, L. (2005). Determination of diffusion coefficients for sub-alpine fir. *Wood-Science-and-Technology, 39*(2), 153-162.

Cave, I. D. (1968). The anisotropic elasticity of the plant cell wall. *Wood-Sci-Technol,-NY, 2*(4), 268-278.

Chen, Y., Choong, E. T., andWetzel, D. M. (1995). Evaluation of diffusion coefficient and surface emission coefficient by an optimization technique. *Wood-and-Fiber-Science, 27*(2), 178-182.

Choong, E. T. (1963). Movement of moisture through a softwood in the hygroscopic range. *For-Prod-J, 13*(11), 489-498.

Choong, E. T., andSkaar, C. (1969). Separating internal and external resistance to moisture removal in wood drying. *Wood-Sci,-Madison, 1*(4), 200-202.

Choong, E. T., andSkaar, C. (1972). Diffusivity and surface emissivity in wood drying. *Wood-and-Fiber, 4*(2), 80-86.

Coleman, T. F., andLi, Y. Y. (1996a). An interior trust region approach for nonlinear minimization subject to bounds. *Siam Journal on Optimization, 6*(2), 418-445.

Coleman, T. F., andLi, Y. Y. (1996b). A reflective Newton method for minimizing a quadratic function subject to bounds on some of the variables. *Siam Journal on Optimization, 6*(4), 1040-1058.

Comstock, G. L. (1963). Moisture diffusion coefficients in wood as calculated from adsortion, desorption, and steady state data. *For-Prod-J, 13*(3), 97-103.

Cown, D. J. (1975). Variation in tracheid dimensions in the stem of a 26-year-old Radiata Pine tree. *Appita-, 28*(4), 237-245.

Cown, D. J., Haslett, A. N., Kimberley, M. O., andMcConchie, D. L. (1996). The influence of wood quality on lumber drying distortion. *Annales-des-Sciences-Forestieres, 53*(6), 1177-1188.

Cown, D. J., andMcConchie, D. L. (1980). Wood property variations in an old-crop stand of radiata pine. *New-Zealand-Journal-of-Forestry-Science, 10*(3), 508-520.

Cown, D. J., andMcConchie, D. L. (1983). Radiata pine wood properties survey (1977-1982). *FRI-Bulletin,-Forest-Research-Institute,-New-Zealand*(50), i.

Cown, D. J., Young, G. D., andKimberley, M. O. (1991). Spiral grain patterns in plantation-grown Pinus radiata. *New-Zealand-Journal-of-Forestry-Science, 21*(2-3), 206-216.

Crank, J. (1956). *The mathematics of diffusion*. Oxford: Clarendon Press.

Danborg, F. (1994a). Drying properties and visual grading of juvenile wood from fast grown Picea abies and Picea sitchensis. *Scandinavian-Journal-of-Forest-Research, 9*(1), 91-98.

Danborg, F. (1994b). Spiral grain in plantation trees of Picea abies. *Canadian-Journal-of-Forest-Research, 24*(8), 1662-1671.

Danvind, J., andEkevad, M. (2006). Local water vapor diffusion coefficient when drying Norway spruce sapwood. *Journal-of-Wood-Science, 52*(3), 195-201.

Dinwoodie, J. M. (1975). Timber: a review of the structure-mechanical property relationship. *Journal-of-Microscopy, 104*(1), 3-32.

Dixon, H. H. (1914). *Transpiration and the ascent of sap in plants*. London: MacMillan.

Donaldson, L. A. (1992). Within- and between-tree variation in microfibril angle in Pinus radiata. *New-Zealand-Journal-of-Forestry-Science, 22*(1), 77-86.

Donaldson, L. A. (1993). Variation in microfibril angle among three genetic groups of Pinus radiata trees. *New-Zealand-Journal-of-Forestry-Science, 23*(1), 90-100.

Droin-Josserand, A., Taverdet, J. L., andVergnaud, J. M. (1989). Modeling of Moisture Absorption within a Section of Parallelepipedic Sample of Wood by Considering Longitudinal and Transversal Diffusion. *Holzforschung, 43*(5), 297-302.

Droin, A., Taverdet, J. L., andVergnaud, J. M. (1988). Modelling the kinetics of moisture adsorption by wood. *Wood-Science-and-Technology, 22*(1), 11-20.

Echols, R. M. (1955). Linear relation of fibrillar angle to tracheid length, and genetic control of tracheid length in Slash Pine. *Trop-Woods*(102), 11-22.

Ekevad, M. (2005). Twist of wood studs: dependence on spiral grain gradient. *Journal-of-Wood-Science, 51*(5), 455-461.

Eklund, L., andSall, H. (2000). The influence of wind on spiral grain formation in conifer trees. *Trees:-Structure-and-Function, 14*(6), 324-328.

Fakhouri, B., Mounji, H., andVergnaud, J. M. (1993). Comparison of the absorption and desorption of water between Scots pine and spruce after submersion in water. *Holzforschung-, 47*(4), 271-277.

Fridley, K. J., andTang, R. C. (1993). Modeling 3-Dimensional Distortion of Wood Due to Anisotropic Shrinkage. *Mathematical and Computer Modelling, 17*(9), 23-30.

Gaby, L. I. (1972). Warping in Southern Pine studs. *USDA-Forest-Service-Research-Paper,-Southeastern-Forest-Experiment-Station*(SE-96), 8.

Geankoplis, C. J. (2003). *Transport processes and separation process principles : (includes unit operations)* (4th ed.). Upper Saddle River, NJ: Prentice Hall Professional Technical Reference.

Harrington, J., Ilic, J., Jones, T., Xu, P., McKinely, R., Northway, R.*, et al.* (2005). WQI STA. 1.5 Evaluate Methods for Predicting Warp - Final Report [unpublished report]. (WQI).

Harris, J. M. (1961). The dimensional stability, shrinkage intersection point, and related properties of New Zealand timbers. *Tech-Pap-For-Res-Inst-NZ-For-Serv*(36), 17.

Harris, J. M. (1977). Shrinkage and density of radiata pine compression wood in relation to its anatomy and mode of formation. *New-Zealand-Journal-of-Forestry-Science, 7*(1), 91-106.

Harris, J. M. (1989). *Spiral grain and wave phenomena in wood formation*. Berlin ; New York: Springer-Verlag.

Harris, J. M., andMeylan, B. A. (1965). The influence of microfibril angle on longitudinal and tangential shrinkage in Pinus radiata. *Holzforschung,-Berlin, 19*(5), 144-153.

Hartley, I. D., Avramidis, S., andMacKay, A. L. (1996). H-NMR studies of water interactions in sitka spruce and western hemlock: moisture content determination and second moments. *Wood-Science-and-Technology, 30*(2), 141-148.

Hartley, I. D., Kamke, F. A., andPeemoeller, H. (1994). Absolute moisture content determination of aspen wood below the fiber saturation point using pulsed NMR. *Holzforschung-, 48*(6), 474-479.

Hukka, A. (1999). The effective diffusion coefficient and mass transfer coefficient of nordic softwoods as calculated from direct drying experiments. *Holzforschung-, 53*(5), 534-540.

Hunter, A. J. (1991). On the basic equation of sorption and the isosteric heat. *Wood-Science-and-Technology, 25*(2), 99-111.

Hunter, A. J. (1992). On the activation energy of diffusion of water in wood. *Wood-Science-and-Technology, 26*(2), 73-82.

Johansson, M., andKliger, R. (2002). Influence of material characteristics on warp in Norway spruce studs. *Wood-and-Fiber-Science, 34*(2), 325-336.

Johansson, M., Kliger, R., andPerstorper, M. (1999). The influence of material variation on quality of Norway spruce timber. *Forest-Research-Bulletin*(212), 314-321.

Johansson, M., Perstorper, M., Kliger, R., andJohansson, G. (2001). Distortion of Norway spruce timber Part 2. Modelling twist. *Holz Als Roh-Und Werkstoff, 59*(3), 155-162.

Kang, W., andLee, N. H. (2002). Mathematical modeling to predict drying deformation and stress due to the differential shrinkage within a tree disk. *Wood Science and Technology, 36*(6), 463-476.

Kelsey, K. E. (1956). The shrinkage intersection point its significance and the method of its determination. *For-Prod-J, 6*(10), 411-417.

Khalili, S., Nilsson, T., andDaniel, G. (2001). The use of soft rot fungi for determining the microfibrillar orientation in the S2 layer of pine tracheids. *Holz-als-Roh--und-Werkstoff, 58*(6), 439-447.

Kininmonth, J. A., andWhitehouse, L. J. (1991). *Properties and uses of New Zealand radiata pine*. Rotorua, N.Z: N.Z. Ministry of Forestry Forest Research Institute with assistance from the New Zealand Lottery Grants Board.

Klaiber, V., andSeeling, U. (2004). The influence of drying method on the warp behavior of Norway spruce (Picea abies (L.) Karst.) sawn timber. *Forest-Products-Journal, 54*(4), 79-87.

Kliger, I. R., Perstorper, M., Johansson, G., andPellicane, P. J. (1995). Quality of timber products from Norway spruce. *Wood-Science-and-Technology, 29*(6), 397-410.

Kliger, R., Johansson, M., Perstorper, M., andJohansson, G. (2003). Distortion of Norway spruce timber. Part 3: Modelling bow and spring. *Holz-als-Roh--und-Werkstoff, 61*(4), 241-250.

Kloot, N. H., andPage, M. W. (1959). A study of distortion in Radiata Pine scatlings. *Div-for-Prod-Technol-Pap-for-Prod-Aust*(7), 24.

Kollmann, F. F. P., andCote, W. A. (1968). *Principles of wood science and technology*. Berlin: Springer.

Kubler, H. (1991). Function of spiral grain in trees. *Trees:-Structure-and-Function, 5*(3), 125-135.

Lavery, P. B. (1986). *Plantation forestry with Pinus radiata : review papers*. Christchurch, N.Z.: School of Forestry University of Canterbury.

Lavery, P. B. (1990). Radiata pine statistics NEFD and notes of Chilean, Australian and other resource descriptions. *New Zealand Forestry*(35), 24-29.

Leelavanichkul, S., andCherkaev, A. (2004). Why the grain in tree trunks spirals: a mechanical perspective. *Structural and Multidisciplinary Optimization, 28*(2-3), 127-135.

Liu, J. Y., Simpson, W. T., andVerrill, S. P. (2001). An inverse moisture diffusion algorithm for the determination of diffusion coefficient. *Drying Technology, 19*(8), 1555-1568.

Madgwick, H. A. I. (1994). *Pinus radiata : biomass, form and growth*. Rotorua, N.Z: H.A.I. Madgwick.

MAF (2007). *THE NEW ZEALAND FORESTRY INDUSTRY*: The Ministry of Agriculture and Forestry, N.Z. Retrieved 20.01. 2007, from http://www.maf.govt.nz/mafnet/rural-nz/overview/nzoverview015.htm

Martensson, A., andSvensson, S. (1997a). Stress-strain relationship of drying wood. Part 1: Development of a constitutive model. *Holzforschung-, 51*(5), 472-478.

Martensson, A., andSvensson, S. (1997b). Stress-strain relationship of drying wood. Part 2: verification of a one-dimensional model and development of a two-dimensional model. *Holzforschung-, 51*(6), 565-570.

McBride, C. F. (1967). Some economic losses in producing lumber from spiral grained logs. *Inform-Rep-For-Prod-Lab,-Vancouver*(VP-X-17), 12.

Megraw, R. A., Leaf, G., andBremer, D. (1998). *Longitudinal shrinkage and microfibril angle in Lobolly pine.* Paper presented at the Microfibril Angle in Wood: Proccedings of the IAWA/IUFRO International Workshop on the Significance of Microfibril Angle, Christchuch, New Zealand.

Mishiro, A., andBooker, R. E. (1989). Warping in new crop radiata pine 100x50 mm (2 by 4) boards. *IAWA-Bulletin, 10*(3), 340-341.

Mishiro, A., Cown, D. J., andWalford, G. B. (1986). A further examination of the clearwood properties of radiata pine grown in New Zealand. *FRI-Bulletin,-Forest-Research-Institute,-New-Zealand*(104), 23.

Nicholls, J. W. P., andDadswell, H. E. (1962). Tracheid length in Pinus radiata D. Don. *Div-For-Prod-technol-Pap-For-Prod-Aust*(24), 19.

Nicholls, J. W. P., andDadswell, H. E. (1965). Assessment of wood qualities for tree breeding. III. In Pinus radiata D. Don. *Div-For-Prod-technol-Pap-For-Prod-Aust*(37), 34.

NZFI. (2006). *Facts&Figures 2005/2006*.

Olek, W., Perre, P., andWeres, J. (2005). Inverse analysis of the transient bound water diffusion in wood. *Holzforschung, 59*(1), 38-45.

Orman, H. R. (1955). The response of New Zealand timbers to fluctuations in atmospheric moisture conditions. *Tech-Pap-For-Res-Inst-NZ-For-Serv*(8), 32.

Ormarsson, S. (1999). *Numerical analysis of moisture-related distortions in sawn timber.* PhD thesis Thesis. Chalmers University of Technology.

Ormarsson, S., Dahlblom, O., andPetersson, H. (1998). A numerical study of the shape stability of sawn timber subjected to moisture variation - Part 1: Theory. *Wood Science and Technology, 32*(5), 325-334.

Ormarsson, S., Dahlblom, O., andPetersson, H. (1999). A numerical study of the shape stability of sawn timber subjected to moisture variation - Part 2: Simulation of drying board. *Wood Science and Technology, 33*(5), 407-423.

Ormarsson, S., Dahlblom, O., andPetersson, H. (2000). A numerical study of the shape stability of sawn timber subjected to moisture variation Part 3: Influence of annual ring orientation. *Wood Science and Technology, 34*(3), 207-219.

Ormarsson, S., Petersson, H., andDahlblom, O. (2000). Numerical and experimental studies on influence of compression wood timber distortion. *Drying Technology, 18*(8), 1897-1919.

Pang, S. (1994). *High-temperature drying of Pinus radiata boards in a batch kiln.* PhD Thesis. University of Canterbury.

Pang, S. (2000). Modelling of stress development during drying and relief during steaming in Pinus radiata lumber. *Drying Technology, 18*(8), 1677-1696.

Pang, S. (2001, July, 2001). *Anisotropic shrinkage, equilibrium moisture content and fibre saturation point of earlywood and latewood of radiata pine.* Paper presented at the 7th International IUFRO Wood Drying Conference, Tsukuba, Japan, July, 2001.

Pang, S. (2002). Predicting anisotropic shringkage of softwood - Part 1: Theories. *Wood Science and Technology, 36*(1), 75-91.

Pang, S., andHaslett, A. N. (2002). Effects of sawing pattern on drying rate and residual drying stresses of Pinus radiata lumber. *Maderas:-Ciencia-y-Technologia, 4*(1), 40-49.

Pang, S., andHerritsch, A. (2005). Physical properties of earlywood and latewood of Pinus radiata D. Don: anisotropic shrinkage, equilibrium moisture content and fibre saturation point. *Holzforschung-, 59*(6), 654-661.

Perre, P., andPassard, J. (1995). A Control-Volume Procedure Compared with the Finite-Element Method for Calculating Stress and Strain during Wood Drying. *Drying Technology, 13*(3), 635-660.

Perre, P., andTurner, I. (2001a). Determination of the material property variations across the growth ring of softwood for use in a heterogeneous drying model - Part 2. Use of homogenisation to predict bound liquid diffusivity and thermal conductivity. *Holzforschung, 55*(4), 417-425.

Perre, P., andTurner, I. (2001b). Determination of the material property variations across the growth ring of softwood for use in a heterogeneous drying model part 1. Capillary pressure, tracheid model and absolute permeability. *Holzforschung, 55*(3), 318-323.

Perstorper, M., Johansson, M., Kliger, R., andJohansson, G. (2001). Distortion of Norway spruce timber. *Holz-als-Roh--und-Werkstoff, 59*(1/2), 94-103.

Preston, R. D. (1948). The fine structure of the wall of the conifer tracheid. III. Dimensional relationships in the central layer of the secondary wall. *Biochimica-et-Biophysica-Acta*(2), 370-383.

Preston, R. D. (1974). *The physical biology of plant cell walls*. London: Chapman and Hall.

Rault, J. P., andMarsh, E. K. (1952). The incidence abd sylvicultural implications of spiral grain in Pinus longifolia Roxb. in South Africa and its effect on converted timber. *6th-British-Commonwealth-Forestry-Conference,-Canada,-1952*.

Rock, D. A. (1975). Why does Radiata Pine grow so vigorously in New Zealand? *Forest Industries Review*(7), 2-3.

Rosenkilde, A., andArfvidsson, J. (1997). Measurement and evaluation of moisture transport coefficients during drying of wood. *Holzforschung-, 51*(4), 372-380.

Rosenkilde, A., andGlover, P. (2002). High resolution measurement of the surface layer moisture content during drying of wood using a novel Magnetic Resonance Imaging technique. *Holzforschung-, 56*(3), 312-317.

Salin, J. G. (1992). Numerical prediction of checking during timber drying and a new mechano-sorptive creep model. *Holz-als-Roh--und-Werkstoff, 50*(5), 195-200.

Salin, J. G. (2003). *External Heat and Mass Transfer - Some Remarks.* Paper presented at the 8th International IUFRO Wood Drying Conference, Brasov, Romania, 24 - 29 August 2003.

Sanio, K. (1872). On the size of the wood cells of the scoth pine (Pinus Sylvestris). *Jahrbücher für Wissenschaftle Botanik*(8), 401-420.

Saren, M. P., Serimaa, R., Andersson, S., Saranpaa, P., Keckes, J., andFratzl, P. (2004). Effect of growth rate on mean microfibril angle and cross-sectional shape of tracheids of Norway spruce. *Trees-Structure and Function, 18*(3), 354-362.

Shampine, L. F., andReichelt, M. W. (1997). The MATLAB ODE suite. *Siam Journal on Scientific Computing, 18*(1), 1-22.

Sharp, A. R., Riggin, M. T., Kaiser, R., andSchneider, M. H. (1978). Determination of moisture content of wood by pulsed nuclear magnetic resonance. *Wood-and-Fiber, 10*(2), 74-81.

Shelly, J. R., Arganbright, D. G., andBirnbach, M. (1979). Severe warp development in young-growth ponderosa pine studs. *Wood-and-Fiber, 11*(1), 50-56.

Shepherd, K. R. (1964). Some observations on the effect of drought on the growth of Pinus radiata D. Don. *Aust-For, 28*(1), 7-22.

Siau, J. F. (1984). *Transport processes in wood*. Berlin ; New York: Springer-Verlag.

Siau, J. F. (1995). *Wood--influence of moisture on physical properties*. [Blacksburg, VA]: Dept. of Wood Science and Forest Products Virginia Polytechnic Institute and State University.

Simpson, W. T., andGerhardt, T. D. (1984). Mechanism of crook development in lumber during drying. *Wood-and-Fiber-Science, 16*(4), 523-536.

Simpson, W. T., andLiu, J. Y. (1991). Dependence of the water vapor diffusion coefficient of aspen (Populus spec.) on moisture content. *Wood-Science-and-Technology, 26*(1), 9-21.

Simpson, W. T., andTschernitz, J. L. (1998). Effect of thickness variation on warp in high-temperature drying plantation-grown loblolly pine 2 by 4's. *Wood-and-Fiber-Science, 30*(2), 165-174.

Skaar, C. (1954). Analysis of methods for determining the coefficient of moisture diffusion in wood. *J-For-Prod-Res-Soc, 4*(6), 403-410.

Skaar, C. (1988). *Wood-water relations*. Berlin ; New York: Springer-Verlag.

Skaar, C., andBabiak, M. (1982). A model for bound-water transport in wood. *Wood-Science-and-Technology, 16*(2), 123-138.

Skatter, S., andKucera, B. (1998). The cause of the prevalent directions of the spiral grain patterns in conifers. *Trees-Structure and Function, 12*(5), 265-273.

Söderström, O., andSalin, J. G. (1993). On Determination of Surface Emission Factors in Wood Drying. *Holzforschung, 47*(5), 391-397.

Stamm, A. J. (1946). Passage of liquids, vapors and dissolved materials through softwoods. *Tech-Bull-US-Dep-Agric*(929), 80.

Stamm, A. J. (1959). Bound-water diffusion into wood in the fibre direction. *For-Prod-J, 9*(1), 27-32.

Stamm, A. J. (1964). *Wood and cellulose science*. New York: Ronald Press Co.

Stanish, M. A. (2000). Predicting the crook stability of lumber within the hygroscopic range. *Drying Technology, 18*(8), 1879-1895.

Stevens, W. C., andJohnston, D. D. (1960). Distortion caused by spiralled grain. *Timb-Technol, 68*(2252), 217-218.

Svensson, S., andMartensson, A. (1999). Simulation of drying stresses in wood. Part I: comparison between one- and two-dimensional models. *Holz-als-Roh--und-Werkstoff, 57*(2), 129-136.

Svensson, S., andMartensson, A. (2002). Simulation of drying stresses in wood part II. Convective air drying of sawn timber. *Holz-als-Roh--und-Werkstoff, 60*(1), 72-80.

Tang, R. C. (1973). The microfibrillar orientation in cell-wall layers of Virginia Pine tracheids. *Wood-Science, 5*(3), 181-186.

Taverdet, J. L., andVergnaud, J. M. (1984). Study of Transfer Process of Liquid into and Plasticizer out of Plasticized Pvc by Using Short Tests. *Journal of Applied Polymer Science, 29*(11), 3391-3400.

Taylor, J. R. (1997). *An introduction to error analysis : the study of uncertainties in physical measurements* (2nd ed.). Sausalito, Calif.: University Science Books.

Thomas, F. C., andLi, Y. Y. (1994). On the Convergence of Interior-Reflective Newton Methods for Nonlinear Minimization Subject to Bounds. *Mathematical Programming, 67*(2), 189-224.

Tiemann, H. D. (1906). Effect of moisture upon the strength and stiffness of wood. *USDA For Serv Bull, 70*, 144 pp.

Time, B. (2002a). Studies on hygroscopic moisture transport in Norway spruce (Picea abies) - Part 1: Sorption measurements of spruce exposed to cyclic step changes in relative humidity. *Holz Als Roh-Und Werkstoff, 60*(4), 271-276.

Time, B. (2002b). Studies on hygroscopic moisture transport in Norway spruce (Picea abies) - Part 2: Modelling of transient moisture transport and hysteresis in wood. *Holz Als Roh-Und Werkstoff, 60*(6), 405-410.

Timell, T. E. (1986). Compression wood in Gymnosperms. Volume 1. Bibliography, historical background, determination, structure, chemistry, topochemistry, physical properties, origin, and formation of compression wood. *Compression-wood-in-Gymnosperms-Volume-1-Bibliography,-historical-background,-determination,-structure,-chemistry,-topochemistry,-physical-properties,-origin,-and-formation-of-compression-wood*.

Turner, I., andMujumdar, A. S. (1997). *Mathematical modeling and numerical techniques in drying technology*. New York: Marcel Dekker.

Uprichard, J. M. (1971). Cellulose and lignin content in Pinus radiata D. Don. Within-tree variation in chemical composition, density and tracheid length. *Holzforschung-, 25*(4), 97-105.

Wolf, M., Walker, J. E., andKapsalis, J. G. (1972). Water Vapor Sorption Hysteresis in Dehydrated Food. *Journal of Agricultural and Food Chemistry, 20*(5), 1073-&.

Xu, P., Donaldson, L., Walker, J., Evans, R., andDownes, G. (2004). Effects of density and microfibril orientation on the vertical variation of low-stiffness wood in radiata pine butt logs. *Holzforschung-, 58*(6), 673-677.

Yeo, H., andSmith, W. B. (2005). Development of a convective mass transfer coefficient conversion method. *Wood and Fiber Science, 37*(1), 3-13.

Yeo, H., Smith, W. B., andHanna, R. B. (2002). Mass transfer in wood evaluated with a colorimetric technique and numerical analysis. *Wood and Fiber Science, 34*(4), 657-665.

Zagorska-Marek, B., andLittle, C. H. A. (1986). Control of fusiform initial orientation in the vascular cambium of Abies balsamea stems by indol-3-ylacetic acid. *Canadian-Journal-of-Botany, 64*(6), 1120-1128.

Zimmermann, M. H. (1983). *Xylem structure and the ascent of sap*. Berlin ; New York: Springer-Verlag.

Appendix

Appendix

Content:

A Environment Chamber ..... - 1 -
A.1 Humidification System ..... - 2 -
A.2 Environment Chamber ..... - 4 -
B Basic Sample Properties ..... - 6 -
B.1 1. Experiment ..... - 6 -
B.2 2. Experiment ..... - 9 -
B.3 3. Experiment ..... - 13 -
B.4 4. Experiment ..... - 16 -
C Moisture Diffusion Summary Page ..... - 21 -
D Schematic Flow Diagram of the Twist Model (Chapter 4) ..... - 22 -

List of Figures

Figure 1: Schematic sketch of air humidification system ..... - 1 -
Figure 2: Detailed flow diagram humidification column ..... - 3 -
Figure 3: Sample container ..... - 4 -
Figure 4: Chamber drawings ..... - 5 -
Figure 5: Tree A2 bottom and top cross section (from left to right) ..... - 6 -
Figure 6: Tree A1 bottom and top cross section (from left to right) ..... - 6 -
Figure 7: 1. Experiment average green moisture content ..... - 7 -
Figure 8: 1. Experiment average basic density ..... - 7 -
Figure 9: 1. Experiment equilibrium moisture content reference samples ..... - 8 -
Figure 10: 1. Experiment average tangential and radial shrinkage ..... - 9 -
Figure 11: Compression wood tree 2 at breast height ..... - 10 -
Figure 12: 2. Experiment average green moisture content ..... - 10 -
Figure 13: 2. Experiment average basic density ..... - 11 -
Figure 14: 2.Experiment equilibrium moisture content reference samples ..... - 12 -
Figure 15: 2. Experiment average tangential and radial shrinkage ..... - 12 -
Figure 16: 3. Experiment average green moisture content ..... - 13 -
Figure 17: 3. Experiment average basic density ..... - 14 -
Figure 18: 3.Experiment equilibrium moisture content reference samples ..... - 15 -
Figure 19: 3. Experiment average tangential and radial shrinkage ..... - 15 -
Figure 20: Cross section at BH: Tree C1 ..... - 16 -
Figure 21: Cross section at BH: Tree C2 ..... - 16 -
Figure 22: 4. Experiment average green moisture content ..... - 17 -
Figure 23: 4. Experiment average basic density ..... - 17 -
Figure 24: 4. Experiment EMC 1 ..... - 18 -
Figure 25: 4. Experiment EMC 2 ..... - 19 -
Figure 26: 4. Experiment EMC 3 ..... - 19 -
Figure 27: 4. Experiment average tangential and radial shrinkage ..... - 20 -

List of Tables:

Table 1: 1. Experiment main sample location and tree information ..... - 6 -
Table 2: 1. Experiment basic properties summary ..... - 8 -
Table 3: 2. Experiment main sample location and tree information ..... - 9 -
Table 4: 2. Experiment basic properties summary ..... - 11 -
Table 5: 3. Experiment main sample location and tree information ..... - 13 -
Table 6: 3. Experiment basic properties summary ..... - 14 -
Table 7: 4. Experiment main sample location and tree information ..... - 16 -
Table 8: 4. Experiment basic properties summary ..... - 18 -

A Environment Chamber

The apparatus was originally built by Laura-Beth Keep (1999). She used it to determine creep strain during the kiln drying of timber. With the old set-up it was possible to achieve various relative humidities at high temperatures (up 140 °C) above ambient conditions.
The task of the experiment was to determine the diffusion coefficient of small specimens of radiata pine for a relative humidity (RH) range between 20% and 85% at 30 °C. The existing apparatus was not designed to achieve this kind of conditioned air, and therefore the air humidification system had to be modified. In addition to the humidification system there was the requirement of a chamber, which allowed easy access and sufficient space for a number of specimens. Furthermore, sample containers were manufactured to establish constant air flow rates over the tested specimens.

The air humidification system is based on one of the simplest and most common method for cooling and/or humidifying air via a counter current contact with water in a packed tower (Figure 1). The incoming air, supplied from the department's compressor, is depending on the desired relative humidity either cooled or heated within the humidification column. Simultaneously the air will be humidified (saturated). After leaving the column the saturated air is heated to the dry bulb temperature and the conditioned air leaves the humidification system into the environment chamber.

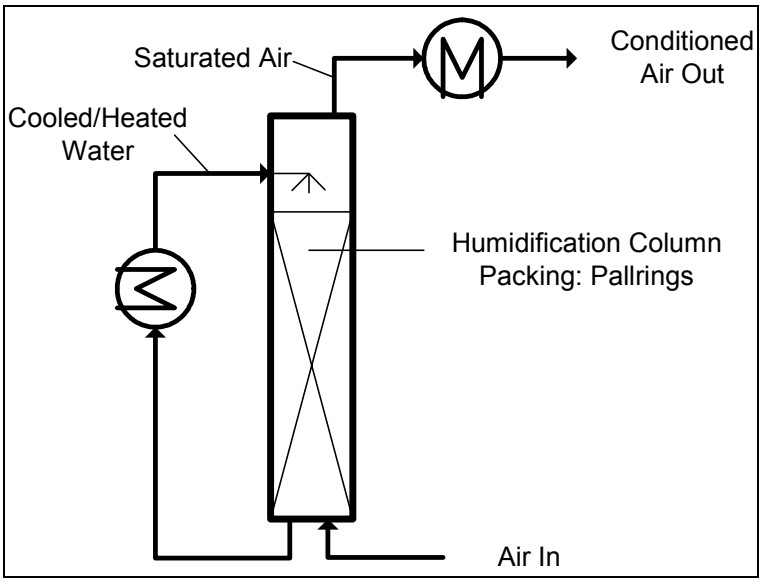

Figure 1: Schematic sketch of air humidification system.

Firstly, the individual parts of the humidification system are discussed, followed by the chamber and sample container specifications.

A.1 Humidification System

The modification of the humidification system included the manufacturing of a new bath below the column due to corrosion of the original. Additionally, a siphon was designed and manufactured to allow access into the bath during operation, which allowed the time required to establish new stable conditions to be decreased especially for low humidities, by adding ice cubes into the bath.

A separate water circuit was established to allow water cooling below ambient conditions. The chiller heater recirculation unit (Grant GP 200) is capable of controlling its own water bath temperature with an accuracy of ±0.1C°. Additionally, a temperature probe (PT 100) was installed at the top of the column for measuring the saturated air outlet temperature.

Recalculation of the column, based on Larson (1985), have shown that the column is capable of saturating and heating air up to 70°C for an air flow rate of 150 l/min and water inlet temperature of 70°C. Above 70°C water inlet temperature, the air still leaves the column saturated but with a lower outlet temperature than the water inlet temperature.

Figure 2 shows the flow diagram of the humidification column. Three control circuits are used to control the apparatus:

1. ***Bath temperature control:***
   To heat the water inside the bath of the column two 4kW heating elements are used. These elements are controlled by a Schimaden SR10 controller (PT100 Temperature Probe). Actual temperature reading and set temperature adjustment are located in the front operating panel.
2. ***Air temperature control***
   A 1 kW element (from a hot water cylinder) is used to heat the saturated air. This element is controlled by Schimaden SR25 (PT100 Temperature Probe). Actual temperature reading and set temperature adjustment are located in the front operating panel. The actual temperature is also passed on to a computer interface module (Advantech 889) for data acquisition.
3. ***Top water inlet temperature control***
   To achieve the requested water inlet temperature at the top of the column the water is cooled or heated by a shell heat exchanger, which is connected to an accurate water heating and chilling recirculation bath (Grant GP 200).

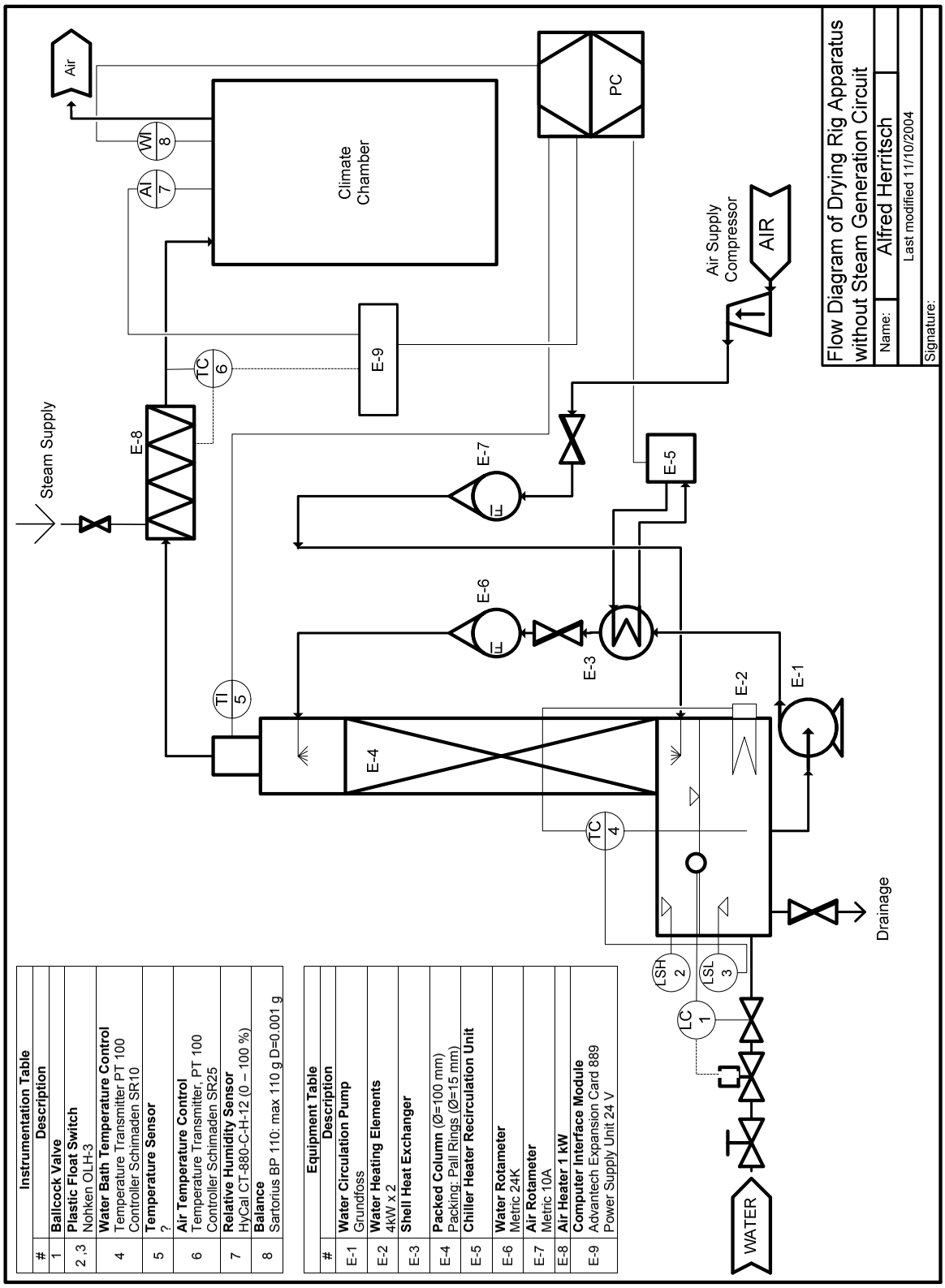

Figure 2: Detailed flow diagram humidification column.

A.2 Environment Chamber

The environment chamber was made out of stainless steel. Figure 4 contains the design drawings of the chamber. Several openings were included for multiple purposes. The round openings and the top square one are cover with a Perspex sheet. The square opening between the two round ones is currently not used and sealed with a stainless steel lid and was currently hidden behind the insulation. This opening can be used for attaching air lock systems to place samples within the chamber with hardly any disturbance within the main chamber. Between the insulation and the outer walls of the chamber trace heating elements are attached to maintain stable conditions within the chamber. The trace heating is controlled by a separate control circuit and located beneath the actual chamber, where you can also find the control unit of the fans for the sample container (Figure 3). The attached fans are capable of generating an air velocity up to 4.5 m/s (tested with hot wire anemometer).

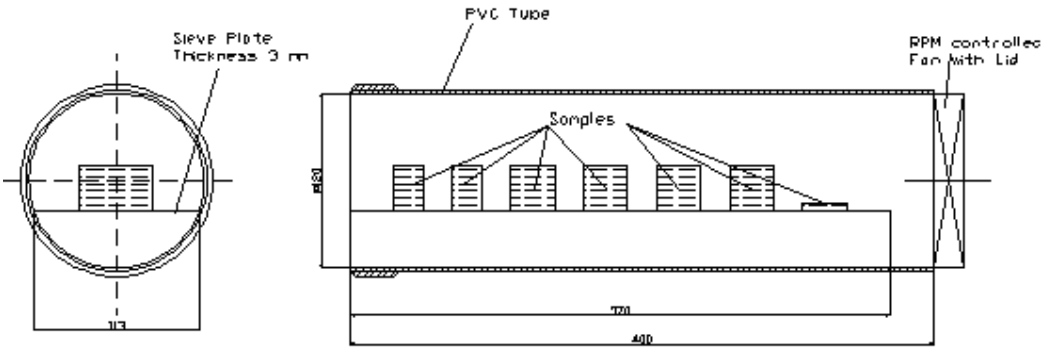

Figure 3: Sample container.

In the design phase the position of the balance was on top of the chamber, so that the sample mass could be measured within the chamber. In the trail runs prior the experiment, severe condensation occurred below the balance which affected the readings of the balance. This denied continuous measurements of one sample. Further the created turbulences by the fans also influenced the readings of the balance and therefore the balance was placed next to the experiment.

The chamber has been proven to reach and maintain constant temperature and relative humidities during the moisture diffusion experiments. The temperature in this experiment was 30°C and the relative humidity ranged from 23.5%RH to 85%RH. The chamber itself is currently designed for temperature up to 50°C (trace heating cut off elements set to 50°C). Design calculations have shown that higher temperatures are achievable, if this is desired. The author recommends the installation of a water trap at the air outlet of the chamber.

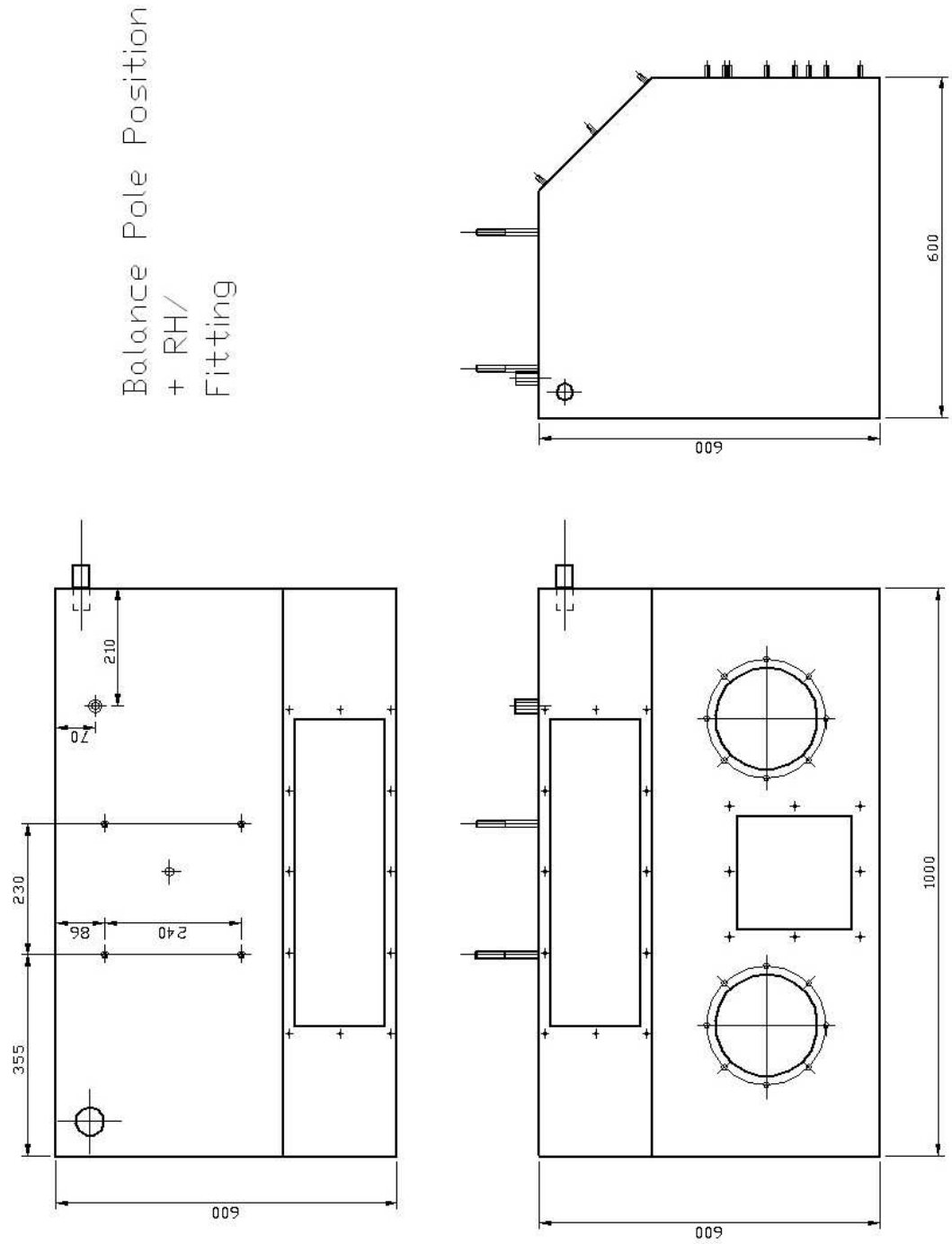

Figure 4: Chamber drawings.

References:

Keep, L.-B. (1998). *The determination of time-dependent strains in Pinus radiata under kiln-drying conditions,* University of Canterbury, New Zealand.

Larson, R. S. (1985). On the Design of Recirculated-Liquid Gas Cooler Humidifiers. *Industrial & Engineering Chemistry Process Design and Development, 24*(4), 1023-1026.

B Basic Sample Properties

B.1 1. Experiment

The variation of the diffusion coefficient between heart and sap wood was the objective of this experiment. Therefore five 19 year old Radiata Pine trees were cut down from the inside of the University trial stand (Southern Plantation Forest) located in Christchurch, Canterbury during spring. From each butt log (4 m long) two discs were cut (top and bottom) and were placed in a cooling room the same day. For the first experiment the trees A2 and A1 were chosen for the initial experiment.

These trees were chosen because of their most evenly distributed and concentrical year rings from the five available trees (Figures 5 and 6).

Figure 5: Tree A2 bottom and top cross section (from left to right).

Figure 6: Tree A1 bottom and top cross section (from left to right).

Table 1 includes the information of the location for the main samples of each disc.

Table 1: 1. Experiment main sample location and tree information

1. Experiment					
Tree: A2			***Tree: A1***		
Disc ID	***Total yearrings***		***Disc ID***	***Total yearrings***	
A2B	19		A1B	19	
A2T	15		A1T	15	
Sample ID	***Location within tree***		***Sample ID***	***Location within tree***	
	Year No.	***Height***		***Year No.***	***Height***
A2BC	3-7	BH	A1BC	3-7	BH
A2BO	12-17	BH	A1BO	9-16	BH
A2TC I	3-7	5m	A1TC	3-7	5m
A2TO I	9-13	5m	A1TO	8-13	5m
A2TC II	2-4	5m			
A2TO II	10-14	5m			

The average green moisture content of the four samples from each location within the tree is, in general lower within the heartwood (identified by the letter C→Core) with the only exception being sample 2BC (Figure 7).

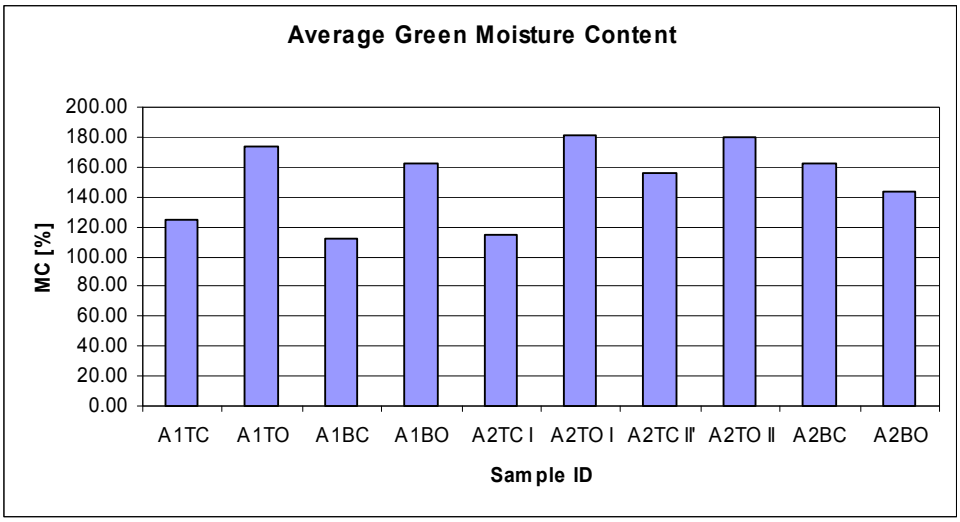

Figure 7: 1. Experiment average green moisture content.

The average basic density for all samples from tree A1 was 353 kg/m^3, with very little deviation between the samples (±2%), and the density distribution followed the general trend of an increasing density from the pith to the bark. For tree A2, the deviation around the mean basic density of 349 kg/m^3 was higher (-7% +8%). Four main samples have been cut from the top disc of tree A2. The basic density of the centre sample A2TCI was slightly higher (343 kg/m^3) than for the corresponding A2TCI sample (326 kg/m^3).

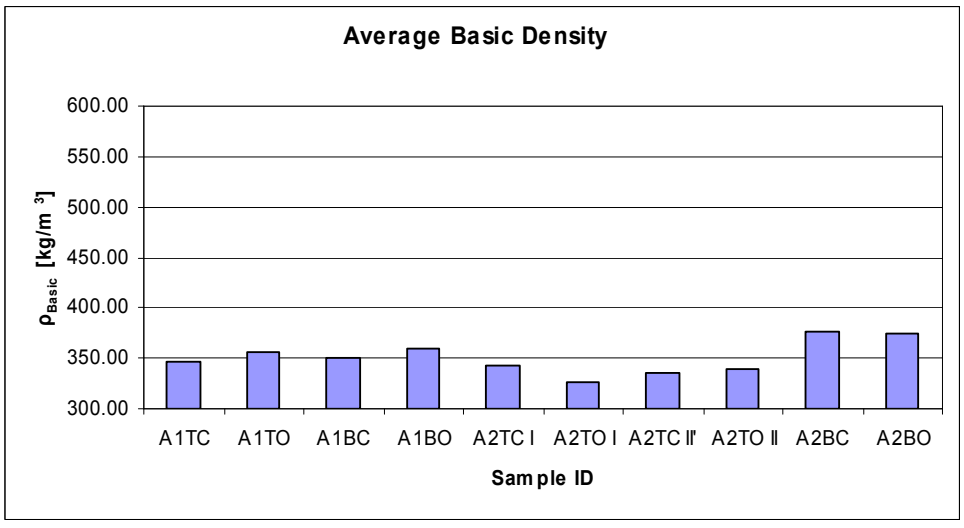

Figure 8: 1. Experiment average basic density

Equilibrium moisture contents (EMC) for the three relative humidity (RH) set points of the environment chamber are listed in Table 2. Both trees showed similar EMC values for the three different conditions.

Table 2: 1. Experiment basic properties summary.

1. Experiment @ 30°C						
		Basic	**Green**	**EMC 1**	**EMC 2**	**EMC 3**
		Density	**MC**	**85%RH**	**23.5%RH**	**84.5%RH**
		[kg/m3]	**[%]**	**[%]**	**[%]**	**[%]**
Tree A1	**Mean**	**352.87**	**143.26**	**21.50**	**6.25**	**18.58**
	Minimum	346.64	112.38	20.80	6.11	18.30
	Maximum	359.13	174.04	21.83	6.36	18.97
	Min. relative	-1.77%	-21.56%	-3.26%	-2.32%	-1.51%
	Max relative	1.78%	21.49%	1.53%	1.71%	2.13%
Tree A2	**Mean**	**348.98**	**155.92**	**21.77**	**6.20**	**18.62**
	Minimum	326.16	113.88	21.55	6.08	18.16
	Maximum	375.69	180.65	22.22	6.30	18.93
	Min. relative	-6.54%	-26.96%	-1.04%	-1.83%	-2.49%
	Max relative	7.65%	15.86%	2.05%	1.69%	1.64%

Average EMC values for the main samples are shown in Figure 9.

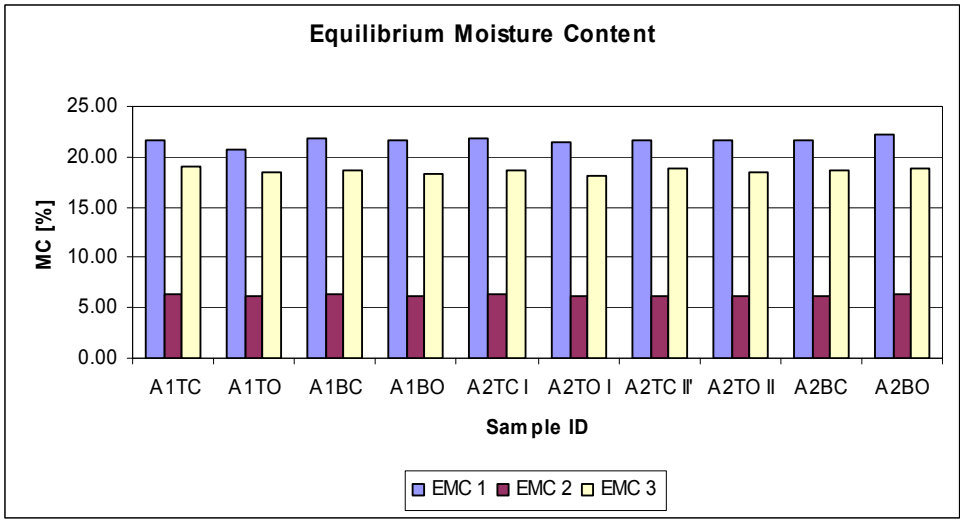

Figure 9: 1. Experiment equilibrium moisture content reference samples.

Average tangential and radial shrinkage from tree A1 was found to vary between 4% - 6.1% and 2% - 3.8% respectively. Tangential shrinkage for tree A2 ranged from 4.3% to 6% and 1.5% to 3.3% in radial direction. The average tangential and radial shrinkage for each sample can be found in Figure 10.

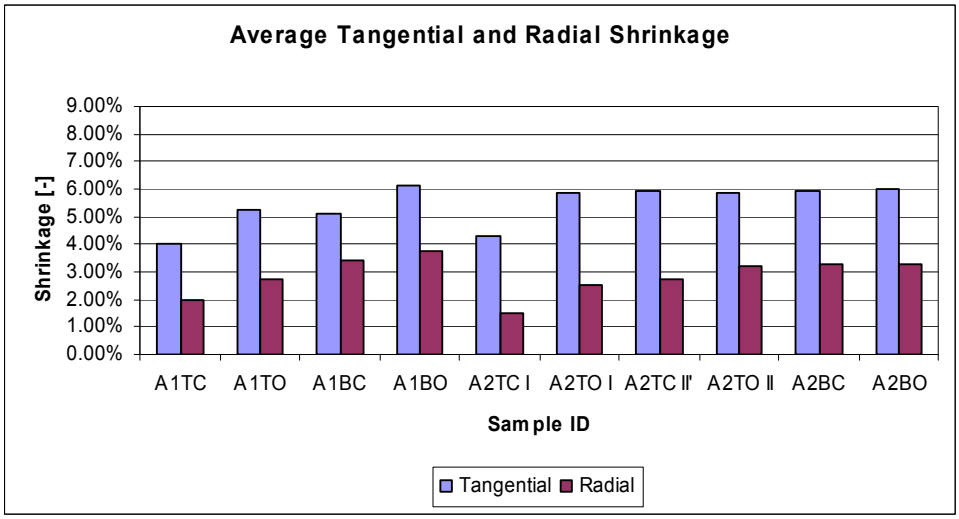

Figure 10: 1. Experiment average tangential and radial shrinkage.

B.2 2. Experiment

Two trees were cut from a forest owned by Selwyn Plantation Board Ltd (autumn). The plantation has been established in 1986 (20 year old), currently 580 stems/ha, average diameter breast height 28 cm, mean top height 20 m. 2.6 m pruning in 1995 and production pruning in 1996.

The trees were located approximately 50 meters from the forest's edge. From each tree, three discs were extracted from different heights and were placed in a cooling room the same day.

Table 3: 2. Experiment main sample location and tree information.

2. Experiment					
Tree: 1			***Tree: 2***		
Disc ID	***Total yearrings***		***Disc ID***	***Total yearrings***	
1/1.2m	18		2/1.2m	18	
1/5m	16		2/10m	13	
1/10m	13		2/15m	11	
Sample ID	***Location within tree***		***Sample ID***	***Location within tree***	
	Year No.	***Height***		***Year No.***	***Height***
1/1.2m/1	1-4	BH	2/1.2m/1	9-12	BH
1/1.2m/2	9-16	BH	2/1.2m/2	9-12	BH
1/5m/1	1-4	5m	2/10m/1	1-6	10m
1/5m/2	5-9	5m	2/10m/2	7-11	10m
1/10m/1	1-5	10m	2/15m/1	1-4	15m
1/10m/2	6-10	10m	2/15m/2	5-9	15m

The breast height disc for tree number two was believed to contain compression wood. Therefore a compression sample and an opposite sample were cut out of the disc (Figure 11).

Figure 11: Compression wood tree 2 at breast height.

Average green moisture content was in general lower for samples closer to the pith (Figure 12).

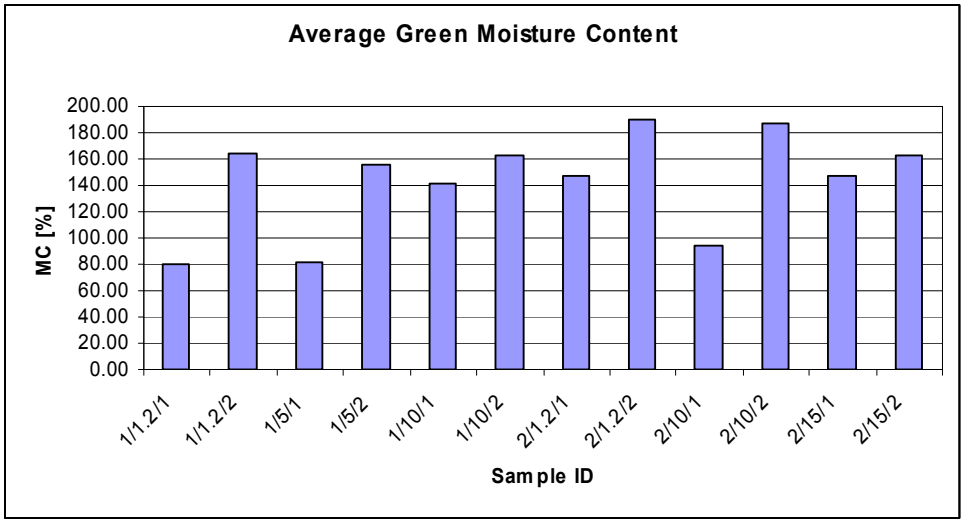

Figure 12: 2. Experiment average green moisture content.

The average basic density for all samples from tree 1 was 341 kg/m^3, with a deviation between the samples (±7%), and the density distribution followed the general trend of an increasing density from the pith to the bark. For tree 2, the deviation around the mean basic density of 359 kg/m^3 was -10% and +19%. Average basic densities for each sample are shown in Figure 13.

Sample 2/1.2/1 was the compression wood sample. This sample had a basic density of 427 kg/m^3. Sample 2/1.2/2 was located within the same year ring but on the opposite side of the compression wood sample, and it had a density of 357 kg/m^3.

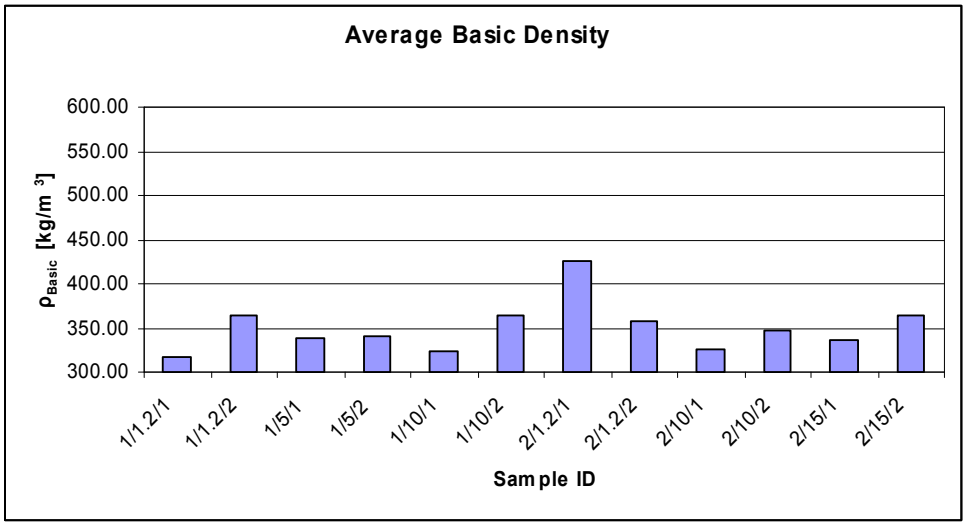

Figure 13: 2. Experiment average basic density.

Equilibrium moisture contents (EMC) for the three relative humidity (RH) set points for the environment chamber are listed in Table 4. Both trees showed similar EMC values for the three different conditions. Tree 2 for the second experiment showed a higher deviation between each sample. Tree 2 was believed to contain compression wood.

Table 4: 2. Experiment basic properties summary.

2. Experiment @ 30°C						
		Basic	**Green**	**EMC 1**	**EMC 2**	**EMC 3**
		Density	**MC**	**83%RH**	**25.5%RH**	**83%RH**
		[kg/m3]	**[%]**	**[%]**	**[%]**	**[%]**
Tree 1	**Mean**	**341.08**	**131.08**	**18.24**	**6.29**	**16.55**
	Minimum	316.98	79.44	17.97	6.09	16.19
	Maximum	363.67	164.88	18.63	6.48	16.93
	Min. relative	-7.07%	-39.39%	-1.49%	-3.28%	-2.18%
	Max relative	6.62%	25.78%	2.12%	2.91%	2.31%
Tree 2	**Mean**	**359.23**	**154.36**	**17.91**	**6.40**	**16.13**
	Minimum	322.91	93.75	17.31	6.09	15.74
	Maximum	426.45	189.65	19.23	6.70	16.48
	Min. relative	-10.11%	-39.27%	-3.32%	-4.84%	-2.39%
	Max relative	18.71%	22.86%	7.39%	4.78%	2.19%

EMC values for the compression wood sample (2/1.2/1) for the three environment condition were 18.3%MC, 6.7%MC and 16.5%MC, respectively. The opposite wood sample (2/1.2/2) had a higher EMC 1 value of 19.2%MC, a lower EMC 2 of 6.3%MC and a lower EMC 3 value of 15.9%MC.

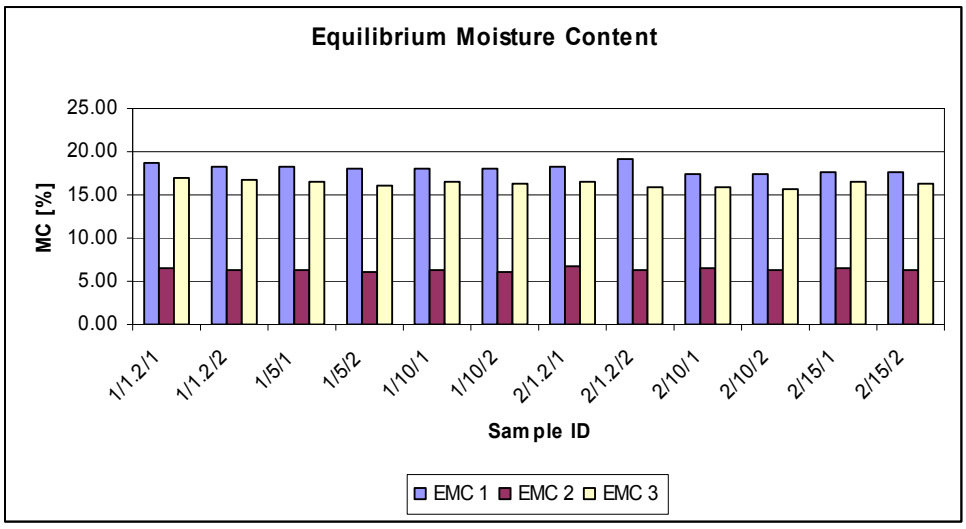

Figure 14: 2.Experiment equilibrium moisture content reference samples.

Average tangential shrinkage for tree 1 followed the commonly known trend of an increasing shrinkage from the pith to the bark. The compression wood sample (2/1.2/1) had a lower tangential and radial shrinkage than the opposite sample (2/1.2/2). The tangential and radial shrinkage values for the compression wood and opposite wood were 5.1% and 3%, 7.1% and 4.1%, respectively.

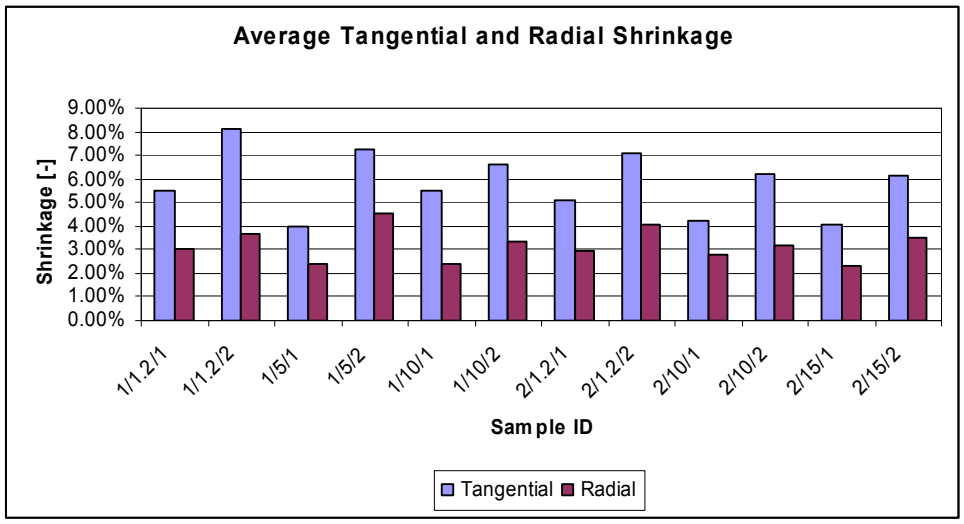

Figure 15: 2. Experiment average tangential and radial shrinkage.

B.3 3. Experiment

Two trees were cut from a forest owned by Selwyn Plantation Board Ltd (winter). From each tree, three discs were extracted from different heights and placed in a cooling room the same day.

Table 5: 3. Experiment main sample location and tree information.

3. Experiment					
Tree: 3			***Tree: 4***		
Disc ID	***Total yearrings***		***Disc ID***	***Total yearrings***	
3/1.2m	27		4/1.2m	25	
3/5m	20		4/10m	20	
3/10m	17		4/18m	18	
Sample ID	***Location within tree***		***Sample ID***	***Location within tree***	
	Year No.	***Height***		***Year No.***	***Height***
3/1.2m/1	1-4	BH	4/1.2/1	2-4	BH
3/1.2m/2	9-16	BH	4/1.2/2	7-10	BH
3/5m/1	1-4	5m	4/10/1	2-3	10m
3/5m/2	5-9	5m	4/10/2	11-15	10m
3/10m/1	1-5	10m	4/18/1	2-4	18m
3/10m/2	6-10	10m	4/18/2	9-16	18m

Average green moisture content varied substantially between heart wood and sap wood for both trees (Figure 16).

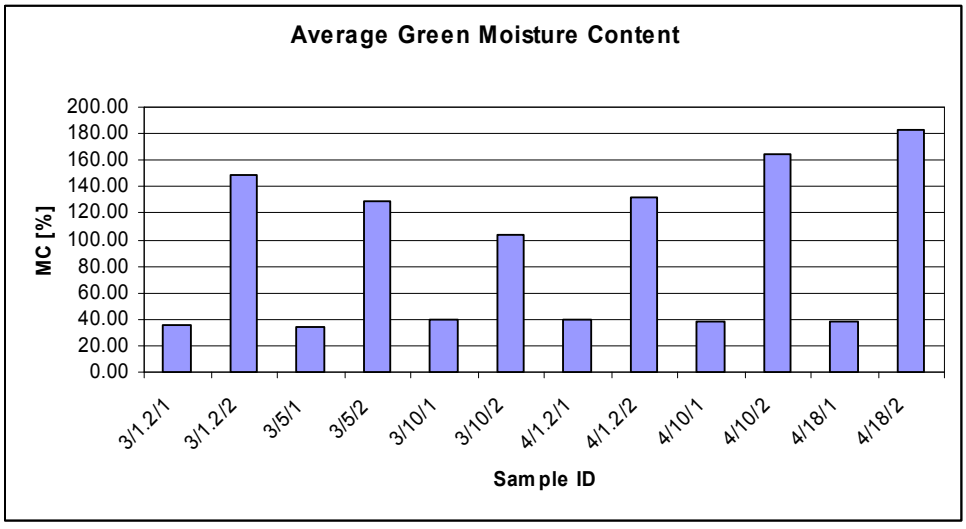

Figure 16: 3. Experiment average green moisture content.

A similar trend as for the green moisture content was observed for the basic density. Heart wood densities were in general much lower than for the sap wood samples (Figure 17).

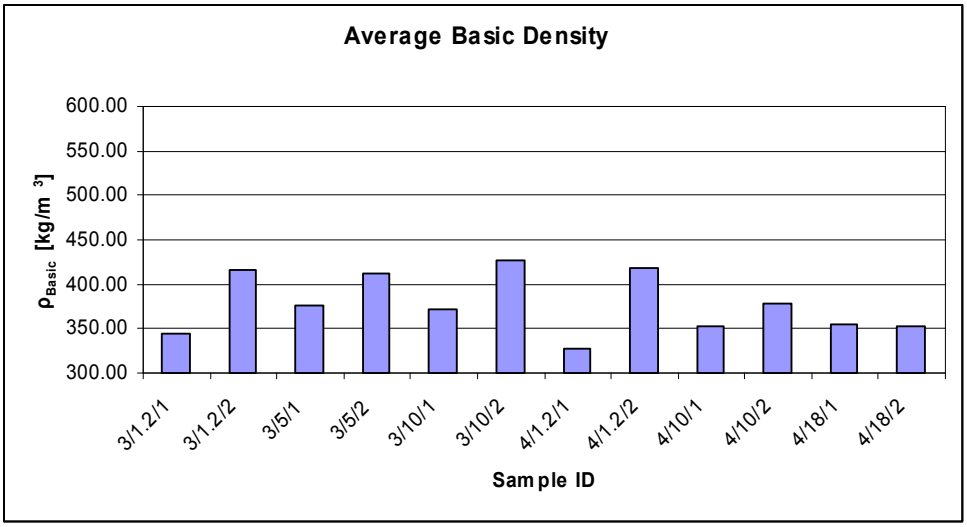

Figure 17: 3. Experiment average basic density.

Equilibrium moisture contents (EMC) for the three relative humidity (RH) set points for the environment chamber are listed in Table 6. Both trees showed similar EMC values for the three different conditions.

Table 6: 3. Experiment basic properties summary.

3. Experiment @ 30°C						
		Basic	**Green**	**EMC 1**	**EMC 2**	**EMC 3**
		Density	**MC**	**83%RH**	**25.5%RH**	**83%RH**
		[kg/m3]	**[%]**	**[%]**	**[%]**	**[%]**
Tree 3	**Mean**	**390.70**	**81.72**	**19.88**	**6.60**	**17.37**
	Minimum	343.93	34.23	19.60	6.39	17.11
	Maximum	426.91	148.62	20.22	6.96	17.73
	Min. relative	-11.97%	-58.11%	-1.41%	-3.22%	-1.48%
	Max relative	9.27%	81.87%	1.71%	5.45%	2.09%
Tree 4	**Mean**	**364.65**	**99.05**	**19.34**	**6.20**	**17.02**
	Minimum	327.58	37.90	18.82	6.13	16.71
	Maximum	418.95	182.50	19.82	6.38	17.66
	Min. relative	-10.17%	-61.74%	-2.70%	-1.08%	-1.84%
	Max relative	14.89%	84.25%	2.49%	2.83%	3.77%

Equilibrium Moisture contents for the third experiment are shown in Figure 18.

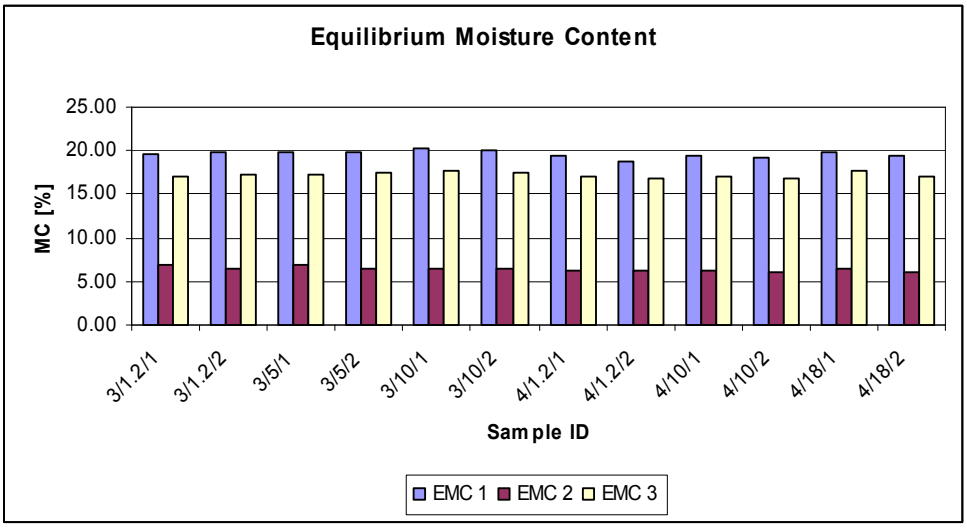

Figure 18: 3.Experiment equilibrium moisture content reference samples.

Average tangential and radial shrinkage for the third experiment are shown in Figure 19.

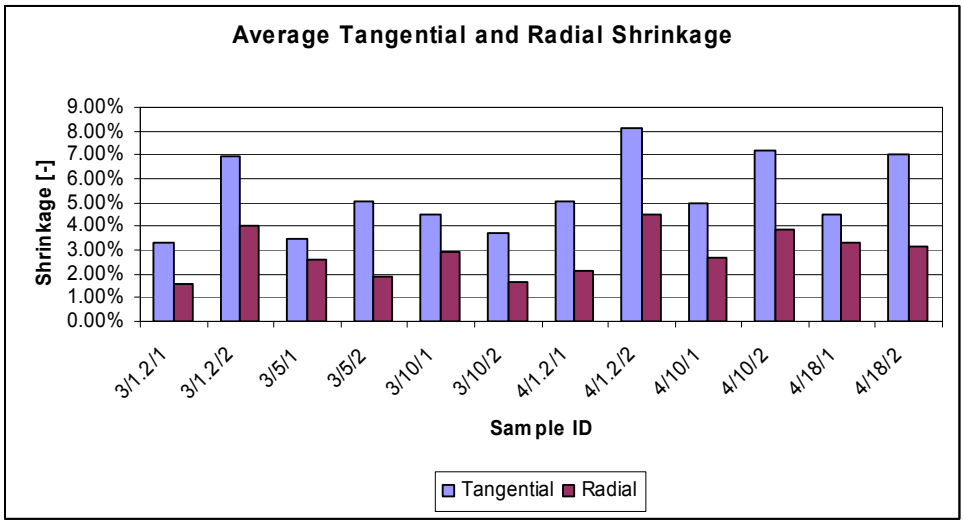

Figure 19: 3. Experiment average tangential and radial shrinkage.

B.4 4. Experiment

The objective of the fourth experiment was to measure the diffusion coefficient variation between opposite and compression wood. The samples were taken from trees at the North West facing edge of the same plantation as in the third experiment.

Figure 20: Cross section at BH: Tree C1.

Figure 21: Cross section at BH: Tree C2.

Table 7: 4. Experiment main sample location and tree information.

4. Experiment					
Tree: C1			***Tree: C2***		
Disc ID	***Total yearrings***		***Disc ID***	***Total yearrings***	
C1/1.2m	29		C2/1.2m	26	
C1/3m	25		C2/3m	23	
C1/10m	21		C2/10m	21	
Sample ID	***Location within tree***		***Sample ID***	***Location within tree***	
	Year No.	***Height***		***Year No.***	***Height***
C1/1.2/1	12-15	BH	C2/1.2/1	7-10	BH
C1/1.2/2	9-13	BH	C2/1.2/2	7-11	BH
C1/3/1	16-18	5m	C2/3/1	10-17	10m
C1/3/2	16-20	5m	C2/3/2	13-19	10m
C1/6/1	13-17	10m	C2/6/1	6-9	18m
C1/6/2	10-18	10m	C2/6/2	6-13	18m

Average green moisture content was lower for compression wood than for the opposite wood despite for samples taken from tree C2 at 6 meters.

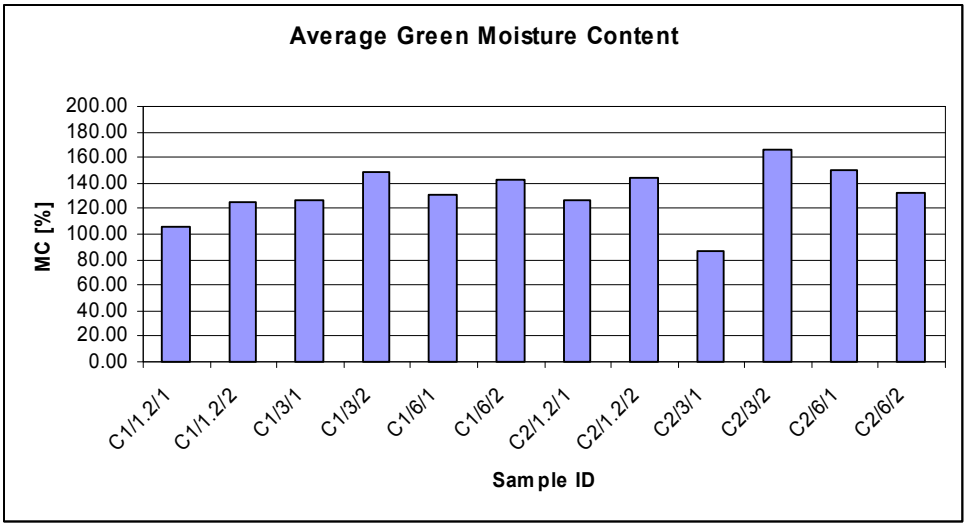

Figure 22: 4. Experiment average green moisture content.

Average basic density was higher for compression than for opposite wood, despite the sample from tree C2 at 6 meters.

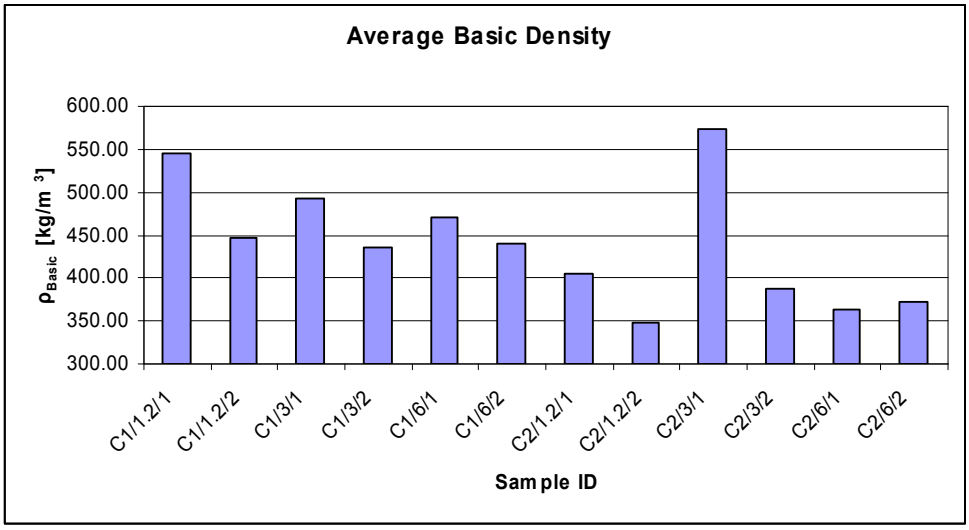

Figure 23: 4. Experiment average basic density.

Table 8: 4. Experiment basic properties summary.

4. Experiment @ 30°C						
		Basic	**Green**	**EMC 1**	**EMC 2**	**EMC 3**
		Density	**MC**	**83%RH**	**25.5%RH**	**83%RH**
		[kg/m3]	**[%]**	**[%]**	**[%]**	**[%]**
Tree C1	**Mean**	**472.12**	**129.71**	**20.95**	**6.46**	**17.78**
	Minimum	434.74	105.34	20.48	6.14	17.55
	Maximum	546.07	148.38	21.35	6.72	18.07
	Min. relative	-7.92%	-18.79%	-2.26%	-5.01%	-1.30%
	Max relative	15.66%	14.40%	1.90%	3.97%	1.66%
Tree C2	**Mean**	**408.53**	**134.39**	**20.47**	**6.45**	**17.70**
	Minimum	348.32	87.22	20.10	6.26	17.41
	Maximum	572.91	165.65	20.63	6.73	18.01
	Min. relative	-14.74%	-35.10%	-1.83%	-2.82%	-1.64%
	Max relative	40.24%	23.25%	0.77%	4.32%	1.71%

The EMC at EMC 1 was lower for compression wood than for the opposite wood (Samples ending with 1 refer to compression wood and 2 for opposite wood).

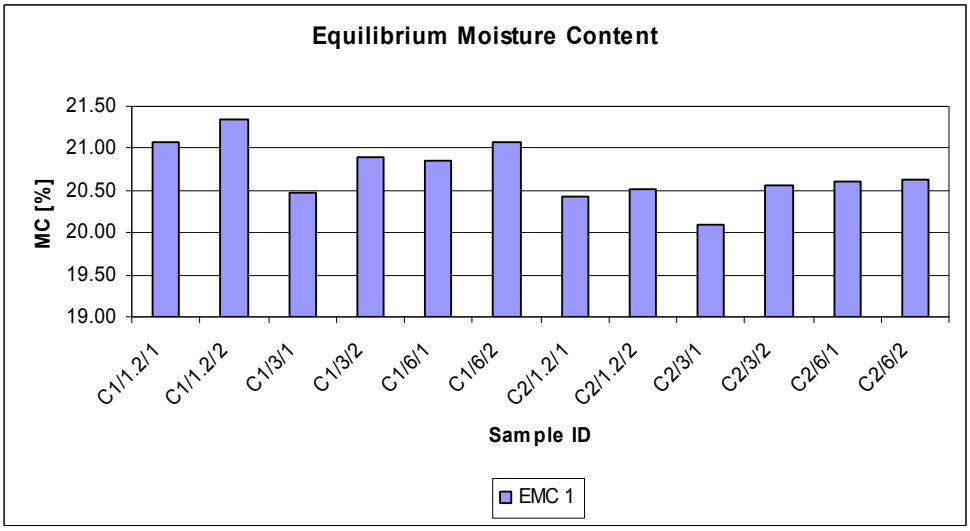

Figure 24: 4. Experiment EMC 1.

The EMC values at EMC 2 were higher for compression wood than opposite wood.

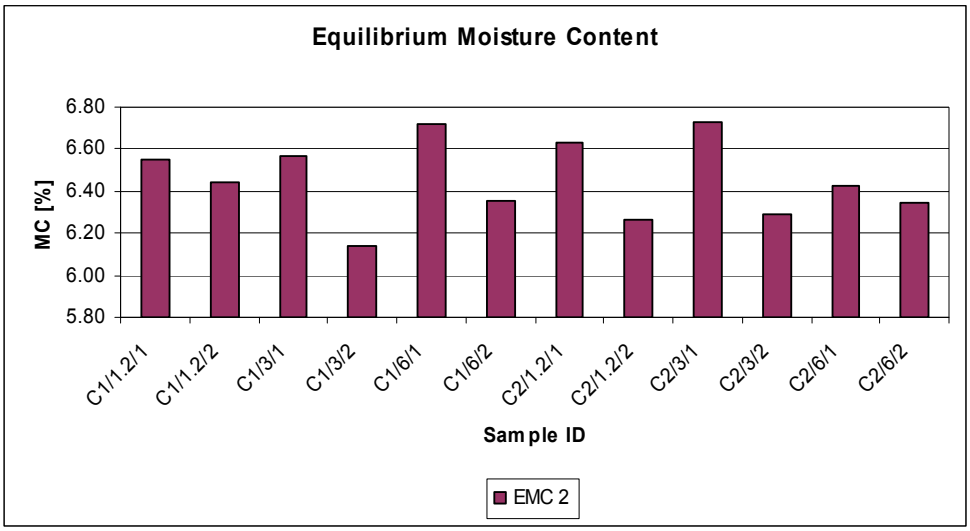

Figure 25: 4. Experiment EMC 2.

The EMC values at EMC 3 were higher for compression wood than opposite wood.

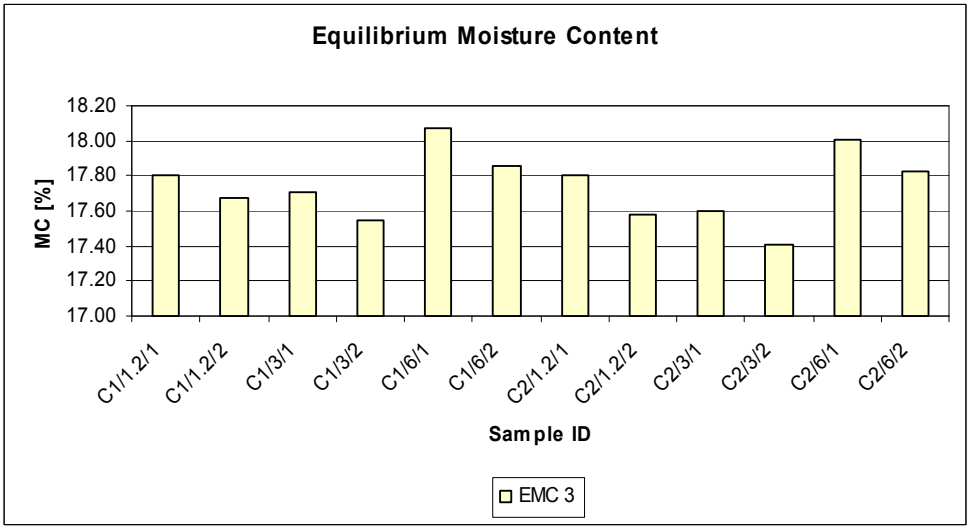

Figure 26: 4. Experiment EMC 3.

For all samples the tangential and radial shrinkage were lower for compression wood than opposite wood.

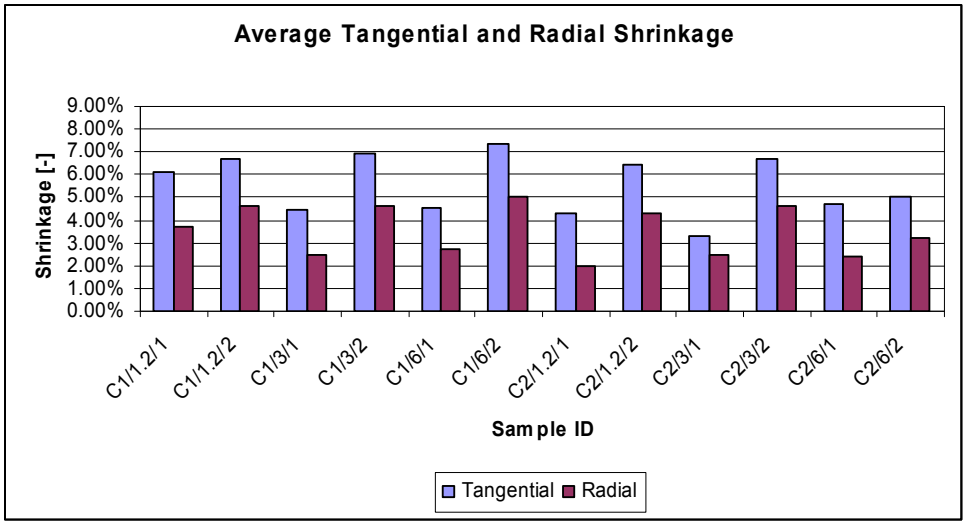

Figure 27: 4. Experiment average tangential and radial shrinkage.

C Moisture Diffusion Summary Page

	Sample ID	Wood Type	Location Yearring from pith	Height	De. Longit.		De. Tangent.		De. Radial		Ad. Longit.		Ad. Tangent.		Ad. Radial	
					D_0	K_0	D_0	K_0	D_0	K_0	D_0	K_0	D_0	K_0	D_0	K_0
					[m^2/s]	[-]	[m^2/s]	[-]	[m^2/s]	[-]	[m^2/s]	[-]	[m^2/s]	[-]	[m^2/s]	[-]
1. Experiment	A1TC	Core	3 - 7	5	1.21E-09	1.10E+01	3.54E-10	4.18E+00	9.18E-10	1.60E-04	3.66E-09	4.68E-02	5.64E-10	1.00E-02	7.58E-10	1.00E-02
	A1TO	Outer	8 - 13	5	2.29E-09	6.16E+00	2.40E-10	6.57E+00	4.45E-10	4.31E+00	7.50E-10	1.08E+01	4.40E-10	5.46E-03	5.69E-10	7.94E-05
	A1BC	Core	3 - 7	BH	1.18E-09	9.96E+00	3.73E-10	5.65E+00	4.09E-10	5.32E+00	1.57E-09	3.86E+00	4.52E-10	1.09E+00	6.55E-10	1.00E-02
	A1BO	Outer	9 - 16	BH	3.77E-09	7.01E-01	4.61E-10	5.15E-02	7.81E-10	1.18E+00	1.12E-09	6.65E+00	4.50E-10	1.81E-02	7.20E-10	1.00E-02
	A2TC I	Core	3 - 7	5	9.85E-10	1.20E+01	3.22E-10	6.01E+00	6.85E-10	1.79E+00	1.04E-09	9.01E+00	6.62E-10	1.00E-02	7.62E-10	9.25E-01
	A2TO I	Outer	9 - 13	5	3.72E-09	3.36E+00	1.70E-10	1.07E+01	4.08E-10	7.01E+00	3.66E-09	9.03E-03	4.49E-10	3.62E-08	6.61E-10	1.00E-02
	A2TC II'	Core	2 - 4	5	1.40E-09	1.10E+01	3.09E-10	5.11E+00	7.97E-10	4.11E-01	2.78E-09	1.11E+00	4.88E-10	5.76E-03	3.31E-10	5.03E+00
	A2TO II	Outer	10 - 14	5	3.15E-09	3.66E+00	5.77E-10	5.24E-02	8.35E-10	4.85E-03	3.70E-09	1.08E-01	4.82E-10	1.00E-02	5.85E-10	1.68E-10
	A2BC	Core	3 - 7	BH	2.22E-09	5.30E+00	5.30E-10	6.77E-03	8.65E-10	8.99E-03	8.91E-10	9.01E+00	5.34E-10	2.24E-02	6.99E-10	5.00E-04
	A2BO	Outer	12 - 17	BH	8.94E-10	1.18E+01	2.64E-10	5.38E+00	4.79E-10	6.04E+00	1.31E-09	5.46E+00	4.10E-10	3.16E-08	7.06E-10	1.00E-02
2. Experiment	1/1.2/1	Core	1 - 4	BH	1.60E-09	1.00E+01	2.95E-10	1.04E+01	1.46E-09	4.35E-02	5.29E-09	1.00E-02	1.02E-09	7.58E-03	4.99E-10	9.59E+00
	1/1.2/2	Outer	9 - 16	BH	1.75E-09	8.97E+00	6.63E-10	1.80E-01	1.84E-10	1.33E+01	4.72E-09	1.00E-02	3.13E-10	6.62E+00	1.33E-09	1.25E-06
	1/5/1	Core	1 - 4	5	1.47E-09	1.02E+01	5.94E-10	1.87E+00	3.55E-10	6.42E+00	5.47E-09	3.46E-02	7.04E-10	1.71E-01	1.06E-09	1.75E-07
	1/5/2	Outer	5 - 9	5	1.79E-09	8.83E+00	8.65E-10	1.98E+00	3.35E-10	1.11E+01	2.36E-09	7.10E+00	5.75E-10	6.07E+00	9.62E-10	1.62E+00
	1/10/1	Core	1 - 5	10	1.75E-09	9.70E+00	3.17E-10	7.94E+00	2.95E-10	1.27E+01	6.09E-09	1.00E-02	5.03E-10	4.56E+00	6.18E-10	3.30E+00
	1/10/2	Outer	6 - 10	10	1.34E-09	1.13E+01	3.56E-10	8.01E+00	3.02E-10	9.87E+00	1.58E-09	9.58E+00	8.85E-10	9.38E-03	9.20E-10	1.95E+00
	2/1.2/1	Compression	9 - 12	BH	9.20E-10	1.20E+01	1.84E-10	7.93E+00	5.11E-10	1.45E+00	3.62E-09	7.52E-07	5.27E-10	9.23E-01	6.75E-10	6.25E-08
	2/1.2/2	Opposite	9 - 12	BH	2.03E-09	7.38E+00	7.60E-11	2.08E+01	4.30E-10	6.33E+00	5.19E-09	4.94E-06	3.30E-10	7.01E+00	5.16E-10	5.63E+00
	2/10/1	Core	1 - 6	10	1.45E-09	1.20E+01	1.81E-10	1.74E+01	9.59E-10	1.97E-03	6.08E-09	3.15E-02	9.83E-10	7.42E-02	4.87E-10	7.35E+00
	2/10/2	Outer	7 - 11	10	1.44E-09	1.10E+01	1.78E-10	1.25E+01	5.42E-10	4.69E+00	5.81E-09	6.25E-08	6.89E-10	1.25E-06	1.03E-09	1.29E+00
	2/15/1	Core	1 - 4	15	1.80E-09	9.42E+00	2.67E-10	8.05E+00	9.18E-10	1.32E-06	2.01E-09	8.26E+00	6.44E-10	6.93E-01	1.21E-09	5.44E-02
	2/15/2	Outer	7 - 11	15	1.64E-09	9.01E+00	5.53E-10	2.74E+00	3.86E-10	8.63E+00	5.14E-09	2.15E-05	1.29E-09	1.50E+00	4.30E-10	6.99E+00
3. Experiment	3/1.2/1	Core	1 - 4	BH	9.60E-10	1.28E+01	2.24E-10	9.98E+00	7.66E-11	2.04E+01	1.25E-09	9.61E+00	5.35E-10	2.86E+00	4.83E-10	4.10E+00
	3/1.2/2	Outer	9 - 16	BH	1.48E-09	8.57E+00	6.71E-10	3.84E-09	6.38E-10	7.70E-01	9.72E-10	1.00E+01	3.90E-10	5.89E+00	8.51E-10	3.69E-01
	3/5/1	Core	1 - 4	5	1.10E-09	1.10E+01	3.18E-10	1.16E+01	2.88E-10	7.17E+00	2.04E-09	4.09E+00	9.56E-10	7.12E-01	1.71E-10	9.57E+00
	3/5/2	Outer	5 - 9	5	1.48E-09	7.88E+00	7.53E-10	4.87E-06	2.61E-10	1.10E+01	1.15E-09	9.01E+00	6.12E-10	3.69E+00	6.53E-10	3.20E+00
	3/10/1	Core	1 - 5	10	1.69E-09	7.81E+00	2.67E-10	1.08E+01	2.03E-10	1.18E+01	1.31E-09	7.27E+00	9.48E-10	4.85E-01	5.60E-10	2.47E+00
	3/10/2	Outer	6 - 10	10	1.43E-09	8.16E+00	5.28E-10	1.03E+00	2.87E-10	6.91E+00	3.74E-09	1.24E-01	1.57E-10	1.06E+01	3.98E-10	4.64E+00
	4/1.2/1	Core	2 - 4	BH	1.30E-09	1.20E+01	2.12E-10	1.24E+01	2.07E-10	1.20E+01	4.15E-09	3.69E-06	3.53E-10	5.50E+00	5.74E-10	1.69E+00
	4/1.2/2	Outer	7 - 10	BH	1.81E-09	7.29E+00	5.73E-10	5.19E-02	3.92E-10	5.01E+00	3.66E-09	6.25E-08	3.31E-10	5.01E+00	7.27E-10	1.05E-02
	4/10/1	Core	2 - 3	10	1.29E-09	1.10E+01	2.57E-10	1.10E+01	4.21E-10	5.46E+00	1.68E-09	7.01E+00	8.49E-10	4.86E-01	4.88E-10	2.64E+00
	4/10/2	Outer	11 - 15	10	1.24E-09	1.20E+01	4.28E-10	3.66E+00	3.21E-10	7.56E+00	4.47E-09	1.58E-07	5.02E-10	2.25E+00	7.97E-10	2.55E-02
	4/18/1	Core	2 - 4	18	1.19E-09	9.93E+00	1.17E-10	1.80E+01	6.24E-10	1.86E-06	3.90E-09	6.25E-08	8.08E-10	3.61E-01	5.90E-10	1.01E+00
	4/18/2	Outer	9 - 16	18	1.30E-09	1.11E+01	1.96E-10	1.02E+01	3.31E-10	8.48E+00	4.84E-09	6.44E-03	4.93E-10	3.02E+00	4.85E-10	4.89E+00
4.Experiment	C1/1.2/1	Compression	12 - 15	BH	1.44E-09	4.23E+00	3.51E-10	3.10E+00	2.28E-10	4.97E+00	1.13E-09	5.26E+00	4.46E-10	1.92E-04	4.86E-10	1.25E-06
	C1/1.2/2	Opposite	9 - 13	BH	1.50E-09	6.81E+00	3.49E-10	3.97E+00	7.23E-10	2.36E-03	3.34E-09	2.88E-03	4.37E-10	2.54E+00	4.58E-10	2.70E+00
	C1/3/1	Compression	16 - 18	3	9.92E-10	9.44E+00	1.33E-10	9.34E+00	3.33E-10	2.97E+00	2.52E-09	1.03E+00	4.87E-10	3.45E-05	5.43E-10	1.25E-06
	C1/3/2	Opposite	16 - 20	3	1.76E-09	5.89E+00	7.70E-10	1.57E-02	2.02E-10	8.03E+00	1.31E-09	6.72E+00	8.87E-10	1.55E+00	4.39E-10	1.96E+00
	C1/6/1	Compression	13 - 17	6	1.32E-09	7.47E+00	2.40E-10	3.90E+00	4.95E-10	3.21E-02	2.03E-09	1.73E+00	3.79E-10	6.25E-08	4.89E-10	7.43E-03
	C1/6/2	Opposite	10 - 18	6	1.23E-09	9.03E+00	4.51E-10	1.18E+00	4.84E-10	4.96E+00	1.42E-09	5.38E+00	4.78E-10	5.85E-01	9.28E-10	1.00E-02
	C2/1.2/1	Compression	7 - 10	BH	1.25E-09	9.79E+00	2.38E-10	5.77E+00	2.85E-10	5.48E+00	2.28E-09	3.34E+00	4.69E-10	2.08E-08	5.70E-10	2.57E-01
	C2/1.2/2	Opposite	1 - 11	BH	1.75E-09	9.01E+00	3.49E-10	7.05E+00	1.87E-10	1.30E+01	1.07E-09	1.00E+01	6.38E-10	1.17E-10	7.53E-10	1.33E+00
	C2/3/1	Compression	10 - 17	3	6.39E-10	1.10E+01	1.63E-10	3.28E+00	1.73E-10	5.10E+00	2.39E-09	1.35E-06	3.30E-10	4.89E-08	3.58E-10	1.00E-02
	C2/3/2	Opposite	13 - 19	3	1.23E-09	1.12E+01	2.79E-10	8.40E+00	2.28E-10	8.64E+00	1.47E-09	7.67E+00	7.70E-10	4.01E-01	6.11E-10	8.83E-01
	C2/6/1	Compression	6 - 9	6	1.20E-09	1.31E+01	1.50E-10	1.18E+01	9.71E-11	1.83E+01	4.08E-09	6.24E-02	5.62E-10	1.00E-02	4.19E-10	4.04E+00
	C2/6/2	Opposite	6 - 13	6	1.34E-09	1.20E+01	1.60E-10	1.27E+01	4.76E-10	4.90E+00	9.19E-10	1.10E+01	6.03E-10	5.63E-01	6.92E-10	1.04E+00

	Sample ID	Wood Type	Location Yearring from pith	Height	OD Shrinkage		Basic Density	Green MC	EMC 1	EMC 2	EMC 3
					Tang	Radial					
					[-]	[-]	[kg/m^3]	[%]	[%]	[%]	[%]
1. Experiment	A1TC	Core	3 - 7	5	4.01%	1.97%	346.64	124.17	21.65	6.33	18.97
	A1TO	Outer	8 - 13	5	5.25%	2.71%	356.15	174.04	20.80	6.21	18.47
	A1BC	Core	3 - 7	BH	5.13%	3.39%	349.56	112.38	21.83	6.36	18.58
	A1BO	Outer	9 - 16	BH	6.11%	3.75%	359.13	162.44	21.73	6.11	18.30
	A2TC I	Core	3 - 7	5	4.26%	1.50%	342.72	113.88	21.74	6.30	18.61
	A2TO I	Outer	9 - 13	5	5.85%	2.52%	326.16	180.65	21.55	6.08	18.16
	A2TC II'	Core	2 - 4	5	5.93%	2.74%	334.95	155.50	21.73	6.23	18.86
	A2TO II	Outer	10 - 14	5	5.86%	3.23%	339.28	179.94	21.70	6.10	18.54
	A2BC	Core	3 - 7	BH	5.95%	3.26%	375.69	162.00	21.71	6.20	18.62
	A2BO	Outer	12 - 17	BH	5.97%	3.26%	375.06	143.56	22.22	6.27	18.93
2. Experiment	1/1.2/1	Core	1 - 4	BH	5.46%	3.04%	316.98	79.44	18.63	6.48	16.93
	1/1.2/2	Outer	9 - 16	BH	8.14%	3.63%	363.67	164.88	18.28	6.32	16.65
	1/5/1	Core	1 - 4	5	3.95%	2.39%	338.45	81.49	18.34	6.40	16.60
	1/5/2	Outer	5 - 9	5	7.23%	4.52%	341.01	156.17	18.08	6.18	16.19
	1/10/1	Core	1 - 5	10	5.48%	2.40%	322.91	141.80	18.14	6.31	16.62
	1/10/2	Outer	6 - 10	10	6.63%	3.38%	363.46	162.69	17.97	6.09	16.31
	2/1.2/1	Compression	9 - 12	BH	5.11%	2.98%	426.45	146.79	18.32	6.70	16.48
	2/1.2/2	Opposite	9 - 12	BH	7.07%	4.05%	356.62	189.65	19.23	6.31	15.94
	2/10/1	Core	1 - 6	10	4.18%	2.81%	325.71	93.75	17.31	6.43	15.94
	2/10/2	Outer	7 - 11	10	6.23%	3.21%	345.93	186.70	17.38	6.22	15.74
	2/15/1	Core	1 - 4	15	4.04%	2.30%	336.60	146.96	17.63	6.44	16.42
	2/15/2	Outer	7 - 11	15	6.09%	3.48%	364.06	162.33	17.57	6.29	16.23
3. Experiment	3/1.2/1	Core	1 - 4	BH	3.29%	1.56%	343.93	35.86	19.60	6.96	17.11
	3/1.2/2	Outer	9 - 16	BH	6.95%	4.04%	415.89	148.62	19.85	6.39	17.20
	3/5/1	Core	1 - 4	5	3.47%	2.57%	375.25	34.23	19.76	6.82	17.24
	3/5/2	Outer	5 - 9	5	5.02%	1.93%	411.45	128.42	19.90	6.47	17.38
	3/10/1	Core	1 - 5	10	4.54%	2.95%	370.80	39.80	20.22	6.39	17.73
	3/10/2	Outer	6 - 10	10	3.72%	1.63%	426.91	103.39	19.94	6.56	17.55
	4/1.2/1	Core	2 - 4	BH	5.03%	2.13%	327.58	39.53	19.46	6.33	17.07
	4/1.2/2	Outer	7 - 10	BH	8.13%	4.51%	418.95	132.08	18.82	6.18	16.74
	4/10/1	Core	2 - 3	10	4.95%	2.68%	353.69	37.90	19.29	6.19	16.96
	4/10/2	Outer	11 - 15	10	7.18%	3.86%	379.00	164.04	19.23	6.13	16.71
	4/18/1	Core	2 - 4	18	4.53%	3.33%	354.91	38.25	19.82	6.38	17.66
	4/18/2	Outer	9 - 16	18	7.04%	3.20%	353.78	182.50	19.44	6.01	17.00
4.Experiment	C1/1.2/1	Compression	12 - 15	BH	6.14%	3.69%	546.07	105.34	21.07	6.55	17.80
	C1/1.2/2	Opposite	9 - 13	BH	6.72%	4.63%	446.23	125.20	21.35	6.45	17.67
	C1/3/1	Compression	16 - 18	3	4.46%	2.50%	493.13	126.13	20.48	6.56	17.71
	C1/3/2	Opposite	16 - 20	3	6.92%	4.64%	434.74	148.38	20.89	6.14	17.55
	C1/6/1	Compression	13 - 17	6	4.57%	2.73%	471.72	131.02	20.84	6.72	18.07
	C1/6/2	Opposite	10 - 18	6	7.34%	5.03%	440.82	142.19	21.08	6.35	17.86
	C2/1.2/1	Compression	7 - 10	BH	4.26%	1.98%	405.62	127.06	20.42	6.63	17.80
	C2/1.2/2	Opposite	1 - 11	BH	6.47%	4.30%	348.32	144.16	20.51	6.26	17.57
	C2/3/1	Compression	10 - 17	3	3.32%	2.46%	572.91	87.22	20.10	6.73	17.60
	C2/3/2	Opposite	13 - 19	3	6.68%	4.63%	387.48	165.65	20.57	6.29	17.41
	C2/6/1	Compression	6 - 9	6	4.72%	2.41%	364.11	149.94	20.60	6.43	18.01
	C2/6/2	Opposite	6 - 13	6	5.05%	3.19%	372.75	132.35	20.63	6.35	17.83

Input:

- *Board specifications:*
  - Width
  - Thickness
  - Length
  - R_B,R_T
  - Θ_B, Θ_T

Input:

- *Log specifications*
  (Radial distribution of)
  - $SH_{Tang}(r)$
  - $SH_{Long}(r)$
  - SGA*(r)*
  - CA*(r)*

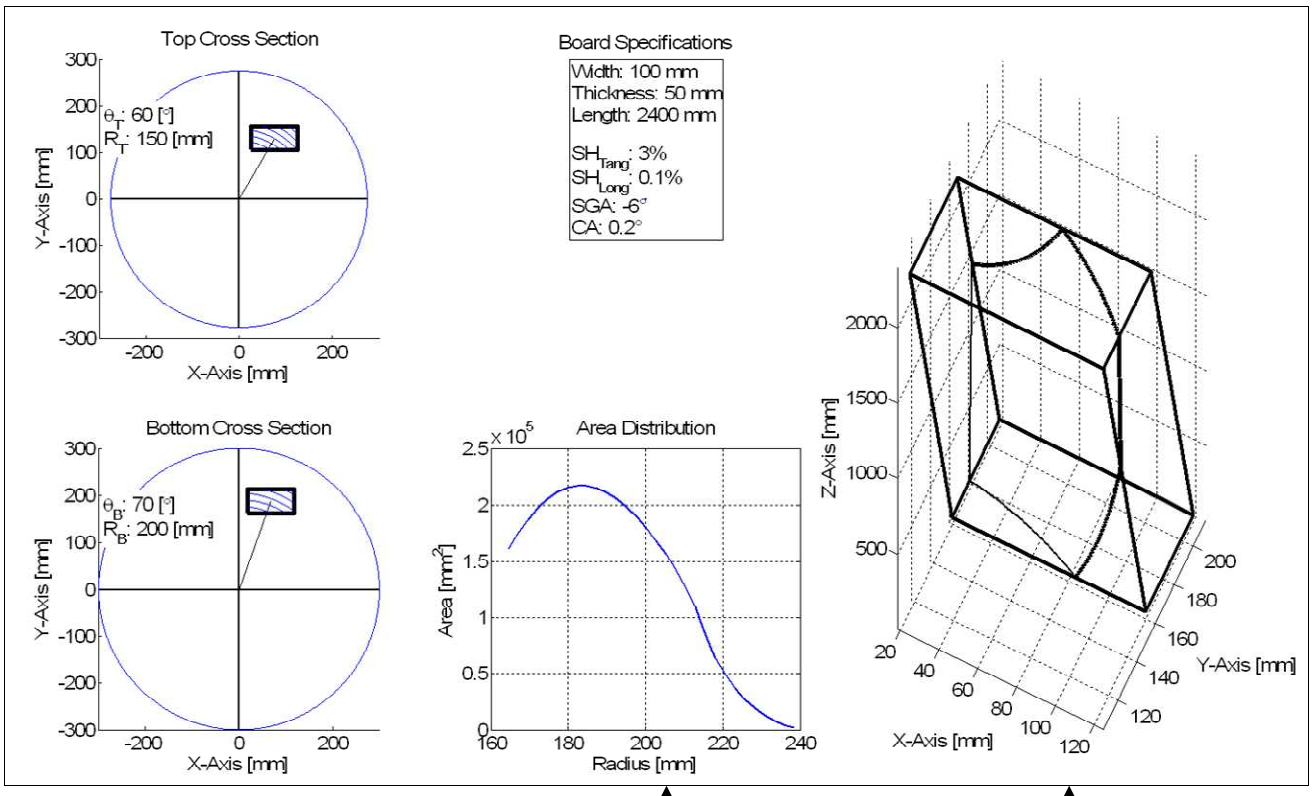

Area distribution

Maximum area

Max. layer shrinkage
(P1', P2', P3', S')

Rotation of cross section
(P2r, Sr)

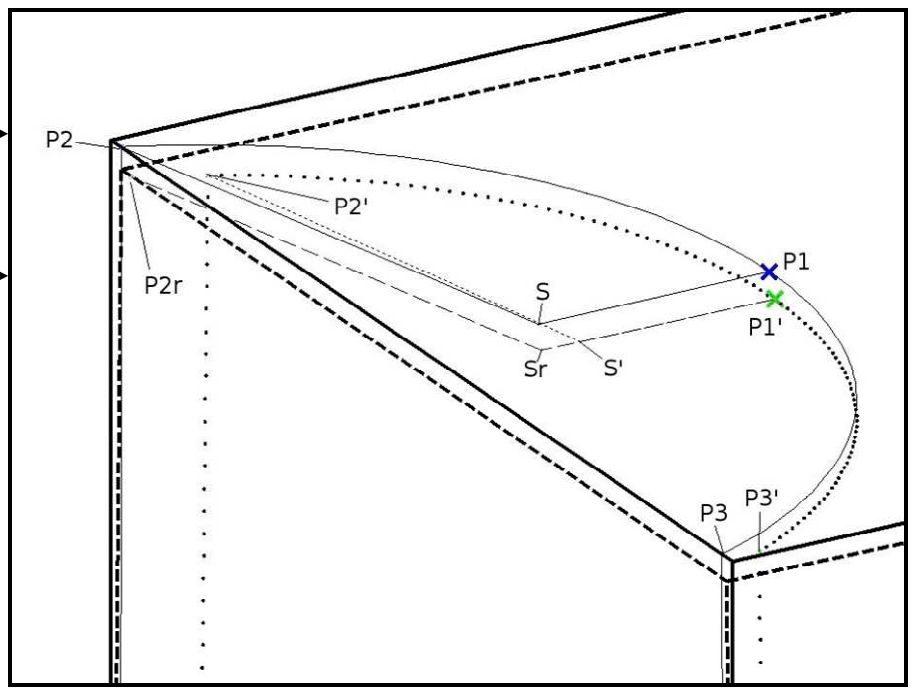

Distortion:

- Twist

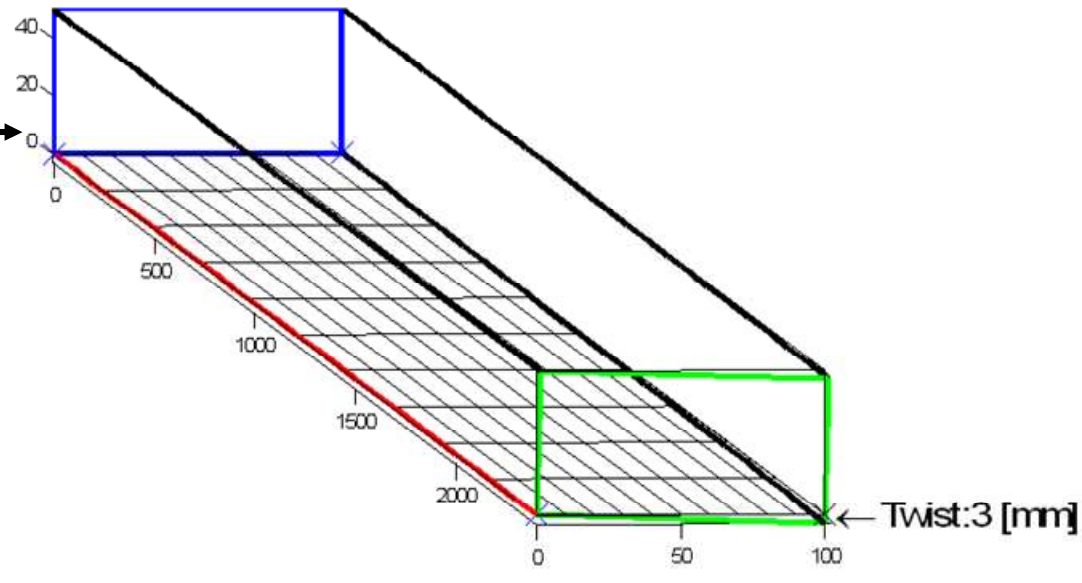

D Schematic Flow Diagram of the Twist Model (Chapter 4)